PB87-227278

Development of Computer Modules of Particulate Processes for Regional Particulate Model

Systems Applications, Inc., San Rafael, CA

Prepared for

Environmental Protection Agency
Research Triangle Park, NC

Jun 87

U.S. Department of Commerce
National Technical Information Service
NTIS

TECHNICAL REPORT DATA
(Please read Instructions on the reverse before completing)

1. REPORT NO. EPA/600/3-87/021	2.	3. RECIPIENT'S ACCESSION NO. PB87 227278/AS
4. TITLE AND SUBTITLE DEVELOPMENT OF COMPUTER MODULES OF PARTICULATE PROCESSES FOR REGIONAL PARTICULATE MODEL		5. REPORT DATE June 1987
		6. PERFORMING ORGANIZATION CODE
7. AUTHOR(S) A. Belle Hudischewskyj, Pradeep Saxena and Christial Seigneur		8. PERFORMING ORGANIZATION REPORT NO.
9. PERFORMING ORGANIZATION NAME AND ADDRESS Systems Applications, Inc. 101 Lucas Valley Road San Rafael, California 94903		10. PROGRAM ELEMENT NO. A101/B/64/03 - 3047 (FY-87)
		11. CONTRACT/GRANT NO. Contract No. 68-02-4076
12. SPONSORING AGENCY NAME AND ADDRESS ATMOSPHERIC SCIENCES RESEARCH LABORATORY - RTP, NC OFFICE OF RESEARCH AND DEVELOPMENT U.S. ENVIRONMENTAL PROTECTION AGENCY RESEARCH TRIANGLE PARK, NORTH CAROLINA 27711		13. TYPE OF REPORT AND PERIOD COVERED Final
		14. SPONSORING AGENCY CODE EPA/600/09

15. SUPPLEMENTARY NOTES

16. ABSTRACT

The development of an aerosol model for inclusion in the EPA Regional Particulate Model is described. Existing computer modules of particulate processes developed under EPA contract by Professors Brock, Seinfeld, and Whitby are compared to determine efficient and accurate methods of simulating particulate behavior. These methods are incorporated into an aerosol model, which is accurate and efficient in its treatment of the dynamics, thermodynamics, and chemical composition of atmospheric aerosols.

Evaluation of the aerosol model is described using simulations for a regional environment and an urban plume. The model performs well under a variety of atmospheric and meteorological conditions. The results indicate the aerosol model is a useful tool for PM-10 and visibility studies.

17. KEY WORDS AND DOCUMENT ANALYSIS

a. DESCRIPTORS	b. IDENTIFIERS/OPEN ENDED TERMS	c. COSATI Field/Group

18. DISTRIBUTION STATEMENT RELEASE TO PUBLIC	19. SECURITY CLASS *(This Report)* UNCLASSIFIED	21. NO. OF PAGES 270
	20. SECURITY CLASS *(This page)* UNCLASSIFIED	22. PRICE

EPA Form 2220-1 (Rev. 4-77) PREVIOUS EDITION IS OBSOLETE

PB87-227278

EPA/600/3-87/021
June 1987

DEVELOPMENT OF COMPUTER MODULES OF PARTICULATE PROCESSES FOR REGIONAL PARTICULATE MODEL

by

A. Belle Hudischewskyj, Pradeep Saxena and Christian Seigneur
Systems Applications, Inc.
101 Lucas Valley Road
San Rafael, California 94903

Contract No. 68-02-4076

Project Officer

Harold M. Barnes
Atmospheric Chemistry and Physics Division
Atmospheric Sciences Research Laboratory
Research Triangle Park, North Carolina 27711

ATMOSPHERIC SCIENCES RESEARCH LABORATORY
OFFICE OF RESEARCH AND DEVELOPMENT
U.S. ENVIRONMENTAL PROTECTION AGENCY
RESEARCH TRIANGLE PARK, NORTH CAROLINA 27711

REPRODUCED BY
U.S. DEPARTMENT OF COMMERCE
NATIONAL TECHNICAL
INFORMATION SERVICE
SPRINGFIELD, VA. 22161

DISCLAIMER

The information in this document has been funded wholly or in part by the United States Environmental Protection Agency under Contract No. 68-02-4076 to Systems Applications, Inc. It has been subject to the Agency's peer and administrative review, and it has been approved for publication as an EPA document.

Mention of trade names or commercial products does not constitute endorsement or recommendation for use.

ABSTRACT

The development of an aerosol model for inclusion in the EPA Regional Particulate Model is described. Existing computer modules of particulate processes developed under EPA Contract by Professors Brock, Seinfeld, and Whitby are compared to determine efficient and accurate methods of simulating particulate behavior. These methods are incorporated into an aerosol model, which is accurate and efficient in its treatment of the dynamics, thermodynamics, and chemical composition of atmospheric aerosols.

Evaluation of the aerosol model is described using simulations for a regional environment and an urban plume. The model performs well under a variety of atmospheric and meteorological conditions. The results indicate the aerosol model is a useful tool for PM-10 and visibility studies.

CONTENTS

ABSTRACT iii

LIST OF FIGURES vii

LIST OF TABLES xii

ACKNOWLEDGMENTS xiv

1 INTRODUCTION 1-1

2 REVIEW OF AEROSOL MODELS 2-1

- Modeling of Aerosol Thermodynamics 2-2
- Modeling of Aerosol Coagulation 2-5
- Modeling of Aerosol Growth/Shrinkage 2-6

3 FORMULATION OF THE AEROSOL MODEL 3-1

- Introduction 3-1
- Mathematical Formulation of the Aerosol Model 3-3
- Coagulation 3-8
- Condensation/Evaporation 3-10
- New Aerosol Formation 3-13
- Thermodynamic Equilibrium 3-15
- Secondary Organic Aerosol Formation 3-17
- Aerosol Chemical Kinetics 3-20
- Removal Processes 3-21
- Light Scattering 3-24
- Specific Formulation of the Aerosol Model for the EPA Regional Particulate Model 3-24

4 DEVELOPMENT OF THE REGIONAL PARTICULATE MODEL 4-1

- Description of the Regional Oxidant Model 4-1
- Gas-Phase Chemical Kinetic Mechanism 4-5
- Emissions 4-11

Dry Deposition..4-11
Production of Aerosols in Clouds...........................4-12

5 APPLICATION OF THE REGIONAL TRAJECTORY PARTICULATE MODEL........ 5-1

Introduction.. 5-1
Description of the Modeling Conditions...................... 5-1
Regional Base Case--Columbus, Ohio.......................... 5-8
Urban Plume Base Case--St. Louis, Missouri..................5-40

6 CONCLUSIONS.. 6-1

REFERENCES.. R-1

Appendix A: TECHNICAL CONSIDERATIONS IN REGIONAL AEROSOL MODELING.. A-1

Appendix B: A COMPARATIVE STUDY OF EQUILIBRIUM APPROACHES TO THE CHEMICAL CHARACTERIZATION OF SECONDARY AEROSOLS.................................... B-1

Appendix C: SIMULATION OF AEROSOL DYNAMICS: A COMPARATIVE REVIEW OF MATHEMATICAL MODELS.......................... C-1

Appendix D: DEVELOPMENT OF A PARAMETERIZED CHEMICAL KINETIC MECHANISM FOR ORGANIC AEROSOL FORMATION................ D-1

Appendix E: ON THE OXIDATION OF SO_2 TO SULFATE IN ATMOSPHERIC AEROSOLS................................... E-1

Appendix F: REDUCTION OF THE CARBON-BOND MECHANISM X (CBM-X) USING VARIATIONAL SENSITIVITY ANALYSIS......... F-1

Appendix G: FORMATION OF AEROSOLS IN CLOUDS........................ G-1

Appendix H: MATHEMATICAL MODELING OF THE DYNAMICS OF MULTICOMPONENT ATMOSPHERIC AEROSOLS.................... H-1

Appendix I: MATHEMATICAL MODELING OF LIGHT SCATTERING BY ATMOSPHERIC AEROSOLS................................... I-1

Appendix J: USER'S GUIDE TO THE AEROSOL MODEL...................... J-1

FIGURES

2-1 Simulation of aerosol coagulation for urban conditions..... 2-8

2-2 Simulation of aerosol condensation for urban conditions....2-11

3-1 Procedure flow chart for the aerosol model................. 3-7

3-2 Brownian coagulation coefficient (Beta) for aerosols of diameters d_i and d_j...................................3-11

3-3 Diffusion-limited condensation coefficient for a vapor pressure of P and an aerosol diameter of d.................3-14

3-4 Steady-state dimensionless new particle formation rates as a function of the total dimensionless sink term, L......3-16

3-5 Example of a size-distributed aerosol concentration and chemical composition calculated by the aerosol model.......3-26

3-6 Application of the aerosol model to clear conditions.......3-27

4-1 Schematic illustration of the "dynamic" layer structure of the regional-scale model and the phenomena each layer is designed to treat................................. 4-3

5-1 Structure of the trajectory model with treatment of vertical mixing... 5-2

5-2 Concentrations of major chemical species for the Columbus, Ohio base case, August 23-24, 1981...............5-13

5-3 Concentrations of major aerosol species for the Columbus, Ohio base case, August 23-24, 1981...............5-15

5-4(a) Size distributed chemical composition of the aerosol for the Columbus, Ohio base case at the time of the maximum aerosol nitrate and PM10 concentrations on the second day of the simulation (August 24, 1981, 9 a.m.)........5-17

5-4(b) Size distributed chemical composition of the aerosol for the Columbus, Ohio base case at the time of the maximum aerosol sulfate concentration on the second day of the simulation (August 24, 1981, 6 p.m.)........5-18

5-5 Concentrations of major chemical species for the Columbus, Ohio base case and 50% SO_2 reduction simulations for August 23-24, 1981........5-20

5-6 Concentrations of major aerosol species for the Columbus, Ohio base case and 50% SO_2 reduction simulations for August 23-24, 1981........5-21

5-7(a) Size distributed chemical composition of the aerosol for the Columbus, Ohio 50% SO_2 reduction case at the time of the maximum aerosol nitrate and PM10 concentrations on the second day of the simulation (August 24, 1981, 9 a.m.)........5-22

5-7(b) Size distributed chemical composition of the aerosol for the Columbus, Ohio 50% SO_2 reduction case at the time of the maximum aerosol sulfate concentration on the second day of the simulation (August 24, 1981, 5 p.m.)........5-23

5-8 Concentrations of major chemical species for the Columbus, Ohio base case and 50% NO_x reduction simulations for August 23-24, 1981........5-24

5-9 Concentrations of major aerosol species for the Columbus, Ohio base case and 50% NO_x reduction simulations for August 23-24, 1981........5-25

5-10(a) Size distributed chemical composition of the aerosol for the Columbus, Ohio 50% NO_x reduction case at the time of the maximum aerosol nitrate concentration on the second day of the simulation. (August 24, 1981, 7 a.m.)........5-26

5-10(b) Size distributed chemical composition of the aerosol for the Columbus, Ohio 50% NO_x reduction case at the time of the maximum PM10 concentration on the second day of the simulation. (August 24, 1981, 9 a.m.)....................5-27

5-10(c) Size distributed chemical composition of the aerosol for the Columbus, Ohio 50% NO_x reduction case at the time of the maximum aerosol sulfate concentration on the second day of the simulation. (August 24, 1981, 5 p.m.)..........5-28

5-11 Concentrations of major chemical species for the Columbus, Ohio base case and 50% NH_3 reduction simulations for August 23-24, 1981..5-30

5-12 Concentrations of major aerosol species for the Columbus, Ohio base case and 50% NH_3 reduction simulations for August 23-24, 1981 (PM10 includes water aerosol)...........5-31

5-13(a) Size distributed chemical composition of the aerosol for the Columbus, Ohio 50% NH_3 reduction case at the time of the maximum aerosol nitrate concentration on the second day of the simulation. (August 24, 1981, 7 a.m.)..........5-32

5-13(b) Size distributed chemical composition of the aerosol for the Columbus, Ohio 50% NH_3 reduction case at the time of the maximum PM10 concentration on the second day of the simulation. (August 24, 1981, 9 a.m.)....................5-33

5-13(c) Size distributed chemical composition of the aerosol for the Columbus, Ohio 50% NO_x reduction case at the time of the maximum aerosol sulfate concentration on the second day of the simulation. (August 24, 1981, 6 p.m.)..........5-34

5-14 Concentrations of major chemical species for the Columbus, Ohio base case and 50% reactive hydrocarbon reduction simulations for August 23-24, 1981........................5-35

5-15 Concentrations of major aerosol species for the Columbus, Ohio base case and 50% reactive hydrocarbon reduction simulations for August 23-24, 1981........................5-36

5-16(a) Size distributed chemical composition of the aerosol for the Columbus, Ohio 50% reactive hydrocarbon reduction case at the time of the maximum aerosol nitrate concentration on the second day of the simulation. (August 24, 1981, 9 a.m.)..5-37

5-16(b) Size distributed chemical composition of the aerosol for the Columbus, Ohio 50% reactive hydrocarbon reduction case at the time of the maximum PM10 concentration on the second day of the simulation. (August 24, 1981, 10 a.m.)....................5-38

5-16(c) Size distributed chemical composition of the aerosol for the Columbus, Ohio 50% reactive hydrocarbon reduction case at the time of the maximum aerosol sulfate concentration on the second day of the simulation. (August 24, 1981, 6 p.m.)....................5-39

5-17 Concentrations of major chemical species for the Columbus, Ohio August 23-24, 1981, base case and December 23-24, 1981 winter simulations....................5-41

5-18 Concentrations of major aerosol species for the Columbus, Ohio August 23-24, 1981 base case and December 23-24 1981 winter simulations....................5-42

5-19(a) Size distributed chemical composition of the aerosol for the Columbus, Ohio winter case at the time of the maximum PM10 concentration on the second day of the simulation (December 24, 1981, 8 a.m.)....................5-43

5-19(b) Size distributed chemical composition of the aerosol for the Columbus, Ohio winter case at the time of the maximum aerosol sulfate concentration on the second day of the simulation. (December 24, 1981, 4 p.m.)....................5-44

5-19(c) Size distributed chemical composition of the aerosol for the Columbus, Ohio winter case at the time of the maximum aerosol nitrate concentration on the second day of the simulation. (December 24, 1981, 8 p.m.)....................5-45

5-20 Concentrations of major chemical species for the St. Louis base case and 85% relative humidity simulations for August 23-24, 1981....................5-48

5-21 Concentrations of major aerosol species for the St. Louis base case and 85% relative humidity simulations for August 23-24, 1981....................5-50

5-22(a) Size distributed chemical composition of the aerosol for the St. Louis base case at the time of the maximum aerosol nitrate and PM10 concentrations on the second day of the simulation. (August 24, 1981, 6 a.m.)..........5-52

5-22(b) Size distributed chemical composition of the aerosol for the St. Louis base case at the time of the maximum aerosol sulfate concentration on the second day of the simulation. (August 24, 1981, 7 p.m.)....................5-53

5-23(a) Size distributed chemical composition of the aerosol for the St. Louis 85% relative humidity case at the time of the maximum aerosol nitrate and PM10 concentrations on the second day of the simulation. (August 24, 1981, 6 a.m.)...5-55

5-23(b) Size distributed chemical composition of the aerosol for the St. Louis 85% relative humidity case at the time of the maximum aerosol sulfate concentration on the second day of the simulation. (August 24, 1981, 8 p.m.)...5-56

TABLES

2-1 Comparison of performance and computational efficiency of KEQUIL, EQUIL, and MARS.................................. 2-4

2-2 Comparison of model simulation results for coagulation..... 2-7

2-3 Comparison of model simulation results for condensation....2-10

3-1 Sectional coagulation coefficients with geometric constraint....................................... 3-9

3-2 Sectional condensational growth coefficients with aerosol number conservation constraint.............................3-12

3-3 Treatment of the aerosol chemical composition..............3-18

3-4 Sectional coefficients for aerosol growth/shrinkage due to changes in the aerosol chemical composition.............3-19

3-5 Chemical kinetic expressions for the aerosol-phase chemical reactions...3-22

3-6 Sectional coefficients for aerosol growth due to aerosol chemical reactions.................................3-23

4-1 The Carbon-Bond Mechanism IV............................... 4-6

4-2 Aerosol deposition velocities (for a friction velocity v* = 10 cm/s)..................................4-13

5-1 Dry deposition velocities................................. 5-4

5-2 Emission rates.. 5-5

5-3 Initial concentrations for the regional simulation......... 5-6

5-4 Initial concentrations for the urban plume simulation...... 5-7

5-5 Minimum concentrations for the base case and sensitivity simulations for Columbus, Ohio, August 23, 1981 5-9

5-6 Minimum concentrations for the base case and sensitivity simulations for Columbus, Ohio, August 24, 1981............5-10

5-7 Maximum concentrations for the base case and sensitivity simulations for Columbus, Ohio, August 23, 1981............5-11

5-8 Maximum concentrations for the base case and sensitivity simulations for Columbus, Ohio, August 24, 1981............5-12

5-9 Minimum concentrations for the base case and 85% relative humidity simulations for St. Louis, Missouri, August 23-24, 1981...5-46

5-10 Maximum concentrations for the base case and 85% relative humidity simulations for St. Louis, Missouri, August 23-24, 1981...5-47

ACKNOWLEDGMENTS

This study was sponsored by the EPA-ASRL Aerosol Research Branch. We would like to thank the Project Officer, Dr. H. M. Barnes, for suggesting this study and for his support.

We thank Professors K. T. Whitby, J. H. Seinfeld, and J. R. Brock for providing us with their aerosol models and giving us useful advice during the course of this work. We thank Mr. E. Whitby and Professor P. H. McMurry for helpful discussions concerning the AGRO model and its computational implementation. Informative discussions with Dr. Tate Tsang, University of Kentucky, Dr. K. Yom, University of Texas, and Mr. Dale Warren, California Institute of Technology, are also very much appreciated. We would also like to thank Ms. Judy A. Rodich for her editorial effort.

1 INTRODUCTION

Systems Applications, Inc. has been under contract to the U.S. Environmental Protection Agency (EPA) to (1) review existing computer models of particulate processes, (2) on the basis of this review, develop a computer model of the dynamics, thermodynamics, and chemistry of atmospheric particulate matter (i.e., aerosols), and (3) incorporate this model into the EPA Regional Oxidant Model to constitute a Regional Particulate Model. Such a model is of primary importance in addressing air quality issues related to particulate matter concentration levels (particularly, PM-10 levels), visibility degradation, and acid deposition.

The tasks conducted in this project include the following:

(1) Installation and operation of the aerosol models developed under EPA contracts on the EPA computer. The models included those developed at the University of Minnesota by Professor K. T. Whitby, Mr. E. R. Whitby, and co-workers; at the University of Texas by Professor J. R. Brock and co-workers; and at the California Institute of Technology by Professor J. H. Seinfeld and co-workers.

(2) Evaluation of the computational requirements, predictive accuracy, and application range of these models.

(3) Based on this review, selection of a technical approach for aerosol modeling suitable to the EPA regional model. (If the available models did not meet the accuracy and computational requirements of regional modeling, further model development would have been carried out.)

(4) Development of chemical kinetic mechanisms for the gas-to-aerosol conversion of sulfate, nitrate, and organic species.

(5) Development of an aerosol model that includes a comprehensive treatment of aerosol dynamics, thermodynamics, and chemistry and is computationally manageable.

(6) Incorporation of this aerosol model in the EPA Regional Oxidant Model.

(7) Development of modules to treat specific aerosol processes, such as dry deposition and aerosol formation in clouds.

(8) Condensation/reduction of a chemical kinetic mechanism for the EPA Regional Oxidant and Particulate Model.

(9) Application and evaluation of the chemical and aerosol submodules in conjunction with a regional trajectory particulate model.

(10) Preparation of a user's guide to the aerosol submodules developed during the course of this project.

This report presents the work that was done.

In Section 2 we summarize the comparative evaluation of the models of aerosol dynamics and thermodynamics that were considered in this study, and discuss the rationale for selecting our technical approach to aerosol modeling. In Section 3 we present the formulation of the aerosol model that is to be incorporated into the EPA Regional Model. Our technical approach to incorporating the aerosol module into the EPA regional model, as well as developing modules for dry deposition and aerosol formation in clouds, is discussed in Section 4. The application and evaluation of the aerosol model are presented in Section 5. Conclusions are presented in Section 6.

Several technical aspects of this work are presented in greater detail in the appendixes. Technical considerations in regional aerosol modeling are discussed in Appendix A. Several models of aerosol thermodynamics are compared in Appendix B, and models of aerosol dynamics are compared in Appendix C. Organic aerosol formation is reviewed in Appendix D. Our investigation of aerosol chemical kinetic processes is summarized in Appendix E. The use of variational sensitivity analysis in the reduction of the chemical kinetic mechanism is explained in Appendix F. Aerosol formation in clouds, which is presented in Section 3, is discussed in detail in Appendix G. The mathematical modeling of the dynamics of multicomponent atmospheric aerosols and of light scattering by atmospheric aerosols is presented in Appendixes H and I, respectively. A user's guide for the aerosol submodules is presented in Appendix J.

2 REVIEW OF AEROSOL MODELS

In this section we review models of aerosol thermodynamics and dynamics and, on the basis of this review, select a modeling technique to simulate atmospheric aerosol thermodynamics and dynamics at the regional scale. Such a modeling technique must treat the aerosol physicochemical processes that are important at the regional scale. These processes have been reviewed by Seigneur and Barnes [(1985)--see Appendix A], who concluded that the following processes must be considered:

Coagulation,

Growth/shrinkage due to condensation/evaporation,

Formation of fresh aerosols at a lower threshold size,

Thermodynamic equilibrium of volatile aerosol species between the aerosol and gas phases,

Chemical reactions in the aerosol phase,

Removal processes (dry and wet depostion), and

Formation of aerosols through cloud chemistry and evaporation.

The treatments of coagulation, growth/shrinkage, and fresh aerosol formation are generally addressed together as aerosol dynamics.

The treatments of aerosol coagulation, growth/shrinkage, and thermodynamics are those that may require the most detailed mathematical models and, consequently, the most expensive computational techniques. Thus, we reviewed models having different levels of detail (and, conversely, different levels of computational requirements) for each one of these processes.

Our reviews have been presented in detail by Saxena et al. [(1986)--see Appendix B] for aerosol thermodynamics modeling, and by Seigneur et al.

[(1986)--see Appendix C] for aerosol dynamics (coagulation and growth/shrinkage) modeling. These reviews are summarized in the following paragraphs.

MODELING OF AEROSOL THERMODYNAMICS

The treatment of the thermodynamic equilibrium between the aerosol and gas phases is central to the determination of the chemical composition of aerosols that results from the condensation of sulfuric acid (H_2SO_4), nitric acid (HNO_3), ammonia (NH_3), and water (H_2O). Other species, such as HCl and organic compounds, also affect the thermodynamic equilibrium of aerosols. The thermodynamics of organic aerosols is discussed in Appendix D, and HCl, which is generally present in low concentrations in the atmosphere, can be neglected. Sulfate and nitrate aerosols generally occur in significant concentrations in polluted areas and are of primary interest in acid deposition and visibility impairment considerations. Therefore, we focus here on models of sulfate/nitrate/ammonium/water aerosols.

Three models were considered in the review: the Model for an Aerosol Reacting System (MARS), EQUIL, and KEQUIL. MARS was developed for this study by Saxena and Seigneur at Systems Applications, Inc. EQUIL and KEQUIL were developed by Bassett and Seinfeld at the California Institute of Technology. Brief descriptions of these models are given next; more detailed descriptions are given in Appendix B.

MARS is based on fundamental thermodynamics (Saxena et al., 1986). The treatment of chemical and interfacial equilibria focuses only on major species for each given set of ambient conditions. Thus, the number of equations to be solved is minimized. The various species treated in MARS include H_2SO_4, HNO_3, NH_3, and H_2O in the gas phase; SO_4^{2-}, HSO_4^-, NH_4^+, NO_3^-, H^+, and $H_2O(\ell)$ in the liquid phase; and $(NH_4)_2SO_4$, $(NH_4)_3H(SO_4)_2$, NH_4HSO_4, and NH_4NO_3 in the solid phase. Note that the solid phase, when present, is assumed to be an external mixture of compounds such as $(NH_4)_2SO_4$, $(NH_4)_3H(SO_4)_2$, NH_4HSO_4, and NH_4NO_3. Therefore, each of these solid compounds, in reality, constitutes a phase in itself. The mixed sulfate-nitrate salts $(NH_4)_2SO_4 \cdot 2NH_4NO_3$ and $(NH_4)_2SO_4 \cdot 3NH_4NO_3$ are considered to be dissociated as $(NH_4)_2SO_4$ and NH_4NO_3. Not all of the species treated by MARS are present in a particular aerosol/gas system. The presence and amounts of these species are dictated by the total concentrations of H_2SO_4, HNO_3, NH_3, the relative humidity, and temperature. For example, for a particular set of concentrations there may not be a solid phase at all, and for another the aqueous phase may be devoid of nitrate. Relative humidity and the molar ratio of ammonia to sulfuric acid are the two most important variables in determining the composition of each phase. Another important consideration is the relative humidity of deliquescence for the sulfate and nitrate salts.

The distinguishing feature of MARS is its division of the entire regime of aerosol species into several subdomains. Since each subdomain contains fewer viable species than does the entire domain of concentrations, the number of equations to be solved and therefore the computational cost are minimized. MARS does not consider the effect of the aerosol surface curvature--the so-called Kelvin effect--on the aerosol/gas equilibrium.

EQUIL is a rigorous model that explicitly solves for 17 species in eight phases by minimizing the Gibbs free energy of the system (Bassett and Seinfeld, 1983). There are 13 equilibrium reactions among these species. The temperature dependence of all thermodynamic properties is taken into account. In addition to the species treated by MARS, EQUIL treats $(NH_4)_2SO_4 \cdot 2NH_4NO_3(s)$ and $(NH_4)_2SO_4 \cdot 3NH_4NO_3(s)$. The thermodynamic properties of these compounds are approximated by those of $((NH_4)_2SO_4 + 2NH_4NO_3)$ and $((NH_4)_2SO_4 + 3NH_4NO_3)$, respectively; for the prediction of $(NH_4)_2SO_4$ and NH_4NO_3 masses, the model produces results that are essentially the same as those obtained by treating $(NH_4)_2SO_4$ and NH_4NO_3 in separate phases. Like MARS, EQUIL does not consider the Kelvin effect.

KEQUIL is derived from EQUIL and does incorporate the Kelvin effect (Bassett and Seinfeld, 1984). In all other respects, KEQUIL is identical to EQUIL.

The results of MARS and EQUIL were compared with those of KEQUIL, the most comprehensive model currently available. Such comparisons were made for a broad spectrum of atmospheric conditions. Results were compared for concentrations of aerosol-phase ammonium, nitrate, total mass, and light scattering coefficients (b_{scat}). Since all three models treat sulfate as a nonvolatile species, there was no disagreement among model predictions regarding aerosol-phase sulfate concentration. The results of this comparative model evaluation are presented in Table 2-1. Calculations by EQUIL and MARS agreed closely with those of KEQUIL. However, MARS was determined to be on average 400 times faster than KEQUIL and about 60 times faster than EQUIL. This substantial difference in computational efficiency was attained without significant loss of accuracy; the average errors for nitrate, ammonium, total mass, and b_{scat} were all well within 10 percent. These results would be slightly different had we used a different initial size distribution or temperature.

TABLE 2-1. Comparison of performance and computational efficiency of KEQUIL, EQUIL, and MARS.

Performance Measure[a]	Parameter	KEQUIL	EQUIL	MARS
Average Error[b] (percent)	Nitrate	--	3	7
	Ammonium	--	0	1
	Total	--	2	4
	b_{scat}	--	4	6
Average Bias[c] (percent)	Nitrate	--	3	0
	Ammonium	--	0	0
	Total	--	2	3
	b_{scat}	--	-1	0
Correlation Coefficient	Nitrate	--	1.000	1.000
	Ammonium	--	1.000	1.000
	Total	--	1.000	0.997
	b_{scat}	--	0.999	0.996
Average Simulation Time (CPUs)[d]		72.4	9.7	0.17

[a] These performance measures are computed with respect to KEQUIL. For nitrate, if the predicted concentration is less than 0.1 $\mu g\ m^{-3}$ (about 0.04 ppb) it is assumed to be zero. For comparison, the measurement threshold for nitrate ranges from 0.04 to about 1 ppb (Anlauf et al., 1985; Kelly et al, 1984). There are 23 cases for which all three models predict nitrate concentrations below 0.1 $\mu g\ m^{-3}$. Perfect agreement among the three models is assumed for these cases.

[b] Defined as $\frac{1}{N} \sum_{i=1}^{N} \left| \frac{X_i - Y_i}{Y_i} \right| \times 100$,

where X_i is the value predicted by EQUIL or MARS, and Y_i is that predicted by KEQUIL. N is the total number of cases.

[c] Defined as $\frac{1}{N} \sum_{i=1}^{N} \frac{X_i - Y_i}{Y_i} \times 100$.

[d] On a Prime 750 computer.

On the basis of the results of this study, we selected MARS as an efficient and accurate model of aerosol thermodynamics for incorporation into the regional model.

MODELING OF AEROSOL COAGULATION

Aerosol coagulation is governed by the following mathematical equation:

$$\frac{\partial n(v, t)}{\partial t} = \frac{1}{2} \int_{v^*}^{v} \beta(v - \tilde{v}, \tilde{v})\, n(\tilde{v}, t)\, n(v - \tilde{v}, t)\, d\tilde{v} - \int_{0}^{\infty} \beta(v, \tilde{v})\, n(v, t)\, n(\tilde{v}, t)\, d\tilde{v}$$

$$n(v, 0) = n_0(v)$$

$$n(v, t) = 0, \qquad v < v^* \qquad (2\text{-}1)$$

where

$n(v, t)$ = the density function of the aerosol number size distribution,

v = the aerosol volume,

t = the time,

β = the coagulation coefficient, and

v^* = the minimum aerosol volume.

Difficulties in solving this equation arise in the evaluation of the integrals on the right side. Three major types of approaches have been developed to solve the equation:

(1) Continuous representation
(2) Discrete representation
(3) Parameterized representation

Each of these approaches is a numerical technique for solving the coagulation equation. They differ only in their degree of approximation of the size distribution. Those techniques that offer any desired degree of approximation are referred to as continuous. Discrete approximations are methods in which the size domain is divided into discrete segments or sections. In principle, discrete approaches can be implemented at an arbitrary degree of approximation; however, there are practical constraints on the number of sections that can be used. Finally, parameterized representations are those methods in which the size distribution is assumed to adhere to a known form depending on a small number of parameters. Both continuous and discrete approaches necessarily assume a certain form of the size distribution but generally at a much finer level of representation than do the approaches that we classify as parameterized.

The three models that were chosen as representative of these approaches were COAGUL (Yom and Brock, 1984) for the continuous representation, ESMAP (Warren and Seinfeld, 1985) for the sectional representation, and AGRO (Whitby, 1981; Whitby, 1985) for the parameterized representation. ESMAP was applied with two different size resolutions, 12 and 39 sections, over the 0.001 μm to 10 μm size range. These models were exercised to simulate aerosol coagulation over 12 hours for atmospheric aerosol concentrations typical of clear, hazy, and urban conditions. COAGUL was shown to provide an accurate solution of the coagulation equation. The detailed results of this comparative model evaluation are described by Seigneur et al. (1986). The results are summarized here in Table 2-2. Figure 2-1 compares the different aerosol size distributions calculated after 12 hours for urban conditions.

The computational times on a Prime 750 computer were as follows: AGRO required less than 1 CPUs, and COAGUL required from 100 to 1000 CPUs depending on the case study. ESMAP with 39 sections required from 180 to 2500 CPUs; with 12 sections it required from 40 to 350 CPUs.

ESMAP with either 39 or 12 sections performs very well relative to COAGUL. AGRO performs well for the case studies with clear and hazy conditions (in which coagulation has little effect on the initial size distributions) but is less accurate for the urban case study. This poor performance of AGRO is due to the assumption of a lognormal distribution, which leads to overprediction of the coagulation rate.

MODELING OF AEROSOL GROWTH/SHRINKAGE

Aerosol growth/shrinkage due to condensation/evaporation is represented by the following equation:

TABLE 2-2. Comparison of model simulation results for coagulation.

Model	Average Absolute Normalized Difference (percent)		
	Clear Conditions	Hazy Conditions	Urban Conditions
COAGUL		(Reference)	
ESMAP (39 sections)	1	1	2
ESMAP (12 sections)	1	1	3
AGRO	2	2	18

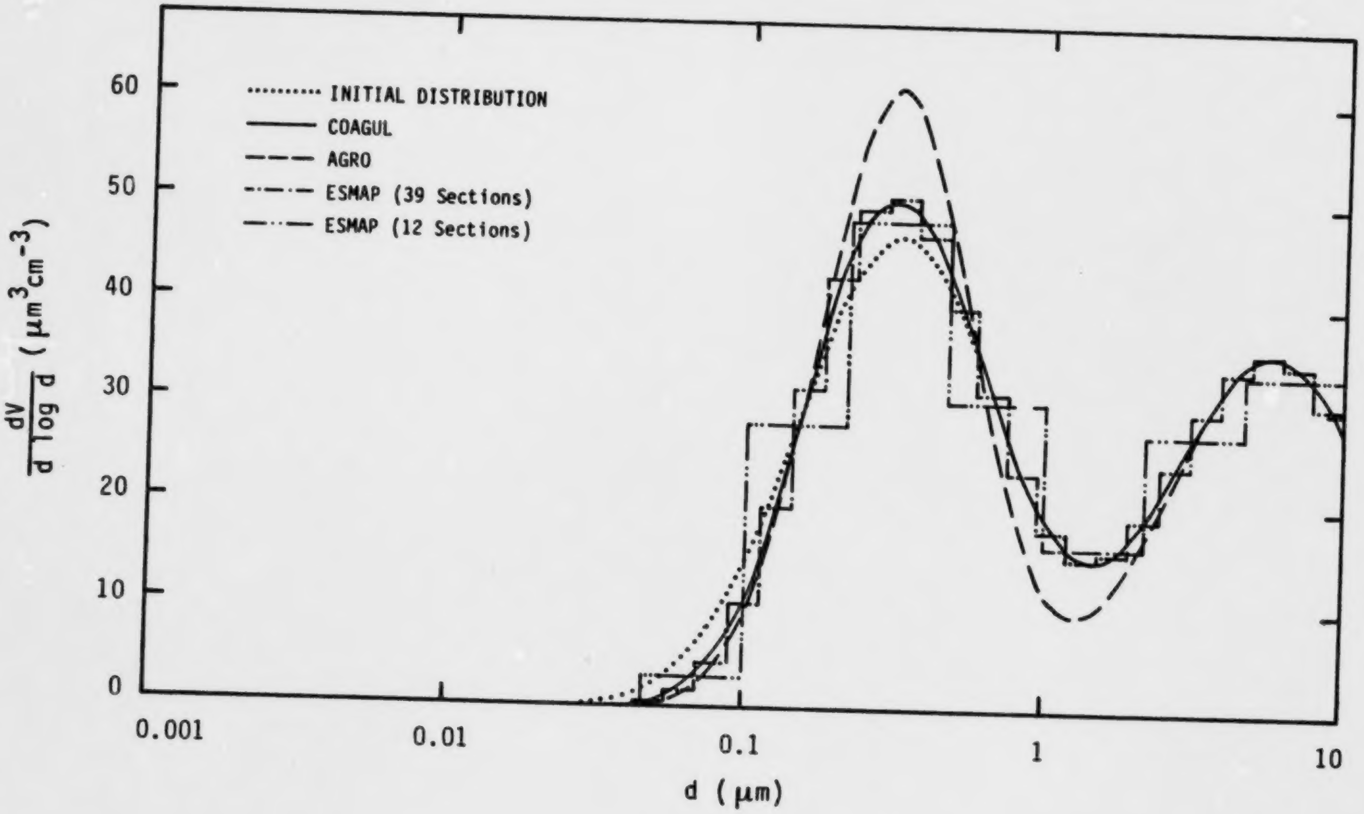

FIGURE 2-1. Simulation of aerosol coagulation for urban conditions.

$$\frac{\partial n(v,\ t)}{\partial t} = - \frac{\partial}{\partial v} [n(v,\ t)\ I(v,\ t)]$$

$$n(v,\ 0) = n_o(v)$$

$$n(v,\ t) = 0 \quad , \quad v < v^* \qquad (2\text{-}2)$$

where $I(v,\ t) = dv/dt$, the rate of growth/shrinkage of a particle of volume v.

This equation is a hyperbolic partial differential equation. The numerical solution of such an equation is hindered by the difficulty in accurately representing the fronts that move with velocity dv/dt. The errors in the solution give rise to numerical diffusion and dispersion. Numerical diffusion leads to a decrease of the peak values of the number distribution and, concurrently, to increases in the values of the number distribution around these peak values. Numerical dispersion leads to wakes in the ranges below and above the area of large values of the number distributions. If one is interested only in growth/shrinkage processes, then this equation can be solved exactly by the method of characteristics. However, in the presence of coagulation, the growth/shrinkage term of the dynamic equation for aerosols must be treated numerically in accordance with the coagulation terms.

The three major approaches that can be used to solve this equation are similar to those described for the treatment of coagulation since they are based on continuous, sectional, and parameterized representations of the aerosol size distribution. The models we selected as representative of these three approaches were CONFEMM (Tsang and Brock, 1983) for the continuous representation, ESMAP (Warren and Seinfeld, 1985) for the sectional representation, and AGRO (Whitby, 1981; Whitby, 1985) for the parameterized representation. For coagulation, ESMAP was applied with two different size resolutions, 12 and 39 sections, over the 0.001 μm to 10 μm size range.

These models were exercised to simulate diffusion-limited condensation of sulfate over 12 hours for atmospheric aerosol concentrations typical of clear, hazy, and urban conditions. CONFEMM provided an accurate solution of the condensation equation. The results are summarized here in Table 2-3. (The detailed results of this comparative model evaluation are described by Seigneur et al., 1986.) Figure 2-2 compares the different aerosol size distributions calculated after 12 hours for urban conditions.

TABLE 2-3. Comparison of model simulation results for condensation.

Model	Average Absolute Normalized Difference (percent) Clear Conditions	Hazy Conditions	Urban Conditions
CONFEMM		(Reference)	
ESMAP (39 sections)	4	12	1
ESMAP (12 sections)	13	35	4
AGRO	6	18	7

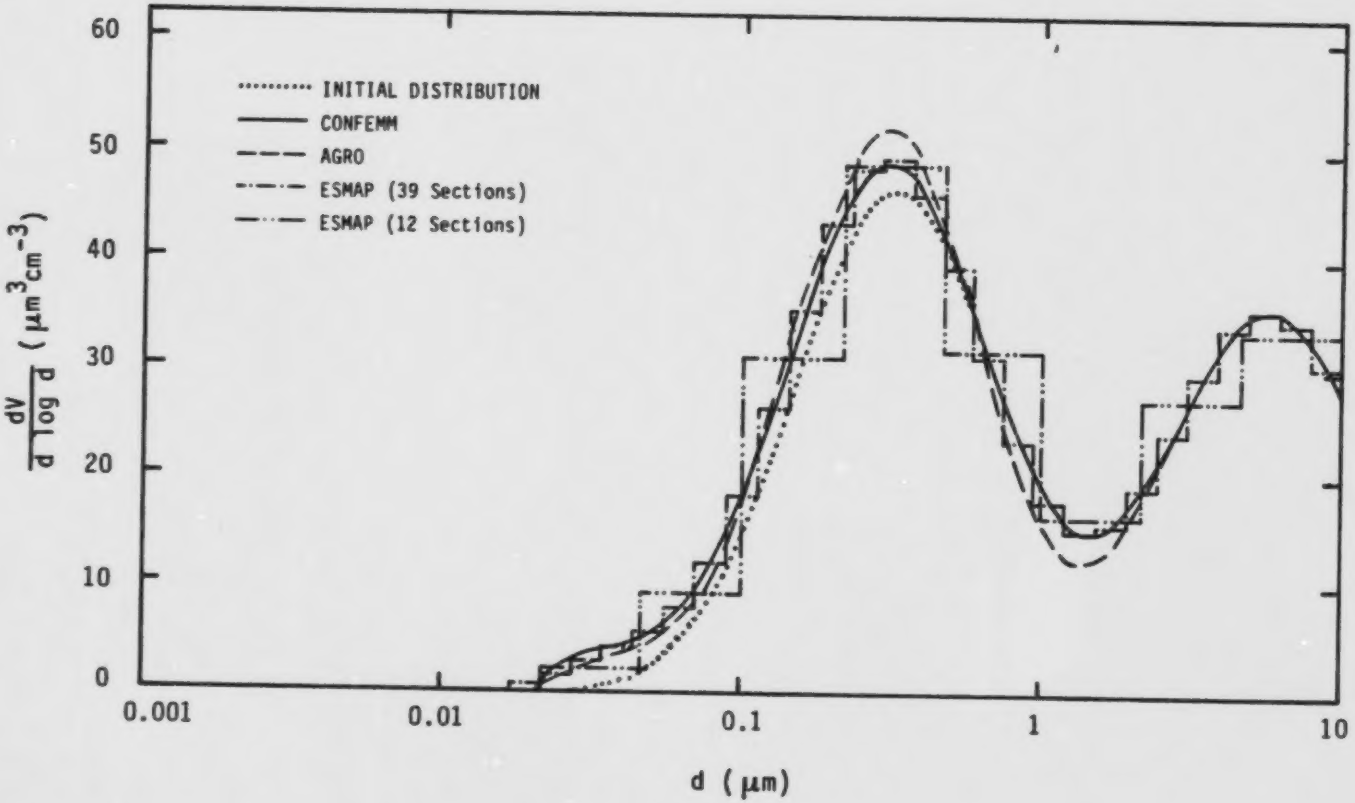

FIGURE 2-2. Simulation of aerosol condensation for urban conditions.

The computational times on a Prime 750 computer were as follows: AGRO required less than 1 CPUs, CONFEMM required about 150 CPUs, ESMAP with 12 sections required about 90 CPUs, and ESMAP with 39 sections required about 300 CPUs.

ESMAP requires a relatively large number of sections to minimize numerical diffusion. The performance of ESMAP with 39 sections is satisfactory for all cases, whereas with 12 sections it produces reasonable results when condensation occurs primarily on the accumulation mode, but poorer results when condensation also occurs on smaller aerosols to form a mode below 0.1 μm in addition to the accumulation mode. AGRO tends to overestimate the peak concentration of the accumulation mode, but it predicts the median diameter of the mode fairly well.

On the basis of these results, we selected the sectional representation with a size resolution of 12 sections over the size range of 0.001 μm to 10 μm to simulate aerosol dynamics. This approach provides a reasonable compromise between model accuracy and computational requirements for both coagulation and growth/shrinkage.

3 FORMULATION OF THE AEROSOL MODEL

INTRODUCTION

Aerosol concentration, size, and chemical composition are affected by many physical and chemical processes. These processes include advection, diffusion, coagulation, gas/aerosol conversion, thermodynamics, chemical kinetics, sedimentation, dry deposition on surfaces, and emissions of new aerosols. The evolution of the aerosol population (characterized by its concentration and chemical composition as a function of size) is governed by the general dynamic equation, which is expressed as follows (Friedlander, 1977):

$$\frac{\partial n_i}{\partial t} = - \nabla(n_i \cdot \underline{v}) + \nabla \underline{\underline{K}} \, \nabla n_i + \left[\frac{\partial n_i}{\partial t}\right]_{\text{growth}} + \left[\frac{\partial n_i}{\partial t}\right]_{\text{coagulation}} - \left[\frac{\partial n_i}{\partial t}\right]_{\text{removal}} + \left[\frac{\partial n_i}{\partial t}\right]_{\text{emission}} . \tag{3-1}$$

The term on the left side represents the evolution of the size-distributed number concentration of aerosol species i. The total aerosol number is then given by the following relationship:

$$N = \sum_{i=1}^{L} \int_0^{\infty} n_i \, d(d_p) \quad , \tag{3-2}$$

where L is the total number of aerosol chemical species, and d_p is the aerosol diameter.

The terms on the right side of Equation 1 represent (1) advection, where $\underline{v}$ is the mean wind field vector, (2) diffusion, where $\underline{\underline{K}}$ is the eddy diffusion coefficient tensor, (3) growth or shrinkage due to condensation of gases on the aerosols, evaporation of gases from the aerosols, changes in the aerosol density, and nucleation of new aerosols, (4) coagulation of aerosols, (5) removal of aerosols by sedimentation and surface dry deposition, and (6) emissions of primary aerosols.

The terms representing advection, diffusion, and emissions will be treated in the same way for both aerosols and gases in the EPA regional model; therefore we do not discuss them in this section. The other three terms--growth, coagulation, and removal--are specific to aerosols, and their treatment is discussed in more detail next.

These three terms constitute the aerosol module of the EPA regional particulate model. The aerosol population is assumed to consist of two categories: (1) fine aerosols of diameter less than 2.5 μm and (2) coarse aerosols of diameter greater than 2.5 μm. Fine aerosols are affected by coagulation, growth or shrinkage due to condensation, evaporation, density changes, and dry deposition; they are little affected by sedimentation. Coarse aerosols are not notably affected by coagulation, growth, or shrinkage; their concentrations are primarily influenced by sedimentation and dry deposition.

Fine aerosols are assumed to consist of three nonvolatile species--primary, sulfate, and organic aerosols--and three volatile species--nitrate, ammonium, and water. Gases such as SO_2, O_2, O_3, and H_2O_2 are allowed to dissolve in the liquid film surrounding the aerosol. This provides the possibility of sulfate formation by chemical reaction in the aerosol. Primary aerosols are affected by coagulation, emission, and removal processes. Sulfate aerosols are affected by coagulation, condensation of sulfuric acid on the aerosol (this process is assumed to be irreversible because of the low vapor pressure of sulfuric acid), new sulfate aerosol formation following nucleation of sulfuric acid, removal processes, chemical reactions in the aerosol, and eventually emissions. Organic aerosols are affected by coagulation and condensation of organic products. Nitrate, ammonium, and water are affected by the thermodynamic equilibrium between the aerosol and the ambient atmosphere, and they are also affected by aerosol removal processes. Coagulation does not directly affect volatile species aerosol concentrations since these are calculated through thermodynamic equilibrium.

Coarse aerosols are assumed to consist of primary aerosols with a fraction of NaCl. These aerosols are affected solely by emissions, sedimentation, and dry deposition. Displacement of hydrogen halide from natural salts (e.g., NaCl, PbBrCl) by HNO_3 and H_2SO_4 has been reported to occur in atmospheric aerosols (e.g., Harrison and Sturges, 1984). To account for this phenomenon, the model allows the species NaCl from the coarse aerosol to react with gaseous HNO_3 or H_2SO_4 through a diffusion-limited process and to yield coarse nitrate aerosol. We describe the treatment of these aerosol processes in detail next.

MATHEMATICAL FORMULATION OF THE AEROSOL MODEL

The sectional representation of an aerosol size distribution allows an efficient treatment of aerosol dynamic processes, equilibrium thermodynamics, and chemical kinetics. We present the equations that govern a model of the sectional aerosol size distribution.

Let the aerosol size distribution be represented by a series of step functions q_ℓ (sectional representation), such that the aerosol mass in section ℓ (for aerosol diameters between $d_{\ell-1}$ and d_ℓ) is defined as Q_ℓ

$$Q_\ell = \int_{x_{\ell-1}}^{x_\ell} q_\ell \, dx, \qquad \ell = 1, \ldots, M \tag{3-3}$$

where

$x = \log(d_p)$,

d_p = aerosol diameter, and

M = the total number of sections.

The function q_ℓ is constant in the size interval $x_{\ell-1}$ to x_ℓ.

$$Q_\ell = q_\ell \, (x_\ell - x_{\ell-1}), \qquad \ell = 1, \ldots, M \tag{3-4}$$

Let the aerosol be constituted of a solid core of primary aerosol, secondary sulfate and organic aerosol that condenses on the primary aerosol, and chemical species (water, ammonium, and nitrate) that are at thermodynamic equilibrium between the aerosol and the ambient gas phase. Let $Q(\ell, 1)$ be the sulfate aerosol, and $Q(\ell, 2)$ be the sum of primary and organic aerosols. It is necessary to differentiate sulfate aerosols from primary and organic aerosols since their size distributions are likely to be different, and the concentrations of nitrate, ammonium, and water in the aerosol are directly related to the sulfate aerosol concentrations. It is possible to lump primary and organic aerosols since both are assumed to be chemically inert.

The concentrations of water, ammonium, and nitrate in an aerosol section depend on relative humidity, temperature, and sulfate concentrations and are calculated assuming thermodynamic equilibrium. If the Kelvin effect (the effect of surface curvature on gas pressure over the aerosol surface) is taken into account, the aerosol chemical composition will be a function of its size. Let the total secondary aerosol mass be defined as follows:

$$Q(\ell,\ s) = \lambda(\ell)\ Q(\ell,\ 1), \qquad \ell = 1,\ \ldots,\ M \tag{3-5}$$

where s refers to secondary inorganic aerosol (i.e., sulfate, nitrate, ammonium, and water; organic aerosols are considered in $Q(\ell,\ 2)$). The parameter $\lambda(\ell)$ depends on the gas-phase concentrations of ammonia and nitric acid, aerosol sulfate concentration, relative humidity, and temperature. This parameter also depends on the aerosol size if the Kelvin effect is taken into account.

If one chooses to neglect the Kelvin effect, the secondary aerosol concentration is written in a simplified form as follows:

$$Q(\ell,\ s) = \lambda\ Q(\ell,\ 1) \qquad \ell = 1,\ \ldots,\ M \tag{3-6}$$

where λ is independent of the section size.

The total aerosol concentration is the sum of inorganic secondary aerosol, organic secondary aerosol, and primary aerosol and is given by the following relationship:

$$Q_\ell = \lambda(\ell)\ Q(\ell,\ 1) + Q(\ell,\ 2) \qquad \ell = 1,\ \ldots,\ M \tag{3-7}$$

This aerosol size distribution will change as a result of coagulation, new aerosol formation, condensation of secondary sulfate, changes in the thermodynamic equilibrium, emissions of primary aerosols (and eventually of sulfate aerosols), and removal of aerosols by dry deposition and sedimentation. The sectional dynamic equations are then written as follows:

$$\begin{aligned}
\frac{dQ(\ell,k)}{dt} = {} & \sum_{i=1}^{\ell-1} {}^{1}\bar{\beta}_{i,\ell}\ Q(\ell-1,\ k)\ Q_i - \sum_{i=1}^{\ell-1} {}^{2a}\bar{\beta}_{i,\ell}\ Q_i\ Q(\ell,\ k) \\
& + \sum_{i=1}^{\ell-1} {}^{2b}\bar{\beta}_{i,\ell}\ Q_\ell\ Q(i,\ k) - \frac{1}{2}\ {}^{3}\bar{\beta}_{\ell}\ Q_\ell\ Q(\ell,\ k) \\
& - Q(\ell,\ k) \sum_{i=\ell+1}^{M} {}^{4}\bar{\beta}_{i,\ell}\ Q_i \\
& + {}^{1}\bar{G}_{s,\ell}\ Q_\ell\ \delta(k-1) - {}^{2}\bar{G}_{s,\ell}\ Q(\ell,\ k) + {}^{2}\bar{G}_{s,\ell-1}\ Q(\ell-1,\ k)
\end{aligned}$$

$$
\begin{aligned}
&+ {}^{1}\overline{G}_{o,\ell}\, Q_\ell\, \delta(k - 2) - {}^{2}\overline{G}_{o,\ell}\, Q(\ell, k) + {}^{2}\overline{G}_{o,\ell-1}\, Q(\ell - 1, k) \\
&- \overline{E}_\ell\, Q(\ell, k) + \overline{E}_{\ell-1}\, Q(\ell - 1, k) \\
&- \overline{H}_\ell\, Q(\ell, k) + \overline{H}_{\ell+1}\, Q(\ell + 1, k) \\
&+ {}^{1}\overline{F}_\ell\, Q_\ell\, \delta(k - 1) - {}^{2}\overline{F}_\ell\, Q(\ell, k) + {}^{2}\overline{F}_{\ell-1}\, Q(\ell - 1, k) \\
&+ \overline{S}_{\ell,k} - \overline{R}_{\ell,k}\, Q(\ell, k) \\
&+ \overline{J}_{s,\ell}\, \delta(\ell - 1)\, \delta(k - 1) \\
&+ \overline{J}_{o,\ell}\, \delta(\ell - 1)\, \delta(k - 2)
\end{aligned}
$$

$$\ell = 1, \ldots, M, \; k = 1, 2 \qquad (3\text{-}8)$$

where

${}^{1}\overline{\beta}_{i,\ell}$, ${}^{2a}\overline{\beta}_{i,\ell}$, ${}^{2b}\overline{\beta}_{i,\ell}$, ${}^{3}\overline{\beta}_{\ell}$, and ${}^{4}\overline{\beta}_{i,\ell}$ = sectional coagulation coefficients,

δ = the Kronecker index,

${}^{1}\overline{G}_{s,\ell}$ and ${}^{1}\overline{G}_{o,\ell}$ = the intrasectional growth term due to sulfate condensation and organic species condensation, respectively

${}^2\overline{G}_{s,\ell}$ and ${}^2\overline{G}_{o,\ell}$ = the intersectional growth terms due to sulfate condensation and organic species condensation, respectively.

$\overline{E}_\ell$ = the intersectional growth term due to the positive change $d\lambda/dt$ in chemical concentrations of equilibrium species (ammonium, nitrate, water),

$\overline{H}_\ell$ = the intersectional shrinkage term due to the negative change $d\lambda/dt$ in chemical concentrations of equilibrium species (ammonium, nitrate, water),

${}^1\overline{F}_\ell$ = the intrasectional growth term due to sulfate formation by aerosol chemical reaction,

${}^2\overline{F}_\ell$ = the intersectional growth term due to sulfate formation by aerosol chemical reaction,

$\overline{S}_{\ell,k}$ = the source rate,

$\overline{R}_{\ell,k}$ = the removal rate, and

$\overline{J}_{s,1}$ and $\overline{J}_{o,1}$ = the new aerosol formation rate for sulfate and organic aerosols, respectively.

The total change in aerosol is given by the following equation:

$$\frac{dQ_\ell}{dt} = \lambda(\ell)\,\frac{dQ(\ell,\,1)}{dt} + \frac{dQ(\ell,\,2)}{dt} + Q(\ell,\,1)\,\frac{d\lambda(\ell)}{dt} \qquad (3\text{-}9)$$

$$\ell = 1,\ \ldots,\ M$$

The change in chemical composition $\frac{d\lambda}{dt}$ must be calculated by a thermodynamic equilibrium model.

These different components are described in detail next. A schematic overview of the procedure used to integrate Equation 8 is presented in Figure 3-1.

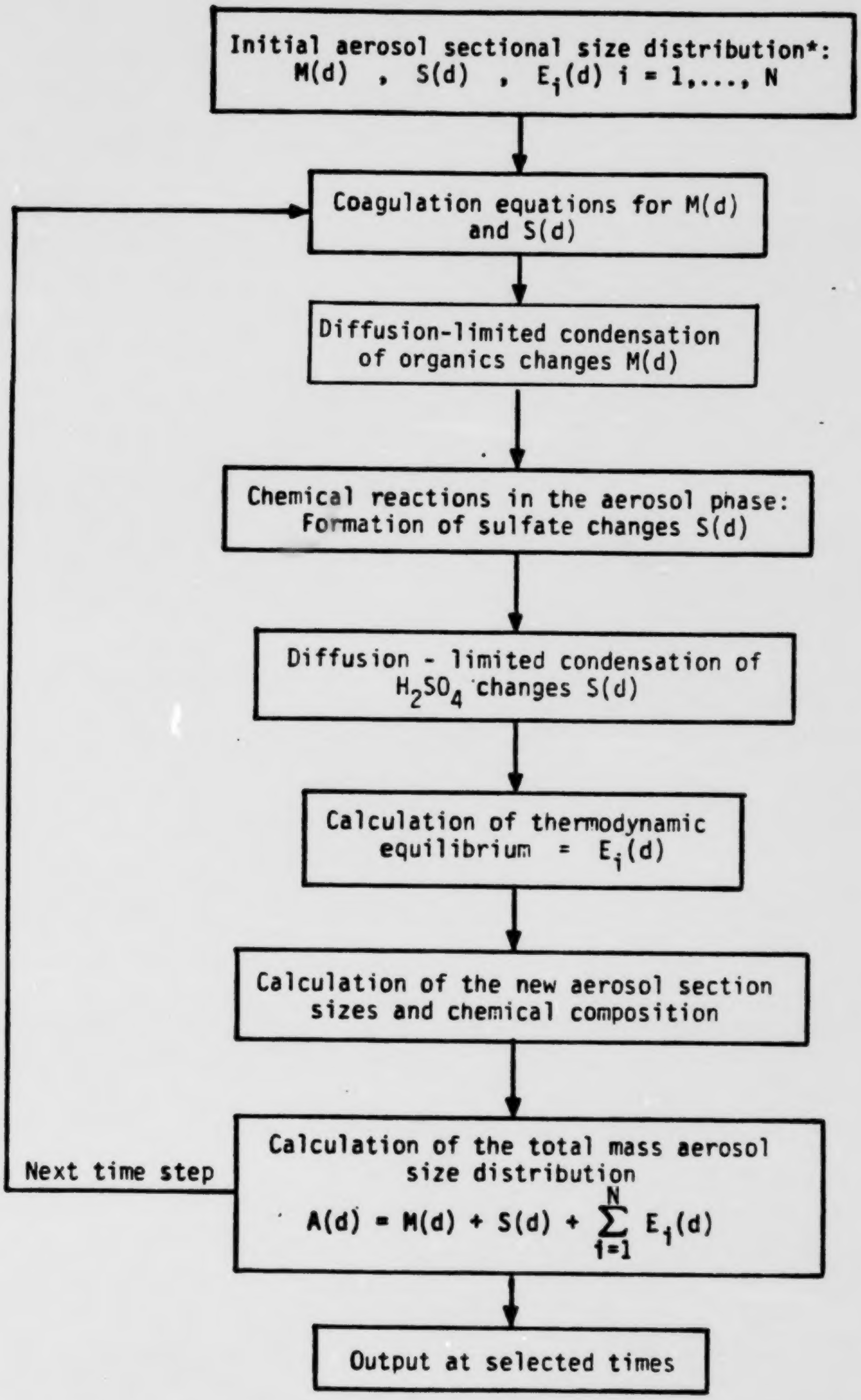
Initial aerosol sectional size distribution*: M(d) , S(d) , E_i(d) i = 1,..., N
Coagulation equations for M(d) and S(d)
Diffusion-limited condensation of organics changes M(d)
Chemical reactions in the aerosol phase: Formation of sulfate changes S(d)
Diffusion - limited condensation of H2SO4 changes S(d)
Calculation of thermodynamic equilibrium = E_i(d)
Calculation of the new aerosol section sizes and chemical composition
Calculation of the total mass aerosol size distribution
A(d) = M(d) + S(d) + Σ_{i=1}^{N} E_i(d)
Next time step
Output at selected times

* $M(d)$ = Size distribution of solid core organic aerosol and metals.
$S(d)$ = Sulfate size distribution.
$E_i(d)$ = size distribution of species at equilibrium with the gas phase.
$A(d)$ = size distribution of total aerosol mass.

86026

FIGURE 3-1. Procedure flow chart for the aerosol model.

COAGULATION

The sectional coagulation coefficients have been calculated by Gelbard and Seinfeld (1980). These coefficients, which are presented in Table 3-1, are a function of the coagulation coefficient β, which depends on the sectional size (i.e., $x_{\ell-1}$ and x_ℓ, the section size boundaries). The form of this coagulation coefficient depends on the coagulation process, i.e., Brownian, turbulent, or gravitational motion. For the purpose of this study, we consider coagulation by Brownian motion since it is the most relevant to coagulation of atmospheric fine aerosols. The aerosol coagulation coefficient used in this study is the Fuchs coefficient, which can be expressed as follows for the coagulation of two aerosols of volumes v_i and v_j (Fuchs, 1964; Sitarski and Seinfeld, 1977):

$$\beta(v_i, v_j) = 4\pi(D_i + D_j)(r_i + r_j)\left(\frac{r_i + r_j}{r_i + r_j + g_{ij}} + \frac{4(D_i + D_j)}{(\overline{C}_i^2 + \overline{C}_j^2)^{1/2}(r_i + r_j)}\right)^{-1} \tag{3-10}$$

where

$r_i = \left(\frac{3v_i}{4\pi}\right)^{1/3}$, the radius of the coagulating aerosol

$D_i = \frac{kT}{6\pi r_i \eta}\{1 + Kn_i[1.257 + 0.4\exp(-1.1\, Kn_i^{-1})]\}$, the aerosol diffusion coefficient

$g_{ij} = (g_i^2 + g_j^2)^{1/2}$

$g_i = \frac{1}{6\, r_i\lambda_i}\left[(2\, r_i + \lambda_i)^3 - (4\, r_i^2 + \lambda_i^2)^{3/2}\right] - 2\, r_i$

$\lambda_i = 8\, D_i/(\pi\, \overline{C}_i)$; the mean free path

$\overline{C}_i = [8\, kT/(\pi\, m_i)]^{1/2}$; the mean thermal velocity

TABLE 3-1. Sectional coagulation coefficients with geometric constraint ($v_{i+1} \geq 2v_i$, $i = 0, 1, 2, \ldots, M - 1$).

Symbol	Remarks	Coefficient*
$^{1}\bar{\beta}_{i,\,\ell}$	$i < \ell - 1$ $j < \ell - 1$	0
$^{1}\bar{\beta}_{i,\,\ell}$	$1 < \ell \leq M$ $i < \ell - 1$	$\int_{x_{i=1}}^{x_i} \int_{f(v_{\ell-1}-v)}^{x_{\ell-1}} \frac{u\ \beta(u,v)}{uv(x_i - x_{i-1})(x_{\ell-1} - x_{\ell-2})}\, dydx$
	$1 < \ell \leq M$ $i = \ell - 1$	$\int_{x_{i-1}}^{f(v_i - v_{i-1})} \int_{f(v_{\ell-1}-v)}^{x_{\ell-1}} \frac{u\ \beta(u,v)}{uv(x_{\ell-1} - x_{\ell-2})^2}\, dydx + \int_{f(v_i-v_{i-\ell})}^{x_i} \int_{x_{\ell-2}}^{x_{\ell-1}} \frac{u\ \beta(u,v)}{uv(x_{\ell-1} - x_{\ell-2})^2}\, dydx$
$^{1}\bar{\beta}_{\ell-1,\,\ell}$	$1 < \ell \leq M$ $i < \ell - 1$	$\int_{x_{i-\ell}}^{x_\ell} \int_{f(v_{\ell-1}-v)}^{x_{\ell-1}} \frac{v\ \beta(u,v)}{uv(x_i - x_{i-1})(x_{\ell-1} - x_{\ell-2})}\, dydx$
$^{2a}\bar{\beta}_{i,\,\ell}$	$1 < \ell \leq M$ $1 \leq i < \ell$	$\int_{x_{i-1}}^{x_i} \int_{f(v_\ell-v)}^{x_i} \frac{u\ \beta(u,v)}{uv(x_i - x_{i-1})(x_\ell - x_{\ell-1})}\, dydx$
$^{2b}\bar{\beta}_{i,\,\ell}$	$1 < \ell \leq M$ $1 \leq i < \ell$	$\int_{x_{i-\ell}}^{x_i} \int_{x_{\ell-1}}^{f(v_\ell-v)} \frac{v\ \beta(u,v)}{uv(x_i - x_{i-1})(x_\ell - x_{\ell-1})}\, dydx$
$^{3}\bar{\beta}_{\ell}$	$1 \leq \ell \leq M$	$\int_{x_{\ell-1}}^{f(v_\ell-v_{\ell-1})} \int_{f(v_\ell-v)}^{x_\ell} \frac{(u + v)\beta(u,v)}{uv(x_\ell - x_{\ell-1})^2}\, dydx + \int_{f(v_\ell-v_{\ell-1})}^{x_\ell} \int_{x_{\ell-1}}^{x_\ell} \frac{(u + v)\beta(u,v)}{uv(x_\ell - x_{\ell-1})^2}\, dydx$
$^{4}\bar{\beta}_{i,\,\ell}$	$1 \leq \ell < M$ $1 < i \leq M$	$\int_{x_{\ell-1}}^{x_\ell} \int_{x_{\ell-1}}^{x_\ell} \frac{u\ \beta(u,v)}{uv(x_i - x_{i-1})(x_\ell - x_{\ell-1})}\, dydx$

---

* $x_i = f(v_i)$; $u = f^{-1}(y)$; $v = f^{-1}(x)$; x_i, x and y are logarithms of aerosol diameters; v_i, u, and v are aerosol volumes.

m_i = aerosol mass

k = the Boltzmann constant

T = the absolute temperature

η = the background gas viscosity

Kn_i = the Knudsen number that is equal to λ/r_i.

The values of this coagulation coefficient are presented in Figure 3-2 for an absolute temperature of 298 K, at a pressure of 1 atm.

CONDENSATION/EVAPORATION

The sectional condensation coefficients have been calculated by Gelbard and Seinfeld (1980) and Seigneur (1982). Their initial derivation was based on a first-order approximation of the condensation equation for a sectional representation. Recently, Warren and Seinfeld (1985) placed the additional constraint that the aerosol number concentration be conserved during condensation. The resulting sectional condensation coefficients are presented in Table 3-2.

The condensation growth law $\phi(v) = dv/dt$ depends on the condensing vapor and aerosol size. It is represented by the Fuchs-Sutugin formula (Fuchs and Sutugin, 1971):

$$\frac{dv}{dt} = \frac{4\pi r D}{1 + \frac{1.333\ Kn + 0.71}{1 + Kn}\ Kn}\ v_m \left(P - P_s \exp\left(\frac{2\sigma v_m}{rkT}\right)\right) , \qquad (3\text{-}11)$$

where

r = the aerosol radius;

D = the diffusion coefficient of the condensing vapor;

Kn = the Knudsen number equal to λ/r;

λ = the mean free path of the condensing vapor;

2

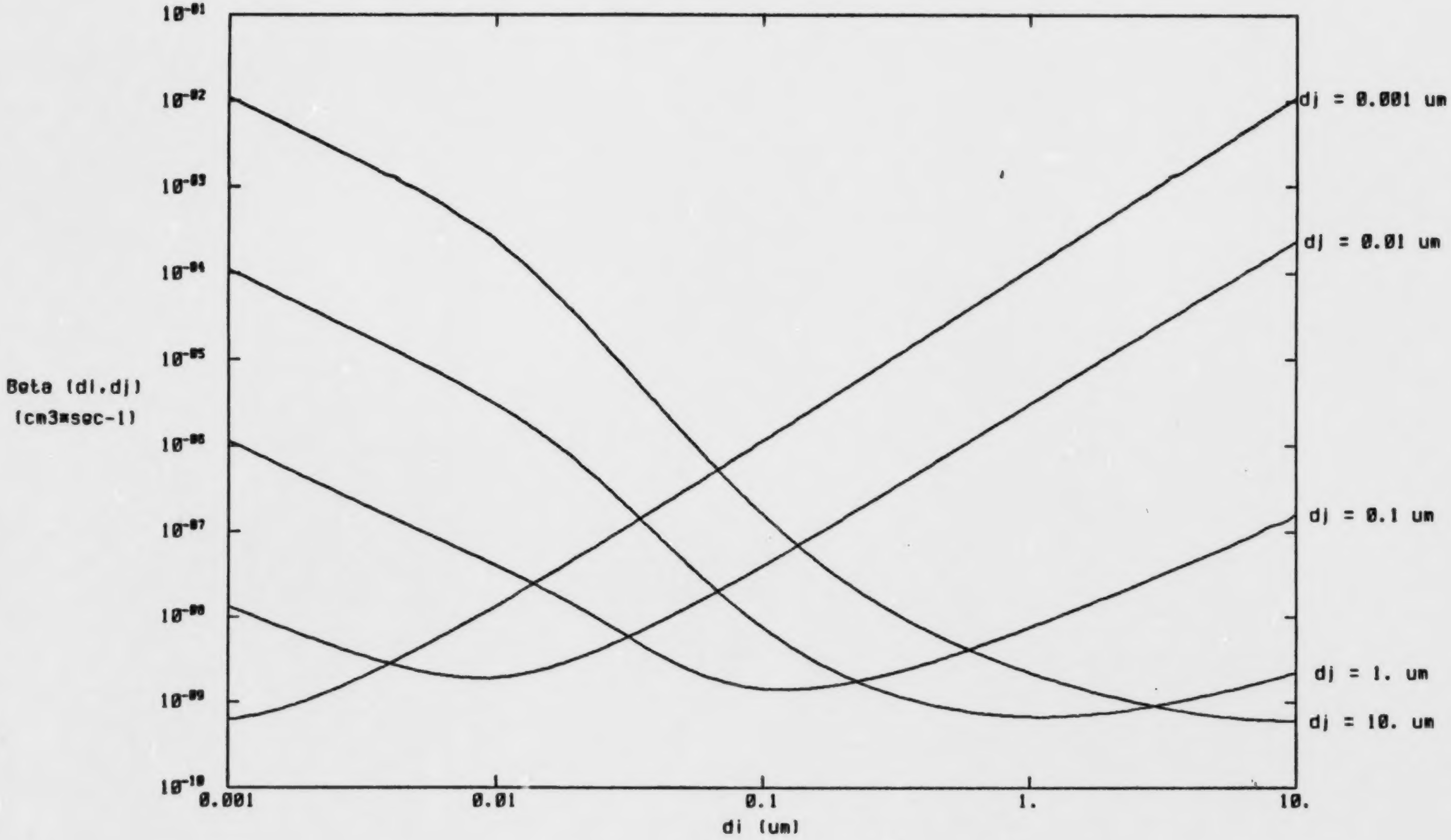

FIGURE 3-2. Brownian coagulation coefficient (Beta) for aerosols of diameters di and dj. Temperature = 298 K, Pressure = 1 atm.

TABLE 3-2. Sectional condensational growth coefficients with aerosol number conservation constraint.

Symbol	Remarks	Coefficient*
${}^{1}\bar{G}_{\ell}$	$1 < \ell < M$	$\int_{x_{\ell-1}}^{x_{\ell}} \frac{\phi(x)}{v(x_{\ell} - x_{\ell-1})} dx$
${}^{2}\bar{G}_{\ell}$	$1 < \ell < M$	$\frac{1}{1 - \exp\left(-\frac{1}{2} \ln\left(\frac{v_{\ell+1}}{v_{\ell-1}}\right)\right)} \int_{x_{\ell-1}}^{x_{\ell}} \frac{\phi(x)}{v(x_{\ell} - x_{\ell-1})} dx$

---

* $x_{\ell} = f(v_{\ell})$, where x is the logarithm of the aerosol diameter, v is the aerosol volume, and $\phi(x)$ is the aerosol growth rate.

v_m = the molecular volume of the condensing vapor;

P and P_s = the ambient and equilibrium vapor pressure of the condensing vapor, respectively, and

the exponential term = the correlation of the Kelvin effect, where σ is the surface tension of the condensed species.

The values of the growth law are shown in Figure 3-3 for sulfuric acid, with a total ambient pressure of 1 atm and an absolute temperature of 298 K. Sulfuric acid and organic condensible products are the two species that are treated via this diffusion-limited condensation process.

In this model the condensation is assumed to be irreversible. Sulfuric acid has a very low vapor pressure and can therefore be assumed to be transferred entirely from the gas phase to the aerosol phase. Organic species that condense on aerosols are also assumed to have a low vapor pressure. All sulfuric acid and organic products may not condense on existing aerosols, but formation of new aerosols via nucleation may occur. This subject is treated in the next section.

Other condensible species such as nitric acid, ammonia, and water have higher saturation vapor pressures. Therefore, they are distributed between the gas phase and the aerosol phase and are treated according to the thermodynamic equilibrium relationship. This treatment is described in a later section.

NEW AEROSOL FORMATION

Because of their low saturation vapor pressure, sulfuric acid and organic condensible species may nucleate to form new aerosols. The mathematical treatment of nucleation of new aerosols has been simulated according to the classical theory of nucleation (e.g., Warren and Seinfeld, 1985). However, this classical theory requires simulating the aerosol size distribution of aerosols as small as 10^{-3} μm in diameter. Such aerosol sizes are not measured in the atmosphere, where generally, reliable measurements only extend to sizes as small as 10^{-2} μm. Therefore, it appears appropriate to use an approach that will focus instead on the rate of aerosol formation at the detectable aerosol size of 10^{-2} μm in diameter.

A theory developed by McMurry (1983) provides the rate of new aerosol formation at a lower given aerosol size in the presence of other existing aerosols. The gas-to-aerosol conversion of sulfuric acid and condensible organics may therefore be distributed between condensation and new aerosol formation. The theory of McMurry is based on several usual assumptions

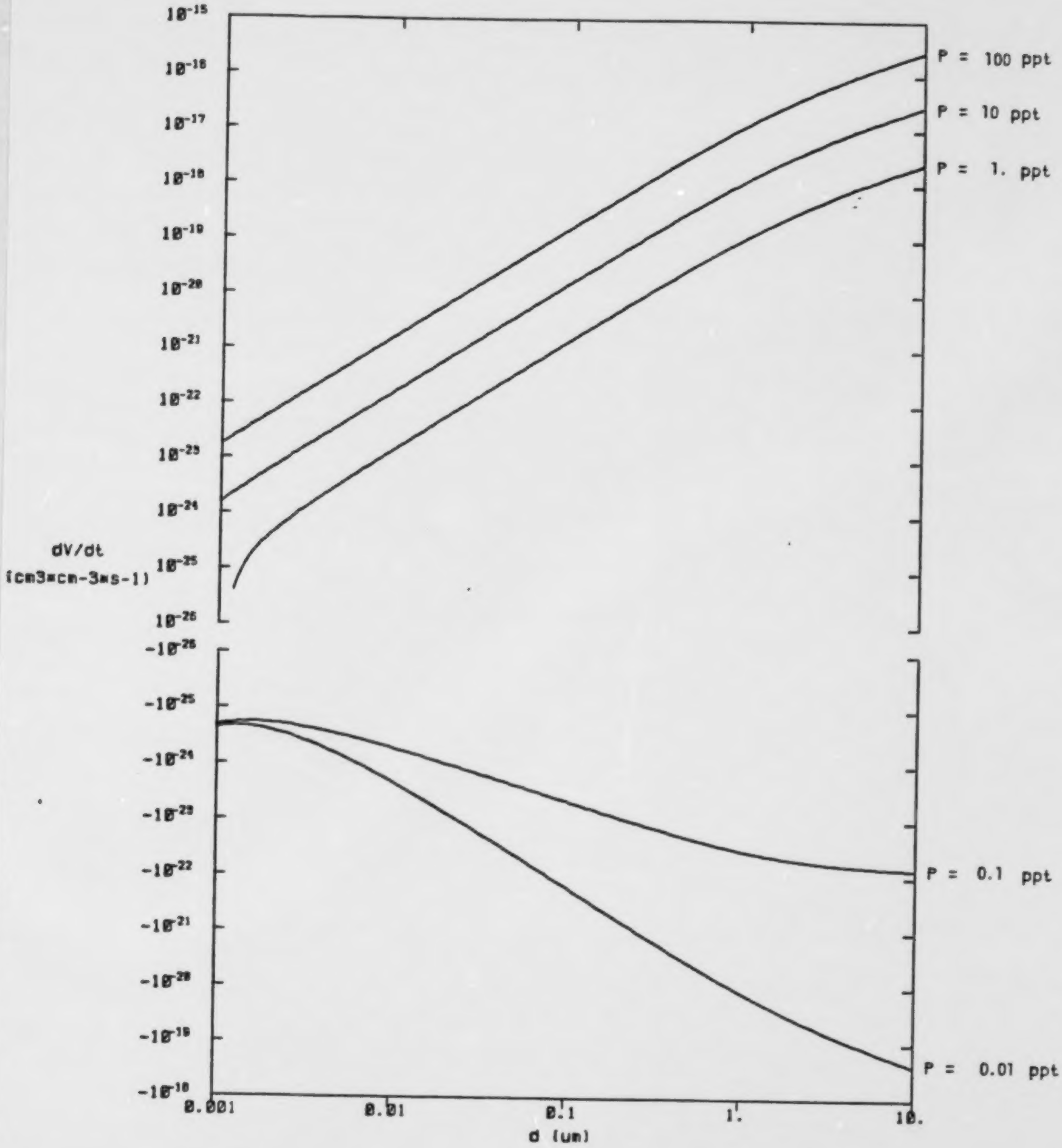

FIGURE 3-3. Diffusion-limited condensation coefficient for a vapor pressure of P and an aerosol diameter of d.

86026
84185
84088

such as pseudo-steady-state of the condensible species formation and slow re-evaporation rate of the condensing molecules. It was developed in a general form (i.e., unsteady-state rate of new aerosol formation) to calculate the rate of new aerosol formation at a given aerosol size (e.g., 10^{-2} μm in diameter), given the rate of condensible vapor formation and the surface area of the existing aerosols. In our model, we used the McMurry solution for steady-state aerosol formation rate. This steady-state assumption is appropriately applied to the atmosphere, where rates of sulfuric acid or condensible organics formation and aerosol concentration are fairly homogeneous, but it may fail near emission stacks, where concentration gradients of gases and aerosols may be high.

The aerosol formation rates are presented in Figure 3-4. The sectional new-aerosol formation coefficient has been calculated by Seigneur (1982) and is given by the following formula:

$$\bar{J}_1 = \gamma R v_m \tag{3-12}$$

where

γ = the ratio of new aerosol formation rate to gas-to-aerosol formation rate,

R = the rate of sulfuric acid or condensible organics formation in the gas phase, and

v_m = the volume of condensing sulfate or organic molecules.

THERMODYNAMIC EQUILIBRIUM

Thermodynamic equilibrium calculations are used to obtain the chemical composition of the aerosol. Since sulfate has a very low saturation vapor pressure, it is assumed to be totally in the aerosol phase. Gases such as nitric acid, ammonia, and water vapor may condense to lead to nitrate, ammonium, and liquid-coated aerosols. Such distributions between the gas phase and the aerosol phase are governed by thermodynamic equilibrium at the aerosol surface and by diffusion in the gas and aerosol phases. We assume that gas-phase concentrations change slowly enough so that diffusion will not be the rate-limiting process, and we focus solely on the thermodynamic equilibrium calculations. The chemical composition and phase distribution (solid phase and liquid phase) of the aerosol are also regulated by thermodynamic constraints. On the basis of the results of our review of aerosol thermodynamic models, we selected MARS for simulating the equilibrium of sulfate, nitrate, and ammonium aerosols.

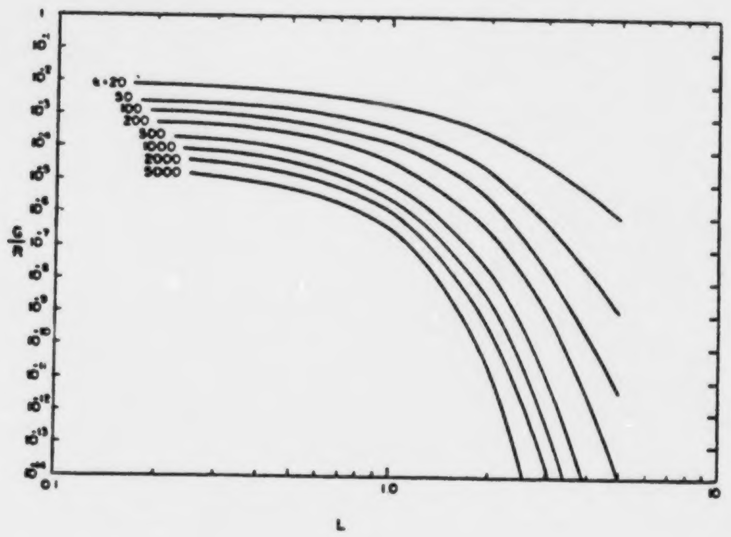

FIGURE 3-4. Steady-state dimensionless new particle formation rates as a function of the total dimensionless sink term, L. The various curves show rates at which particles grow into or past the indicated particle sizes, where k represents the number of condensing monomers. (Source: McMurry, 1983)

The chemical species that are included in the thermodynamic equilibrium calculations are listed in Table 3-3. Our analysis of the thermodynamic equilibrium considers the major chemical compounds containing sulfate, nitrate, ammonium, and water. These compounds include gas phase species $H_2SO_4(g)$, $HNO_3(g)$, $NH_3(g)$ and $H_2O(g)$; liquid-phase species $HSO_4^-(aq)$, $SO_4^{2-}(aq)$, $NO_3^-(aq)$, $H_2O(\ell)$, $H^+(aq)$; and solid phase species $(NH_4)_2SO_4(s)$, $NH_4HSO_4(s)$, $(NH_4)_3H(SO_4)_2(s)$, and $NH_4NO_3(s)$. The liquid-phase species $H_2SO_4(aq)$ and $HNO_3(aq)$ are neglected; this is a fair assumption at pH values above 1 since these are strong acids. The $OH^-(aq)$ ions are not considered explicitly since their concentration can be directly deduced from the $H^+(aq)$ concentration. The solid-state species $(NH_4)_2SO_4 \cdot 2NH_4NO_3$ and $(NH_4)_2SO_4 \cdot 3NH_4NO_3$ are not considered explicitly in this thermodynamic model and are treated instead as the corresponding stoichiometric combination of the individual salts $(NH_4)_2SO_4$ and NH_4NO_3. This approach is required since thermodynamic data for the sulfate-nitrate combined salts are not available. A detailed description of the MARS calculations is provided in Appendix B (Saxena et al., 1986).

Changes in the chemical composition of the aerosol occur due to changes in the gas-phase concentrations of HNO_3, NH_3, and H_2O (relative humidity). The aerosol phase concentration of sulfate (following gas-phase formation of H_2SO_4 and subsequent condensation of aerosol as well as formation of sulfate in the aerosol) and the ambient temperature also lead to changes in the aerosol chemical composition, density, and volume, i.e., growth or shrinkage. This growth/shrinkage of aerosols results in a modification of the aerosol size distribution, which must be reflected in the general dynamic equation. The sectional growth/shrinkage coefficients $\bar{E}_\ell$ account for this effect. The terms E_ℓ represent the coupling between the aerosol dynamics component and the equilibrium thermodynamics component, and are expressed mathematically to account for aerosol mass and number conservation. These terms are given in Table 3-4.

SECONDARY ORGANIC AEROSOL FORMATION

To date, no general chemical kinetic mechanism has been developed to treat the formation of secondary organic aerosols. Therefore, for this study, we developed a simple organic aerosol model that is based on the experimental data currently available. Clearly, there is a paucity of data, and large uncertainties necessarily remain in the formulation of such a model. However, the treatment of organic aerosol formation proposed here should provide reasonable estimates of the mass of organic aerosol formed under typical atmospheric conditions.

TABLE 3-3. Treatment of the aerosol chemical composition. For a given relative humidity and ratio of total ammonia to total sulfur concentrations, the model calculates the chemical composition of the aerosol from the possible chemical species listed in the matrix.

<table>
<tr><th rowspan="2">Relative Humidity</th><th colspan="4">Ratio of Total Ammonia to Total Sulfate</th></tr>
<tr><th>0</th><th>1</th><th>1.5</th><th>2</th></tr>
<tr><td>100 percent</td><td rowspan="4">$NH_4^+(aq)$
$SO_4^{2-}(aq)$
$HSO_4^-(aq)$
$H^+(aq)$
$H_2O(\ell)$</td><td colspan="2">$NH_4^+(aq)$
$SO_4^{2-}(aq)$
$HSO_4^-(aq)$
$H^+(aq)$
$H_2O(\ell)$</td><td>$NH_4^+(aq)$
$SO_4^{2-}(aq)$
$NO_3^-(aq)$
$H^+(aq)$
$H_2O(\ell)$</td></tr>
<tr><td>80 percent</td><td>$NH_4^+(aq)$, $SO_4^{2-}(aq)$
$HSO_4^-(aq)$, $H^+(aq)$
$H_2O(\ell)$, $(NH_4)_2SO_4(c)$</td><td>$NH_4^+(aq)$, $SO_4^{2-}(aq)$
$HSO_4^-(aq)$, $H^+(aq)$
$H_2O(\ell)$, $(NH_4)_2SO_4(c)$</td><td rowspan="2">$NH_4^+(aq)$
$SO_4^{2-}(aq)$
$NO_3^-(aq)$
$H^+(aq)$
$H_2O(\ell)$
$(NH_4)_2SO_4(c)$</td></tr>
<tr><td>69 percent</td><td rowspan="2">$NH_4^+(aq)$
$SO_4^{2-}(aq)$
$HSO_4^-(aq)$
$H^+(aq)$
$H_2O(\ell)$
$(NH_4)_3H(SO_4)_2(c)$</td><td rowspan="4">$(NH_4)_2SO_4(c)$
$(NH_4)_3(SO_4)_2(c)$</td></tr>
<tr><td>62 percent</td><td rowspan="3">$(NH_4)_2SO_4(c)$
$NH_4NO_3(c)$</td></tr>
<tr><td>40 percent</td><td rowspan="2">$NH_4^+(aq)$
$SO_4^{2-}(aq)$
$HSO_4^-(aq)$
$H^+(aq)$
$H_2O(\ell)$
$NH_4HSO_4(c)$</td><td rowspan="2">$(NH_4)_3H(SO_4)_2(c)$
$NH_4HSO_4(c)$</td></tr>
<tr><td>0 percent</td></tr>
</table>

TABLE 3-4. Sectional coefficients for aerosol growth/shrinkage due to changes in the aerosol chemical composition.

Symbol	Remarks	Coefficient
$\overline{E}_\ell$	$1 \le \ell \le M$ $d\lambda/dt > 0$	$\dfrac{1}{1 - \exp\left(-\frac{1}{2} \ln\left(\frac{v_{\ell+1}}{v_{\ell-1}}\right)\right)} \; \dfrac{Q(\ell, 1)}{Q_\ell} \; \dfrac{d\lambda}{dt}$
$\overline{H}_\ell$	$1 \le \ell \le M$ $d\lambda/dt < 0$	$\dfrac{-1}{1 - \exp\left(-\frac{1}{2} \ln\left(\frac{v_{\ell+1}}{v_{\ell-1}}\right)\right)} \; \dfrac{Q(\ell, 1)}{Q_\ell} \; \dfrac{d\lambda}{dt}$

where $\frac{d\lambda}{dt}$ is the change in the aerosol chemical composition, v is the aerosol volume, $Q(\ell, 1)$ is the sulfate aerosol mass in section ℓ, and Q_ℓ is the total aerosol mass in section ℓ.

Our knowledge of the chemistry of organic aerosol formation is still insufficient to develop a detailed chemical kinetic mechanism. Consequently, we opted for the development of a lumped mechanism in which the stoichiometric coefficients are derived from smog chamber experiments. The development of this mechanism is described in Appendix D. The chemical reactions involved in the mechanism are as follows:

$$\mathrm{TOL} + \mathrm{OH} \rightarrow 206\ \mathrm{AERO}$$

$$\mathrm{XYL} + \mathrm{OH} \rightarrow 68\ \mathrm{AERO}$$

$$\mathrm{OLE} + \mathrm{OH} \rightarrow 42\ \mathrm{AERO}$$

$$\mathrm{OLE} + \mathrm{O_3} \rightarrow 56\ \mathrm{AERO}$$

$$\mathrm{ISOP} + \mathrm{O_3} \rightarrow 46\ \mathrm{AERO}$$

where κ is the fraction of olefins leading to condensible products (i.e., long chain, cyclic, and diolefins); TOL, XYL, OLE, and ISOP are toluene, xylenes, olefinic bonds, and isoprene according to the carbon-bond formulation of gas-phase chemistry (expressed in ppm); and AERO is the organic aerosol product (expressed in $\mu g/m^3$).

Because of large uncertainties that exist in the value of the saturation vapor pressure of organic condensible species and because of the additional computational cost that would be involved in the treatment of organics as volatile/condensible species, we assume that organic species condensation is irreversible. (The treatment of volatile organic species would require the treatment of additional aerosol species.) In our model, organic aerosols are lumped with primary aerosol. This approach does not provide the size distribution of organic aerosols; however, its computational costs are much less than those incurred when organic and primary aerosols are treated independently.

AEROSOL CHEMICAL KINETICS

Chemical reactions may occur in the liquid film coating the aerosols. Seigneur and Saxena (1984) showed that nitrate formation in the liquid phase occurs too slowly to be important. Nitrate formation by heterogeneous hydrolysis of N_2O_5 at the aerosol surface is an important process. It is treated in the gas-phase chemical kinetic mechanism and, therefore, is not discussed here. Sulfate formation in the liquid phase may occur at an appreciable rate.

Reactions that lead to sulfate formation in aerosols include oxidation of SO_2 by O_2 (catalyzed by trace metals such as Mn^{2+} and Fe^{3+}) and H_2O_2. Other reactions are negligible because of the low pH of atmospheric aerosols. Appendix E presents the results of our investigation of the chemical reactions that lead to sulfate formation in liquid-coated aerosols. Oxidation of SO_2 by carbonaceous aerosols may occur at a nonnegligible rate; it is not included in the present model since carbon aerosols are not currently considered, but it could be included if appropriate. The chemical kinetic expressions used to simulate the aerosol phase oxidation of SO_2 to sulfate are listed in Table 3-5. The sectional reaction terms are given in Table 3-6. These terms represent the growth of aerosols due to sulfate formation in the aerosol phase; they account for aerosol mass and number conservation.

REMOVAL PROCESSES

Removal processes include dry deposition and sedimentation. The removal rate is calculated for the sectional representation as follows:

$$\overline{R}_{\ell,k} = \frac{1}{x_\ell - x_{\ell-1}} \int_{x_{\ell-1}}^{x_\ell} R(x)\, dx \quad , \qquad (3\text{-}13)$$

where R(x) is the removal rate, which is size-dependent. A size-dependent dry deposition rate (e.g., Sehmel and Hodgson, 1980) will eventually be incorporated in this model. The sedimentation rate is calculated according to Stokes's formula, as modified by the Cunningham correction factor:

$$R = \frac{V_s(d_p)}{H_z} \quad , \qquad (3\text{-}14)$$

where

V_s = the sedimentation velocity, which is dependent on the aerosol diameter d_p, and

H_z = the height of the model grid cell.

The sedimentation velocity is given by the following expression (Fuchs, 1964):

$$V_s = \frac{1}{18} \frac{\rho\, d_p^2\, g}{\eta} Cu \quad , \qquad (3\text{-}15)$$

where

ρ = the aerosol density,

TABLE 3-5. Chemical kinetic expressions for the aerosol-phase chemical reactions.

Reaction*	$\frac{d[\text{Sulfate}]}{dt}$ (M·min^{-1}) Kinetic Expression (25°C)	Reference
$S(IV)(aq) + \frac{1}{2} O_2(aq) \xrightarrow{Mn^{2+},\ Fe^{3+}} S(VI)(aq)$	$\frac{282\ [Mn^{2+}]^2}{[H^+]} + \frac{49\ [Fe^{3+}][S(IV)]}{[H^+]} \left(1 + \frac{1.7 \times 10^3\ [Mn^{2+}]^{1.5}}{6.31 \times 10^{-6} + [Fe^{3+}]}\right)$	Martin (1984)
$S(IV)(aq) + H_2O_2(aq) \rightarrow S(VI)(aq) + H_2O(aq)$	$\frac{6.84 \times 10^7\ [H_2O_2(aq)][SO_2(aq)]}{1.0 + 16\ [H^+]}$ ‡	McArdle and Hoffmann (1983)

---

* Species S(IV) and S(VI) represent two different sulfur oxidation states corresponding to, respectively, sulfur dioxide (H_2SO_3, HSO_3^-, and SO_3^{2-}) and sulfate (H_2SO_4, HSO_4^-, and SO_4^{2-}).

‡ Rate constant measured at 15°C is corrected by a factor of 1.5 for the 25°C temperature according to Martin and Damschen (1981).

TABLE 3-6. Sectional coefficients for aerosol growth due to aerosol chemical reactions.

Symbol	Remarks	Coefficient
$^{1}\bar{F}_{\ell}$	$1 < \ell < M$	$\int_{x_{\ell-1}}^{x_{\ell}} v' \frac{v(aq)}{v} \frac{F}{x_{\ell} - x_{\ell-1}} dx$
$^{2}\bar{F}_{\ell}$	$1 < \ell < M$	$\frac{1}{1 - \exp\left(- \frac{1}{2} \ell n\left(\frac{v_{\ell+1}}{v_{\ell-1}}\right)\right)} \int_{x_{\ell-1}}^{x_{\ell}} v_m \frac{v(aq)}{v} \frac{F}{x_{\ell} - x_{\ell-1}} dx$

where v_m is the sulfate molar volume, F is the reaction rate, v(aq) is the aqueous aerosol volume, v is the total aerosol volume, and x is the logarithm of the aerosol diameter.

g = the gravitational acceleration,

η = the viscosity of the air, and

Cu = the Cunningham factor.

$$Cu = 1 + \frac{2\lambda}{d_p} (1.23 + 0.41 \exp(-0.44 \frac{d_p}{\lambda})) \quad , \tag{3-16}$$

where λ is the mean free molecular path.

LIGHT SCATTERING

Aerosols scatter light. The light scattering coefficient depends on the light wavelength and aerosol size. In this model, we considered the scattering of light over the visible light range (i.e., 350 to 700 nm) and calculated sectional scattering coefficients. The sectional scattering coefficient is given by the following relationship:

$$\overline{b}_\ell = \frac{1}{x_\ell - x_{\ell-1}} \int_{x_{\ell-1}}^{x_\ell} b(x)\, dx \quad . \tag{3-17}$$

The scattering coefficient b(x) was calculated according to Mie theory using the optics computer code of the PLUVUE II model (Seigneur et al., 1984). It is expressed as $m^{-1}/(\mu m^3 \cdot cm^{-3})$, i.e., inverse length per aerosol concentration. The total light scattering by aerosols is then given by the following relationship:

$$b_{scat} = \sum_{\ell=1}^{M} \overline{b}_\ell \frac{Q_\ell}{\rho} \tag{3-18}$$

where Q_ℓ is the total aerosol mass in section ℓ, and ρ is the aerosol density. The mathematical modeling of light scattering by aerosols is discussed in detail in Appendix H.

SPECIFIC FORMULATION OF THE AEROSOL MODEL FOR THE EPA REGIONAL PARTICULATE MODEL

The aerosol model incorporated in the regional particulate model is based on Equations 7 and 8, which define the concentration, chemical composition, and size distribution of atmospheric aerosols on the basis of a sectional representation of the aerosol size distribution. Sensitivity studies have shown that a compromise between reasonable accuracy and computational costs was obtained for a sectional size resolution of $V_\ell/V_{\ell-1} = 10$, where V_ℓ and $V_{\ell-1}$ are the upper and lower limits of aerosol volumes in section ℓ (Seigneur, 1982; Seigneur et al., 1986).

The aerosol distribution consists of seven sections in the fine aerosol range with diameters between 0.01 and 2.5 μm, and two sections in the coarse aerosol range with diameters between 2.5 and 10 μm. The chemical species treated in the fine aerosol mode include primary aerosol, sulfate, nitrate, ammonium, organics, and water. Species treated in the coarse aerosol mode include primary aerosol and nitrate. A schematic representation of this aerosol model is given in Figure 3-5. This aerosol model applies to the entire range of relative humidities. The general aerosol model will be incorporated in the regional particulate model as an independent component that is coupled to the gas-phase chemistry mechanism (The Carbon-Bond Mechanism).

An example of the application of the aerosol model is presented in Figure 3-6 for clear conditions typical of those in northern Arizona. In Figure 3-6a, the base-case size distribution shows a peak at 0.15 μm, with solid ammonium sulfate in the accumulation mode. The NH_3 concentration is 10 ppb, and the relative humidity is 16 percent. In Figure 3-6b, the NH_3 concentration increases to 100 ppb, leading to the formation of ammonium nitrate. The evolution of the size distribution yields two peaks in the accumulation mode, at 0.3 and 1.5 μm. In Figure 3-6c, the NH_3 concentration is 10 ppb, and the relative humidity increases to 85 percent. Some nitric acid is dissolved in the aerosol liquid film, and the condensation of water leads to aerosol growth, with a peak at 1.5 μm.

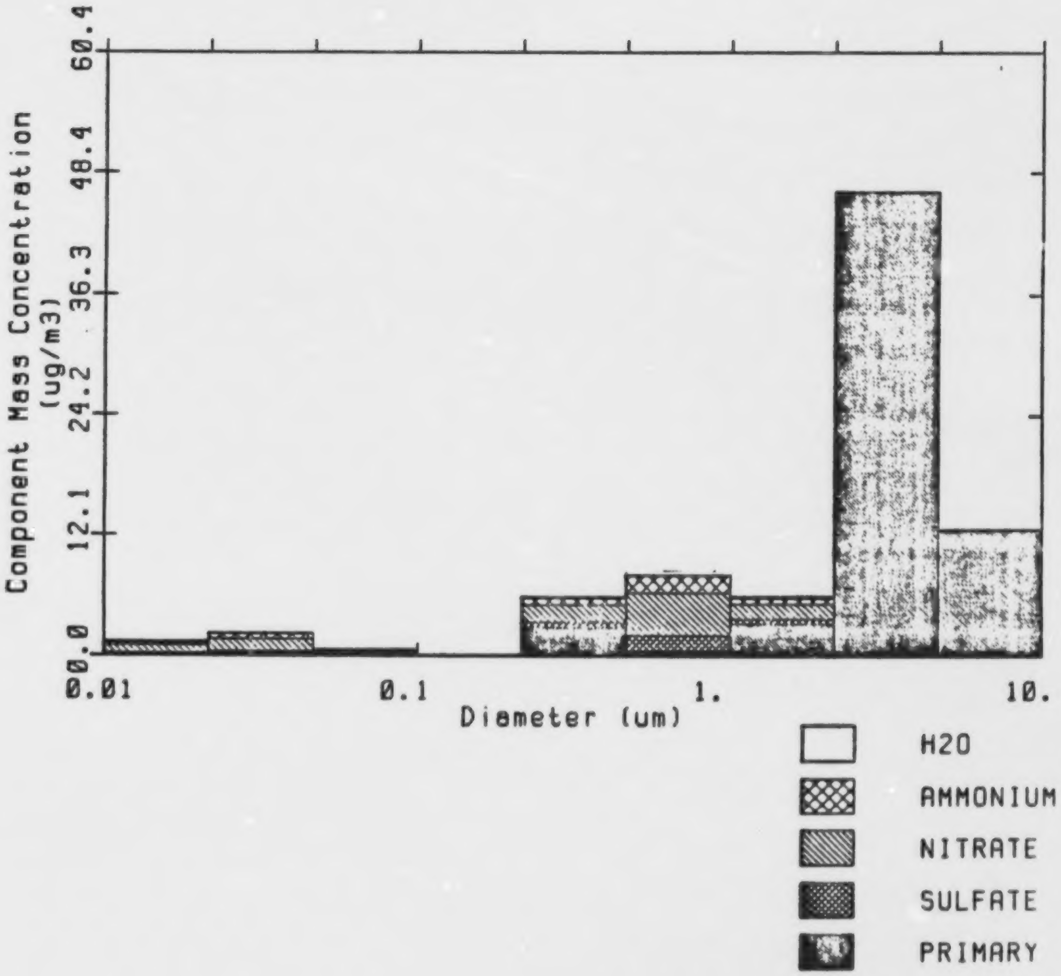

FIGURE 3-5. Example of a size-distributed aerosol concentration and chemical composition calculated by the aerosol model. The aerosol is composed of primary solid ammonium sulfate and solid ammonium nitrate. The nuclei, accumulation, and coarse modes are clearly apparent.

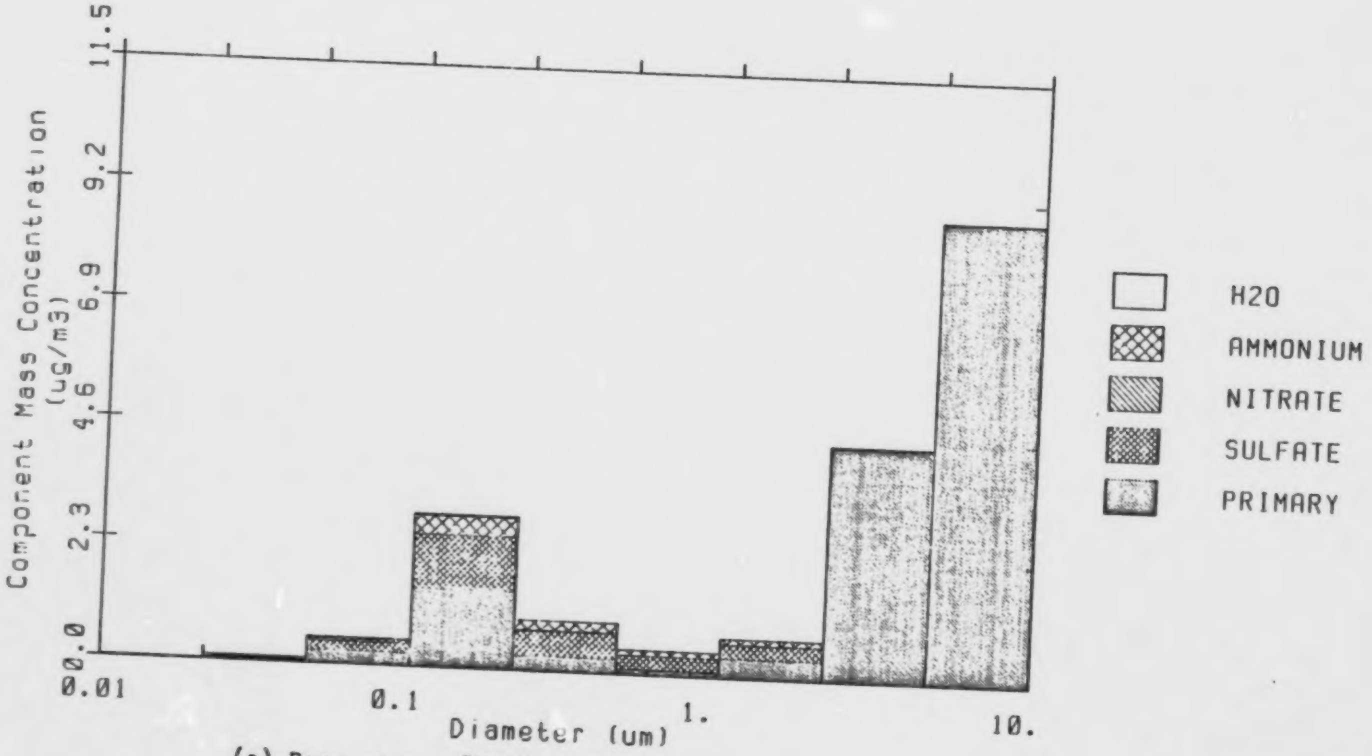

(a) Base case. $[NH_3]$ = 10 ppb, RH = 16%

FIGURE 3-6. Application of the aerosol model to clear conditions.

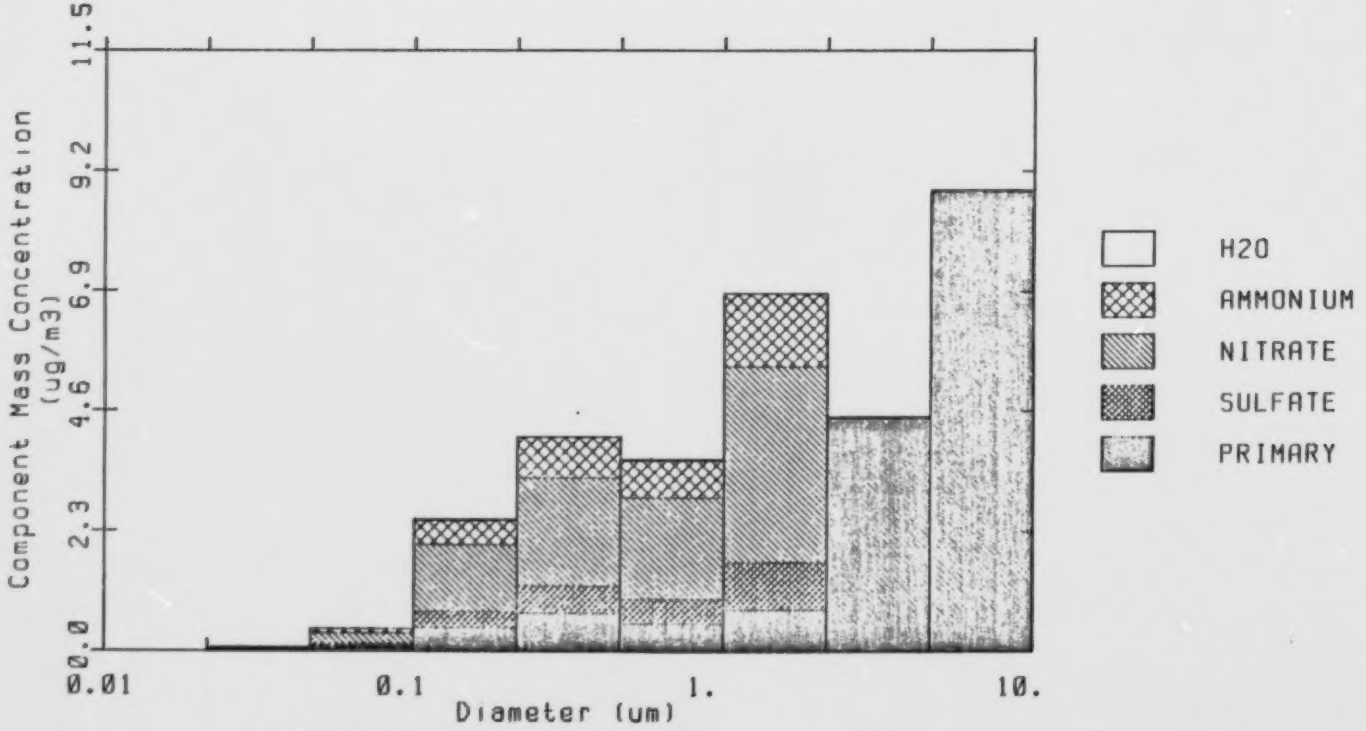

(b) $[NH_3]$ = 100 ppb, RH = 16%

FIGURE 3-6 (continued).

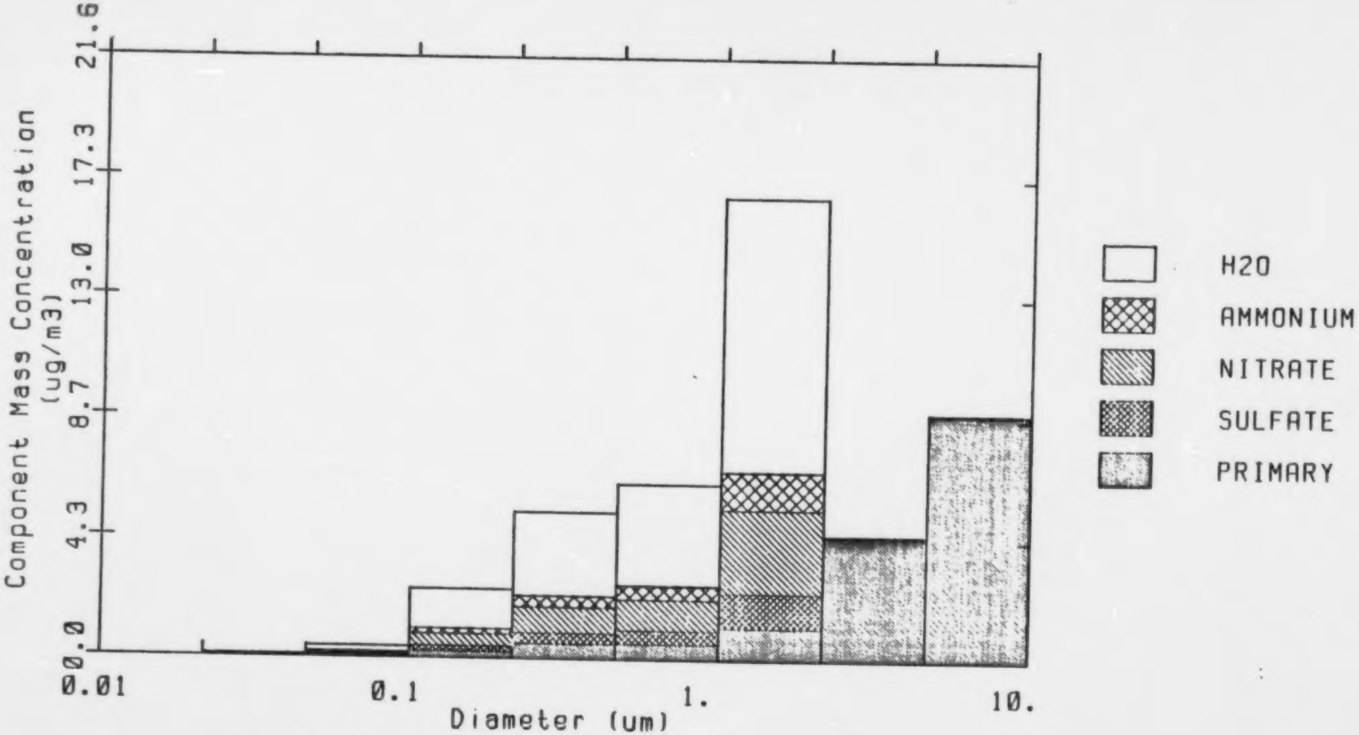

(c) $[NH_3]$ = 10 ppb, RH = 85%

FIGURE 3-6 (concluded).

4 DEVELOPMENT AND APPLICATION OF THE REGIONAL PARTICULATE MODEL

The regional particulate model consists of the EPA regional oxidant model's treatment of emissions, transport and dispersion, dry deposition, and gas-phase chemistry, in addition to the aerosol module described in Section 3. The latter will treat physicochemical processes affecting aerosol concentrations, size distributions, and chemical composition at a fixed location in the regional modeling domain. Other modules related to aerosols that must be added or modified include

Emissions
Dry deposition
Production of aerosols from clouds

This section presents an overview of the EPA regional model, gas-phase chemical mechanism, and aerosol-related modules.

DESCRIPTION OF THE REGIONAL OXIDANT MODEL

The regional oxidant model (ROM) is an Eulerian, grid-based, multiple-layer model capable of treating the following atmospheric processes relevant to regional oxidant distribution (Lamb, 1982):

Horizontal transport;

Photochemistry, including the very slow reactions;

Nighttime chemistry of the products and precursors of photochemical reactions;

Nighttime wind shear, stability stratification, and turbulence "episodes" associated with the nocturnal jet;

Cumulus cloud effects, including the venting of pollutants from the mixed layer, effects on photochemical reaction rates in their shadows, providing sites for liquid-phase reactions, influencing changes in the mixed-layer depth, and perturbing horizontal flow;

Mesoscale vertical motion induced by terrain and horizontal divergence of the large-scale flow;

Mesoscale eddy effects on urban plume trajectories and growth rates;

Terrain effects on horizontal flows, removal, and diffusion;

Sub-grid-scale chemistry processes (those resulting from emissions from sources smaller than the model's grid can resolve);

Emissions of hydrocarbons (anthropogenic and biogenic), oxides of nitrogen (NO_x, anthropogenic only); and

Wet and dry removal processes, e.g., washout and deposition.

Analysis of aerometric data collected by aircraft in the northeastern United States indicates that the model must contain provisions for treating at least three vertical layers to allow treatment of the processes just cited. These layers, which vary both spatially and temporally, are the inversion layer, the mixed layer, and the cloud layer. The model also includes a shallow surface layer adjacent to the ground for the treatment of surface deposition and sub-grid-scale chemistry phenomena. Estimates of ground-level concentrations are also derived from surface-layer concentrations. Schematic illustrations of the conceptual treatment of vertical layers and the important processes represented in each layer for both daytime and nighttime conditions are given in Figure 4-1.

To derive the governing equations for the model, one first performs a spatial integration of the fundamental mass conservation equation for a chemically reactive pollutant in a turbulent flow. This integration is carried out over a volume corresponding to a grid cell (with typical horizontal and vertical dimensions of 18 km and 50 to 1000 m, respectively). At the present time, the horizontal dimension of the model consists of a 60 x 42 cell array. After casting the resulting equations into curvilinear coordinates to take into account the effects of the earth's curvature, a set of coupled partial differential equations describing the dynamic behavior of volume-averaged pollutant concentrations in a latitude-longitude coordinate system remains.

The regional oxidant model is operational on both the IBM and VAX computers at the U.S. Environmental Protection Agency; it uses standard FORTRAN 77 (Novak, private communication, 1984).

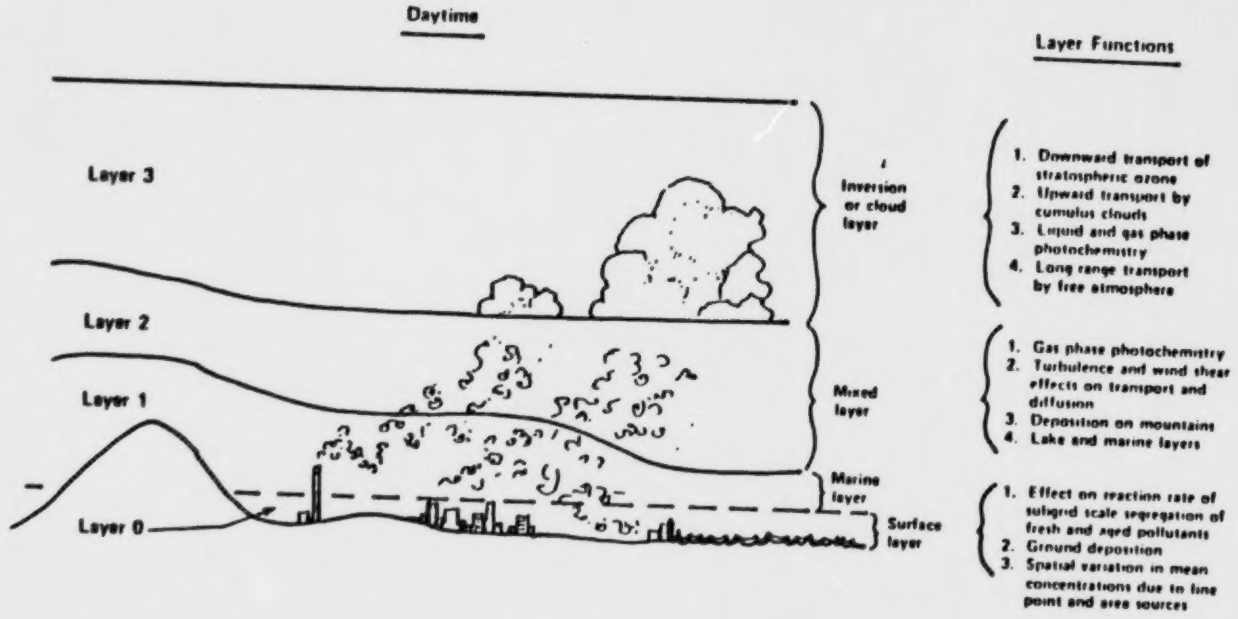
Daytime
Layer Functions
Layer 3
Layer 2
Layer 1
Layer 0
Inversion or cloud layer
Mixed layer
Marine layer
Surface layer
1. Downward transport of stratospheric ozone
2. Upward transport by cumulus clouds
3. Liquid and gas phase photochemistry
4. Long range transport by free atmosphere
1. Gas phase photochemistry
2. Turbulence and wind shear effects on transport and diffusion
3. Deposition on mountains
4. Lake and marine layers
1. Effect on reaction rate of subgrid scale segregation of fresh and aged pollutants
2. Ground deposition
3. Spatial variation in mean concentrations due to line point and area sources

(a) Daytime phenomena

FIGURE 4-1. Schematic illustration of the "dynamic" layer structure of the regional-scale model and the phenomena each layer is designed to treat.

86026
83129
84088

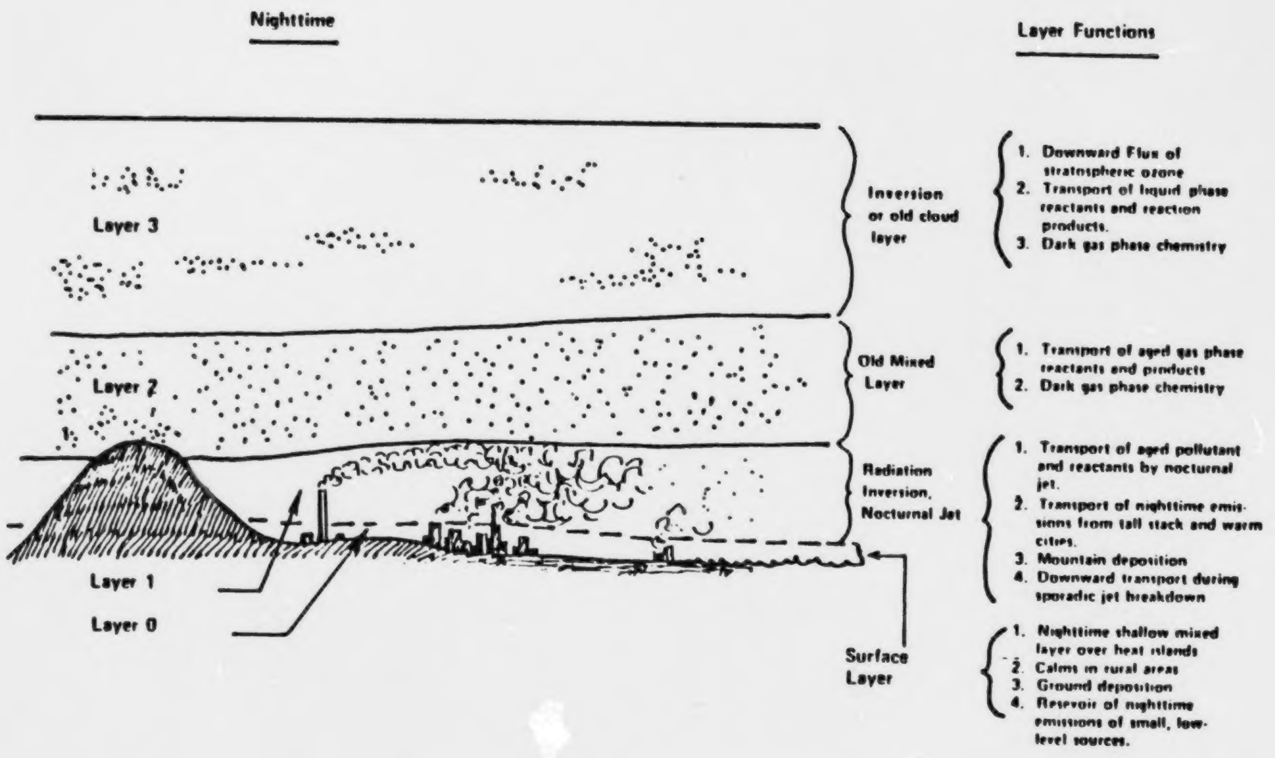
Nighttime
Layer Functions
Layer 3
Layer 2
Layer 1
Layer 0
Inversion or old cloud layer
Old Mixed Layer
Radiation Inversion, Nocturnal Jet
Surface Layer
1. Downward Flux of stratospheric ozone
2. Transport of liquid phase reactants and reaction products.
3. Dark gas phase chemistry
1. Transport of aged gas phase reactants and products
2. Dark gas phase chemistry
1. Transport of aged pollutant and reactants by nocturnal jet.
2. Transport of nighttime emissions from tall stack and warm cities.
3. Mountain deposition
4. Downward transport during sporadic jet breakdown
1. Nighttime shallow mixed layer over heat islands
2. Calms in rural areas
3. Ground deposition
4. Reservoir of nighttime emissions of small, low-level sources.

(b) Nighttime phenomena

FIGURE 4-1. (concluded).

86026
83129
84088

GAS-PHASE CHEMICAL KINETIC MECHANISM

Gas-phase chemistry is treated by means of the Carbon-Bond Mechanism IV (CBM-IV) developed by Whitten and Gery (1985). The mechanism, shown in Table 4-1, describes the chemistry of oxidants, nitrogen oxides, and anthropogenic and natural hydrocarbons. It includes 28 species involved in 70 reactions and is written in a condensed form that facilitates solution of the corresponding chemical kinetic equations. The condensation of the Carbon-Bond Mechanism IV is discussed in detail in Appendix F.

Two gas-phase species--SO_2 and NH_3, and one reaction--the gas-phase oxidation of SO_2 to H_2SO_4, were added to the gas-phase species and reactions described in CB-IV (Stockwell and Calvert, 1984). Since the condensation of H_2SO_4 to aerosol sulfate is rapid (McMurry, Takano, and Anderson, 1983), the product of SO_2 oxidation can be assumed to be aerosol sulfate:

$$SO_2 + OH \rightarrow AERS + HO_2 \qquad k = 1500\ \text{ppm}^{-1}\ \text{min}^{-1} \quad ,$$

where AERS is aerosol sulfate.

Aerosol Module

The aerosol module was described in detail in Section 3. It treats the evolution of the concentration, chemical composition, and size distribution of aerosols undergoing the following processes:

- Coagulation;
- Growth from diffusion-limited condensation of sulfuric acid and organic species;
- Growth/shrinkage from condensation/evaporation of HNO_3, NH_3, and H_2O;
- Oxidation of SO_2 to sulfate by O_2 and H_2O_2 in the liquid-coated aerosols; and
- Formation of small sulfate and organic aerosols.

Aerosols have diameters that range in size from 0.01 μm to 10 μm. Secondary aerosols have diameters that range in size from 0.01 μm to 2.5 μm, with seven size sections. Primary aerosols encompass the entire size range, with nine size sections.

TABLE 4-1. The Carbon-Bond Mechanism IV

	Reaction			Rate constant[a]	Activation energy[b]
1	NO2		= NO +O	vary	
2	O		= O3	4.65 X 10^{+6}	-690.
3	O3	+NO	= NO2	26.6	1430.
4	O	+NO2	= NO	13800.	
5	O	+NO2	= NO3	2320.	-600.
6	O	+NO	= NO2	3120.	-411.
7	NO2	+O3	= NO3	0.0474	2450.
8	O3		= 0.205 OH + 0.897 O	vary	
9	O3		= O	0.042 X k1	
10	O3	+OH	= HO2	100.	940.
11	O3	+HO2	= OH	3.0	580.
12	NO3	+NO	= 2. NO2	28100.	-250.
13	NO3	+NO2	= NO +NO2	0.59	1230.
14	NO3	+NO2	= N2O5	1780.	60.
15	N2O5		= 2. HNO3	0.0285	
16	N2O5		= NO3 +NO2	3.12	10840.
17	NO	+NO2	= 2. HNO2	2.4 X 10^{-7}	
18	HNO2	+HNO2	= NO +NO2	1.5 X 10^{-5}	
19	HNO2		= NO +OH	0.18 X k1	
20	NO2	+OH	= HNO3	16300.	-560.
21	NO	+OH	= HNO2	9770.	-427.

continued

TABLE 4-1. Continued.

	Reaction		Rate constant[a]	Activation energy[b]
22	HO2 +NO	= OH +NO2	12300.	-240.
23	NO +NO	= 2. NO2	1.52×10^{-4}	-530.
24	H2O2	= 2. OH	0.0014 X k1	
25	OH +H2O2	= HO2	2520.	187.
26	OH +HNO2	= NO2	9770.	
27	OH +HNO3	= NO3	192.	-778.
28	NO3	= 0.85NO2 +0.85 O +0.15NO	30.6 X k1	
29	HO2 +HO2	= H2O2	4144.	-1150.
30	HO2 +HO2	= H2O2	3270.	-5800.
31	OH +CO	= HO2	400.	
32	FORM+OH	= HO2 +CO	15000.	
33	FORM	= 2. HO2 +CO	vary	
34	FORM	= CO	vary	
35	FORM+O	= OH +HO2 +CO	237.	1550.
36	FORM+NO3	= HNO3 +HO2 +CO	0.93	
37	ALD2+O	= C2O3 +OH	636.	986.
38	ALD2+OH	= C2O3	24000.	-250.
39	ALD2+NO3	= C2O3 +HNO3	3.7	
40	ALD2	= XO2 +2.HO2 +CO +FORM	vary	
41	ALD2+HO2	= XO2 +2.FORM +HO2	5.	
42	C2O3+NO	= NO2 +XO2 +FORM +HO2	16500.	-250.
43	C2O3+NO2	= PAN	9000.	-250.
44	PAN	= C2O3 +NO2	0.0222	14000.
45	C2O3+C2O3	= 2. XO2 +2.FORM +2.HO2	3700.	
46	C2O3+HO2	=	9600.	

TABLE 4-1. Continued.

	Reaction		Rate constant[a]	Activation energy[b]
47	MGLY	= C203 +H02 +CO	0.02 X k1	
48	MGLY+OH	= X02 +C203	26000.	
49	OH	= X02 +FORM +H02	21.	
50	PAR +OH	= 1.49X02 +0.067X02N + 0.93H02 +0.45ALD2 -0.75PAR	1150.0	
51	O +OLE	= 0.95ALD2 +0.35H02 + 0.20X02 +0.15CO + 0.05FORM +0.05C203 + -0.35PAR	5920.	324.
52	OH +OLE	= FORM +ALD2 +X02 +H02 -PAR	42000.	-537.
53	03 +OLE	= 0.5ALD2 +0.66FORM + 0.212CO +0.28H02 + 0.144X02 +0.08 OH -PAR	0.018	1897.
54	N03 +OLE	= 0.91X02 +0.91H02 + 0.09X02N	11.4	
55	O +ETH	= FORM +X02 +CO +2.H02	1080.	800.
56	OH +ETH	= X02 +2.FORM +H02	12000.	-382.
57	03 +ETH	= FORM +0.37CO + 0.13H02	0.0027	2840.
58	TOL +OH	= H02 +0.64X02 +1.13FORM + 0.56MGLY +0.36PHEN + 0.36PAR +1.13CO	9750.	
59	PHEN+N03	= PHO +HN03	14000.	
60	PHO +N02	=	20000.	
61	XYL +OH	= H02 +0.72X02 +0.67CO + 1.33MGLY +0.28PHEN + 0.56PAR +0.06TLA + 0.67FORM	36000.	
62	TLA +OH	= X02 +PHO +2. PAR	20000.	
63	ISOP+O	= H02 +0.8ALD2 +0.55OLE + 0.5X02 +0.5CO + 0.45ETH -0.1PAR	28000.	

TABLE 4-1. Concluded.

	Reaction		Rate constant[a]	Activation energy[b]
64	ISOP+OH	= 0.87XO2 +0.87FORM + 0.87HO2 +0.29PAR 0.29OLE +0.58ETH 0.29ALD2	126000.	
65	ISOP+O3	= FORM +0.45ALD2 + 0.55ETH +0.98HO2 + 0.10OLE +0.06CO -0.25PAR	0.018	
66	ISOP+NO3	= XO2N	165.	
67	XO2N+NO	=	1000.	
68	XO2 +NO	= NO2	12000.	
69	XO2 +HO2	=	5000.	-1300.
70	XO2 +C2O3	= XO2 +HO2 +FORM	2400.	

[a] All rate constants are in appropriate ppm and min units at 298K and one atmosphere of air. That is, all unimolecular and photolysis reactions (+ hν) are in units of min^{-1}; all bimolecular reactions are in units of $\text{ppm}^{-1}\ \text{min}^{-1}$; and all termolecular reactions are in units of $\text{ppm}^{-2}\ \text{min}^{-1}$. Rate constants designated as "vary" are defined in Whitten, Killus, and Johnson (1985a and b).

[b] The numbers listed are Arrhenious temperature coefficients in degrees Kelvin for B in the expression $k_T = k_{298} \exp(B \times (\frac{1}{298} - \frac{1}{T}))$.

The aerosol module contains 37 variables:

Nine size-segregated primary aerosol categories (QP_1 to QP_9);

Seven sulfate aerosol categories (QS_1 to QS_7);

AERS (total aerosol sulfate, which is simply the sum of these seven sulfate aerosol categories);

AERN (total aerosol nitrate);

AERA (total aerosol ammonium);

AERW (total aerosol water);

AERO (total aerosol organics);

Fe^{3+} and Mn^{2+} (trace metals that catalyze SO_2 aqueous oxidation to sulfate);

AB (a surrogate for NaCl or $CaCO_3$, i.e., coarse aerosols that may react with HNO_3 to form coarse nitrate);

CAN (coarse aerosol nitrate);

Seven size-segregated categories of total aerosol mass (Q_1 to Q_7) (note that $Q_8 = QP_8$ and $Q_9 = QP_9$);

PM10 (total aerosol mass below 10 μm);

RHO (aerosol density);

BSCAT (aerosol scattering coefficient);

PH (aerosol pH); and

λ (parameter equal to the ratio of the total of sulfate, nitrate, ammonium, and water aerosol to sulfate aerosol; λ = (AERS + AERN + AERA + AERW)/AERS).

Of these 37 variables, 22 are solved forward in time through differential equations--so-called state variables. The remaining 15 variables are calculated from the values of the 22 state variables through algebraic equations.

EMISSIONS

The emissions required for the regional particulate model include nitrogen oxides (NO_x), reactive hydrocarbons (RHC), sulfur dioxide (SO_2), ammonia (NH_3), and size-segregated particulate matter. The National Acid Precipitation Assessment Program (NAPAP) version 5.2 emission inventory will be used in the application of the regional particulate model (J. Novak, private communication, 1985). This inventory is for 1980 and includes NO_x, SO_2, RHC, NH_3, and particulate matter segregated into three size ranges (0 μm to 2.5 μm, 2.5 μm to 5 μm, and 5 μm to 10 μm). No emission data are currently available for trace metals (Fe^{3+}, Mn^{2+}) or the chemical composition of fugitive dust or sea salts (NaCl, $CaCO_3$, etc.). Concentration values for these aerosol species will be derived from ambient experimental data.

DRY DEPOSITION

The rate of dry deposition of gaseous species is calculated in the EPA regional model by means of deposition resistances and velocities. First, a deposition resistance is calculated that depends on land use and atmospheric stability (represented by the Monin-Obukhov length). The functional dependence of deposition resistance on land use and stability is obtained from published empirical data. The deposition velocity, V_d, is then calculated from the following equation (Sheih et al., 1979):

$$V_d = 0.4\, u^* \left[\ln\left(\frac{z}{z_0}\right) + 2.6 + 0.4\, u^* r - \psi_c \right]^{-1} , \qquad (4\text{-}1)$$

where

u^* = the friction velocity,

z_0 = the surface roughness,

z = a reference height for the deposition flux calculation (equal to 10 m), and the function ψ_c depends on atmospheric stability through the Monin-Obukhov length.

$$\psi_c = \exp[0.598 + 0.390 \ln(-\frac{z}{L}) - 0.09 (\ln(-\frac{z}{L}))^2] \quad \text{for } L < 0$$

$$\psi_c = -5 \frac{z}{L} \quad \text{for } L > 0 .$$

Experimental data and theoretical calculations for aerosol species are reported in the literature as deposition velocities rather than deposition resistance. Deposition velocity depends on the size of the aerosol diameter, with the minimum deposition velocity in the size range 0.235 μm to 0.516 μm (Section 5 of the sectional aerosol representation). We constructed a table of deposition velocities for aerosols that depends on friction velocity and the land use categories described by the EPA regional model. We used the review of Sehmel (1980) to develop this file of aerosol dry deposition velocities. Deposition velocities were calculated for friction velocities of 10, 20, 50, 100, 150, and 200 cm s^{-1}. Deposition velocities for a friction velocity of 10 cm s^{-1} are presented in Table 4-2.

PRODUCTION OF AEROSOLS IN CLOUDS

The turbulent odyssey of sulfur species through cumulus clouds results in the formation of aerosols from the oxidation of SO_2 in cloud droplets. The size distribution of aerosols flowing out of the cloud depends on the cloud droplet size distribution and the chemical composition of the cloud droplets.

The oxidation of SO_2 in liquid droplets is assumed to take place via the reaction of HSO_3^- with H_2O_2(aq). This reaction is rapid and may be assumed to be instantaneous since the residence time of an air parcel in a cumulus cloud is of the order of 20 minutes, i.e., longer than the (HSO_3^- + H_2O_2) reaction time.

Calculation of the chemical composition of cloud droplets is based on the aerosol concentrations that enter the cloud and the sulfate formed within the cloud. As the air parcel leaves the cloud and evaporates, the cloud droplet evaporates until a thermodynamic equilibrium is reached between the droplet and the surrounding air. This thermodynamic calculation is carried out with MARS (see Section 2 for a description of MARS). The new aerosol size distribution is calculated using as input the cloud droplet initial size distribution; the total amount of primary, organic, and sulfate aerosol; nitric acid and ammonia concentrations; relative humidity; and temperature. The formation of aerosols in clouds is discussed in detail in Appendix G.

TABLE 4-2. Aerosol deposition velocities (cm/s) (for a friction velocity $u^* = 10$ cm/s).

Land Use Type	Aerosol Size Section 1	2	3	4	5	6	7	8	9
Urban	0.4	0.35	0.2	0.15	0.12	0.15	0.25	0.35	0.45
Agriculture	0.26	0.23	0.16	0.10	0.08	0.1	0.2	0.27	0.42
Rangeland	0.2	0.18	0.14	0.08	0.06	0.08	0.18	0.25	0.4
Deciduous forest	0.5	0.45	0.3	0.2	0.15	0.2	0.3	0.4	0.5
Coniferous	0.5	0.45	0.3	0.2	0.15	0.2	0.3	0.4	0.5
Mixed forest including wetlands	0.4	0.35	0.2	0.15	0.12	0.15	0.25	0.35	0.45
Water	0.15	0.12	0.08	0.05	0.04	0.07	0.1	0.2	0.35
Outside study area	0	0	0	0	0	0	0	0	0
Nonforested wetland	0.3	0.25	0.18	0.12	0.09	0.12	0.22	0.3	0.43
Mixed agriculture and rangeland	0.23	0.20	0.15	0.09	0.07	0.09	0.19	0.26	0.41

5 APPLICATION OF THE REGIONAL TRAJECTORY PARTICULATE MODEL

INTRODUCTION

The aerosol model developed in this study was incorporated into a gridded trajectory model that treats the emission, dry deposition, turbulent diffusion, and gas-phase chemical reactions of pollutants. A Lagrangian concept, in which a wall of cells follows a trajectory determined by the mean horizontal wind, governs the transport. During the model simulations, the grid size remains fixed, but the individual cells may have different dimensions in order to provide the desired spatial resolution. Vertical and lateral turbulent diffusion are treated by the K-theory of turbulence. This trajectory/aerosol model was developed under contract to Southern California Edison Company and was described by Hudischewskyj and Seigneur (1986). We used this trajectory model to simulate the atmospheric formation of secondary aerosols for conditions typical of (1) regional pollution over the northeastern United States, and (2) an urban plume.

DESCRIPTION OF THE MODELING CONDITIONS

The simulations were conducted for 36-hour periods to simulate both daytime and nighttime chemistry. The initial simulation time was 0800 LST, and the final simulation time was 2000 LST the following day. The gridded structure of the trajectory model was designed to simulate the variation in vertical mixing during the various periods of the diurnal cycle. These variations are presented schematically in Figure 5-1. During the day, vertical mixing is important and the pollutant concentrations are homogeneous in the mixing layer; at night, vertical mixing is considerably reduced, and emissions of fresh pollutants released from ground-level sources and dry deposition of pollutants are limited to a relatively shallow layer near the surface. The top of the mixing layer is assumed to be at 1500 m, which is typical of the continental United States (Holzworth, 1972). The vertical structure of the model consists of three layers that constitute the mixing layer: a surface layer, 100-m deep; a second layer, 400-m deep; and a third layer, 1000-m deep, which extends up to the base of the elevated inversion layer. During the day, there is strong vertical

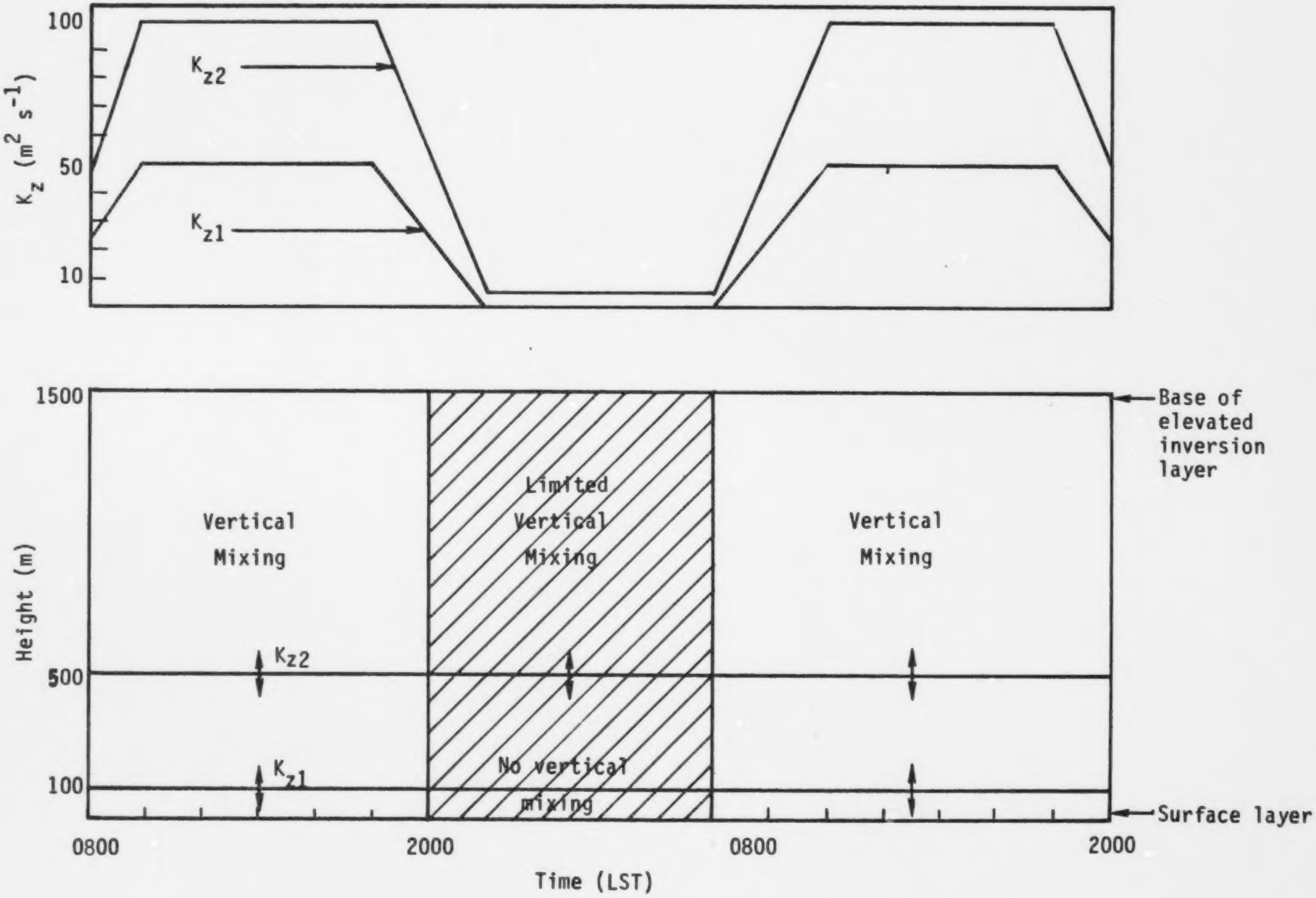

FIGURE 5-1. Structure of the trajectory model with treatment of vertical mixing.

mixing due to unstable conditions. The vertical eddy diffusion coefficient K_z typically varies with height, reaching a maximum value at about midway between the surface and the top of the mixing layer (Lamb and Duran, 1977). The value of K_z is typically of the order of 100 m^2 s^{-1}; values of 50 and 100 m^2 s^{-1} were selected for eddy diffusion between the first and second layers and between the second and third layers, respectively. At night, atmospheric conditions become stable due to the formation of a ground-based inversion of temperatures. Then, the value of the vertical eddy diffusion coefficient considerably decreases, with typical maximum values between 0.5 and 5 m^2 s^{-1} (Businger and Arya, 1974). We selected a value of K_{z1} of 0 m^2 s^{-1} to prevent any vertical diffusion between the first and second layers, and a value of K_{z2} of 5 m^2 s^{-1} to allow some limited diffusion between the second and third layers.

Dry deposition is calculated according to a first-order removal rate that depends on the pollutant-specific deposition velocity. The deposition velocity, in turn, depends on land use and atmospheric stability. We assumed a general surface roughness value of 0.1 typical of agricultural land. Dependence of the deposition velocity on atmospheric stability leads to a diurnal variation in the dry deposition rate. Dry deposition velocities are presented in Table 5-1 for gases and aerosols for daytime and nighttime conditions. Emissions were held constant throughout each simulation.

We selected emissions of primary pollutants that are typical of those found in the northeastern United States. The primary pollutants include SO_2, NO_x, anthropogenic and biogenic reactive hydrocarbons, CO, NH_3, and aerosol mass for aerosols whose diameters are smaller than 10 μm (PM-10). The emission rates are presented in Table 5-2. (Isoprene was selected as typical of biogenic RHC and was represented by two olefinic bonds and one paraffinic carbon, according to the carbon-bond formulation). Emissions were held constant throughout each simulation.

We assumed an average wind speed of 5 m s^{-1}, which is typical of summertime conditions in the northeastern United States (Holzworth, 1972). The temperature was assumed to vary between a maximum value of 25°C at noon and a minimum value of 10°C at night. The relative humidity was assumed to be 60 percent.

We selected initial concentrations that are typical of a moderately polluted regional background in the northeastern United States for the first case study, and of an urban plume such as the St. Louis urban plume for the second case study. These initial concentrations are presented in Tables 5-3 and 5-4 for each case study, respectively.

TABLE 5-1. Dry deposition velocities.

Species	Deposition Velocity (cm s^{-1})	
	Daytime	Nighttime
SO_2	1	0.2
NO_x	0.7	0.14
O_3	0.35	0.07
HNO_3	1	0.2
NH_3	1	0.2
RHC	1	0.2
PAN	0.25	0.05
H_2O_2	1	0.2
QP1 and QS1	0.5	0.1
QP2 and QS2	0.45	0.09
QP3 and QS3	0.2	0.04
QP4 and QS4	0.08	0.016
QP5 and QS5	0.06	0.012
QP6 and QS6	0.12	0.024
QP7 and QS7	0.4	0.08
Q8	0.8	0.16
Q9	1.25	0.26

TABLE 5-2. Emission rates.

Species	Emission rate	Reference
SO_2	108 kg ha^{-1} y^{-1}	(NRC, 1986)
NO_x	45 kg ha^{-1} y^{-1}	(NRC, 1986)
Anthropogenic RHC		(based on NEDS, 1982 ratio of RHC/NO_x)
PAR	36 kg ha^{-1} y^{-1}	
OLE	1 kg ha^{-1} y^{-1}	
ETH	4 kg ha^{-1} y^{-1}	
ARO	4 kg ha^{-1} y^{-1}	
CARB	5 kg ha^{-1} y^{-1}	
Biogenic RHC	50 kg ha^{-1} y^{-1}	(based on background concentration estimate)
CO	400 kg ha^{-1} y^{-1}	(based on NEDS, 1982 ratio of CO/SO_2)
NH_3	5 kg ha^{-1} y^{-1}	(based on background concentration estimate)
PM-10	10 kg ha^{-1} y^{-1}	(based on background concentration estimate)

TABLE 5-3. Initial concentrations for the regional simulation.

Species	Concentration	Reference
NO_x	5.3×10^{-3} ppm	EPRI, 1982
SO_2	1.1×10^{-2} ppm	EPRI, 1982
O_3	4.8×10^{-2} ppm	EPRI, 1982
H_2O_2	1.0×10^{-3} ppm	Heikes et al., 1985
S(VI)	$4.0\ \mu g\ m^{-3}$	EPRI, 1982
HNO_3	1.8×10^{-3} ppm	Mohnen, 1985
NH_3	5.0×10^{-3} ppm	Tanner, 1982
PAR	3.5×10^{-2} ppm	Ferman et al., 1985
OLE	7.0×10^{-4} ppm	Ferman et al., 1985
ETH	2.0×10^{-3} ppm	Ferman et al., 1985
ARO	7.0×10^{-4} ppm	Ferman et al., 1985
CARB	4.5×10^{-3} ppm	Ferman et al., 1985
PAN	2.0×10^{-4} ppm	Singh, 1987
CO	2.0×10^{-1} ppm	Kelly et al., 1984
NaCl	$1.0\ \mu g\ m^{-3}$	Lazrus et al., 1983
Fe^{3+}	$6.0 \times 10^{-3}\ \mu g\ m^{-3}$	Pratt et al., 1984
Mn^{2+}	$2.0 \times 10^{-3}\ \mu g\ m^{-3}$	Lindberg, 1982
Q1	$1.2 \times 10^{-4}\ \mu g\ m^{-3}$	Whitby, 1981
Q2	$7.03 \times 10^{-2}\ \mu g\ m^{-3}$	Whitby, 1981
Q3	$4.151 \times 10^{-1}\ \mu g\ m^{-3}$	Whitby, 1981
Q4	$2.082\ \mu g\ m^{-3}$	Whitby, 1981
Q5	$2.578\ \mu g\ m^{-3}$	Whitby, 1981
Q6	$9.986 \times 10^{-1}\ \mu g\ m^{-3}$	Whitby, 1981
Q7	$2.257\ \mu g\ m^{-3}$	Whitby, 1981
Q8	$7.134\ \mu g\ m^{-3}$	Whitby, 1981
Q9	$9.56\ \mu g\ m^{-3}$	Whitby, 1981
b_{scat}	$1.75 \times 10^{-4}\ m^{-1}$	Wolff et al., 1983

TABLE 5-4. Initial concentrations for the urban plume simulation.

Species	Concentration	Reference
NO_x	6.0×10^{-2} ppm	Seigneur et al., 1983
SO_2	1.0×10^{-2} ppm	Gillani et al., 1978
O_3	2.0×10^{-2} ppm	Seigneur et al., 1983
H_2O_2	1.0×10^{-3} ppm	Heikes et al., 1985
S(VI)	20 $\mu g\ m^{-3}$	Wilson, 1978
HNO_3	2.5×10^{-3} ppm	Cadle et al., 1982
NH_3	5.0×10^{-3} ppm	Tanner, 1982
PAR	1.45×10^{-1} ppm	Haney and Seigneur, 1985
OLE	7.5×10^{-3} ppm	Haney and Seigneur, 1985
ETH	1.0×10^{-2} ppm	Haney and Seigneur, 1985
ARO	4.75×10^{-2} ppm	Haney and Seigneur, 1985
CARB	1.25×10^{-2} ppm	Haney and Seigneur, 1985
PAN	2.0×10^{-4} ppm	Singh, 1987
CO	5.0×10^{-1} ppm	Seigneur et al., 1983
NaCl	1.0 $\mu g\ m^{-3}$	Lazrus et al., 1984
Fe^{3+}	6.0×10^{-1} $\mu g\ m^{-3}$	Cass and McRae, 1986
Mn^{2+}	1.0×10^{-2} $\mu g\ m^{-3}$	Cass and McRae, 1986
Q1	1.067×10^{-1} $\mu g\ m^{-3}$	Whitby, 1978
Q2	5.186×10^{-1} $\mu g\ m^{-3}$	Whitby, 1978
Q3	2.48 $\mu g\ m^{-3}$	Whitby, 1978
Q4	9.18 $\mu g\ m^{-3}$	Whitby, 1978
Q5	14.68 $\mu g\ m^{-3}$	Whitby, 1978
Q6	9.82 $\mu g\ m^{-3}$	Whitby, 1978
Q7	5.365 $\mu g\ m^{-3}$	Whitby, 1978
Q8	9.112 $\mu g\ m^{-3}$	Whitby, 1978
Q9	11.19 $\mu g\ m^{-3}$	Whitby, 1978
b_{scat}	1.75×10^{-4} m^{-1}	Gillani et al., 1978 Wilson, 1978

In addition to the two base case studies, six sensitivity studies were conducted--five based on the data for the regional environment base case (Columbus, Ohio), and one on the data for the urban plume (St. Louis, Missouri). The parameters were varied as follows:

Columbus case study:

1. Base case SO_2 emissions and initial SO_2 concentrations were reduced by 50 percent.
2. Base case NO_x emissions and initial NO_x concentrations were reduced by 50 percent.
3. Base case NH_3 emissions and initial NH_3 concentrations were reduced by 50 percent.
4. Base case RHC emissions and initial RHC concentrations were reduced by 50 percent.
5. Base case simulation time was changed from summer to winter, which included lowering the mixing height, decreasing the initial H_2O_2 and O_3 concentrations and the temperature, and shortening the period of daylight hours.

St. Louis case study:

1. Relative humidity was increased from 60 percent to 85 percent.

A grid composed of three vertical cells was used in the computer simulations. The results and discussions that follow address the lowest (surface) of these three cells. We discuss the base case simulations and compare the results of the base case and sensitivity simulations.

REGIONAL BASE CASE--COLUMBUS, OHIO

Results for the regional environment base case simulation are presented in Tables 5-5 through 5-8 and in Figures 5-2 through 5-4. The diurnal variations in the gas-phase species--NO_2, O_3, and HNO_3--are significant, as shown in Figure 5-2(a-c). During the daytime NO_2 decreases as it is transformed to HNO_3 and organic nitrate. The O_3 concentration peaks at 10 pphm the second day. The H_2O_2 concentration rises to about 1 ppb during the simulation. Sulfate formation occurs primarily during the daytime when SO_2 is oxidized by OH radicals in the gas phase. The nitrate aerosol concentration increases at night when low temperatures favor ammonium nitrate formation. Decreases in NH_3 result in increases in the ammonium aerosol (AERA). The size-distributed chemical composition of the aerosol at the time of maximum aerosol sulfate (AERS), aerosol nitrate (AERN), and

TABLE 5-5. Minimum concentrations for the base case and sensitivity simulations for Columbus, Ohio, August 23, 1981 (Day 1, 8am to Midnight).

Species	Base Case	50% SO2	50% NOX	50% NH3	50% RHC	Winter+
NO2 (ppm)	0.396E-02*	0.391E-02*	0.183E-02*	0.393E-02*	0.433E-02*	0.310E-02*
NO (ppm)	0.409E-05	0.412E-05	0.305E-05	0.408E-05	0.596E-05	0.482E-04
O3 (ppm)	0.402E-01	0.402E-01	0.429E-01	0.402E-01	0.375E-01	0.569E-02
HNO3 (ppm)	0.121E-02	0.122E-02	0.956E-03	0.159E-02	0.114E-02	0.106E-03
H2O2 (ppm)	0.359E-03	0.358E-03	0.639E-03	0.360E-03	0.308E-03	0.204E-04
SO2 (ppm)	0.116E-01*	0.577E-02*	0.115E-01*	0.116E-01*	0.116E-01*	0.686E-02*
Aerosol Sulfate (ug/m3)	4.07*	3.91	4.12*	4.07*	4.00	3.44
Aerosol Nitrate (ug/m3)	0.00	0.00	0.00	0.00	0.00	3.03*
NH3 (ppm)	0.103E-02	0.169E-02	0.129E-02	0.342E-03	0.112E-02	0.862E-03
Ammonium Aerosol (ug/m3)	1.45*	1.39*	1.46*	1.41*	1.78*	2.18*
BSCAT (m-1)	0.270E-04	0.266E-04	0.271E-04	0.259E-04	0.268E-04	0.365E-04
Organic Aerosol (ug/m3)	0.168E-01*	0.169E-01*	0.194E-01*	0.167E-01*	0.981E-02*	0.812E-02*
OLEF (ppm)	0.308E-02*	0.308E-02*	0.302E-02*	0.309E-02*	0.290E-02*	0.274E-02*
CARB (ppm)	0.511E-02*	0.513E-02*	0.528E-02*	0.510E-02*	0.279E-02*	0.312E-02
PM10# (ug/m3)	18.5	17.2	18.8	18.5	17.9	17.3

* If the minimum concentration on day 1 was the initial concentration, then the second minimum value was used.

+ Winter simulation was for December 23, 1981.

# Water aerosol is included in the PM10 concentration.

TABLE 5-6. Minimum concentrations for the base case and sensitivity simulations for Columbus, Ohio, August 24, 1981 (Day 2, Midnight to 8pm).

Species	Base Case	50% SO2	50% NOX	50% NH3	50% RHC	Winter+
NO2 (ppm)	0.467E-02	0.465E-02	0.242E-02	0.467E-02	0.487E-02	0.320E-02
NO (ppm)	0.391E-05	0.386E-05	0.279E-05	0.383E-05	0.555E-05	0.991E-05
O3 (ppm)	0.186E-01	0.185E-01	0.229E-01	0.186E-01	0.141E-01	0.362E-05
HNO3 (ppm)	0.434E-03	0.407E-03	0.358E-03	0.196E-02	0.260E-02	0.139E-04
H2O2 (ppm)	0.897E-03	0.108E-02	0.129E-02	0.353E-02	0.520E-03	0.381E-04
SO2 (ppm)	0.124E-01	0.617E-02	0.125E-01	0.124E-01	0.123E-01	0.679E-02
Aerosol Sulfate (ug/m3)	9.84	6.08	8.69	9.86	9.27	3.66
Aerosol Nitrate (ug/m3)	0.00	0.00	0.00	0.336E-06	0.00	3.78
NH3 (ppm)	0.110E-02	0.185E-02	0.131E-02	0.315E-03	0.103E-02	0.734E-03
Ammonium Aerosol (ug/m3)	5.18	3.27	3.65	5.21	4.41	2.50
BSCAT (m-1)	0.864E-04	0.692E-04	0.655E-04	0.644E-04	0.764E-04	0.544E-04
Organic Aerosol (ug/m3)	0.412	0.393	0.364	0.392	0.329	0.109
OLEF (ppm)	0.353E-02	0.352E-02	0.415E-02	0.353E-02	0.351E-02	0.326E-02
CARB (ppm)	0.962E-02	0.963E-02	0.875E-02	0.962E-02	0.808E-02	0.271E-02
PM10# (ug/m3)	37.0	29.6	29.6	29.9	32.8	24.2

+ Winter simulation was for December 23, 1981.

Water aerosol is included in the PM10 concentration.

TABLE 5-7. Maximum concentrations for the base case and sensitivity simulations for Columbus, Ohio, August 23, 1981 (Day 1, 8am to Midnight).

Species	Base Case	50% SO2	50% NOX	50% NH3	50% RHC	Winter+
NO2 (ppm)	0.115E-01	0.115E-01	0.584E-02	0.115E-01	0.121E-01	0.127E-01
NO (ppm)	0.160E-02*	0.159E-02*	0.602E-03*	0.159E-02*	0.199E-02*	0.157E-02*
O3 (ppm)	0.785E-01	0.783E-01	0.682E-01	0.785E-01	0.660E-01	0.251E-01*
HNO3 (ppm)	0.306E-02	0.306E-02	0.147E-02*	0.305E-02	0.303E-02	0.883E-03*
H2O2 (ppm)	0.976E-03*	0.968E-03*	0.143E-02	0.976E-03*	0.706E-03*	0.157E-03
SO2 (ppm)	0.225E-01	0.112E-01	0.226E-01	0.225E-01	0.225E-01	0.201E-01
Aerosol Sulfate (ug/m3)	10.6	6.61	9.29	10.5	9.87	4.60
Aerosol Nitrate (ug/m3)	1.65	2.34	1.29	0.164E-03	1.56	4.53
NH3 (ppm)	0.261E-02*	0.274E-02*	0.326E-02*	0.707E-03*	0.263E-02*	0.283E-02*
Ammonium Aerosol (ug/m3)	4.31	3.07	3.38	3.57	4.05	2.91
BSCAT (m-1)	0.697E-04*	0.620E-04*	0.583E-04*	0.611E-04*	0.680E-04*	0.520E-04*
Organic Aerosol (ug/m3)	0.374	0.374	0.346	0.373	0.314	0.117
OLEF (ppm)	0.120E-01	0.120E-01	0.125E-01	0.120E-01	0.121E-01	0.138E-01
CARB (ppm)	0.129E-01	0.129E-01	0.119E-01	0.129E-01	0.107E-01	0.616E-02
PM10# (ug/m3)	31.3	26.9	27.4	28.8	30.2	24.2

* If the maximum concentration on day 1 was the initial condition, then the second maximum value was used.

+ Winter simulation was for December 23, 1981.

# Water aerosol is included in the PM10 concentration.

TABLE 5-8. Maximum concentrations for the base case and sensitivity simulations for Columbus, Ohio, August 24, 1981 (Day 2, Midnight to 8pm).

Species	Base Case	50% SO2	50% NOX	50% NH3	50% RHC	Winter+
NO2 (ppm)	0.215E-01	0.215E-01	0.102E-01	0.215E-01	0.232E-01	0.153E-01
NO (ppm)	0.244E-02	0.244E-02	0.107E-02	0.244E-02	0.324E-02	0.111E-01
O3 (ppm)	0.106	0.106	0.874E-01	0.106	0.948E-01	0.245E-01
HNO3 (ppm)	0.648E-02	0.627E-02	0.338E-02	0.613E-02	0.598E-02	0.119E-02
H2O2 (ppm)	0.170E-02	0.168E-02	0.237E-02	0.169E-02	0.116E-02	0.367E-03
SO2 (ppm)	0.421E-01	0.210E-01	0.422E-01	0.420E-01	0.421E-01	0.292E-01
Aerosol Sulfate (ug/m3)	17.3	9.47	14.8	17.5	16.8	5.58
Aerosol Nitrate (ug/m3)	11.9	12.3	6.78	5.28	8.88	4.84
NH3 (ppm)	0.399E-02	0.429E-02	0.514E-02	0.119E-02	0.494E-02	0.481E-02
Ammonium Aerosol (ug/m3)	7.52	6.14	5.54	5.21	6.60	3.42
BSCAT (m-1)	0.140E-03	0.127E-03	0.112E-03	0.106E-03	0.125E-03	0.712E-04
Organic Aerosol (ug/m3)	0.738	0.734	0.715	0.745	0.629	0.167
OLEF (ppm)	0.236E-01	0.236E-01	0.236E-01	0.236E-01	0.242E-01	0.218E-01
CARB (ppm)	0.267E-01	0.268E-01	0.251E-01	0.267E-01	0.216E-01	0.687E-02
PM10# (ug/m3)	57.7	50.8	47.8	46.2	51.5	30.0

+ Winter simulation was for December 24, 1981.

Water aerosol is included in the PM10 concentration.

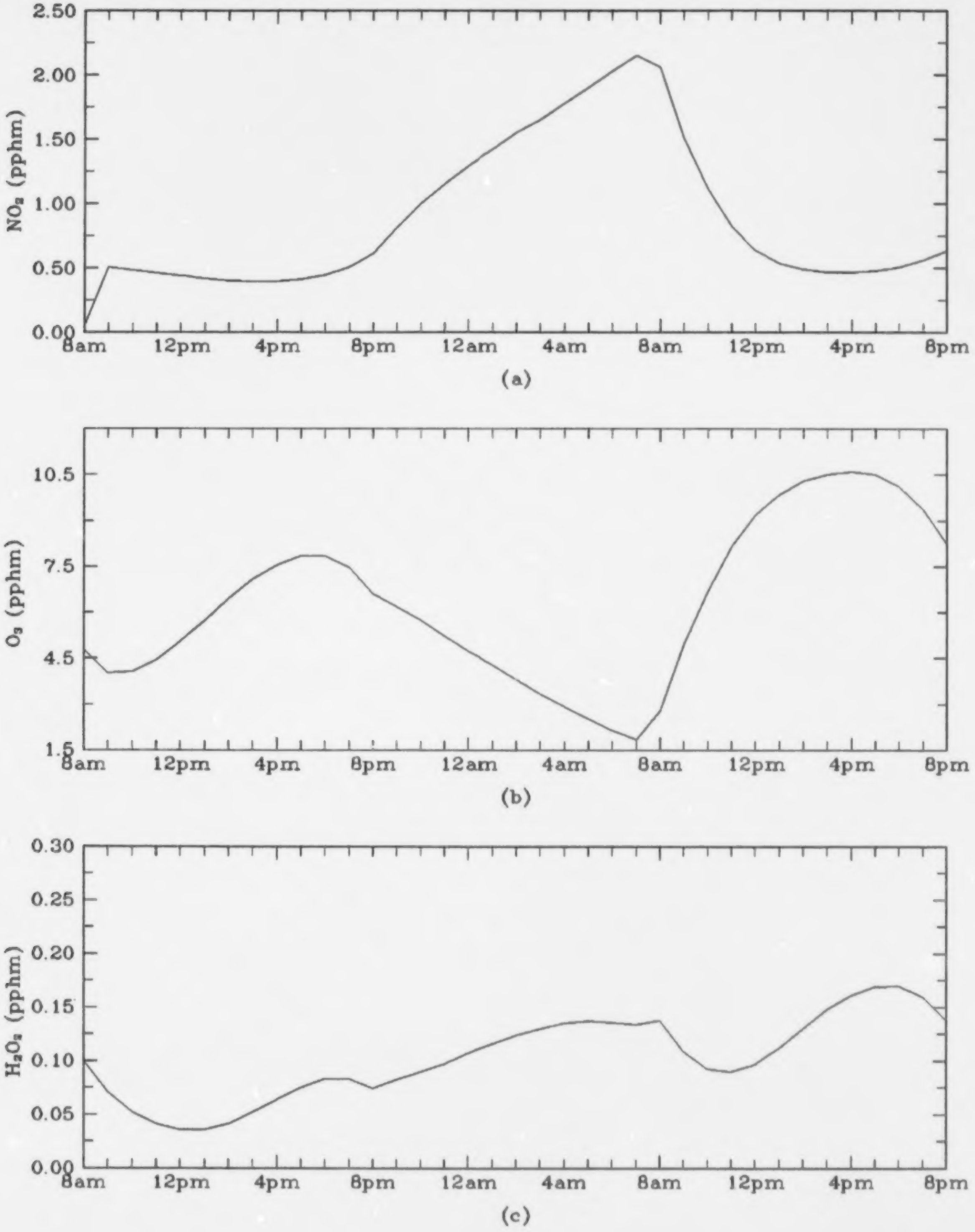

Figure 5–2. Concentrations of major chemical species for the Columbus, Ohio base case, August 23–24, 1981.

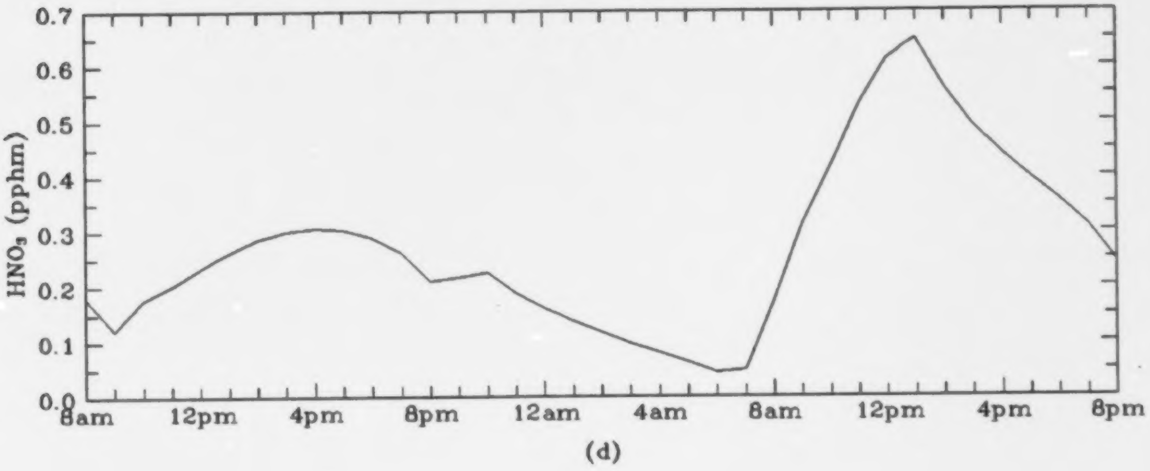

(d)

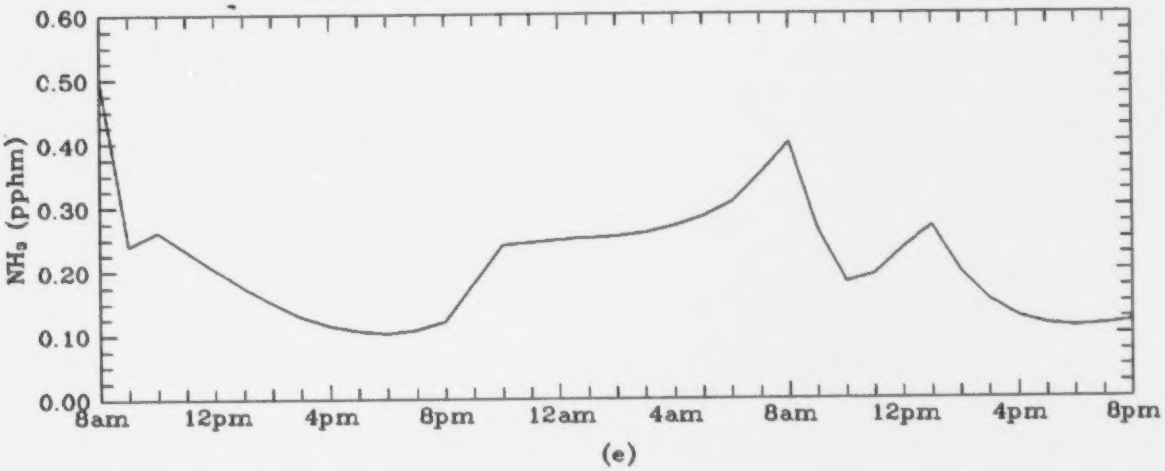

(e)

Figure 5-2 (concluded).

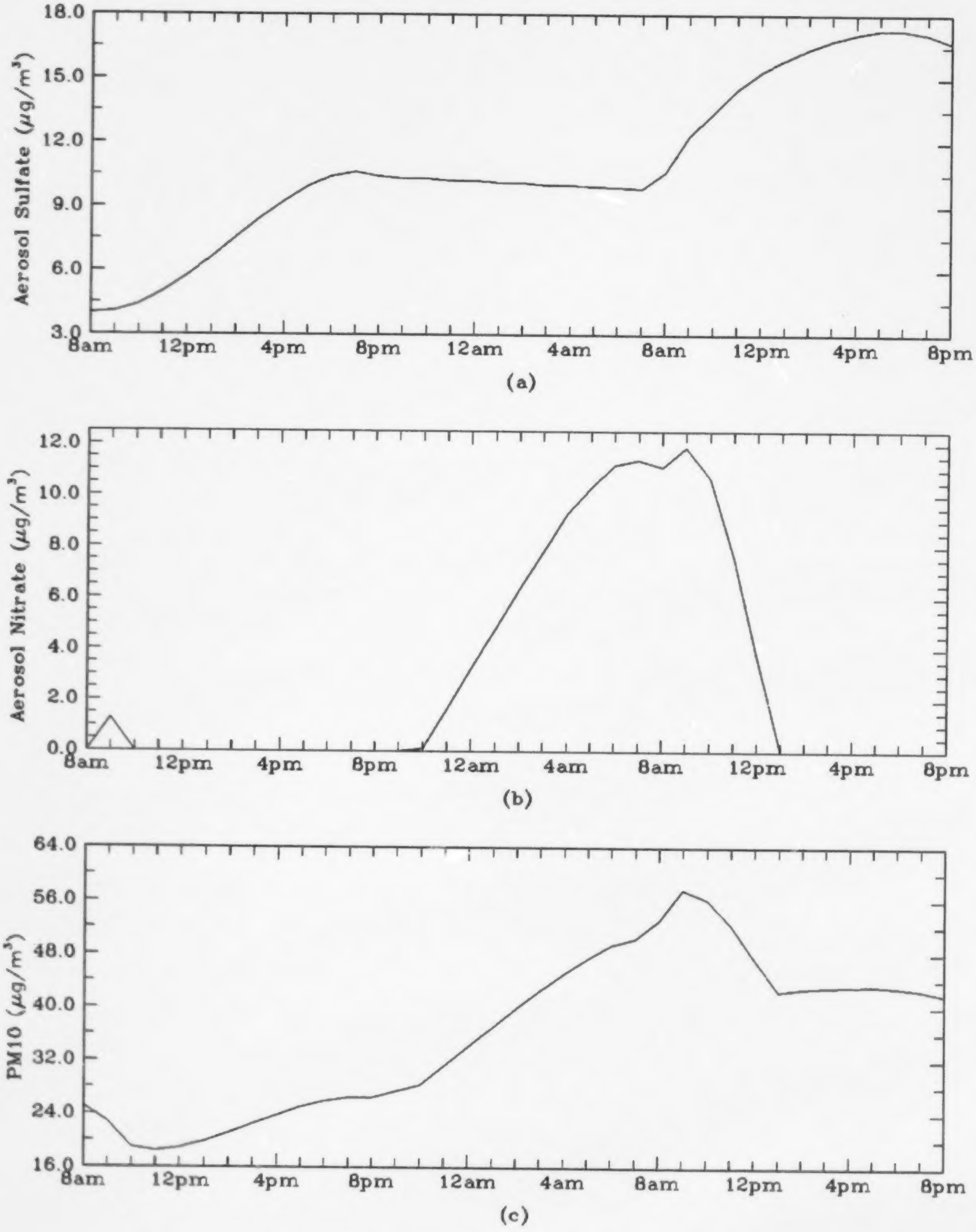

Figure 5–3. Concentrations of major aerosol species for the Columbus, Ohio base case, August 23–24, 1981. (PM10 includes water aerosol).

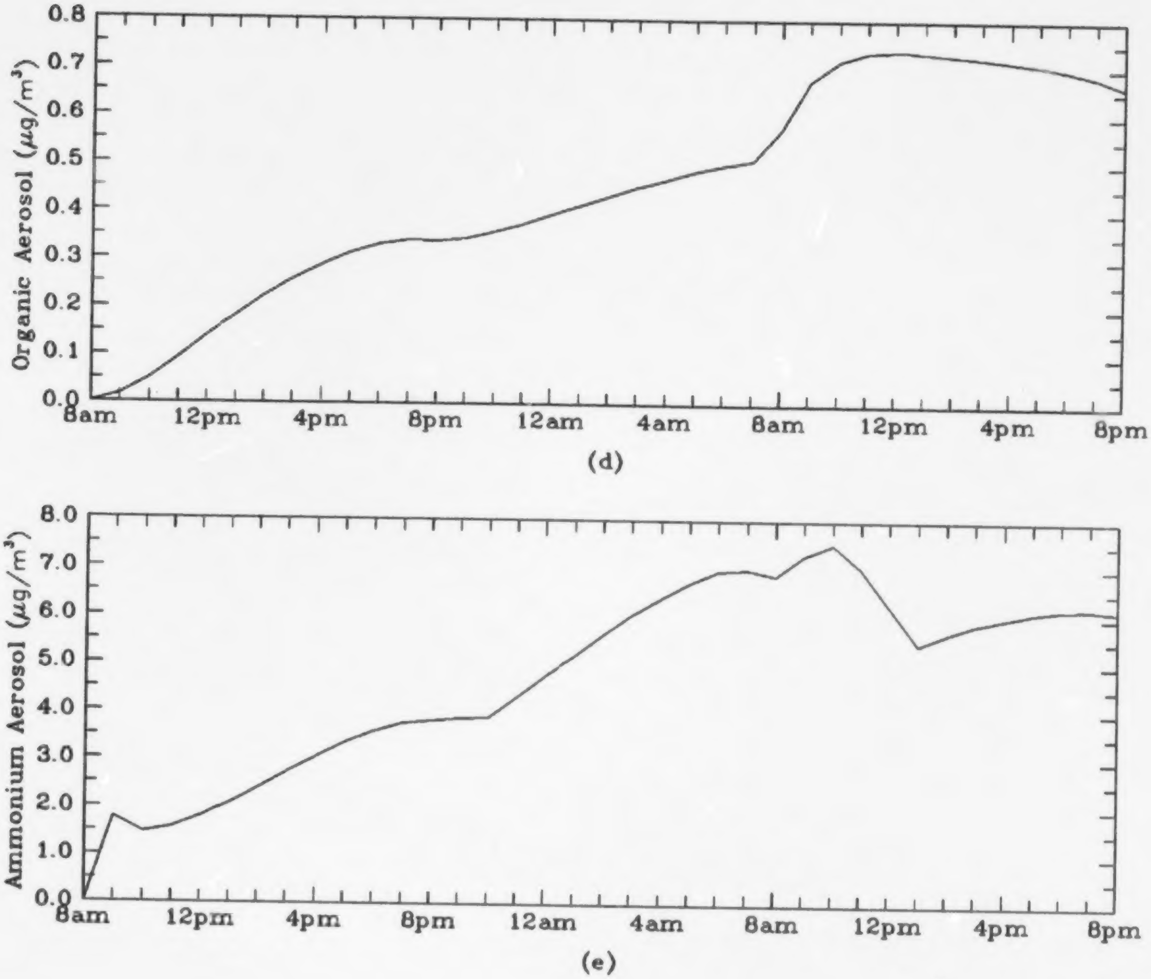

Figure 5–3 (concluded).

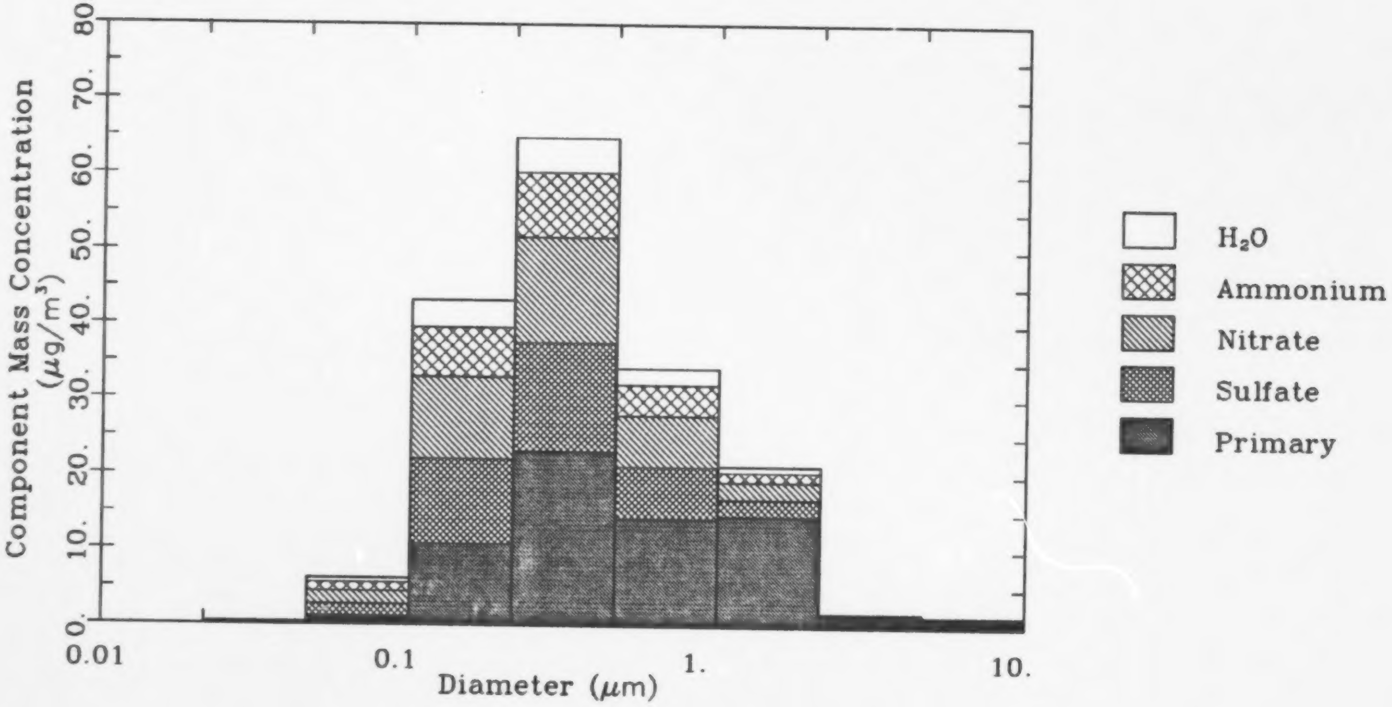

Figure 5–4(a). Size distributed chemical composition of the aerosol for the Columbus, Ohio base case at the time of the maximum aerosol nitrate and PM10 concentrations on the second day of the simulation. (August 24, 1981, 9am).

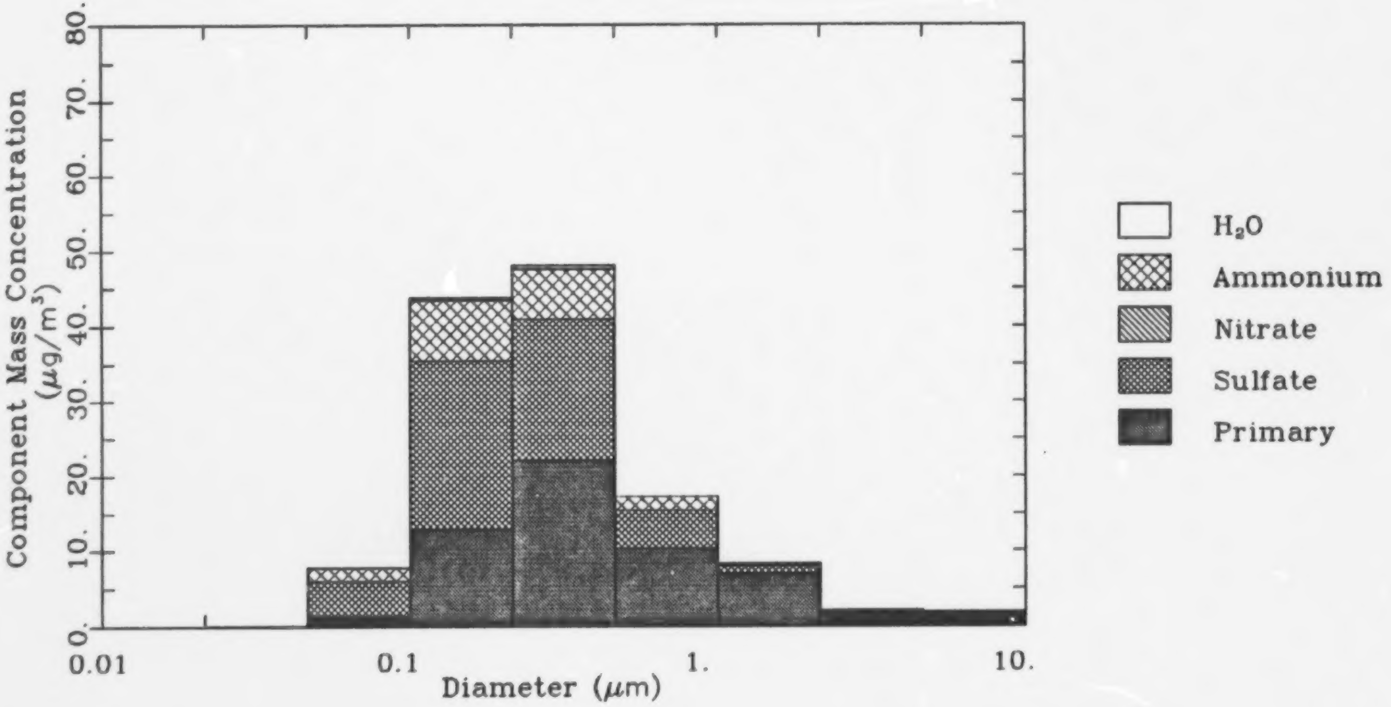

Figure 5–4(b). Size distributed chemical composition of the aerosol for the Columbus, Ohio base case at the time of the maximum aerosol sulfate concentration on the second day of the simulation. (August 24, 1981, 6pm).

PM10 (which includes the water aerosol) is shown in Figure 5-4(a) and (b). As the figure indicates, the peak in the aerosol size distribution is midway between 0.1 μm and 1 μm.

50 Percent SO_2 Reduction--Columbus, Ohio

The first sensitivity study examined the effect of decreasing the SO_2 emissions and initial concentrations by 50 percent. The results of this study are shown in the second column in Tables 5-5 through 5-8, and in Figures 5-5 through 5-7. The maximum and minimum values of SO_2 for the 50 percent SO_2 reduction case are approximately half those for the base case. The change in maximum and minimum aerosol sulfate values varies from 3 percent to 45 percent of the base case values (Tables 5-5 through 5-8 and Figure 5-6(a)). Comparison of Figures 5-4(b) and 5-7(b) at the time of the maximum aerosol sulfate concentration on the second day shows that the largest absolute decreases in aerosol sulfate volume occurred in the fourth and fifth sections of the aerosol size distribution.

The decrease in the aerosol sulfate concentration is also noted in Figure 5-7(a) and (b). The decrease occurred earlier in the day at the time of maximum aerosol nitrate and PM10 concentrations. There is no noticeable difference in the concentrations of NO_2, O_3, or H_2O_2 (Figure 5-5 a-c) since SO_2 does not significantly affect oxidant chemistry. However, the aerosol nitrate concentration does show a slight increase from the base case (Figure 5-6(b)) because the decrease in ammonium sulfate levels produces an increase in ammonia availability.

50 Percent NO_x Reduction--Columbus, Ohio

Results for the case study in which the nitrogen oxides (NO_x) emissions and initial concentrations were reduced by 50 percent are presented in the third column of Tables 5-5 through 5-7 and in Figures 5-8 through 5-10. The lower NO_x concentration affects not only the gas-phase species but also the aerosol species. Lower NO_x concentrations result in a slight increase in sulfate formation for the first five hours of the simulation, as shown in Figure 5-9(a). Lower NO_x concentrations yield lower ozone concentrations (except for the first five hours of simulation, when the NO titration effect occurs, i.e., less ozone is consumed by NO). Since the hydrocarbon concentrations are high enough, lower NO concentrations result in a slower ozone formation rate, and hence lower ozone concentrations. Consequently, the SO_2 oxidation rates are lower, and there is less sulfate formation (Figure 5-9(a)). The aerosol nitrate (AERN) concentration decreases when the NO_x emissions and initial concentrations are decreased

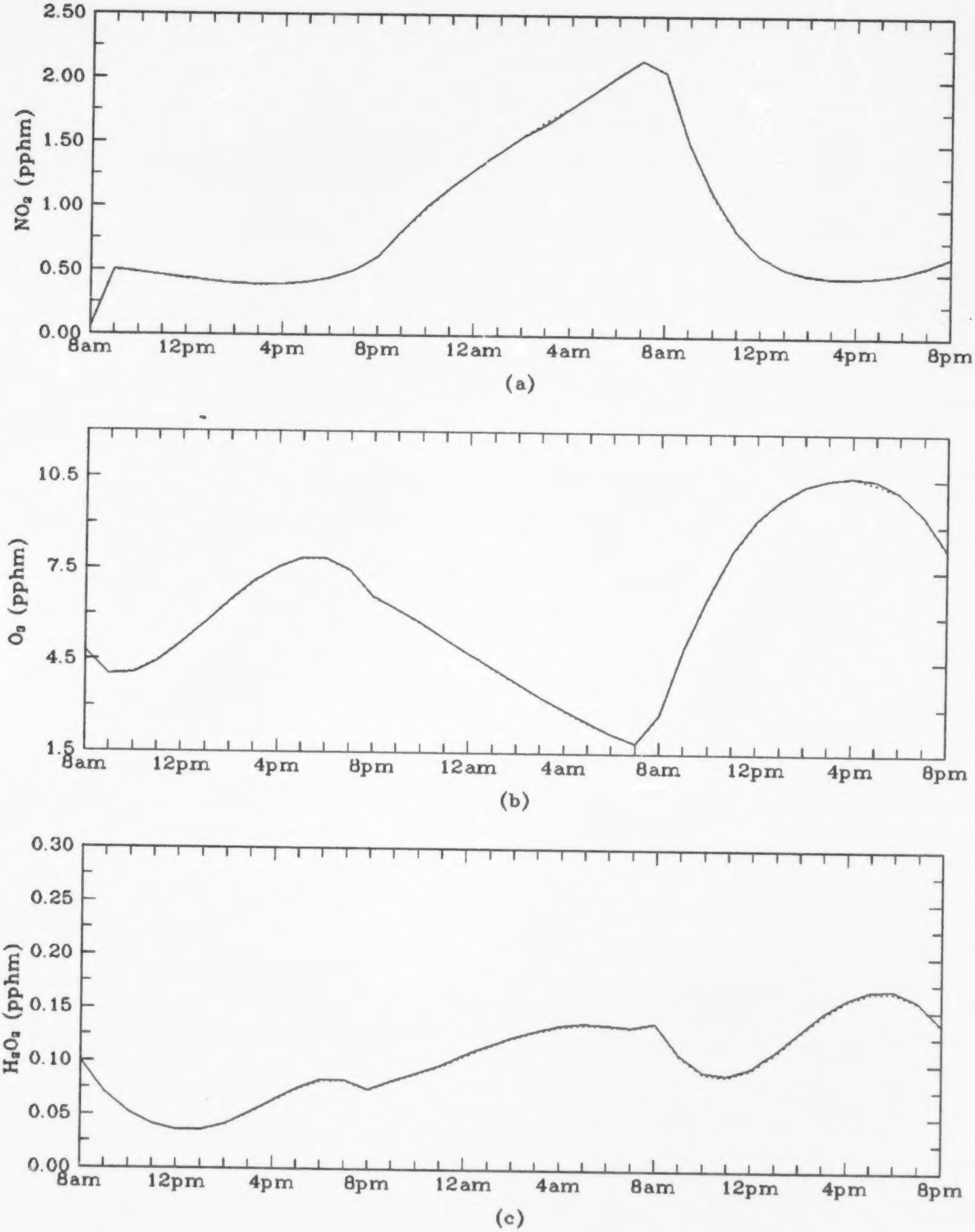

Figure 5-5. Concentrations of major chemical species for the Columbus, Ohio base case (———) and 50% SO_2 reduction (.....) simulations for August 23-24, 1981

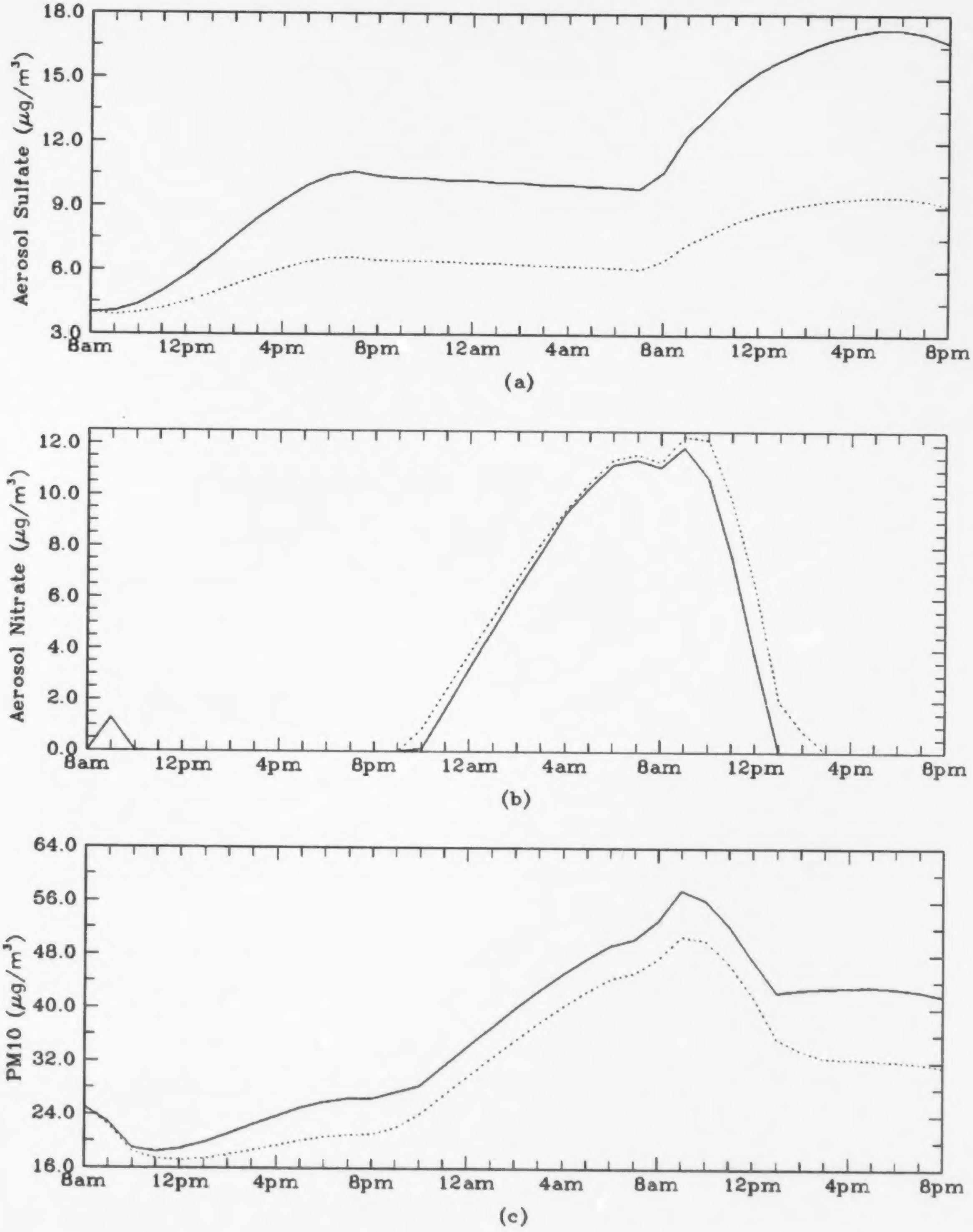

Figure 5-6. Concentrations of major aerosol species for the Columbus, Ohio base case (———) and 50% SO_2 reduction (.....) simulations for August 23-24, 1981. (PM10 includes water aerosol).

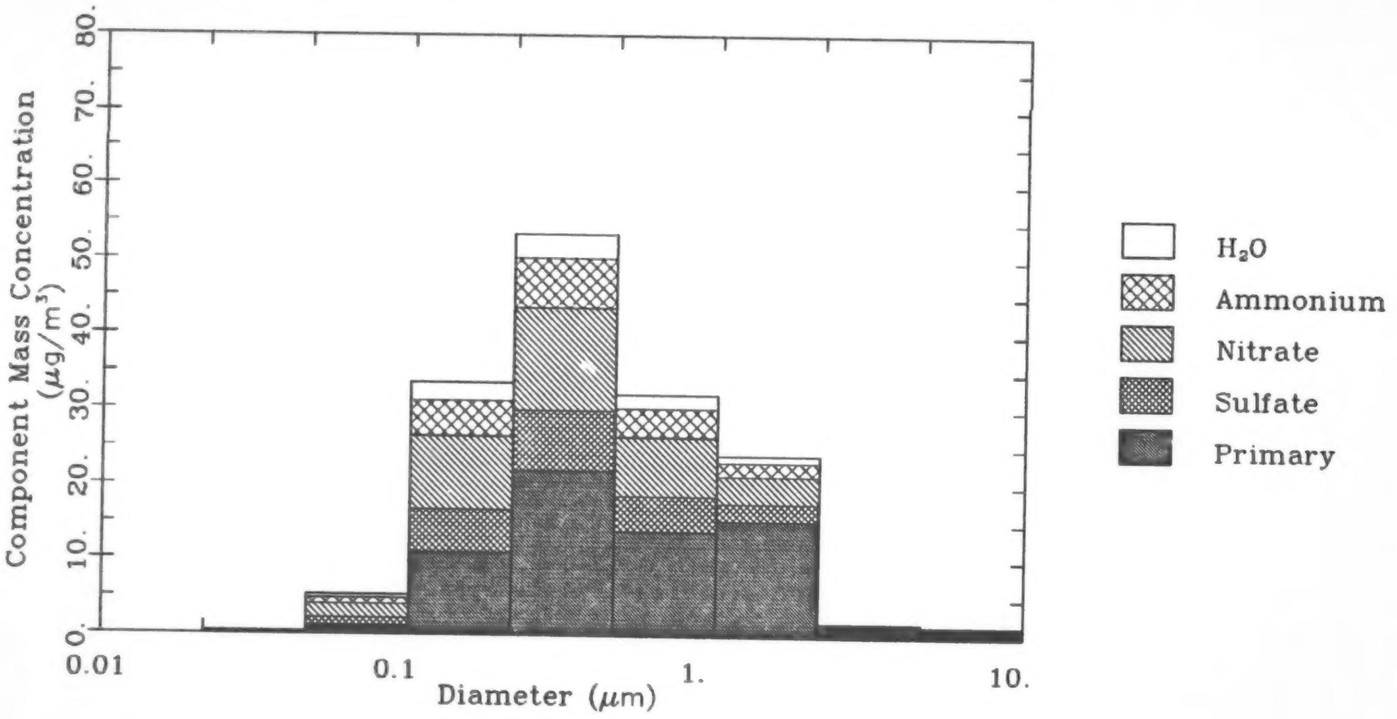

Figure 5–7(a). Size distributed chemical composition of the aerosol for the Columbus, Ohio 50% SO_2 reduction case at the time of the maximum aerosol nitrate and PM10 concentrations on the second day of the simulation. (August 24, 1981, 9am).

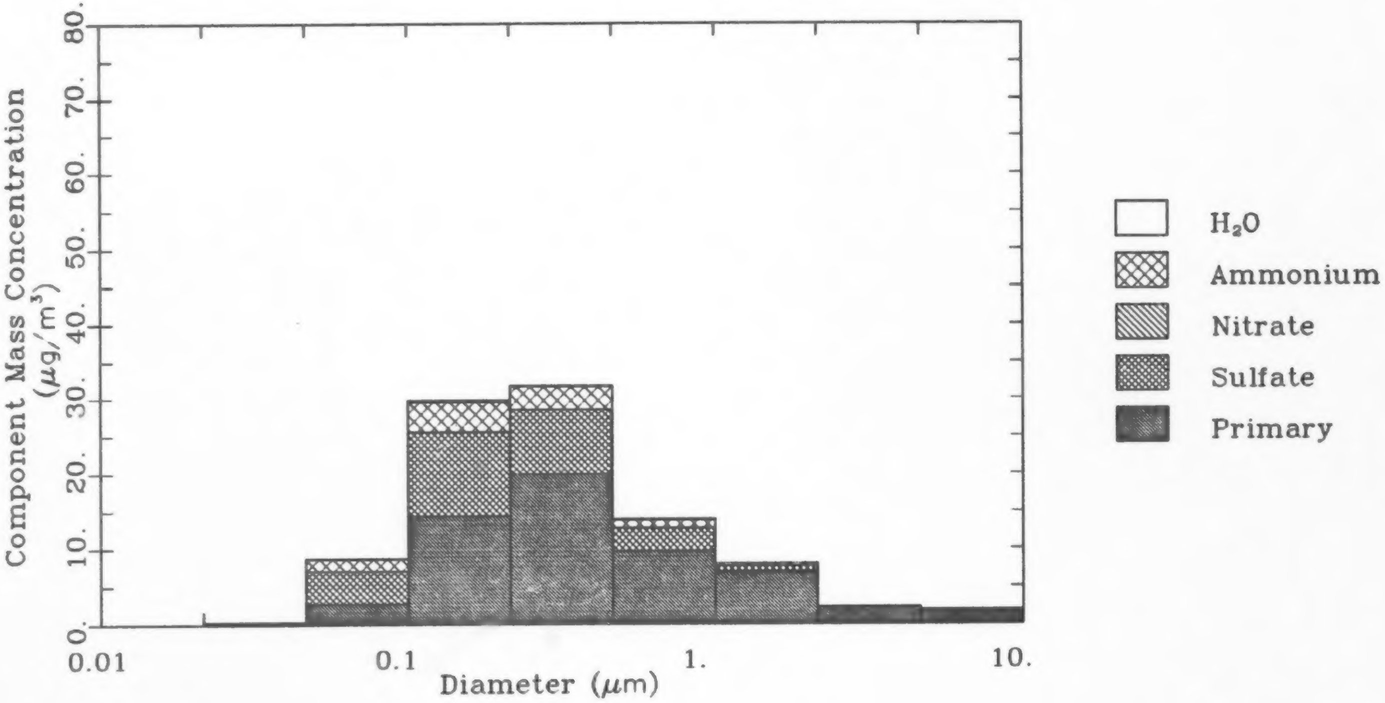

Figure 5–7(b). Size distributed chemical composition of the aerosol for the Columbus, Ohio 50% SO_2 reduction case at the time of the maximum aerosol sulfate concentration on the second day of the simulation. (August 24, 1981, 5pm).

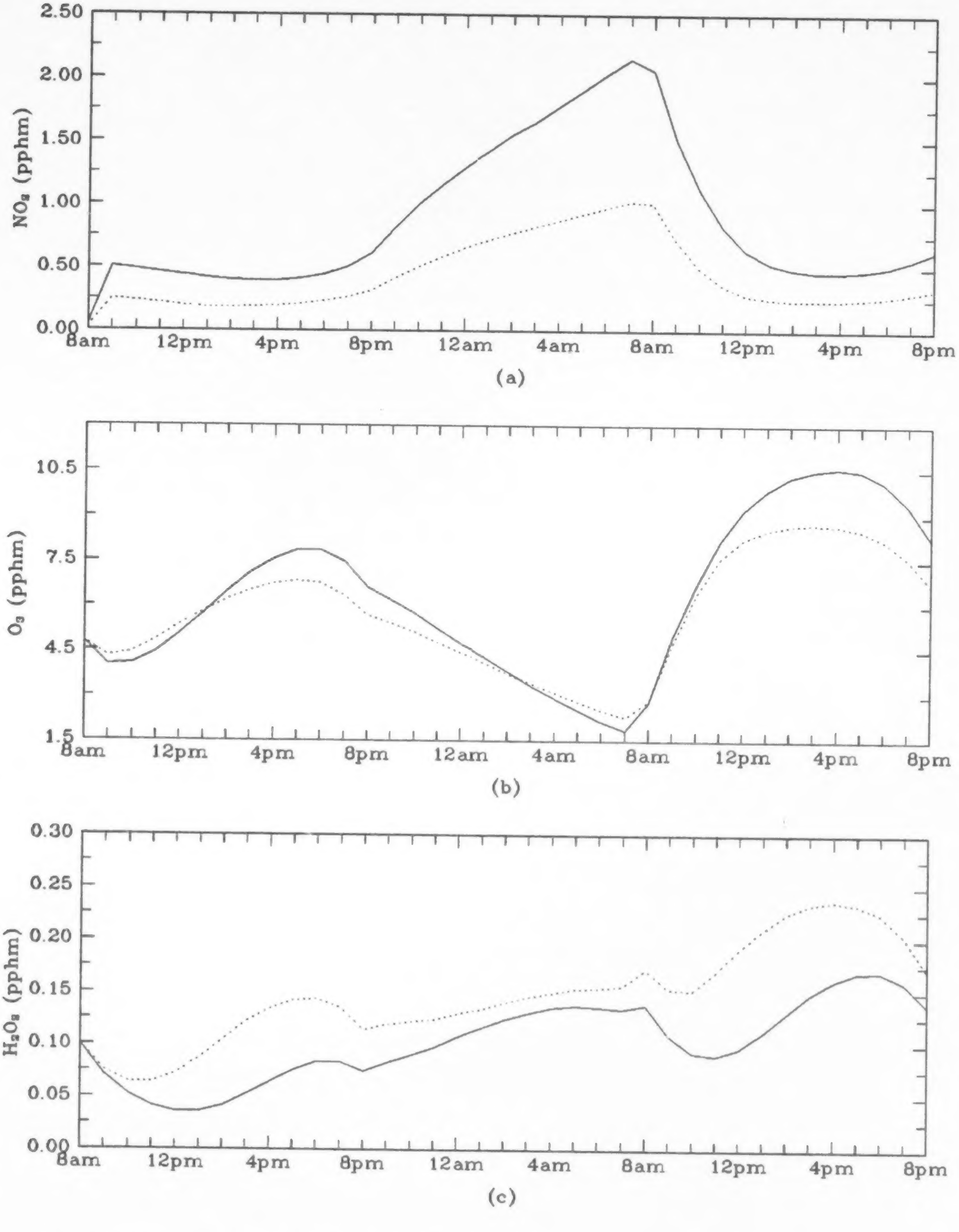

Figure 5–8. Concentrations of major chemical species for the Columbus, Ohio base case (——) and 50% NO$_x$ reduction (.....) simulations for August 23–24, 1981

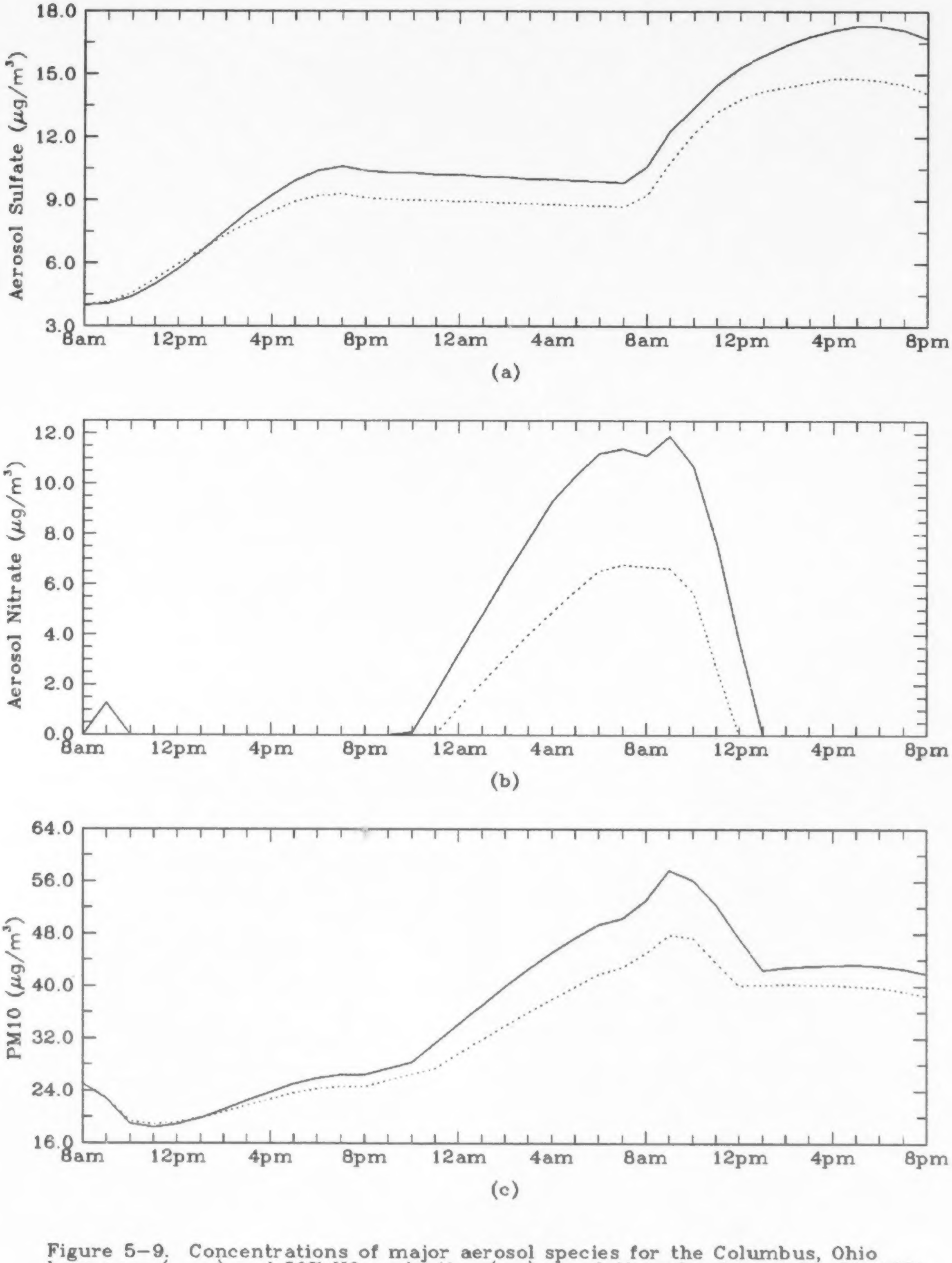

Figure 5-9. Concentrations of major aerosol species for the Columbus, Ohio base case (——) and 50% NO_x reduction (.....) simulations for August 23-24, 1981. (PM10 includes water aerosol).

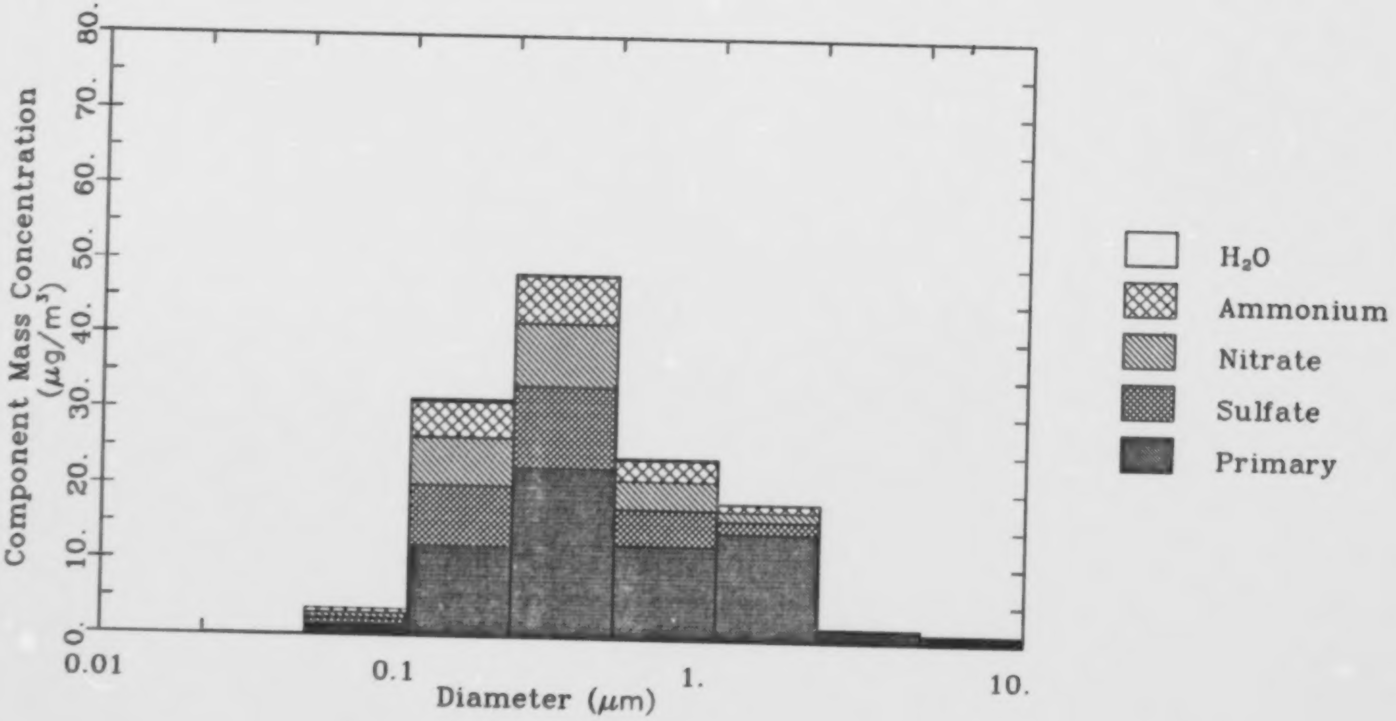

Figure 5-10(a). Size distributed chemical composition of the aerosol for the Columbus, Ohio 50% NO_x reduction case at the time of the maximum aerosol nitrate concentration on the second day of the simulation. (August 24, 1981, 7am).

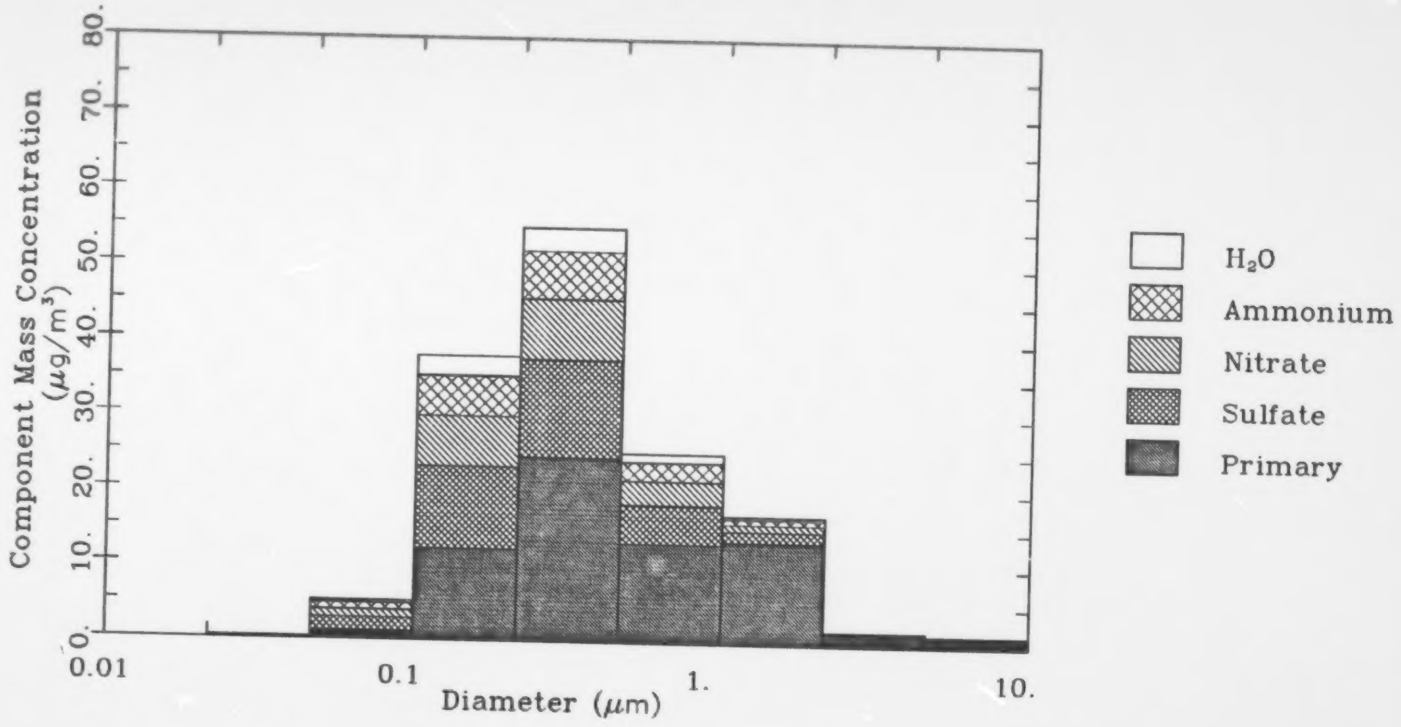

Figure 5–10(b). Size distributed chemical composition of the aerosol for the Columbus, Ohio 50% NO$_x$ reduction case at the time of the maximum PM10 concentration on the second day of the simulation. (August 24, 1981, 9am).

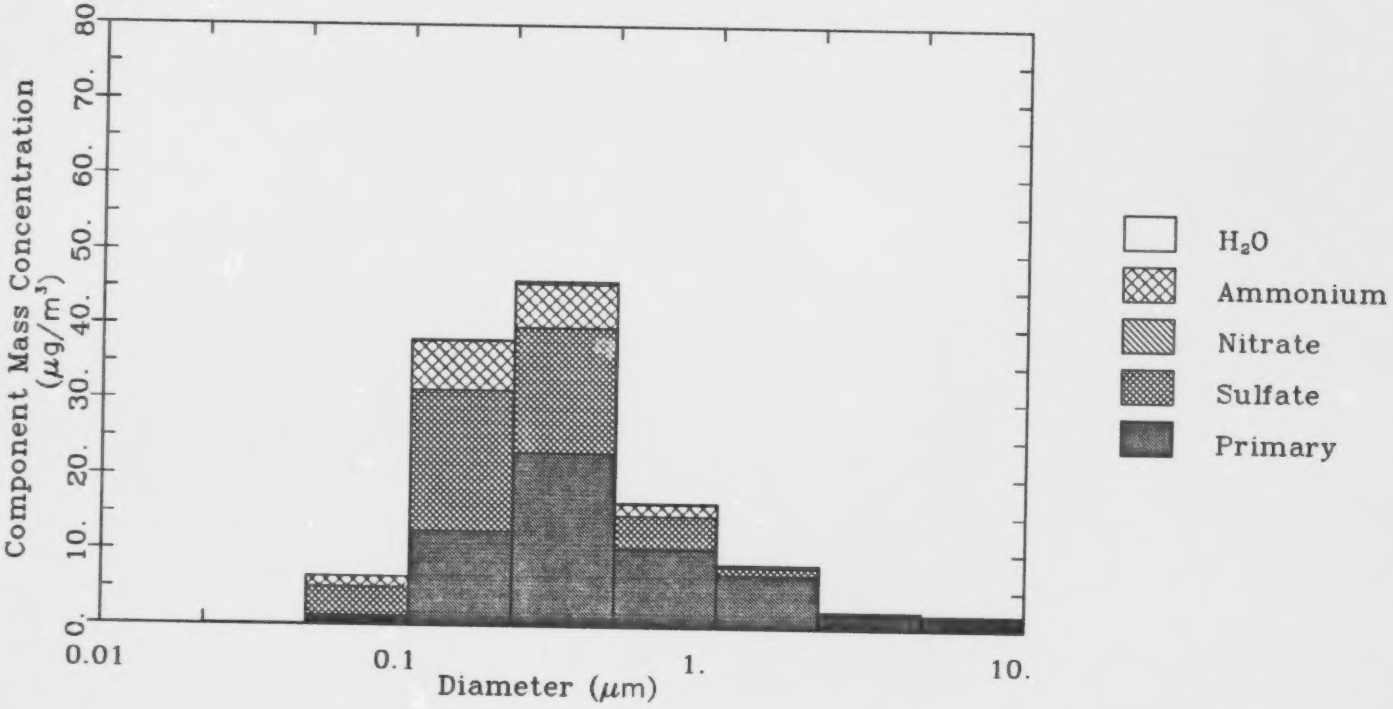

Figure 5-10(c). Size distributed chemical composition of the aerosol for the Columbus, Ohio 50% NO_x reduction case at the time of the maximum aerosol sulfate concentration on the second day of the simulation. (August 24, 1981, 5pm).

(Figure 5-9(b), Figure 5-10, and Figure 5-4). The H_2O_2 concentration is also affected by the decrease in NO_x (Figure 5-8(c)). As the NO_2 concentration increases, the rate of H_2O_2 formation increases, and higher H_2O_2 concentrations result.

50 Percent NH_3 Reduction--Columbus, Ohio

Results for the case study in which the NH_3 emissions and initial concentrations were reduced by 50 percent are presented in the fourth column of Tables 5-5 through 5-7 and in Figures 5-11 through 5-13. The gas-phase species shown in Figure 5-11 (a-c) are not affected by the NH_3 decrease since NH_3 does not affect oxidant formation. The aerosol sulfate concentration is not affected either (Figure 5-12(c), Figure 5-13, and Figure 5-4). Examination of Figure 5-12(b) and comparison of Figures 5-4 and 5-13 show that the aerosol nitrate concentration decreases because of the decrease in the ammonium nitrate concentration, which results from less ammonia being available for reaction. The ammonium nitrate saturation vapor pressure is more sensitive to the ammonia gas-phase concentration than is the ammonium sulfate saturation vapor pressure.

50 Percent RHC Reduction--Columbus, Ohio

Results for the case study in which the reactive hydrocarbon (RHC) emissions and initial concentrations were reduced by 50 percent are shown in the fifth column in Tables 5-5 through 5-8 and in Figures 5-14 through 5-16. As can be seen from these tables and figures, the lower hydrocarbon levels result in lower O_3, H_2O_2, aerosol sulfate, aerosol nitrate, and PM10 levels. The NO_2 concentrations, on the other hand, increase slightly. These results show that reducing RHC emissions is very effective in reducing both oxidant and aerosol levels. Lower oxidant levels lead to slower rates of SO_2 and NO_2 oxidation, and, consequently, to lower levels of sulfate and nitrate.

Winter Simulation--Columbus, Ohio

For the winter simulation, the date was changed from 23-24 August to 23-24 December. The initial concentration of H_2O_2 was decreased from 1×10^{-3} ppm to 5×10^{-5} ppm, and that of O_3 from 4.8×10^{-2} ppm to 2.6×10^{-2} ppm. The temperature was assumed to vary between 10°C at noon to a minimum value of 2.5° at night. The mixing height was decreased from 1500 meters to 800 meters, and the daylight period was shortened. Results for

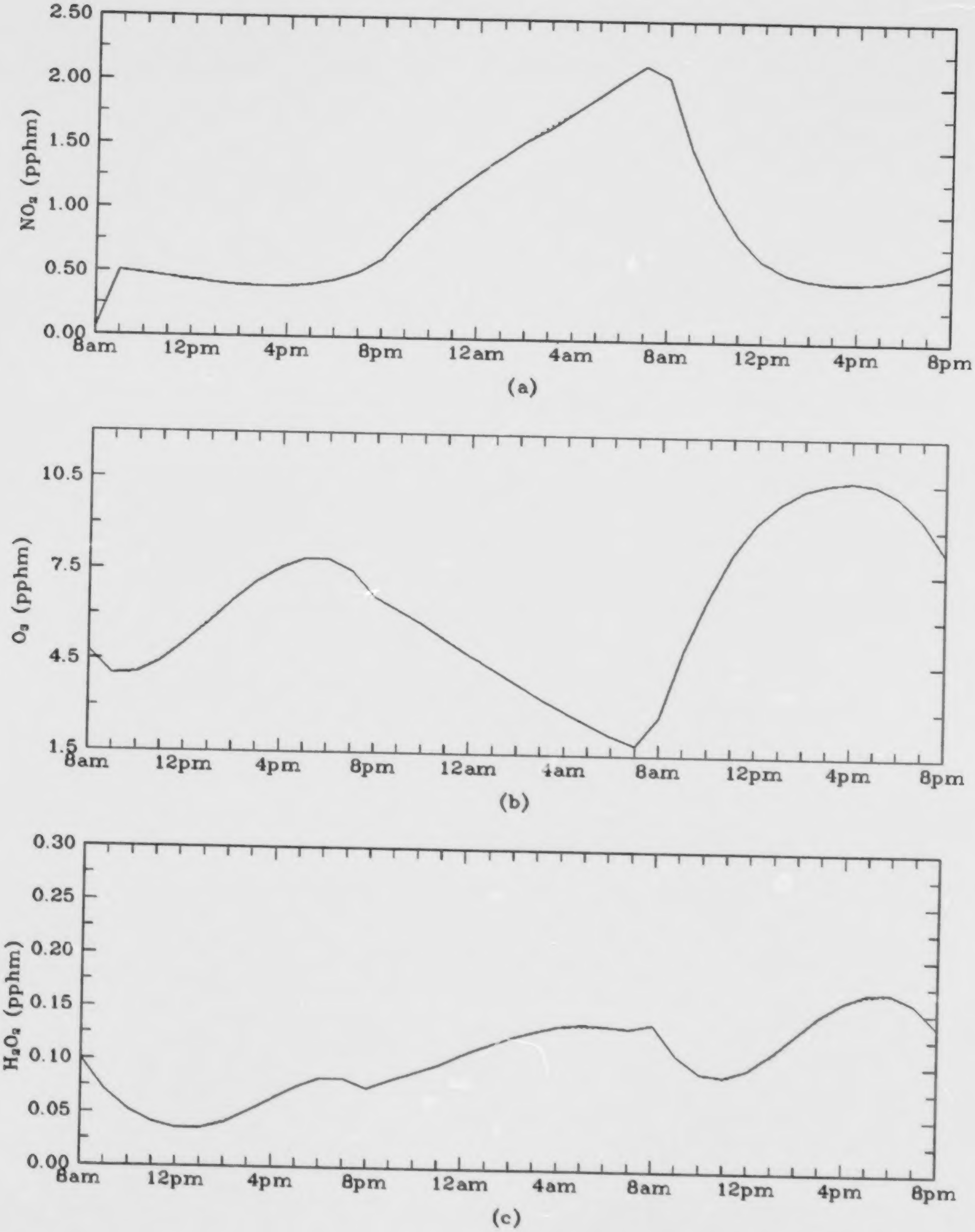

Figure 5-11. Concentrations of major chemical species for the Columbus, Ohio base case (——) and 50% NH$_3$ reduction (.....) simulations for August 23-24, 1981

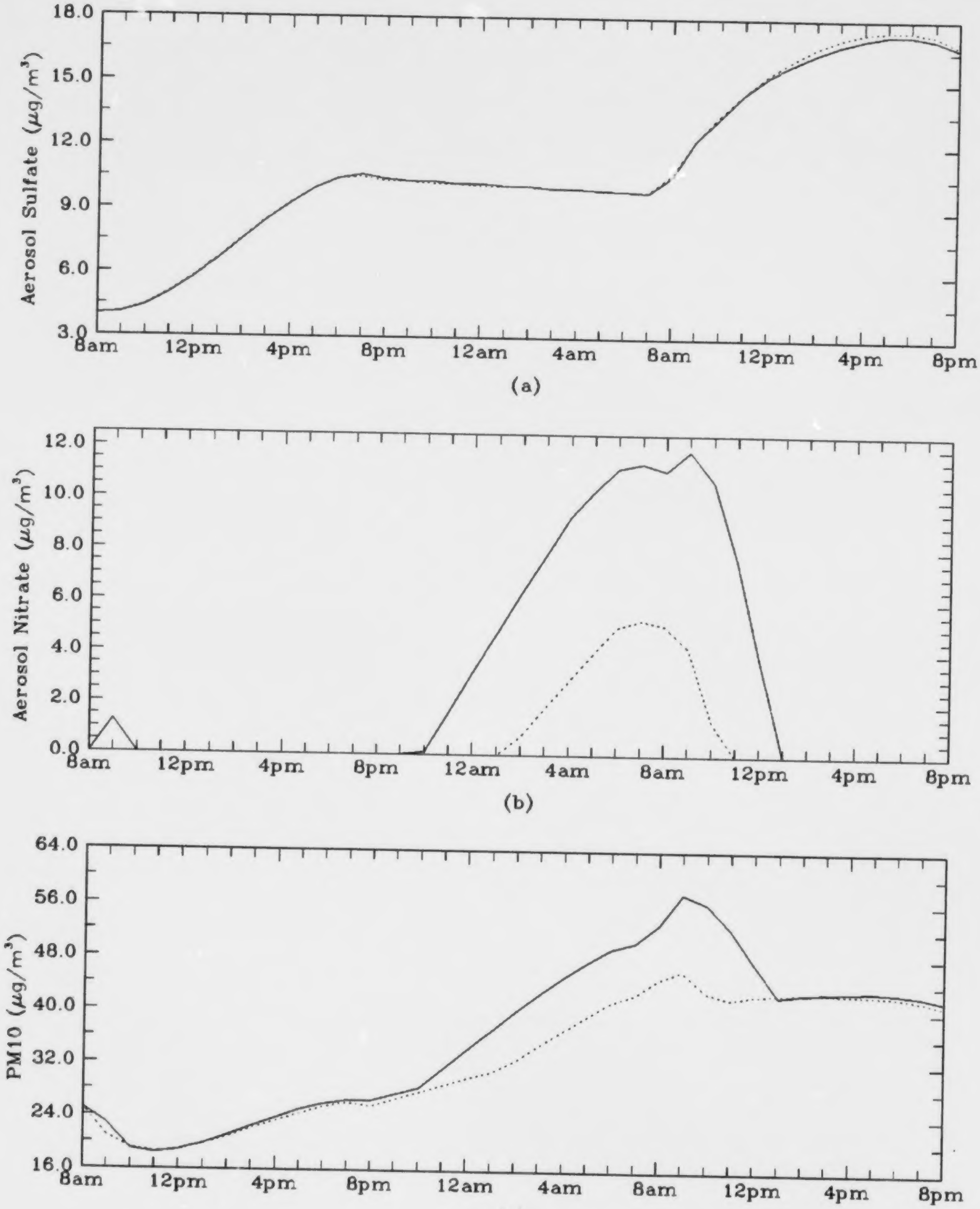

(a)

(b)

(c)

Figure 5-12. Concentrations of major aerosol species for the Columbus, Ohio base case (_____) and 50% NH_3 reduction (.....) simulations for August 23-24, 1981. (PM10 includes water aerosol).

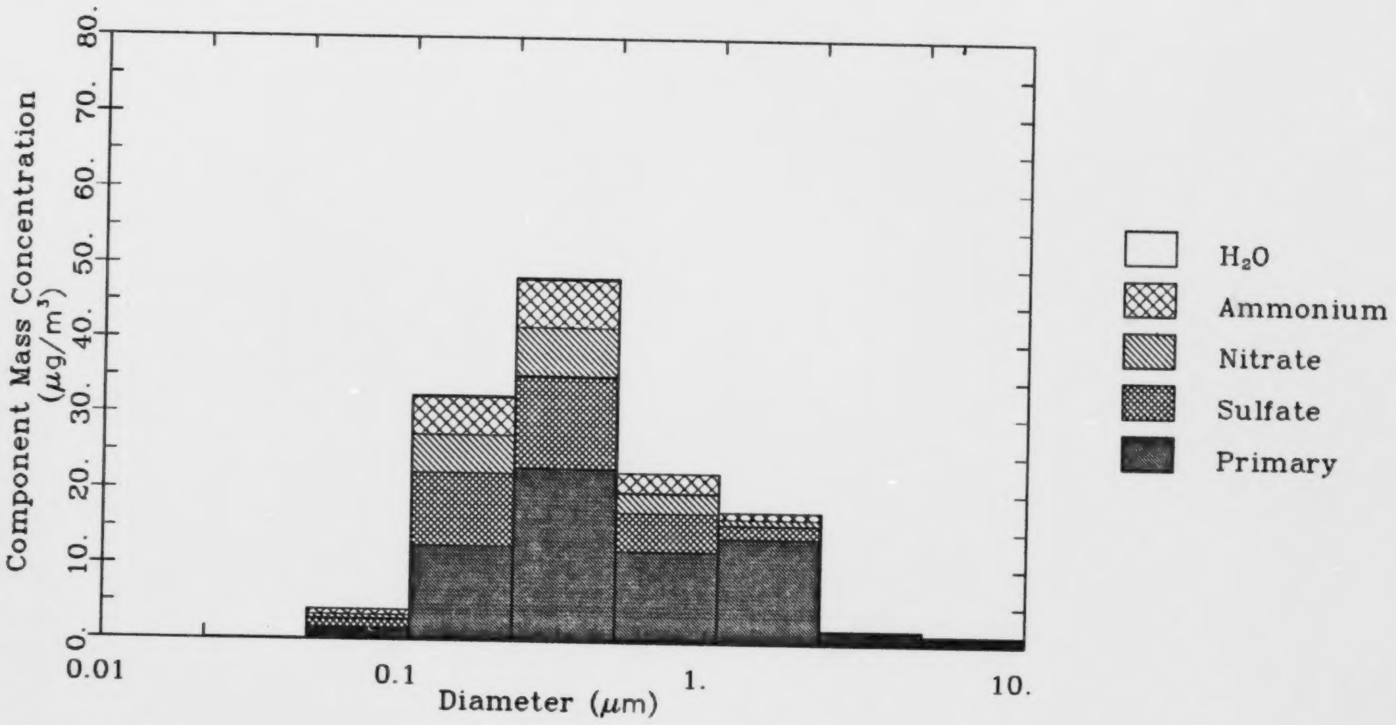

Figure 5–13(a). Size distributed chemical composition of the aerosol for the Columbus, Ohio 50% NH_3 reduction case at the time of the maximum aerosol nitrate concentration on the second day of the simulation. (August 24, 1981, 7am).

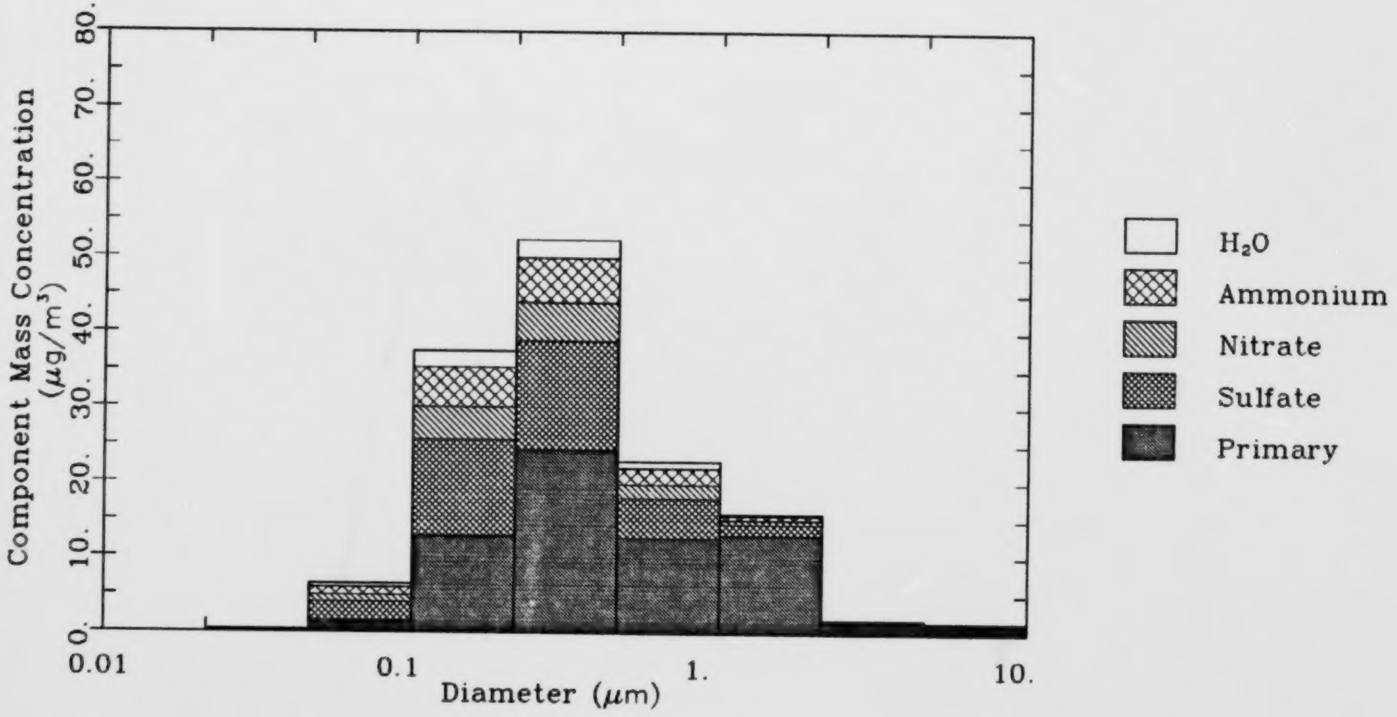

Figure 5–13(b). Size distributed chemical composition of the aerosol for the Columbus, Ohio 50% NH_3 reduction case at the time of the maximum PM10 concentration on the second day of the simulation. (August 24, 1981, 9am).

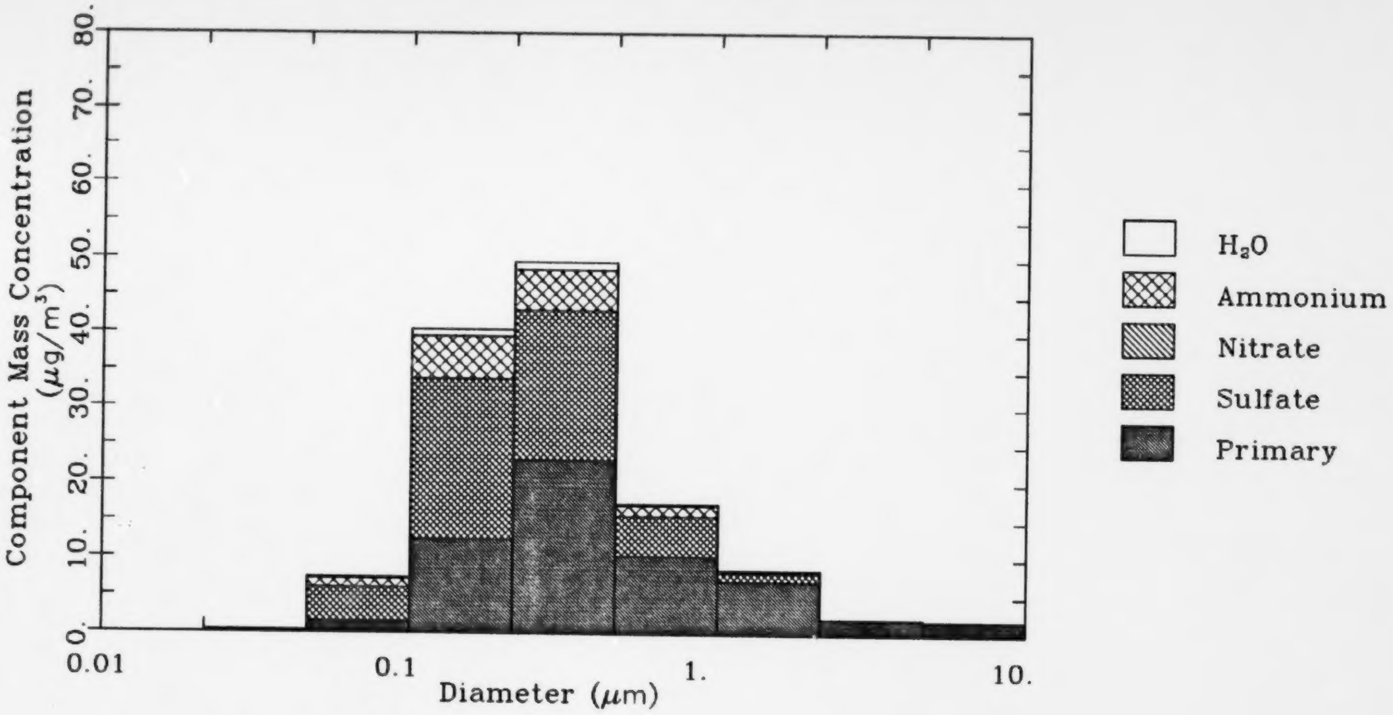

Figure 5–13(c). Size distributed chemical composition of the aerosol for the Columbus, Ohio 50% NO_x reduction case at the time of the maximum aerosol sulfate concentration on the second day of the simulation. (August 24, 1981, 6pm).

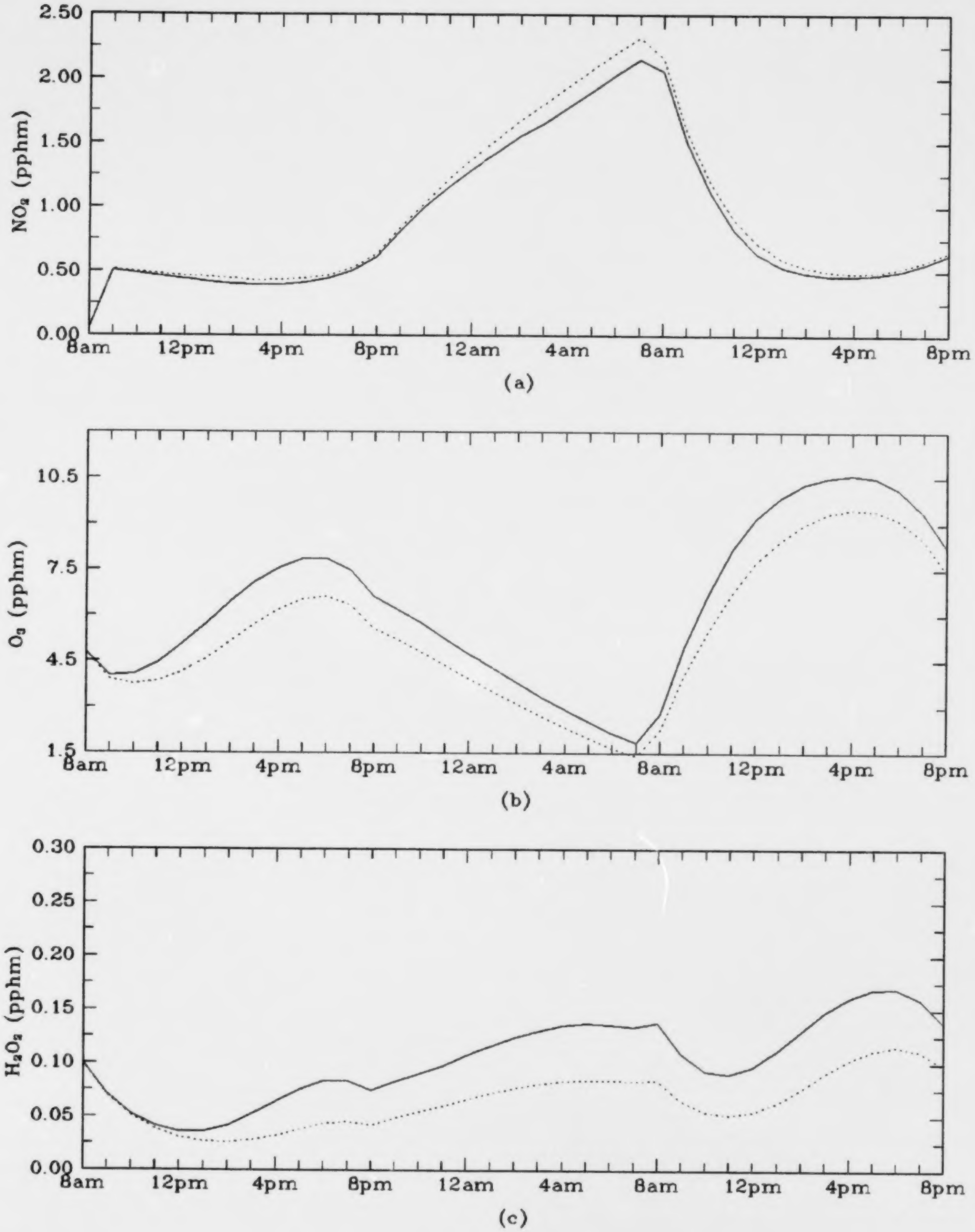

Figure 5–14. Concentrations of major chemical species for the Columbus, Ohio base case (——) and 50% reactive hydrocarbon reduction (.....) simulations for August 23–24, 1981.

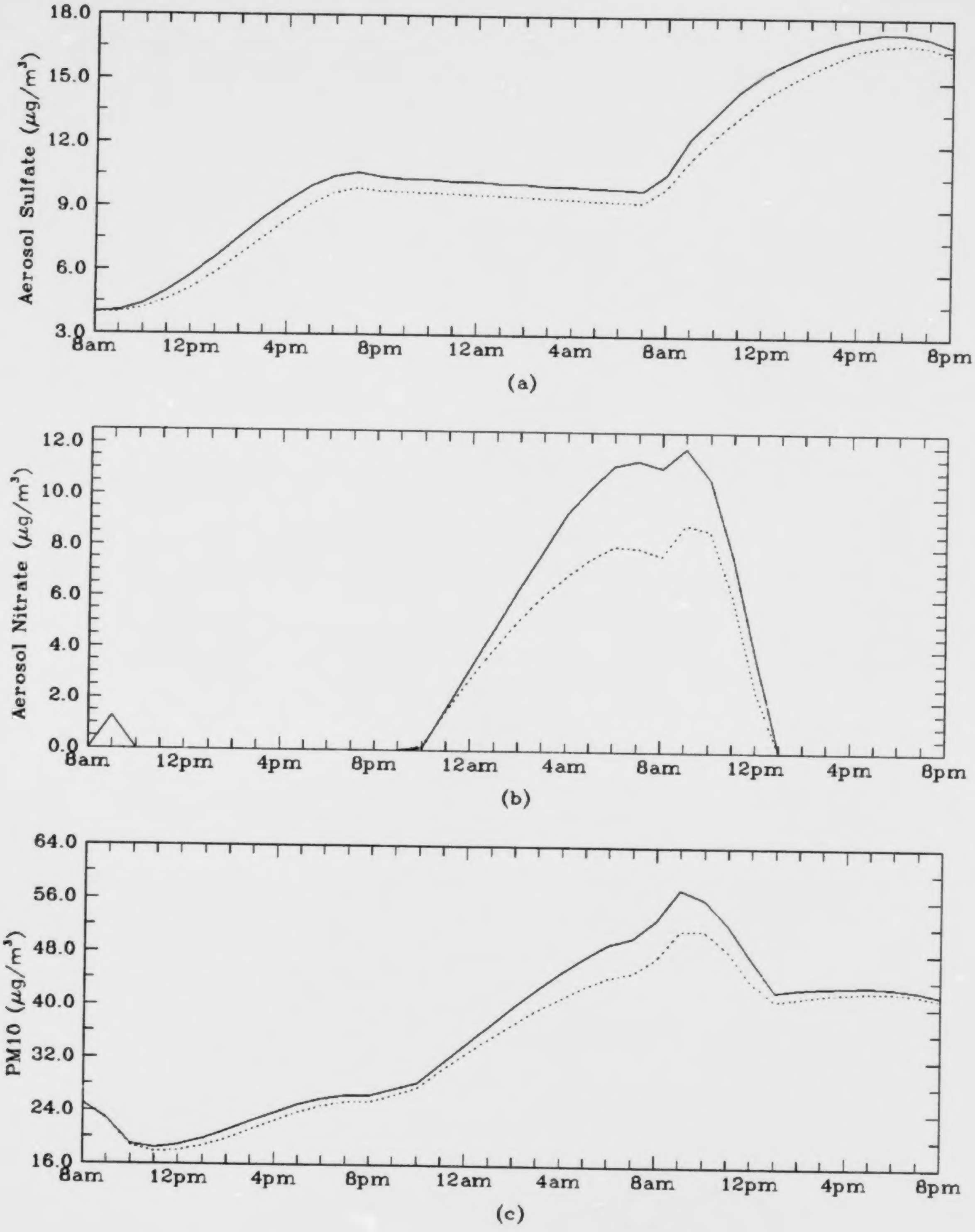

Figure 5–15. Concentrations of major aerosol species for the Columbus, Ohio base case (——) and 50% reactive hydrocarbon reduction (.....) simulations for August 23–24, 1981. (PM10 includes water aerosol).

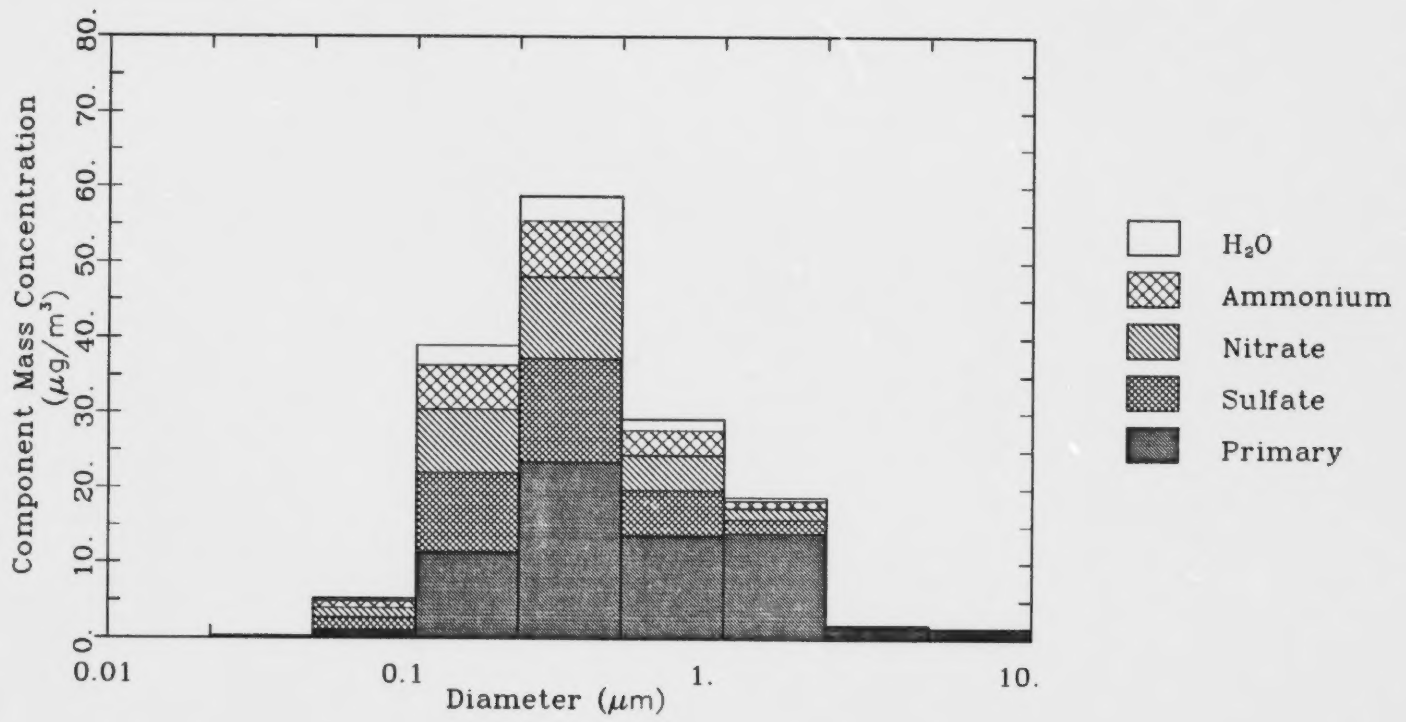

Figure 5–16(a). Size distributed chemical composition of the aerosol for the Columbus, Ohio 50% reactive hydrocarbon reduction case at the time of the maximum aerosol nitrate concentration on the second day of the simulation. (August 24, 1981, 9am).

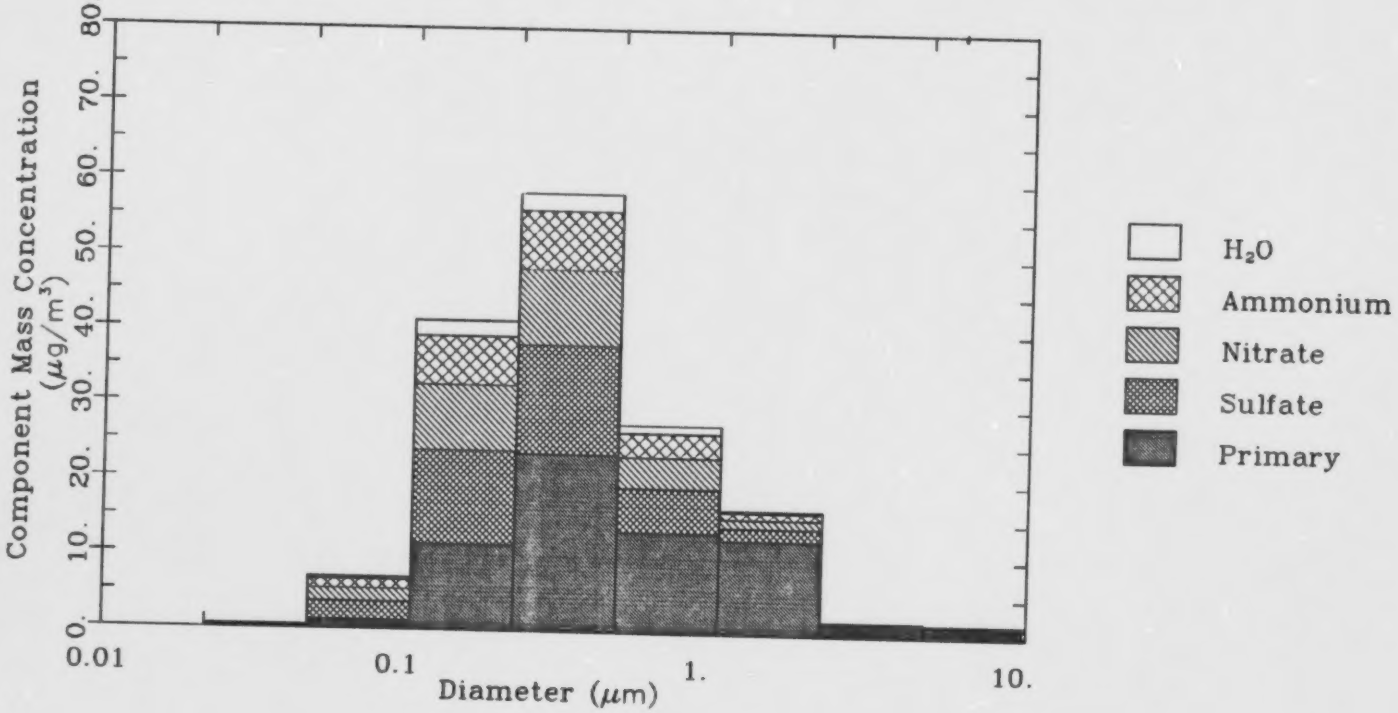

Figure 5-16(b). Size distributed chemical composition of the aerosol for the Columbus, Ohio 50% reactive hydrocarbon reduction case at the time of the maximum PM10 concentration on the second day of the simulation. (August 24, 1981, 10am).

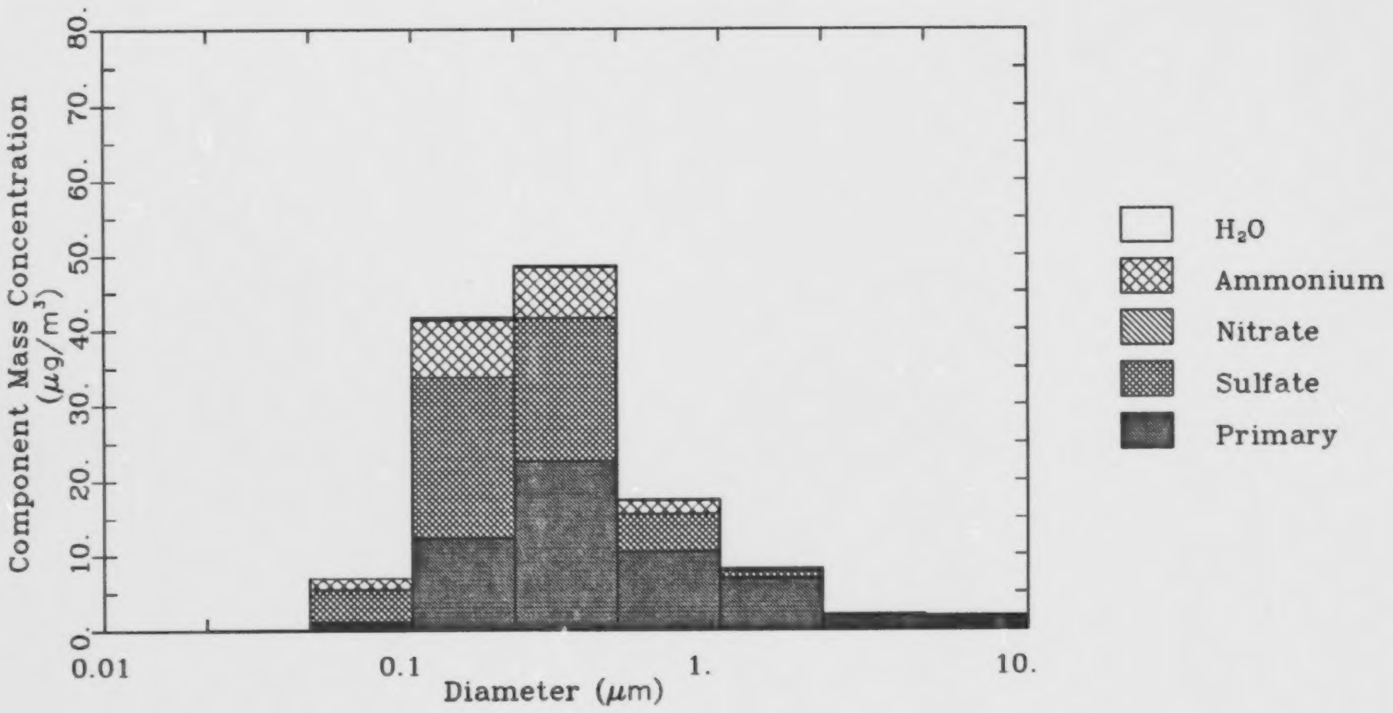

Figure 5–16(c). Size distributed chemical composition of the aerosol for the Columbus, Ohio 50% reactive hydrocarbon reduction case at the time of the maximum aerosol sulfate concentration on the second day of the simulation. (August 24, 1981, 6pm).

the winter case study for Columbus, Ohio are shown in the sixth column in Tables 5-5 through 5-8.

For the most part, the concentrations of gaseous NO_2, O_3, and H_2O_2 and aerosol sulfate and PM10 follow the same diurnal pattern as they do in the summer base case simulation (Figures 5-17 and 5-18). Since the daylight period is shortened, there is less time for sunlight-dependent reactions to occur, and the differences between daytime maximum/minimum values and nighttime maximum/minimum values are not as pronounced as during the summer period. The most notable difference between the winter and summer simulations occurs in the distribution of aerosol nitrate concentrations (Figure 5-18(b), Figure 5-4, and Figure 5-19). The maximum concentration is significantly reduced as is the variation between the minimum and maximum values. The reduction in the maximum concentration of ammonium nitrate results from the fact that less NO_2 oxidation occurs in the winter than in the summer. However, the lower temperatures and mixing height in the winter favor the formation of ammonium nitrate from its gas-phase precursor, ammonia and nitric acid; therefore, less variation occurs between daytime and nighttime concentrations of nitrate in the winter simulation than in the summer simulation (during the daytime, all ammonium nitrate was volatilized in the summer simulation).

URBAN PLUME BASE CASE--ST. LOUIS, MISSOURI

Results for the simulation performed using the urban plume data given in Table 5-4 are presented in Tables 5-9 and 5-10, and in Figures 5-20 through 5-22. The diurnal variations in the gaseous and aerosol species are similar to those in the regional environment simulation (Figures 5-2 and 5-3), but because the initial hydrocarbon concentrations are higher in the urban case, the initial formation of secondary aerosols is greater in the urban case than in the regional environment case (Figures 5-3 and 5-21). However, comparison of the maximum concentrations of both gaseous and aerosol species in the urban plume and the regional environment on the second day of the simulation shows that, as the urban plume becomes more dilute after leaving the urban area, the concentrations become similar to those in the regional environment (Tables 5-8 and 5-10; Figures 5-4 and 5-22). The maximum O_3 concentrations are on the order of 13 pphm on both days. The H_2O_2 concentration appears to be high, although concentrations of the order of a few ppb have been observed in urban environments. Formation of sulfate occurs during daytime as SO_2 is oxidized by OH radicals. The lower temperatures and reduced mixing favor ammonium nitrate formation at night.

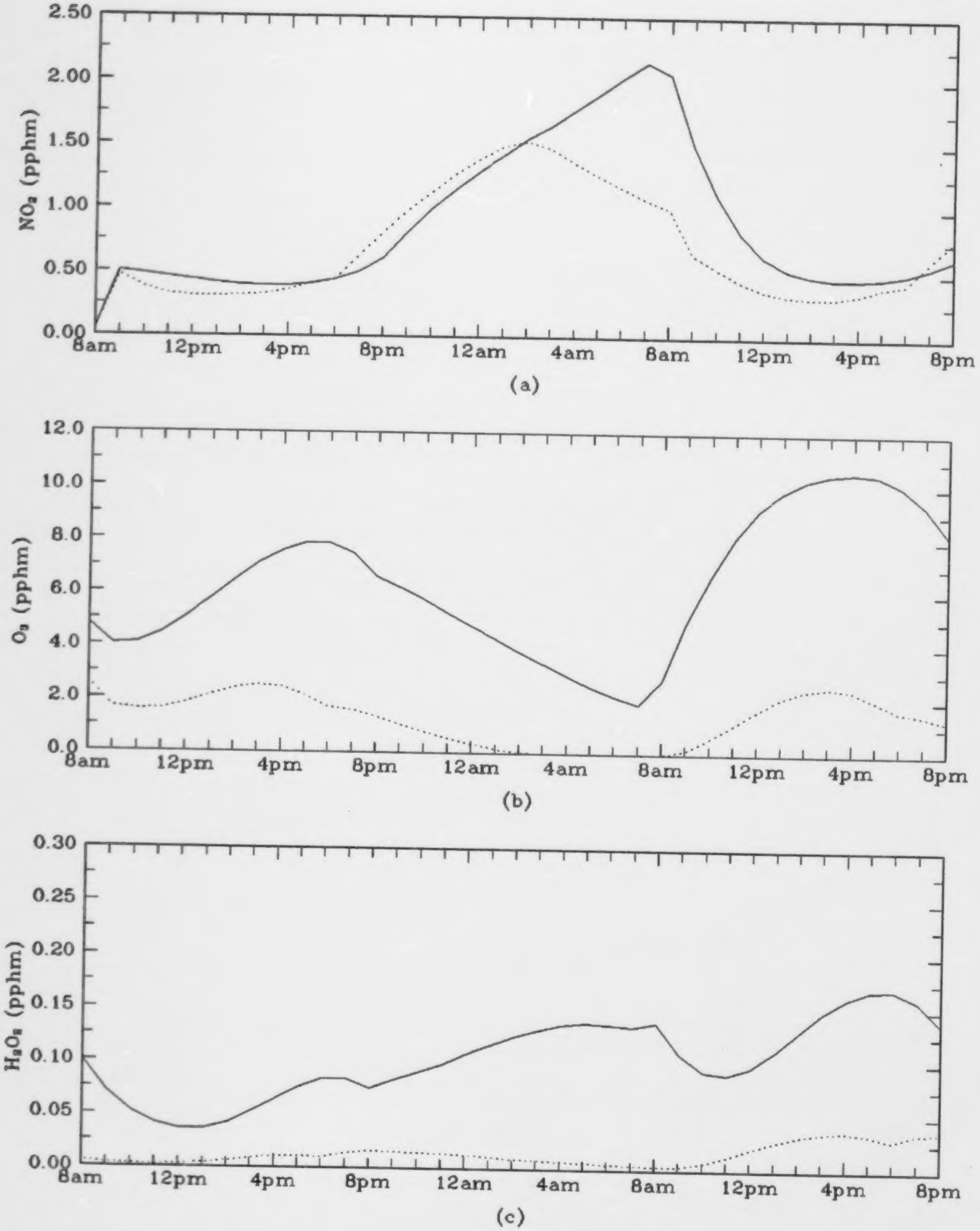

Figure 5-17. Concentrations of major chemical species for the Columbus, Ohio August 23-24, 1981, base case (———) and December 23-24, 1981, winter (.....) simulations.

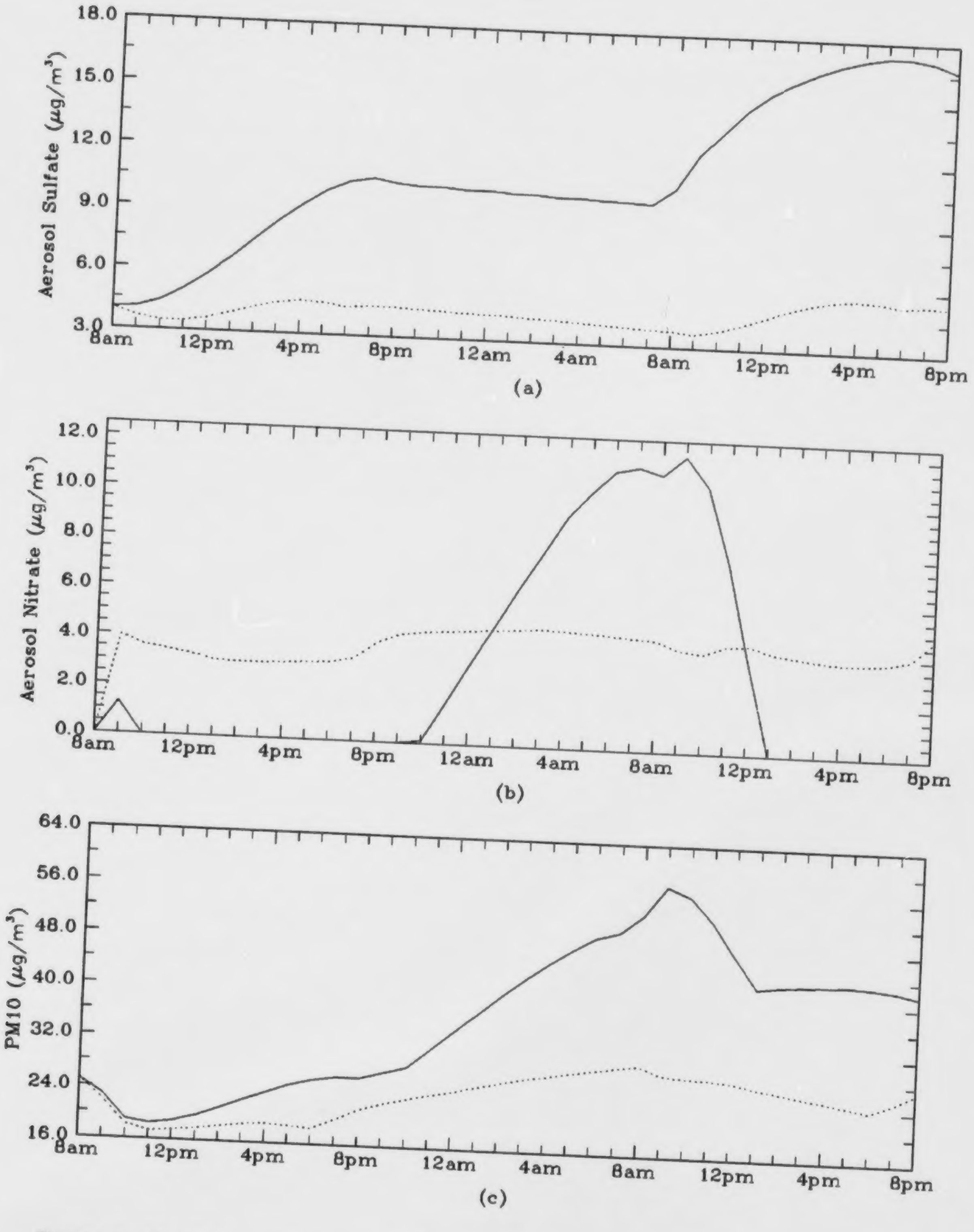

Figure 5–18. Concentrations of major aerosol species for the Columbus, Ohio August 23–24, 1981, base case (——) and December 23–24, 1981, winter (.....) simulations. (PM10 includes water aerosol).

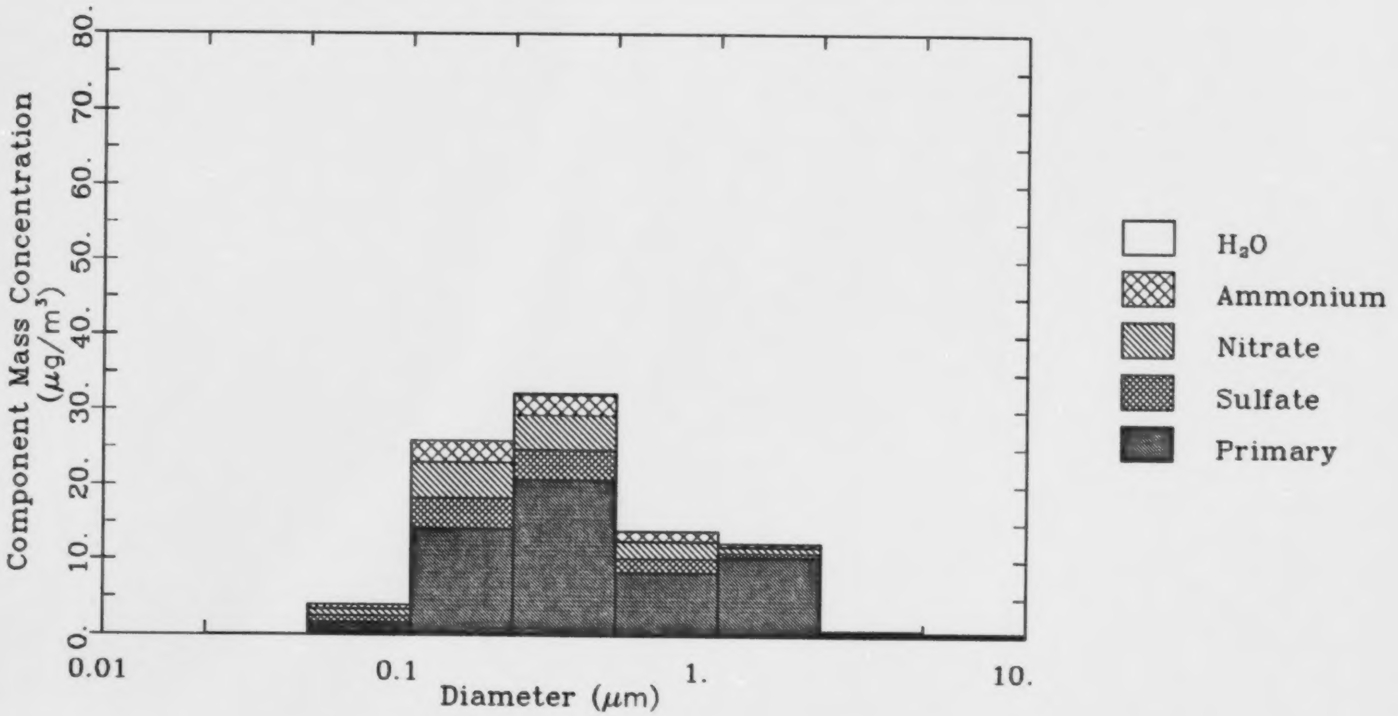

Figure 5-19(a). Size distributed chemical composition of the aerosol for the Columbus, Ohio winter case at the time of the maximum PM10 concentration on the second day of the simulation. (December 24, 1981, 8am).

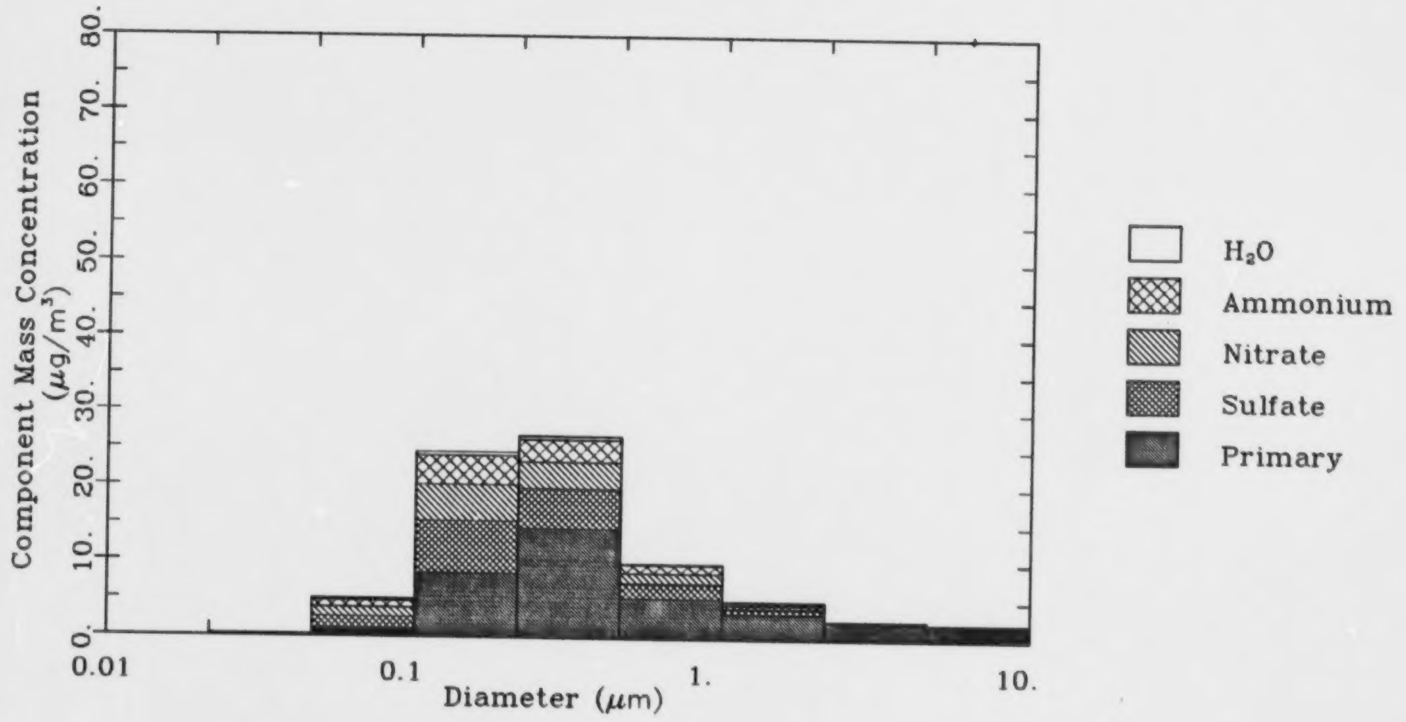

Figure 5–19(b). Size distributed chemical composition of the aerosol for the Columbus, Ohio winter case at the time of the maximum aerosol sulfate concentration on the second day of the simulation. (December 24, 1981, 4pm).

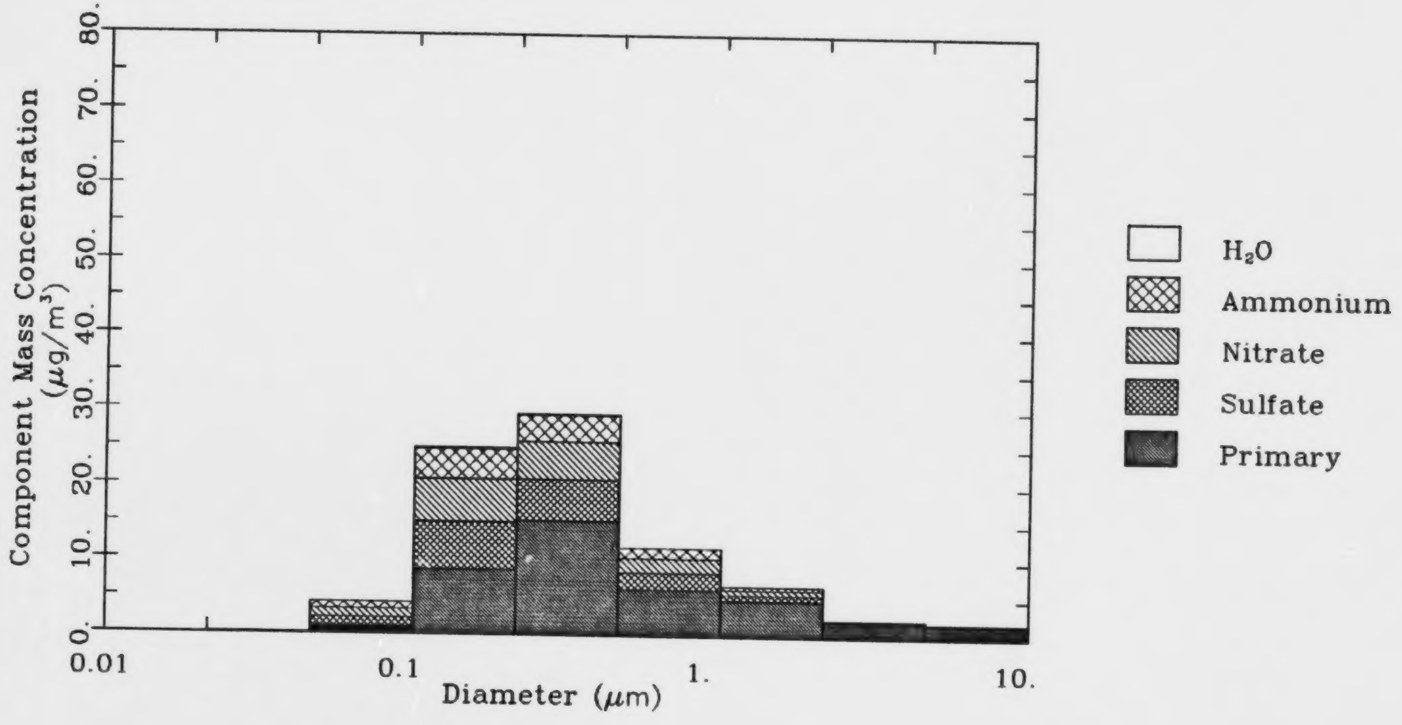

Figure 5–19(c). Size distributed chemical composition of the aerosol for the Columbus, Ohio winter case at the time of the maximum aerosol nitrate concentration on the second day of the simulation. (December 24, 1981, 8pm).

TABLE 5-9. Minimum concentrations for the base case and 85% relative humidity simulations for St. Louis, Missouri, August 23-24, 1981.

Species	Day 1 Base Case	Day 1 85% RH	Day 2 Base Case	Day 2 85% RH
NO2 (ppm)	0.212E-02	0.212E-02	0.211E-02	0.211E-02
NO (ppm)	0.218E-05	0.218E-05	0.499E-07	0.499E-07
O3 (ppm)	0.755E-01*	0.757E-01*	0.581E-01	0.581E-01
HNO3 (ppm)	0.562E-02*	0.534E-02*	0.688E-02	0.712E-02
H2O2 (ppm)	0.113E-02*	0.113E-02*	0.490E-02	0.476E-02
SO2 (ppm)	0.106E-01*	0.106E-01*	0.129E-01	0.125E-01
Aerosol Sulfate (ug/m3)	9.53	9.43	13.0	13.7
Aerosol Nitrate (ug/m3)	0.00	0.180*	0.00	1.30
NH3 (ppm)	0.342E-03	0.342E-03	0.342E-03	0.342E-03
Ammonium Aerosol (ug/m3)	2.45*	2.80*	5.31	5.49
BSCAT (m-1)	0.492E-04	0.989E-03	0.742E-04	0.154E-03
Organic Aerosol (ug/m3)	0.709	0.700	0.880	0.864
OLEF (ppm)	0.157E-02	0.157E-02	0.190E-02	0.190E-02
CARB (ppm)	0.131E-01*	0.131E-01*	0.980E-02	0.980E-02
PM10# (ug/m3)	33.0	58.8	37.5	75.2

* If the minimum concentration on day 1 was the initial concentration, then the second maximum was used.

Water aerosol is included in the PM10 concentration.

TABLE 5-10. Maximum concentrations for the base case and 85% relative humidity simulations for St. Louis, Missouri, August 23-24, 1981.

Species	Day 1		Day 2	
	Base Case	85% RH	Base Case	85% RH
NO2 (ppm)	0.105E-01*	0.105E-01*	0.120E-01	0.120E-01
NO (ppm)	0.129E-02*	0.128E-02*	0.403E-03	0.403E-03
O3 (ppm)	0.130	0.130	0.129	0.129
HNO3 (ppm)	0.714E-02	0.729E-02	0.975E-02	0.947E-02
H2O2 (ppm)	0.501E-02	0.495E-02	0.688E-02	0.646E-02
SO2 (ppm)	0.193E-01*	0.192E-01*	0.375E-01	0.371E-01
Aerosol Sulfate (ug/m3)	13.3*	13.6*	19.8	22.4
Aerosol Nitrate (ug/m3)	1.81	2.22	13.4	12.2
NH3 (ppm)	0.178E-02*	0.132E-02*	0.112E-02	0.829E-03
Ammonium Aerosol (ug/m3)	4.93	5.09	8.71	8.75
BSCAT (m-1)	0.741E-04*	0.136E-03*	0.140E-03	0.298E-03
Organic Aerosol (ug/m3)	0.857	0.840	1.05	1.03
OLEF (ppm)	0.759E-02	0.759E-02	0.164E-01	0.164E-01
CARB (ppm)	0.227E-01	0.228E-01	0.176E-01	0.176E-01
PM10# (ug/m3)	42.5*	82.6	56.6	118.6

* If the maximum concentration on day 1 was the initial concentration, then the second maximum was used.

# Water aerosol is included in the PM10 concentration.

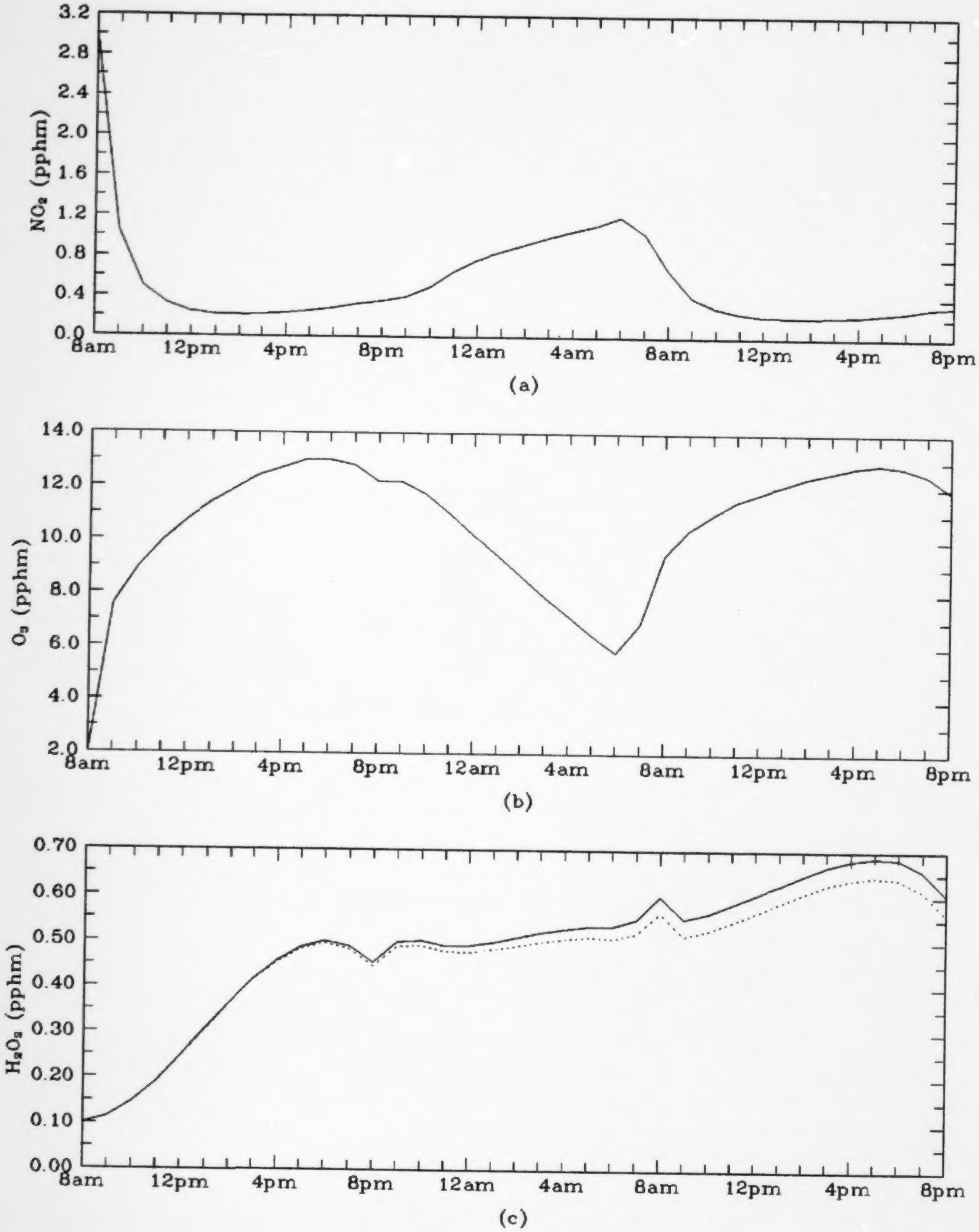

Figure 5–20. Concentrations of major chemical species for the St. Louis base case (_____) and 85% relative humidity (.....) simulations for August 23–24, 1981.

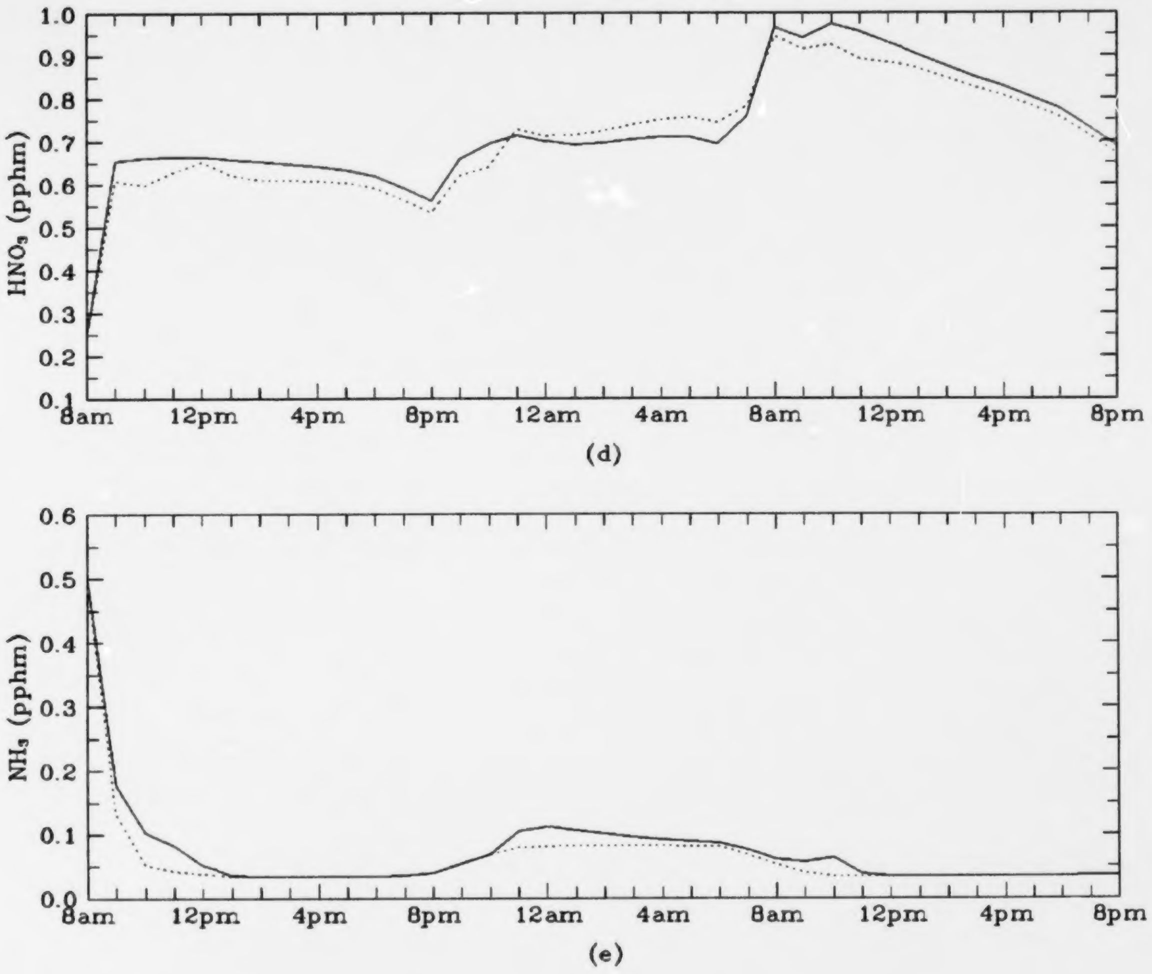

Figure 5–20 (concluded).

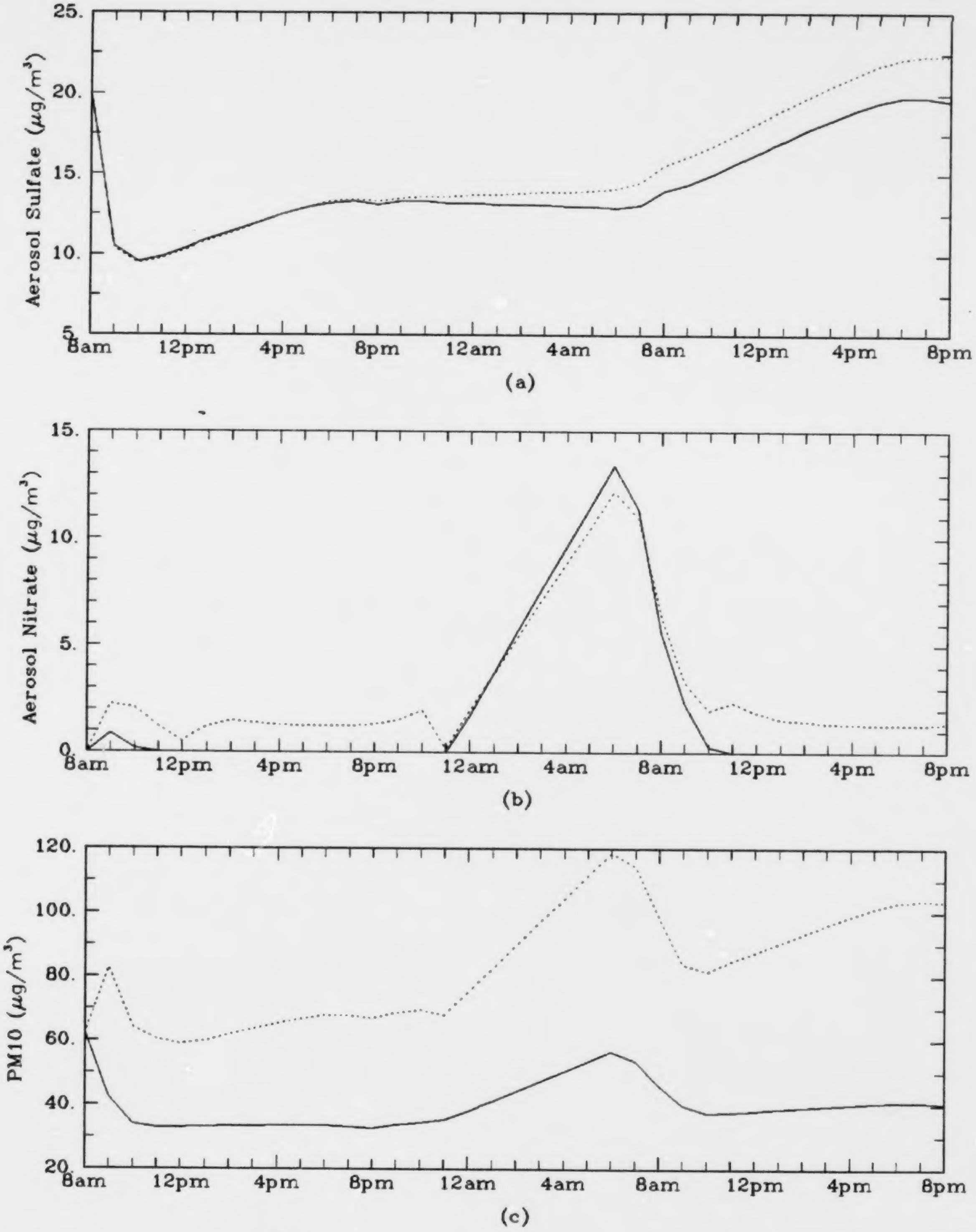

Figure 5–21. Concentrations of major aerosol species for the St. Louis base case (——) and 85% relative humidity (.....) simulations for August 23–24, 1981. (PM10 includes water aerosol).

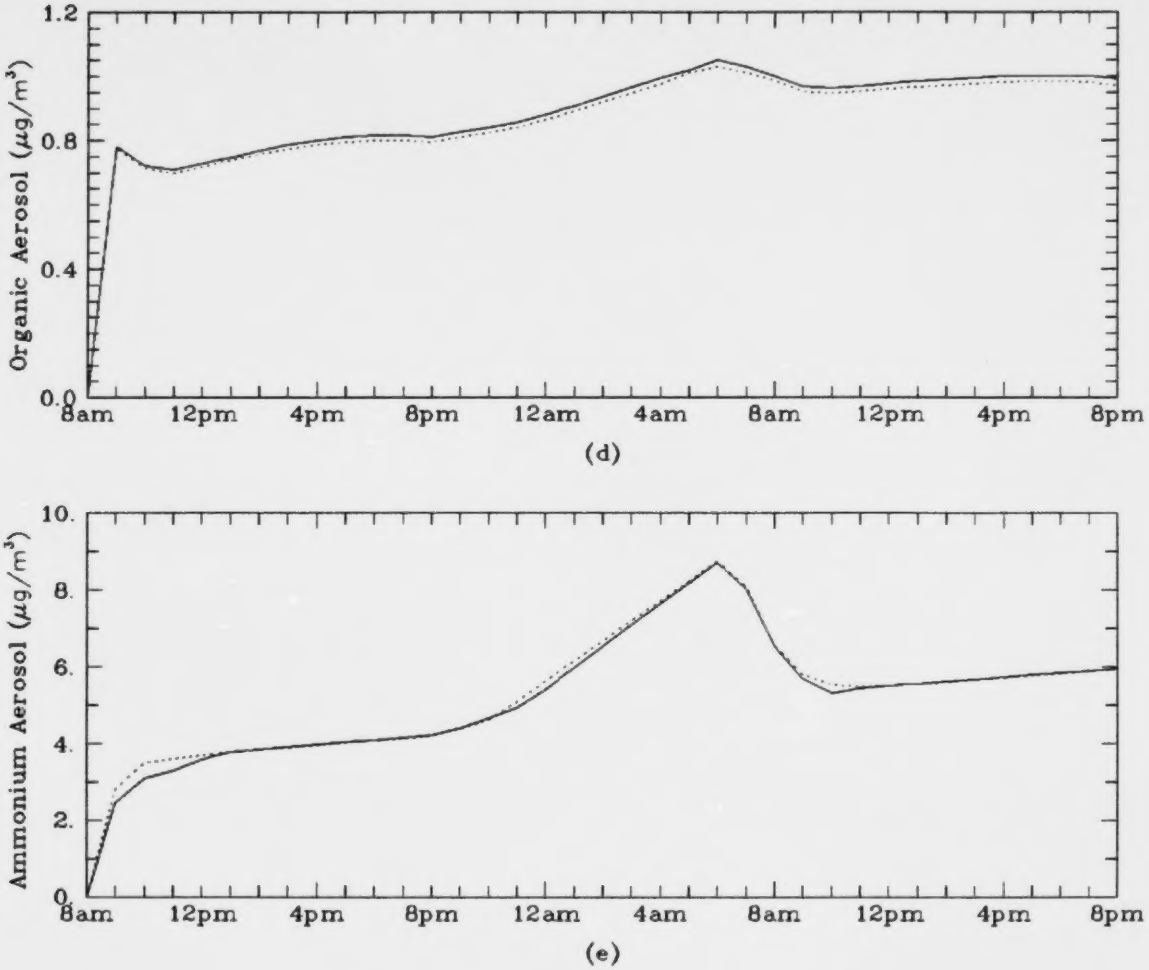

Figure 5–21 (concluded).

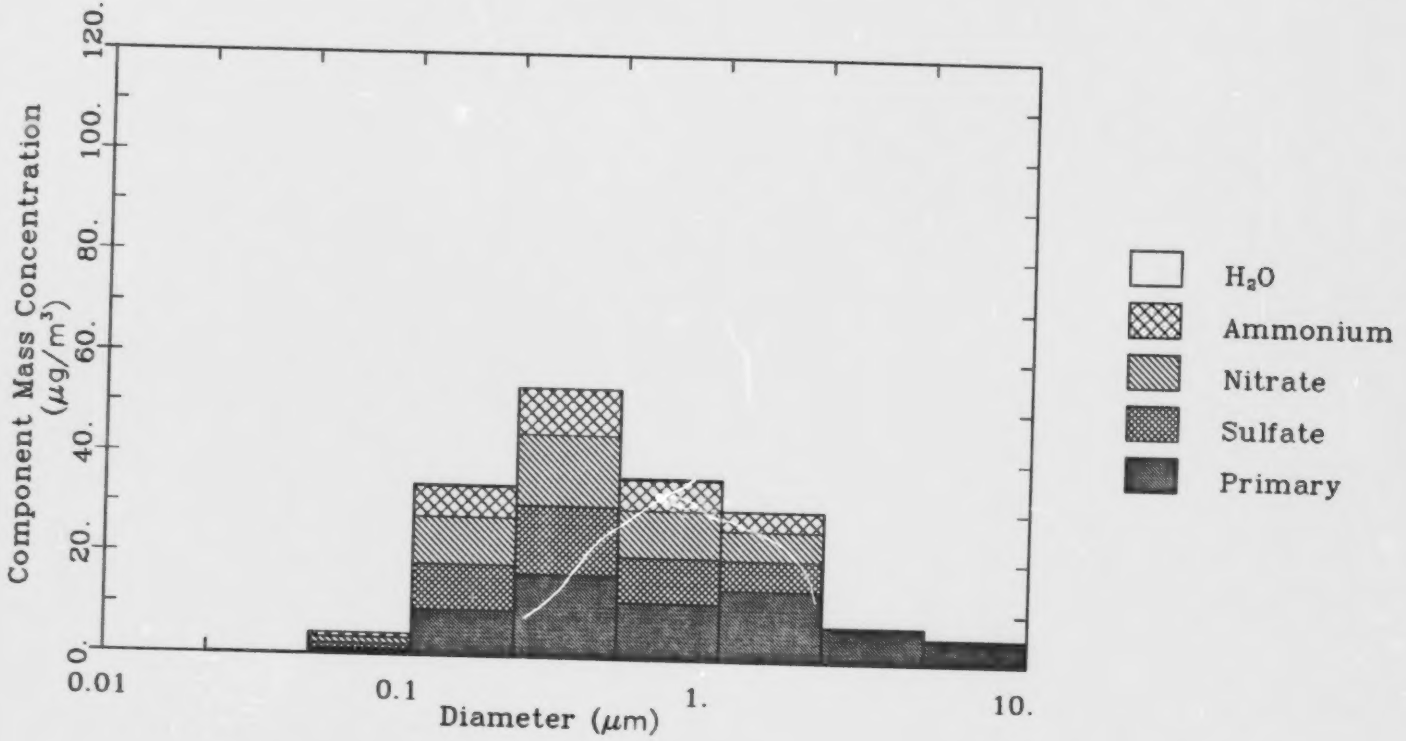

Figure 5-22(a). Size distributed chemical composition of the aerosol for the St. Louis, Mo. base case at the time of the maximum aerosol nitrate and PM10 concentrations on the second day of the simulation. (August 24, 1981, 6am).

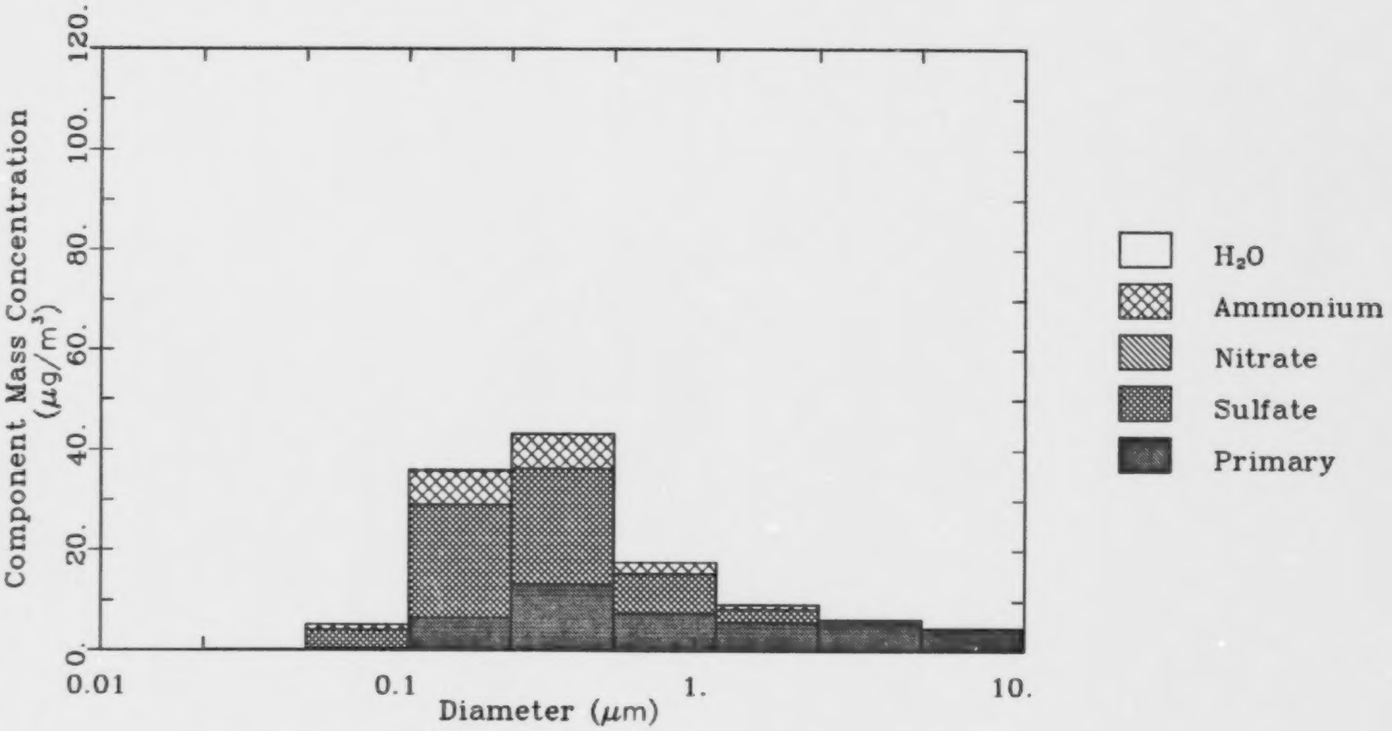

Figure 5-22(b). Size distributed chemical composition of the aerosol for the St. Louis, Mo. base case at the time of the maximum aerosol sulfate concentration on the second day of the simulation. (August 24, 1981, 7pm).

85 Percent Relative Humidity--St. Louis, Missouri

For this case study, the relative humidity was increased from 60 percent in the St. Louis base case to 85 percent. Results of this simulation are presented in Tables 5-9 and 5-10, and in Figures 5-20, 5-21, and 5-23. The change in the gaseous species is only slight; however, the change in the aerosol nitrate and sulfate concentrations is somewhat more pronounced (Figure 5-21(a) and (b)). A slight increase appears in the aerosol sulfate distribution above 1 μm (Figure 5-23(a) compared to Figure 5-22(a)). This increase is due largely to the growth of deliquescent and hygroscopic aerosol sulfate particles. At 7-8 p.m. on day 2, no aerosol nitrate was present in the base case simulation. The presence of a liquid film on the aerosol leads to the presence of nitrate in the aerosol phase despite the fact that the criteria for ammonium nitrate are not met because some amount of nitric acid will dissolve.

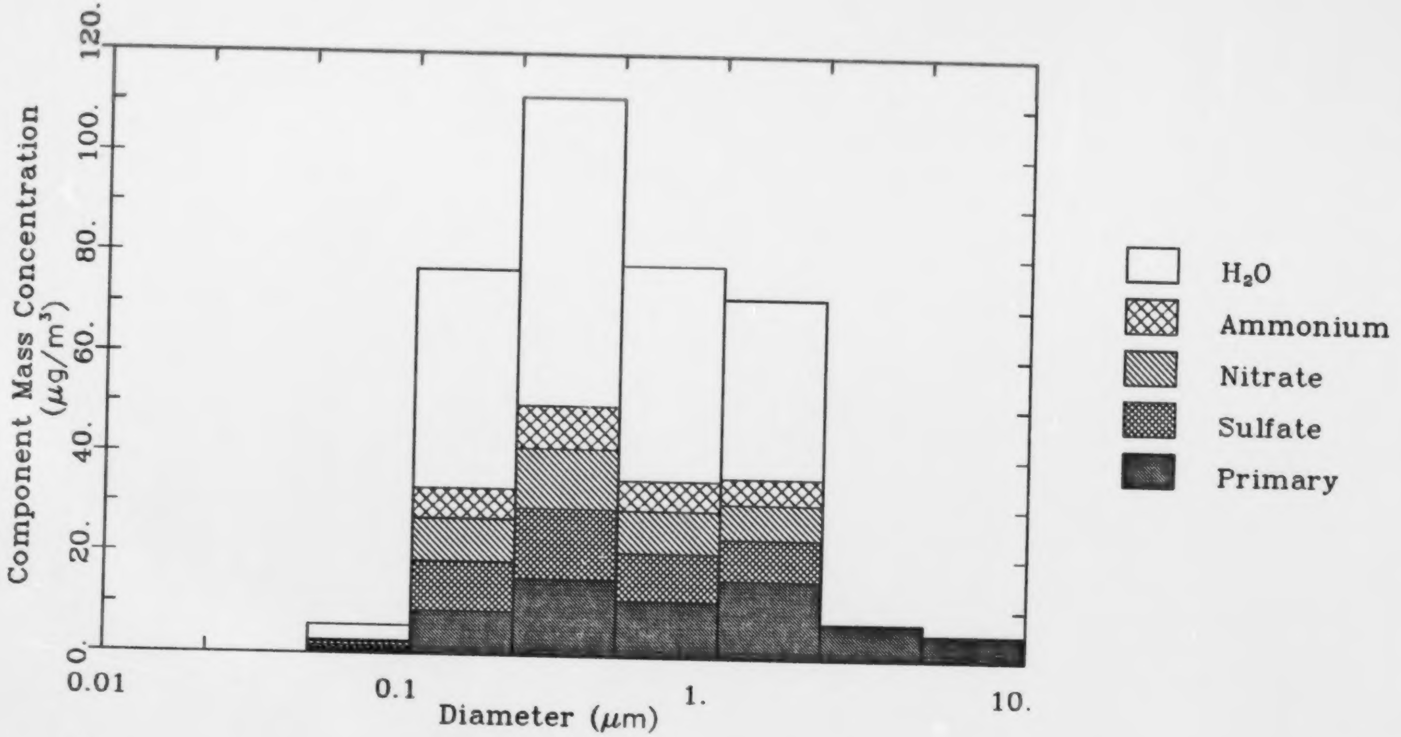

Figure 5–23(a). Size distributed chemical composition of the aerosol for the St. Louis, Mo. 85% relative humidity case at the time of the maximum aerosol nitrate and PM10 concentrations on the second day of the simulation. (August 24, 1981, 6am).

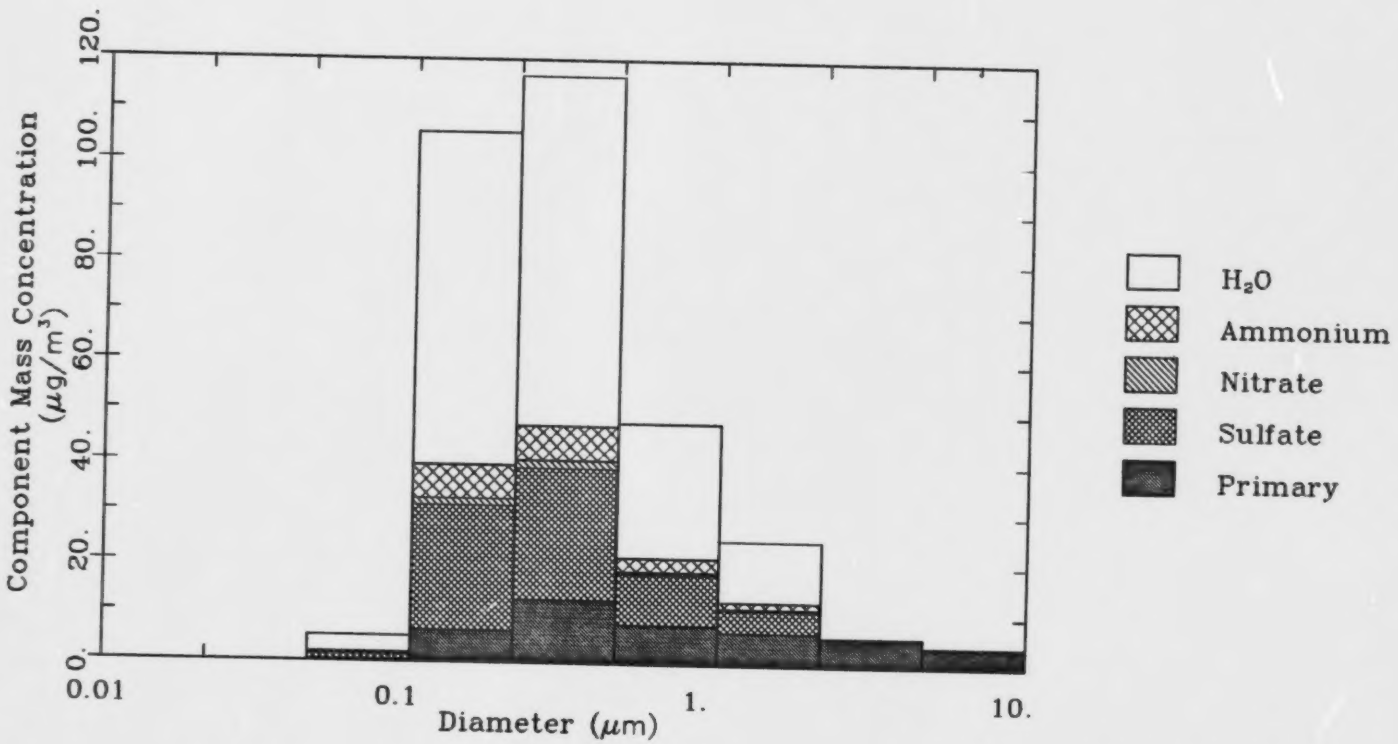

Figure 5–23(b). Size distributed chemical composition of the aerosol for the St. Louis, Mo. 85% relative humidity case at the time of the maximum aerosol sulfate concentration on the second day of the simulation. (August 24, 1981, 8pm).

6 CONCLUSIONS

During the course of this work, we installed and evaluated numerous computer models of particulate processes developed under contract to the EPA to select efficient and accurate models for incorporation into the regional model. These models were developed to treat the dynamics, thermodynamics, and chemistry of atmospheric particulate matter. The evaluation took into consideration the computational requirements, predictive accuracy, and application range of the models.

For our study of the treatment of aerosol dynamics, we compared four models: COAGUL and CONFEMM, developed at the University of Texas by Professor J. R. Brock and co-workers; AGRO, developed at the University of Minnesota by Professor K. T. Whitby, Mr. E. E. Whitby, and co-workers; and ESMAP, developed at the California Institute of Technology by Professor J. H. Seinfeld and co-workers. These four models represent the three major approaches to solving the General Dynamic Equation (GDE) that governs the treatment of aerosol coagulation and condensation. COAGUL and CONFEMM are examples of a continuous representation of the GDE for coagulation and condensation, respectively. ESMAP is an example of a discrete (sectional) representation, and AGRO represents a parameterized approach.

COAGUL, AGRO, and ESMAP were used to simulate aerosol coagulation over 12 hours for atmospheric aerosol concentrations typical of clear, hazy, and urban conditions. ESMAP was applied with two different size resolutions, 12 and 39 sections, over the 0.001 μm to 10 μm size range. COAGUL was shown to provide an accurate solution of the coagulation equation. AGRO performed well for case studies involving both clear and hazy conditions (in which coagulation has little effect on the initial size distributions) but was less accurate for the urban case study. ESMAP, with both 12 and 39 sections, performed well relative to COAGUL.

The computational times were compared on a Prime 750 computer. AGRO required less than 1 CPUs; COAGUL from 100 to 1000 CPUs; and ESMAP from 180 to 2500 CPUs for 39 sections, and from 40 to 350 CPUs for 12 sections.

CONFEMM, AGRO, and ESMAP were then compared in the simulation of aerosol condensation over 12 hours for atmospheric concentrations typical of clear, hazy, and urban conditions. ESMAP was again applied with two different size resolutions, 12 and 39 sections, over the 0.001 μm to 10 μm size range. CONFEMM provided an accurate solution of the condensation equation. The performance of ESMAP with 39 sections was satisfactory for all cases; with 12 sections it produced reasonable results when condensation occurred primarily in the accumulation mode, but poorer results when condensation occurred on smaller aerosols. AGRO overestimated the peak concentration of the accumulation mode, but predicted the median diameter of the mode fairly well. As in the coagulation study, AGRO required the least amount of time, less than 1 CPUs. CONFEMM required about 150 CPUs; ESMAP required 90 CPUs with 12 sections and 300 CPUs with 39 sections.

On the basis of the results of the coagulation and condensation simulation results, we selected the sectional representation with a size resolution of 12 sections over a size range of 0.001 μm to 10 μm to simulate aerosol dynamics. This approach provides a reasonable compromise between model accuracy and computational requirements.

Treatment of the thermodynamic equilibrium between the aerosol phases is central to determination of the chemical composition of aerosols that results from the condensation of sulfuric acid, nitric acid, ammonia, and water. Other species, such as HCl and organic compounds, also affect the thermodynamic equilibrium of aerosols. Since HCl is generally present in low concentrations in the atmosphere, and sulfate and nitrate aerosols generally occur in significant concentrations in polluted areas and are of primary interest in the consideration of acid deposition and visibility impairment, we focused on models of sulfate/nitrate/ammonium/water aerosols.

The three thermodynamic models we reviewed and compared are (1) the Model for an Aerosol Reacting System (MARS), developed for this study by Saxena and Seigneur at Systems Applications, Inc.; (2) EQUIL, developed by Bassett and Seinfeld at the California Institute of Technology; and (3) KEQUIL, also developed by Bassett and Seinfeld at the California Institute of Technology. EQUIL and KEQUIL are rigorous models that explicitly solve for 17 species in eight phases by minimizing the Gibbs free energy of the systems. There are 13 equilibrium reactions among these species, and the temperature dependence of all thermodynamic properties is taken into account. KEQUIL and EQUIL are identical in all respects, except KEQUIL incorporates the Kelvin effect (the effect of aerosol surface curvature), and EQUIL does not. MARS is based on fundamental thermodynamics. Its treatment of chemical and interfacial equilibrium focuses only on major species for given sets of ambient conditions. Therefore, the number of equations to be solved is minimized. MARS, like EQUIL, does not consider the Kelvin effect. The distinguishing feature of MARS is its division of the entire regime of aerosol species into several subdomains. Since each subdomain contains fewer viable species than does the entire domain of concentrations, the number of equations to be solved is reduced, and the computational costs are thus minimized.

Since KEQUIL is the most comprehensive model currently available, the results of MARS and EQUIL were compared with those of KEQUIL. Comparisons were made for a broad spectrum of atmospheric conditions. Results were compared for concentrations of aerosol-phase ammonium, nitrate, total mass, and light scattering coefficients (b_{scat}). Calculations by EQUIL and MARS agreed closely with those of KEQUIL; however, MARS was on the order of 400 times faster than KEQUIL and about 60 times faster than EQUIL. This substantial difference in computational efficiency was attained without significant loss of accuracy. On the basis of this study, we selected MARS as an efficient and accurate model of aerosol thermodynamics for incorporation into the regional model.

On the basis of the results of the previously mentioned model evaluations and comparisons, we formulated an aerosol model that uses a sectional approach to treat the dynamics and the methodologies incorporated into MARS to treat the thermodynamics of atmospheric aerosols. The processes that affect aerosol concentration, size, and chemical composition were also explored. These processes include advection; diffusion; coagulation; gas-to-aerosol conversion of sulfate, nitrate, and organic species; chemical kinetics; sedimentation; dry deposition on surfaces; and emissions of new aerosol formation in clouds.

The aerosol model that we incorporated into the regional particulate model consists of seven sections in the fine aerosol range with diameters between 0.01 µm and 2.5 µm, and two sections in the coarse aerosol range with diameters between 2.5 µm and 10 µm. The chemical species treated in the fine mode include primary aerosol, sulfate, nitrate, ammonium, organics, and water. Species treated in the coarse aerosol mode include primary aerosol and nitrate. The model can be applied to the entire range of relative humidities. It treats the evolution of the concentration, chemical composition, and size distribution of aerosols undergoing the following processes: coagulation; growth from diffusion-limited condensation of sulfuric acid and organic species; growth/shrinkage from condensation/evaporation of HNO_3, NH_3, and H_2O; oxidation of SO_2 to sulfate by H_2O_2 in the liquid-coated aerosols; and formation of small sulfate and organic aerosols.

The gas-phase chemistry is treated by means of the Carbon-Bond Mechanism IV (CBM-IV) developed by Whitten and Gery of Systems Applications, Inc. The mechanism describes the chemistry of oxidants, nitrogen oxides, and anthropogenic and natural hydrocarbons. The Carbon-Bond Mechanism X (CBM-X), developed by Whitten and co-workers, was also examined for incorporation into the regional particulate model, and the number of reactions was condensed through variational sensitivity analysis.

To evaluate the aerosol model, we simulated both a regional environment and an urban plume, using a plume trajectory model, PLMSTAR, developed by Godden and Lurmann of ER&T, into which our aerosol model was incorporated. This trajectory/aerosol model, which also employs the Carbon-Bond Mechanism for the treatment of gas-phase chemistry, was developed under contract to Southern California Edison Company.

Two simulations were conducted for 36-hour periods (23-24 August 1987) to simulate both daytime and nighttime chemistries. The first simulation, for Columbus, Ohio, was selected to represent a regional environment. The second, for St. Louis, Missouri, was selected to represent an urban plume. In addition to the two base case studies, six sensitivity studies were conducted. Five of these studies were based on the data for the regional environment and consisted of simulations performed with (1) the base case SO_2 emissions and initial concentrations reduced by 50 percent, (2) the base case NO_x emissions and initial concentrations reduced by 50 percent, (3) the base case NH_3 emissions and initial concentrations reduced by 50 percent, (4) the base case reactive hydrocarbon emissions and initial concentrations reduced by 50 percent, and (5) the season changed from summer to winter. The sensitivity study based on the data from the St. Louis urban plume consisted of increasing the relative humidity from 60 percent to 85 percent. Results for all the studies were compared and evaluated, and it was concluded that the aerosol model performs well under a variety of atmospheric and meteorological conditions.

REFERENCES

Anlauf, K. G., P. Fellin, H. A. Wiebe, H. I. Schiff, G. I. MacKay, R. S. Braman, and R. Gilbert. 1985. A comparison of three methods for measurement of atmospheric nitric acid and aerosol nitrate and ammonium. Atmos. Environ., 19:325-333.

Bassett, M. E., and J. H. Seinfeld. 1984. Atmospheric equilibrium model of sulfate and nitrate aerosols-II. Particle size analysis. Atmos. Environ., 18:1163-1170.

Bassett, M. E., and J. H. Seinfeld. 1983. Atmospheric equilibrium model of sulfate and nitrate aerosol. Atmos. Environ., 17:2237-2252.

Businger, J. A., and S.P.S. Arya. 1974. Height of the mixed layer in the stably stratified planetary boundary layer. Adv. Geophys., 18A:73-92.

Cadle, S. H., R. J. Countess, and N. A. Kelley. 1982. Nitric acid and ammonium in urban and rural locations. Atmos. Environ., 16:2501.

Calvert, J. G. 1976. Hydrocarbon involvement in photochemical smog formation in Los Angeles atmosphere. Environ. Sci. Technol., 10:256-262.

Cass, G. R., and G. J. McRae. 1986. Emissions and air quality relationships for atmospheric trace metals. Adv. Environ. Sci. Technol., 17:145-171.

EPRI. 1982. "The Sulfate Regional Experiment: Data Base Inventory and Summary of Major Source File Programs." Electric Power Research Institute, Palo Alto, California (EPRI EA-1904).

Ferman, M. A., N. A. Kelly, and G. T. Wolff. 1985. "Nonurban Hydrocarbons and Their Effect on Ozone and Haze." Environmental Science Department, General Motors, Warren, Michigan (GMR-5040, ENV-211).

Fox, D. L., M. Gery, and H. E. Jeffries. 1984. "Organic Aerosol Formation: OH vs. Ozone Oxidation Pathways." Final Report to Coordinating Research Council, Inc., Atlanta, Georgia.

Franzblau, E., C. S. Burton, and G. M. Hidy. 1984. Aerosol particle formation from ozone-terminal olefin reactions. Aerosol Sci. Technol., 3:167-176.

Friedlander, S. K. 1977. Smoke, Dust and Haze--Fundamentals of Aerosol Behavior, John Wiley & Sons, New York.

Fuchs, W. A. 1964. The Mechanics of Aerosols, Pergamon Press, Oxford.

Fuchs, N. A., and A. G. Sutugin. 1971. High dispersed aerosols, in Topics in Current Aerosol Research. Edited by G. M. Hidy and J. R. Brock, Pergamon Press, New York, pp. 6-60.

Gelbard, F., and J. H. Seinfeld. 1980. Simulation of multicomponent aerosol dynamics. J. Colloid Interface Sci., 78:485-501.

Gillani, N. V., R. B. Husar, J. D. Husar, D. E. Patterson, and W. E. Wilson. 1978. Project MISTT: Kinetics of particulate sulfur formation in a power plant plume out to 300 km. Atmos. Environ., 12:589-598.

Grosjean, D. 1984a. Photooxidation of 1-heptene. Sci. Total Environ., 37:195-211.

Grosjean, D. 1984b. Atmospheric reactions of ortho-cresol: gas phase and aerosol products. Atmos. Environ., 18:1641-1652.

Grosjean, D. 1985. Reactions of o-cresol and nitrocresol with NO_x in sunlight and with ozone-nitrogen dioxide mixtures in the dark. Environ. Sci. Technol., 19:968-974.

Grosjean, D., and P. H. McMurry. 1982. "Secondary Organic Aerosol Formation: Homogeneous and Heterogeneous Chemical Pathways." Final Report to Coordinating Research Council, Inc., Atlanta, Georgia.

Haney, J. L., and C. Seigneur. 1985. "Investigation of Reactive Hydrocarbon to NO_x Ratio in the South Coast Air Basin." Technical Memorandum.

Harrison, R. M., and W. T. Sturges. 1984. Physico-chemical speciation and transformation reactions of particulate atmospheric nitrogen and sulfuric compounds. Atmos. Environ., 18:1829-1833.

Hatakeyama, S., T. Tanonaka, J. H. Weng, H. Bandow, H. Takagi, and H. Akimoto. 1985. Ozone-cyclohexene reaction in air: quantitative analysis of particulate products and the reaction mechanism. Environ. Sci. Technol., 19:935-942.

Heikes, B. G., A. L. Lazrus, and G. L. Kok. 1985. "Measurements of H_2O_2 in the Lower Troposphere." 17th International Symposium on Free Radicals, Granby, Colorado (18-23 August).

Heisler, S. L., and S. K. Friedlander. 1977. Gas-to-particle conversion in photochemical smog: aerosol growth laws and mechanisms for organics. Atmos. Environ., 11:157-168.

Holzworth, G. C. 1972. "Mixing Heights, Wind Speeds, and Potential for Urban Air Pollution Throughout the Contiguous United States." U.S. Environmental Protection Agency, Research Triangle Park, North Carolina (AP-101).

Hudischewskyj, A. B., and C. Seigneur. 1986. "Simulation of the Formation of Acidic Aerosol Species in Power Plant and Smelter Plumes." 79th Annual Meeting of the Air Pollution Control Association, Minneapolis, Minnesota (22-27 June).

Kamens, R. M., M. W. Gery, H. E. Jeffries, M. Jackson, and E. I. Cole. 1982. Ozone-isoprene reactions: product formation and aerosol potential. Int. J. Chem. Kinet., 14:955-975.

Kelley, T. J., R. L. Tanner, L. Newman, P. J. Galvin, and J. A. Kadlecek. 1984. Trace gas and aerosol measurements at a remote site in the northeast United States. Atmos. Environ., 12:2565-2576.

Killus, J. P., and G. Z. Whitten. 1982. "A New Carbon-Bond Mechanism for Air Quality Simulation Modeling." U.S. Environmental Protection Agency, Research Triangle Park, North Carolina (EPA-600/3-82-041).

Kopczynski, S. L., W. A. Lonneman, F. D. Sutterfield, and P. E. Darley. 1972. Photochemistry of atmospheric samples in Los Angeles. Environ. Sci. Technol., 6:342-347.

Lamb, R. G. 1982. "A Regional Scale (1000 km) Model of Photochemical Air Pollution, Part 1, Theoretical Formulation." U.S. Environmental Protection Agency, Research Triangle Park, North Carolina.

Lamb, R. G., and D. R. Duran. 1977. Eddy diffusivities derived from a numerical model of the convective boundary layer. Nuov. Cimento, 1C:1-17.

Lazrus, A. L., P. L. Haagenson, G. L. Kok, B. J. Huebert, C. W. Kreitzberg, G. E. Likens, V. A. Mohnen, W. E. Wilson, and J. W. Winchester. 1983. Acidity in air and water in a case of warm frontal precipitation. Atmos. Environ., 17:581-591.

Lindberg, S. E. 1982. Factors influencing trace metal, sulfate, and hydrogen ion concentrations in rain. Atmos. Environ., 16:1701-1709.

Martin, L. R. 1984. Kinetic studies of sulfate oxidation in aqueous solution. In SO_2, NO and NO_2 Oxidation Mechanisms. J. G. Calvert, ed. Butterworth, Boston, Massachusetts, pp. 63-100.

Martin, L. R., and D. E. Damschen. 1981. Aqueous oxidation of sulfur dioxide by hydrogen peroxide at low pH. Atmos. Environ., 15:1615-1621.

McArdle, J. V., and M. R. Hoffmann. 1983. Kinetics and mechanism of the oxidation of aquated sulfur dioxide by hydrogen peroxide at low pH. J. Phys. Chem., 87:5425-5429.

McMurry, P. H. 1983. New particle formation in the presence of an aerosol: Rates, time scales, and sub-0.01 μm size distribution. J. Colloid Interface Sci., 95:72-80.

McMurry, P. H., and D. Grosjean. 1985. Photochemical formation of organic aerosols: growth laws and mechanisms. Atmos. Environ., 19:1445-1451.

McMurry, P. H., H. Takano, and G. R. Anderson. 1983. A study of the ammonia (gas)-sulfuric and (aerosol) reaction rate. Environ. Sci. Technol., 17:347-351.

Mohnen, V. A. 1985. Private communication. Atmospheric Sciences Research Center, State University of New York, Albany, New York.

NAS. 1977. Aerosols. In Ozone and Other Photochemical Oxidants. National Academy of Sciences, Washington, D.C., pp. 45-125.

Pratt, G. C., M. R. Coscio, S. Krupa. 1984. Regional rainfall chemistry in Minnesota and west central Wisconsin. Atmos. Environ., 18:173-182.

Saxena, P., A. B. Hudischewskyj, and C. Seigneur. 1986. The effect of meteorology on the SO_2/sulfate relationship. In The Meteorology of Acidic Deposition.

Saxena, P., A. B. Hudischewskyj, C. Seigneur, and J. H. Seinfeld. 1986. A comparative study of equilibrium approaches to the chemical characterization of secondary aerosols. Atmos. Environ., 20:1471-1483.

Saxena, P., C. Seigneur, and A. K. Pollack. 1986. A critical assessment of existing data bases for acid deposition modeling studies. J. Air Pollut. Control Assoc., 36:48-54.

Sehmel, G. A. 1980. Particle and gas dry deposition: A review. Atmos. Environ., 14:983-1011.

Sehmel, G. A., and W. H. Hodgson. 1980. A model for predicting dry deposition of particles and gases to environmental surfaces. AIChE Symposium Series, 76:218-230.

Seigneur, C. 1982. A model of sulfate aerosol dynamics in atmospheric plumes. Atmos. Environ., 16:2207-2228.

Seigneur, C., and H. M. Barnes. 1986. "Technical Considerations in Regional Aerosol Modeling." In Air Pollution Modeling and Its Application, 5:343-369, C. de Wispelaere, ed., Plenum Press, New York.

Seigneur, C., R. W. Bergstrom, C. D. Johnson, and L. W. Richards. 1984. Measurements and simulations of the visual effects of particulate plumes. Atmos. Environ., 18:2231-2244.

Seigneur, C., A. B. Hudischewskyj, J. H. Seinfeld, K. T. Whitby, E. R. Whitby, J. R. Brock, and H. M. Barnes. 1986. Simulation of aerosol dynamics: a comparative review of mathematical models. Aerosol Sci. Technol., 5:205-222.

Seigneur, C., and P. Saxena. 1984. A study of atmospheric acid formation in different environments." Atmos. Environ., 18:2109-2124.

Seigneur, C., P. Saxena, and P. M. Roth. 1984. Computer simulations of the atmospheric chemistry of sulfate and nitrate formation. Science, 225:1028-1030.

Seigneur, C., T. W. Tesche, P. M. Roth, and M. K. Liu. 1983. On the treatment of point source emissions in urban air quality modeling. Atmos. Environ., 17:1655-1676.

Sheih, C. M., M. L. Wesely, and B. B. Hicks. 1979. Estimated dry deposition velocities of sulfur over the eastern United States and surrounding regions. Atmos. Environ., 13:1361-1368.

Singh, H. B. 1987. Reactive nitrogen in the troposphere. Environ. Sci. Technol., 21:320-327.

Sitarski, M., and J. H. Seinfeld. 1977. Brownian coagulation in the transition regime. J. Colloid Interface Sci., 61:261-271.

Stockwell, W. R., and J. G. Calvert. 1983. The mechanism of HO-SO_2 reaction. Atmos. Environ., 17:2231-2235.

Tanner, R. L. 1982. "Temporal and Spatial Variability of Ammonia Concentrations in the Nonurban Troposphere." Second Symposium on the Composition of the Nonurban Troposphere, Williamsburg, Virginia (25-28 May).

Telford, J. W., T. S. Keck, and S. K. Chai. 1984. Entrainment at cloud tops and the droplet spectra. J. Atmos. Sci., 41:3170-3179.

Tsang, T. H., and J. R. Brock. 1983. Simulation of condensation aerosol growth by condensation and evaporation. Aerosol Sci. Technol., 2:311-320.

Warren, D. R., and J. H. Seinfeld. 1985. Simulation of aerosol size distribution evolution in systems with simultaneous nucleation, condensation, and coagulation. Aerosol Sci. Technol., 4:31-43.

Whitby, E. R. 1985. "The Modal Aerosol Dynamics Model. Part I. Solution of the Internal Terms of the General Dynamic Equation of Aerosols." Report to the U.S. Environmental Protection Agency, Department of Mechanical Engineering, University of Minnesota, Minneapolis, Minnesota.

Whitby, E. R., and K. T. Whitby. 1985a. "The Modal Aerosol Dynamics Model--Part I--Solution of the Internal Terms for the General Dynamics Equation of Aerosols." Department of Mechanical Engineering, University of Minnesota, Minneapolis, Minnesota (Particle Technology Laboratory Publication No. 580).

Whitby, E. R., and K. T. Whitby. 1985b. "AGR01: A Fortran Implementation of the Modal Aerosol Dynamics Model for the IBM PC/XT/AT." Department of Mechanical Engineering, University of Minnesota, Minneapolis, Minnesota (Particle Technology Laboratory Publication No. 581).

Whitby, K. T. 1981a. "Aerosol and Ozone Formation in the Columbus, Ohio, Urban Plume on July 29 and 30, 1980: A Preliminary Report." Particle Technology Laboratory, Department of Mechanical Engineering, University of Minnesota, Minneapolis, Minnesota (No. 447).

Whitby, K. T. 1981b. Determination of aerosol growth rates in the atmosphere using lumped aerosol dynamics. J. Aerosol Sci., 12:174-178.

Whitby, K. T. 1978. The physical characteristics of sulfur aerosols. Atmos. Environ., 12:135-159.

Whitten, G. Z., and M. W. Gery. 1985. "Development of CBM-X Mechanisms for Urban and Regional AQSMs." Systems Applications, Inc., San Rafael, California (SYSAPP-85/189).

Wilson, W. E. 1978. Sulfates in the atmosphere: A progress report on project MISTT. Atmos. Environ., 12:537-547.

Wolff, G. T., N. A. Kelly, M. A. Ferman, and M. L. Morrissey. 1983. Rural measurements of the chemical composition of airborne particles in the eastern United States. J. Geophys. Res., 88C:10769-10775.

Yom, K., and J. R. Brock. 1984. Private communication, Department of Chemical Engineering, University of Texas, Austin, Texas.

Appendix A

TECHNICAL CONSIDERATIONS IN REGIONAL AEROSOL MODELING*

Christian Seigneur
Systems Applications Inc.
101 Lucas Valley Road
San Rafael, California 94903

Harold M. Barnes
U.S. Environmental Protection Agency
Atmospheric Sciences Research Laboratory
Research Triangle Park, North Carolina 27711

INTRODUCTION

Particles that are emitted and formed in our atmosphereyield fumes, mist, and ashes. However, unlike the Greek mythological belief that a beautiful bird can be reborn from its ashes, the beauty of atmospheric ashes and particles appears only under certain angles when the light of Phebus can be directed advantageously by fine particles toward the human eye. Under other conditions, atmospheric particles adversely affect visibility by reducing visual range and delineating contrasting plumes. Fine particles are also inhaled by humans and may disturb the lung physiology when deposited in the tracheobronchial system. Moreover, the chemical species contained in these particles may disturb the ecological balance of our biota; for example, sulfate and nitrate particles that are deposited on the ground and on foliage acidify soils and watersheds.

A comprehensive approach to this variety of environmental issues requires an integrated study of atmospheric particles to assess their sources, evolution, and fate and to characterize their concentration, size distribution, and chemical composition. Such a study must be both theoretical and experimental if our concepts of particle physics and chemistry are to be reconciled with our observations.

We address in this work the theoretical aspects of the behavior of aerosol particles in the atmosphere. In particular, we focus on the mathematical modeling of atmospheric aerosols at the regional scale. Previous modeling studies have concentrated on the simulation of aerosol dynamics in laboratory experiments, chimney plumes, or the stratosphere. No work has been performed so far on the mathematical description of aerosols in the lower layers of the atmosphere over distances of the order of 1000 km. Regional modeling is particularly important to the study of air pollution since pollutants can be transported over long distances and thus may have an environmental impact several thousands of kilometers downwind of the source. In addition, a regional model can also be used to calculate background conditions for urban-scale models. Such an endeavor requires us to consider a wide variety of physical and chemical processes that affect aerosols.

---

*Published in Air Pollution Modeling and Its Application V. C. De Wispelaere, F. A. Schiermeier, and N. V. Gillani, eds. (Plenum Publishing Corporation, 1986).

To that end, we discuss in the following sections the formulation of a regional aerosol model.

We first provide a brief overview of the mathematical formulation of the transport mechanisms used in the regional model. Next, we provide an overview of the physical processes that affect the dynamics of the aerosol population. We then review the chemistry of atmospheric aerosols. Various mathematical models of aerosol dynamics and chemistry, and the formulation of the regional aerosol model are discussed before the presentation of concluding remarks.

OVERVIEW OF THE REGIONAL MODEL

The evolution of aerosol concentrations is treated at the regional scale by means of a three-dimensional gridded structure. Chemical reactions and aerosol dynamics take place within each grid cell. Advective and convective transport, dispersion, emissions of primary pollutants, and removal by dry deposition and sedimentation are treated as transport between grid cells.

The transport processes are treated by the regional model developed at the U.S. Environmental Protection Agency. The mathematical formulation of the model (Lamb, 1983), its computer implementation (Lamb, 1984a; Novak, 1984), and its preliminary application (Schere and Possiel, 1984) have been presented elsewhere. We therefore limit our discussion to a brief overview of the model formulation.

The EPA regional model is an Eulerian, grid-based, multiple-layer model that treats atmospheric processes relevant to the regional distribution of pollutants. The model includes three horizontal layers that vary spatially and temporally--the surface layer, the mixed layer, and the inversion, or cloud, layer. The model also includes a shallow surface layer adjacent to the ground for the treatment of surface processes such as dry deposition and near-ground chemical reactions. The vertical dimensions of the grid vary from 50 to 1000 m. The grid framework follows a latitude-longitude coordinate system with horizontal dimensions of the order of 18 km.

The EPA regional model treats such physical processes as horizontal transport including its nondeterministic aspects (Lamb, 1984b), nighttime wind shear, stability stratification, nocturnal jets, venting of pollutants from the mixed layer by cumulus clouds, mesoscale vertical motions induced by terrain and horizontal wind flow divergence, dry deposition, and emission of primary pollutants.

The EPA regional model also includes a chemical kinetic mechanism (CBM-X) that describes the chemistry of nitrogen oxides, anthropogenic and biogenic hydrocarbons, and photochemical oxidants such as ozone and hydrogen peroxide. This chemical kinetic mechanism currently includes 180 reactions and is based on a carbon-bond representation of hydrocarbon chemistry (Killus and Whitten, 1984). Gas-phase reactions for the chemistry of sulfur dioxide are included (Seigneur, et al., 1985). In its application to the regional aerosol model, the chemical kinetic mechanism must be condensed to fewer chemical species and reactions to allow the incorporation of additional variables describing the aerosol size distribution and chemical composition. This condensation will be based on the results of a recent sensitivity analysis of the CBM-X (Gautier, 1984) that was carried out by means of a variational method (Seigneur et al., 1982).

AEROSOL DYNAMICS

The concentrations and sizes of aerosols are affected by a variety of dynamic processes including coagulation, growth and shrinkage, nucleation, sedimentation, dry deposition, and wet deposition. In this section we review the theoretical basis of these processes and assess their relevance to aerosol modeling at the regional scale.

Coagulation

Coagulation does not affect the total mass of aerosols because mass is conserved during the coagulation of two aerosols. However, coagulation affects the aerosol size distribution and aerosol total number concentration because it is the process by which two aerosols form one larger aerosol. Coagulation occurs via Brownian motion, sedimentation, and turbylent motion (e.g., Friedlander, 1977). In the atmosphere, Brownian motion is the most important mechanism for coagulation, as shown in Figure 1, where the coagulation coefficients are presented for various aerosol sizes. The change in the aerosol size distribution due to coagulation is represented mathematically as follows :

$$\frac{\partial n(v)}{\partial t} = \frac{1}{2} \int_0^v \beta(\tilde{v}, v-\tilde{v})\, n(\tilde{v})\, n(v-\tilde{v})\, d\tilde{v} - \int_0^\infty \beta(v,\tilde{v})\, n(\tilde{v})\, n(v)\, d\tilde{v} \qquad (1)$$

where $n(v)$ is the aerosol number distribution, v is the aerosol volume, and β is the coagulation coefficient. The coagulation rate decreases as the aerosol concentration decreases, i.e., coagulation affects the aerosol size distribution more in polluted air parcels such as stack plumes than in cleaner areas such as pristine airsheds. It is therefore important to assess the contribution of coagulation at the regional scale, where aerosol concentrations are likely to be significantly lower than they are in a stack plume. To that end, we performed simulations of aerosol coagulation for aerosol concentrations typical of those observed at the regional scale.

The aerosol coagulation simulations were conducted by means of a sectional representation of the aerosol volume distribution (Gelbard et al., 1980; Seigneur, 1982). The simulations were conducted for 12 hours. Two initial aerosol size distributions were selected typical of hazy and urban atmospheres. The results of the simulations conducted with and without coagulation are presented in Figure 2. The initial size distributions do not change when coagulation does not occur. Coagulation appears to have a negligible effect in a hazy atmosphere, where the total aerosol volume below 2 μm is about 10 $\mu m^3 \cdot cm^{-3}$. In an urban atmosphere, where the total aerosol volume below 2 μm is about 44 $\mu m^3 \cdot cm^{-3}$, coagulation affects the concentrations of aerosols with diameters smaller than 1 μm, although the changes in aerosol concentrations are less than 10 percent for aerosols whose diameters are larger than 0.1 μm. However, to determine the necessity of including coagulation in aerosol regional modeling, one must also investigate the manner in which coagulation interacts with other dynamic processes such as aerosol growth.

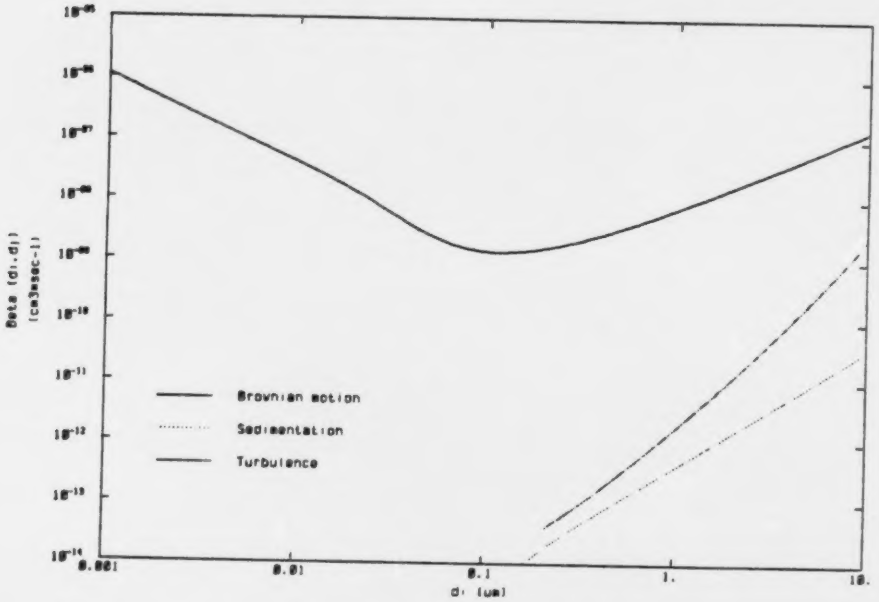

Fig. 1. Coagulation coefficients for an aerosol of 0.1 μm in diameter coagulating with aerosols in the 0.001 - 10 μm diameter range.

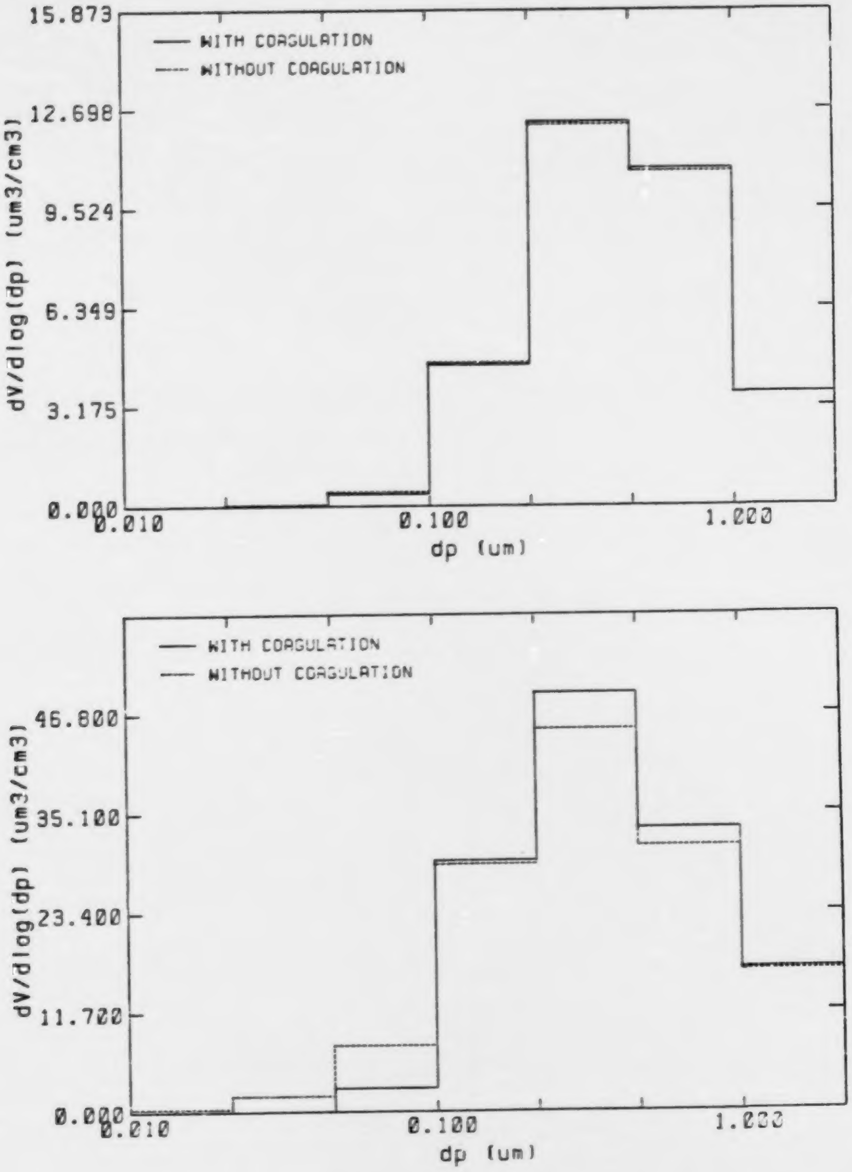

Fig. 2. Evolution of aerosol size distributions with and without coagulation for hazy (top) and urban (bottom) conditions.

Growth/Shrinkage

Aerosols may grow or shrink in size when material condenses or evaporates, respectively, or when its density changes due to a change in chemical composition. Growth or shrinkage does not affect the total aerosol number concentration; however, it affects the total aerosol mass and the aerosol size distribution. The change in the aerosol distribution due to growth or shrinkage of the aerosol is expressed mathematically as follows :

$$\frac{\partial n(v)}{\partial t} = - \frac{\partial}{\partial v} n(v) \frac{dv}{dt} \qquad (2)$$

The growth/shrinkage rate of aerosols depends on their size, and this size dependence in turn depends on the chemical process leading to condensation/evaporation of aerosol material (e.g., Friedlander, 1977; McMurry, 1980; Seinfeld and Bassett, 1980).

Condensation may occur following the gas-phase formation of a condensible species such as H_2SO_4 (a diffusion-limited condensation process), the conversion of a volatile precursor to a condensed product via reaction at the aerosol surface (e.g., oxidation of SO_2 to H_2SO_4 at the surface of carbon soot particles) or in a liquid film coating the aerosol (e.g., aqueous oxidation of SO_2 to H_2SO_4 in the presence of trace metals), and the equilibrium redistribution of a volatile species such as HNO_3 or H_2O between the gas and aerosol phases (e.g., because of a change in temperature, relative humidity, or ambient concentration).

The size dependence of the corresponding growth processes is depicted in Figure 3. Diffusion-limited condensation appears to encourage the growth of smaller aerosols, whereas aerosol droplet reaction and equilibrium displacement favor the growth of larger aerosols; aerosol surface reactions yield a growth process that is intermediate between the other two growth processes. The processes that lead to growth/shrinkage of aerosols and that should be included in a regional aerosol model are presented in Table 1.

Since growth/shrinkage processes affect the aerosol size distribution, it is of interest to investigate how the coupling of growth and coagulation influence the aerosol size distribution. Figure 4 presents the results of 12-hour simulations of the initial aerosol size distributions presented in Figure 2, with diffusion-limited condensation of ammonium sulfate taking place at a rate of 5.4 $\mu m^3 cm^{-3}$/12 hours and 4.4 $\mu m^3 cm^{-3}$/12 hours for the hazy and urban case studies, respectively. The amount of aerosol volume produced during condensation corresponds to 50 and 10 percent of the initial aerosol volume for the hazy and urban cases, respectively. The simulations were performed with and without coagulation.

The results of the urban case study do not differ significantly from those presented in Figure 2 since the aerosol volume is not greatly affected by condensation. However, there are larger discrepancies between the cases with and without coagulation than there are in the cases presented in Figure 2, where no condensation occurs. This result is even more apparent in the hazy case, where condensation leads to a notable increase in aerosol volume. In this case, neglecting coagulation when condensation takes place strongly affects the aerosol size distribution : diffusion-limited condensation leads to the growth of smaller aerosols; if coagulation takes place, these smaller aerosols are scavenged by larger aerosols in the 0.1 to 1.0 μm diameter range; if coagulation is ignored, the concentration of small aerosols increases unrealistically.

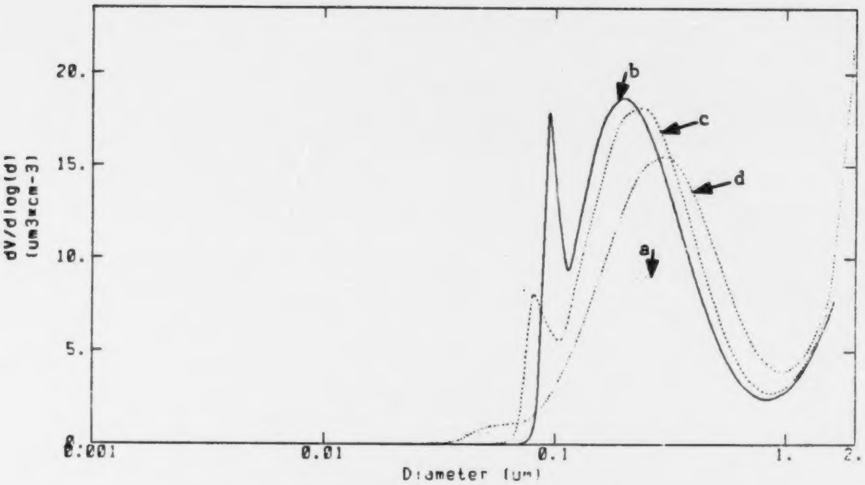

Fig. 3. Growth of an aerosol size distribution for various condensation processes. The amount of condensed material is 5.4 $\mu m^3/cm^{-3}$. Initial size distribution. Columbus, Ohio (Whitby, 1981b) (a = initial distribution; b = diffusion-limited; c = aerosol surface reaction; d = aerosol droplet reaction and equilibrium displacement). Simulations were performed with the CONFEMM model of Tsang and Brock (1983).

Table 1. Aerosol Growth/Shrinkage Processes of the Regional Aerosol Model

Growth/Shrinkage Law	Chemical Process*
Diffusion-limited condensation	Gas-phase formation of H_2SO_4 and condensible organics
Diffusion-limited evaporation	Evaporation of HCl†
Aerosol surface reactions	Oxidation of SO_2 to sulfate on carbon soot†
Aerosol droplet reactions	Oxidation of SO_2 to sulfate by O_2, H_2O_2 and O_3
Equilibrium displacement	Thermodynamic equilibrium of $HNO_3/NH_3/NH_4NO_3$ Deliquescence and hygroscopy of sulfate and nitrate ammonium salts Thermodynamic equilibrium of volatile organics† Change in aerosol density due to change in chemical composition

* The chemical processes are discussed in detail in the next section.

† These processes are not included in the regional model.

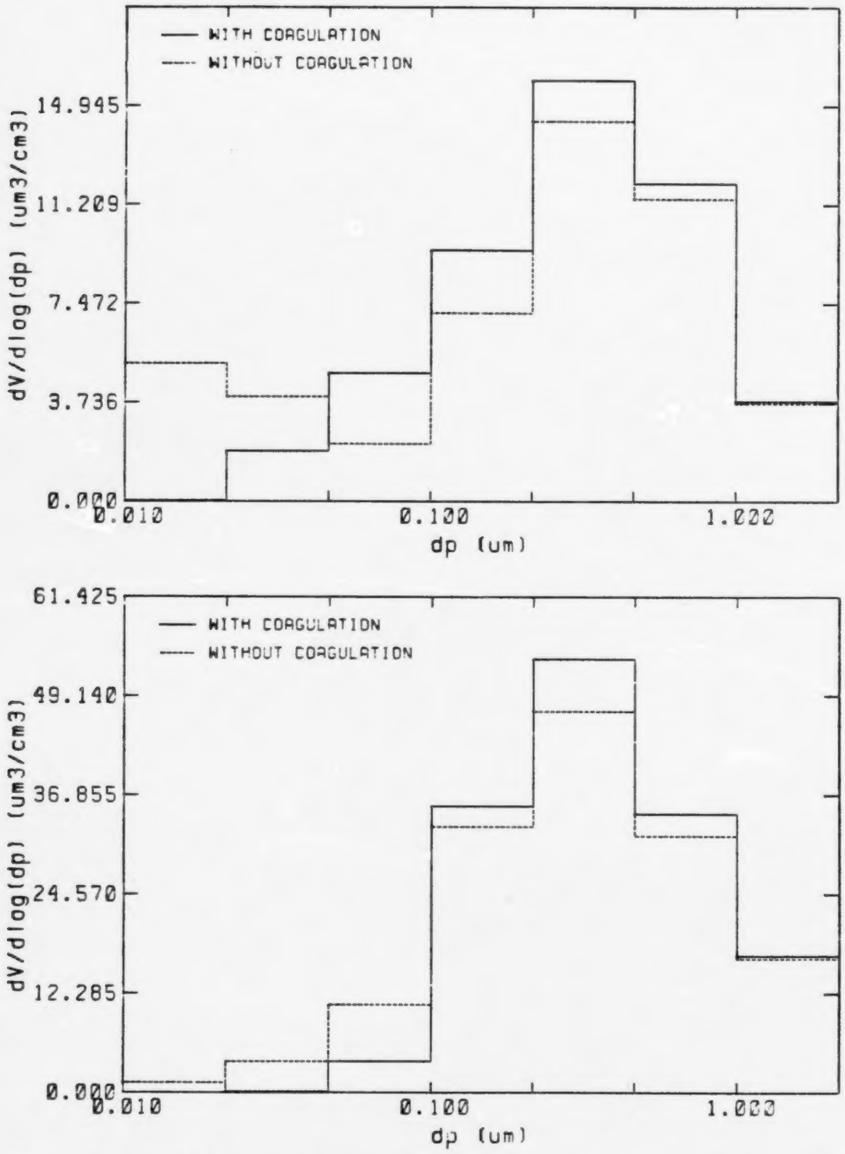

Fig. 4. Evolution of aerosol size distributions with condensation and with and without coagulation for hazy (top) and urban (bottom) conditions.

These results suggest that coagulation can be neglected in cases in which the aerosol volume is nearly constant; however, it is a critical process in the evolution of the aerosol size distribution when the aerosol volume increases due to gas-to-aerosol conversion. Coagulation should therefore be included in the simulation of regional aerosol dynamics.

Nucleation

Vapors that have a low vapor pressure, such as H_2SO_4, nucleate and form new aerosols. These new aerosols, whose size is of the order of 0.001 μm, grow quickly through coagulation with larger aerosols and condensation of additional vapor. Because the calculation of nucleation rates is sensitive to many parameters, these rates are rather uncertain. Also, the explicit treatment of nucleation requires modeling aerosols as small as of the order of 0.001 μm. Since aerosols smaller than 0.01 μm are rarely measured, we opted for an alternative approach that calculates the rate of formation of new aerosols growing beyond a given size. This size will correspond in our model to the lower size range of the aerosol size spectrum. The monomer-balance theory of McMurry (1983) is well suited for this approach and is used in the regional aerosol model.

Removal Processes

Aerosols are removed from the atmosphere via sedimentation, dry deposition, and wet deposition. All these processes are strongly dependent on the size of the aerosol. Figure 5 presents the evolution of an aerosol size distribution that is affected by sedimentation, dry deposition, and washout below precipitating clouds. Aerosols may also be removed by rainout in clouds through nucleation of cloud droplets on aerosols and scavenging of aerosols through coagulation, thermophoresis, diffusiophoresis, and electrophoresis.

Sedimentation primarily removes large aerosols, i.e., those whose diameters are larger than 2 μm. Dry deposition, simulated according to Sehmel and Hodgson (1980), affects both smaller and larger aerosols and is ineffective in removing aerosols whose diameters range from 0.01 to 1.0 μm. Washout by precipitation below clouds was simulated according to Wang et al. (1978). This process also removes larger aerosols and does not scavenge aerosols in the 0.01 to 1.0 μm diameter range, the so-called Greenfield gap (Greenfield, 1957). These results are based on theoretical considerations, and it should be noted that, although qualitative agreement exists between experimental results and model calculations, some discrepancies still need to be resolved (Radke et al., 1980). The regional aerosol model incorporates the treatment of dry deposition and sedimentation. Dry deposition is treated according to the model of Sehmel and Hodgson (1980). Sedimentation is modeled with the Stokes formula (e.g., Friedlander, 1977). Currently, no treatment of wet deposition is considered.

AEROSOL CHEMISTRY

The chemical composition of an aerosol depends upon the condensation of gaseous species on the aerosol and on the chemical transformation of species in the aerosol phase. We review in this section the chemical reactions that lead to condensible species in the gas phase, chemical reactions that occur in the aerosol phase, and equilibrium thermodynamics of aerosols.

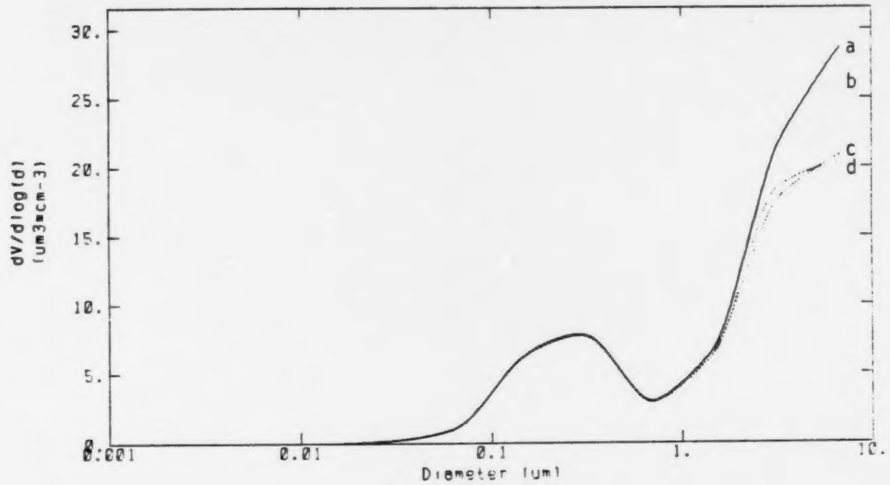

Fig. 5. Evolution of an aerosol size distribution undergoing removal by dry deposition, sedimentation, and washout by raindrops (a = initial distribution; b = sedimentation; c = wet deposition; d = dry deposition). Dry deposition and sedimentation were simulated for 12 hours under stable atmospheric conditions. The total aerosol removal used in simulating wet deposition was the same as that used for dry deposition.

Gas-Phase Chemical Reactions

Condensible species that are considered in the regional aerosol model include H_2SO_4, HNO_3, NH_3, and some organic products. Ammonia will react with H_2SO_4 and HNO_3 to yield ammonium salts. The reaction of NH_3 with H_2SO_4 is fast and may be assumed to be irreversible (McMurry et al., 1983). The reaction of HNO_3 with NH_3 is reversible (Stelson et al., 1979) and is discussed in a later section on aerosol thermodynamics. The reaction of HCl with NH_3 yields NH_4Cl aerosols. However, this species is more elusive than are other ammonium salts and is not considered in our model.

The major reactions that lead to H_2SO_4, HNO_3, and condensible organic species are listed in Table 2. The reaction of SO_2 with OH is the major pathway for the formation of H_2SO_4. The oxidation of SO_2 by Criegee intermediates may be significant only at very low relative humidities. The formation of HNO_3 is believed to occur predominantly via the oxidation of NO_2 by OH during the day and by the chemistry of NO_3 radicals at night. However, the oxidation of NO_2 by OH may also take place at night since high nighttime concentrations of free radicals have been observed. For example, Stedman (1985) reported nighttime concentrations of free radicals of the order of 10^{-7} ppm. The OH radicals could result from the thermal decomposition of peroxyacetylnitrate in the presence of NO (Seigneur and Saxena, 1984). The hydrolysis of N_2O_5 occurs slowly in the gas-phase but may proceed at a faster rate if it takes place heterogeneously at the aerosol surface. Both processes are included in the model. The details of the chemistry of organic aerosol formation are still uncertain. It has been observed, however, that aromatics and long-chain olefins lead to secondary aerosol formation (e.g. Heisler and Friedlander, 1977; Grosjean, 1984; Franzblau et al., 1984, Fox et al., 1984). These reactions are cast in the lumped form of the precursor being oxidized to a condensible product. No mechanistic details are included since they are still unknown. The stoichiometric coefficients will be defined from the results of smog chamber experiments.

Aerosol-Phase Chemical Reactions

The formation of nitrate in liquid droplets occurs too slowly to be of significance (Schwartz and White, 1983; Seigneur and Saxena, 1984). The formation of sulfate may occur at an appreciable rate in liquid droplets and is therefore likely to occur in liquid-coated aerosols. Atmospheric measurements of aerosol growth suggest the existence of such reactions (McMurry and Wilson, 1982, 1983; Gillani and Wilson, 1983). These reactions include the oxidation of SO_2 by O_2 catalyzed with trace metals, by H_2O_2 and by O_3. Preliminary calculations suggest that the oxidation of SO_2 by O_3 is too slow to be significant in liquid aerosols because the pH of the liquid film coating an aerosol is generally below 3, and the oxidation of SO_2 by O_3 is slow at these low pH values. The oxidation of SO_2 by H_2O_2 occurs at a notable rate at low pH values, and it is a major oxidation pathway for SO_2 in fog and cloud droplets. However, since the amount of water contained in aerosols is typically 1000 times less than that present in fog or clouds, the oxidation of SO_2 by H_2O_2 occurs at a slow rate-- of the order of 0.1 percent per hour. The oxidation of SO_2 by trace metals may be the major pathway; the kinetics of this pathway becomes slower as the pH decreases; however, trace metal concentrations tend to increase as the liquid water content decreases and will therefore maintain a faster kinetics than the reactions that involve O_3 and H_2O_2.

Table 2. Gas-Phase Reactions of Condensible Species

Reaction	Rate Parameter (ppm^{-1} min^{-1} and ppm^{-1})	Reference
$SO_2 + OH \rightarrow H_2SO_4 + HO_2$	1500	Atkinson and Lloyd, 1984
$NO_2 + OH \rightarrow HNO_3$	16000	Atkinson and Lloyd, 1984
$NO_2 + NO_3 \rightleftarrows N_2O_5$	1280	Atkinson and Lloyd, 1984
$N_2O_5 + H_2O \rightarrow 2HNO_3$	3.5×10^{-6} *	Tuazon et al., 1983
PHEN† + $NO_3 \rightarrow HNO_3$ + PHO†	15000	Atkinson and Lloyd, 1984
FORM + $NO_3 \rightarrow HNO_3 + HO_2 + CO$	0.93	Kerr and Calvert, 1984
ALD2 + $NO_3 \rightarrow HNO_3 + C_2O_3$	3.7	Kerr and Calvert, 1984
ARO† + OH → α_1 ORG	§	§
OLE† + $O_3 \rightarrow \alpha_2$ ORG	§	§
OLE† + OH → α_3 ORG	§	§

† Nomenclature of the Carbon-Bond Chemical Kinetic Mechanism:
PHEN = phenolic compound; PHO = phenoxy radical;
FORM = formaldehyde; ALD2 = other aldehydes;
C_2O_3 = peroxy radical; ARO = aromatic compound;
OLE = carbon-carbon double bond of olefins.

§ Rate parameters are to be determined.

* Rate parameter for the homogeneous reaction; this reaction may also take place heterogeneously at the aerosol surface.

Aerosol Thermodynamics

Several chemical species are present in both the aerosol and gas phases. The relative distribution of these species between the two phases is governed by equilibrium thermodynamics although diffusion kinetics may also contribute to the partition of a species between the two phases. In the regional aerosol model, it is assumed that chemical species are at thermodynamic equilibrium between the aerosol phase and the gas phase, and within the aerosol phase.

Inorganic species that are considered in the aerosol thermodynamic model include ammonium salts of sulfate and nitrate. These chemical species have been measured in atmospheric aerosols (e.g., Gaarenstroom et al., 1977; Lewis and Macias, 1980; Wolff et al., 1983; Harisson and Sturges, 1984) and are generally present in the fine aerosol range, i.e., in aerosols whose diameters are smaller than 2 μm. These aerosols result from the reactions of H_2SO_4 and HNO_3 with NH_3, as discussed previously.

Certain other sulfate and nitrate species have been measured in atmospheric aerosols that result from the displacement of other aerosol constituents. For example, HCl may be displaced from NaCl in marine aerosols by H_2SO_4 and HNO_3 (Harrison and Pio, 1983) to produce the salts Na_2SO_4 and $NaNO_3$. Similarly, $CaCO_3$ may react with H_2SO_4 to produce $CaSO_4$ and gaseous CO_2, and PbBrCl may be converted by reaction with H_2SO_4 to $PbSO_4$ and gaseous HCl and HBr. These species are not included in the aerosol thermodynamic model since quantitative descriptions of their thermodynamics have not yet been developed.

Another inorganic salt that has been observed in fine aerosols is NH_4Cl, which results from the reaction of NH_3 with HCl. This compound could eventually be included in the aerosol thermodynamic model; however, since its presence in aerosols is generally much less important than that of sulfate and nitrate ammonium salts and appears to be significant only near large sources of Cl_2 and HCl, it is not included in the model.

Several models of aerosol thermodynamics have been developed (Saxena et al., 1983; Bassett and Seinfeld, 1983, 1984; Saxena, 1984). The major characteristics of the behavior of atmospheric sulfate/nitrate/ammonium aerosols may be summarized as follows :

Sulfuric acid is much less volatile than is nitric acid. Since ammonia neutralizes the former preferentially, ammonium sulfate aerosols are formed first. As the ammonia concentration increases from 0 to more than twice the sulfuric acid concentration, the following aerosols are formed :

$[NH_3]^*_T = 0,$	$H_2SO_4(\ell)$
$0 < [NH_3]_T < [H_2SO_4],$	$H_2SO_4\ (\ell),\ NH_4HSO_4(s,\ \ell)$
$[H_2SO_4] < [NH_3]_T < 1.5[H_2SO_4],$	$NH_4HSO_4(s,\ \ell),\ (NH_4)_3H(SO_4)_2(s,\ \ell)$
$1.5[H_2SO_4] < [NH_3]_T < 2[H_2SO_4],$	$(NH_4)_3H(SO_4)_2(s,\ \ell),\ (NH_4)_2SO_4(s,\ \ell)$
$0 < [NH_3]_T - 2[H_2SO_4] < \frac{K_{AN}}{[HNO_3]},$	$(NH_4)_2SO_4(s,\ \ell)$
$\frac{K_{AN}}{[HNO_3]} < [NH_3]_T - 2[H_2SO_4],$	$(NH_4)_2SO_4(s,\ \ell),\ NH_4NO_3(s,\ \ell),$ $(NH_4)_2SO_4 \cdot 2NH_4NO_3(s),\ (NH_4)_2SO_4 \cdot 3NH_4NO_3(s)$

The equilibrium constant K_{AN} for ammonium nitrate is a function of the relative humidity, temperature, and aerosol pH (Stelson and Seinfeld, 1982a, 1982b). Ammonium nitrate aerosols are formed when the product of the gas phase concentrations of NH_3 and HNO_3 exceeds the saturation equilibrium constant K_{AN}.

The aerosol species listed above may be present in a liquid or solid phase. If these species are present in a liquid phase, the ionic species H^+, HSO_4^-, SO_4^{2-}, NO_3^-, and NH_4^+ will result from the ionization of the aerosol salts. It should be noted that if the species are present in a liquid phase, a minute amount of HNO_3 will dissolve, and nitrate will be present in the aerosol.

The existence of a liquid film around the aerosol depends primarily on the deliquescent properties of the aerosol. At an ambient temperature of 25°C, the following relative humidities of deliquescence will determine the state of the aerosol :

Aerosol Species	Relative Humidity of Deliquescence
H_2SO_4	Always liquid
NH_4HSO_4	40 percent
$(NH_4)_3H(SO_4)_2$	69 percent
$(NH_4)_2SO_4$	80 percent
NH_4NO_3	62 percent

---

* $[NH_3]_T$ represents the total ammonia concentration prior to neutralization of H_2SO_4 and HNO_3.

A given salt may be present in the solid phase above its relative humidity of deliquescence if its saturation product in the liquid phase is exceeded. For example, the following relationships are defined for ammonium sulfate and nitrate (Saxena et al., 1983).

$$[NH_4^+]^2 \ [SO_4^{2-}] \leq 1.05 \ mol^3.kg^{-3}$$

$$[NH_4^+] \ [NO_3^-] < 13.06 \ mol^2.kg^{-2}$$

Above their relative humidities of deliquescence, sulfate and nitrate aerosols are hygroscopic, that is, the amount of associated condensed water increases as relative humidity increases.

MATHEMATICAL MODELS OF ATMOSPHERIC AEROSOLS

A model that describes the evolution of the aerosol concentration, size distribution, and chemical composition in a grid cell of a 3-D regional model must treat aerosol dynamics (i.e., coagulation, growth, and shrinkage), thermodynamics (i.e., equilibrium of sulfate, nitrate, and ammonium species), and chemical kinetics (i.e., gaseous, heterogeneous, and aqueous). Emission, transport, and removal processes are included as inter-grid-cell processes in the regional model and are therefore not discussed further here. A mathematical model of aerosol dynamics, thermodynamics, and chemical kinetics does not currently exist. However, individual models that describe the dynamics, thermodynamics, or kinetics, of aerosols do exist. We have discussed mechanisms for the chemical kinetics of aerosol species formation in the previous section. In this section we focus on the selection of models of aerosol dynamics and thermodynamics.

Because of the computational requirements of a regional-scale simulation, it is imperative to develop an aerosol model that offers a reasonably accurate solution and is computationally efficient. To that end, we reviewed several mathematical models of aerosol dynamics and thermodynamics of various degrees of sophistication. This section presents an overview of these mathematical models and general discussions of their comparative accuracies and computational requirements.

Aerosol Dynamics Models

In solving the mathematical equations of aerosol system dynamics, most difficulties are associated with the solution of the coagulation and condensation/evaporation terms. The coagulation term consists of an integro-differential equation, and the condensation/evaporation term consists of a hyperbolic differential equation. Three major approaches have been developed to simulate aerosol dynamics. These approaches differ primarily in their representation of the size distribution of aerosols--continuous, discrete, and parameterized. Examples of an aerosol size distribution modeled with continuous, discrete, and parameterized lognormal representations are presented in Figure 6.

The first approach, based on a continuous representation of the aerosol size distribution, involves finding the exact solution of the mathematical equations using numerical techniques for the evaluation of integrals. This approach requires the use of an accurate numerical technique and may therefore be computationally expensive. In our study, this approach is characterized by the COAGUL model for the simulation of coagulation (Suck and Brock, 1979) and the CONFEMM model for the simulation of condensation (Tsang and Brock, 1982).

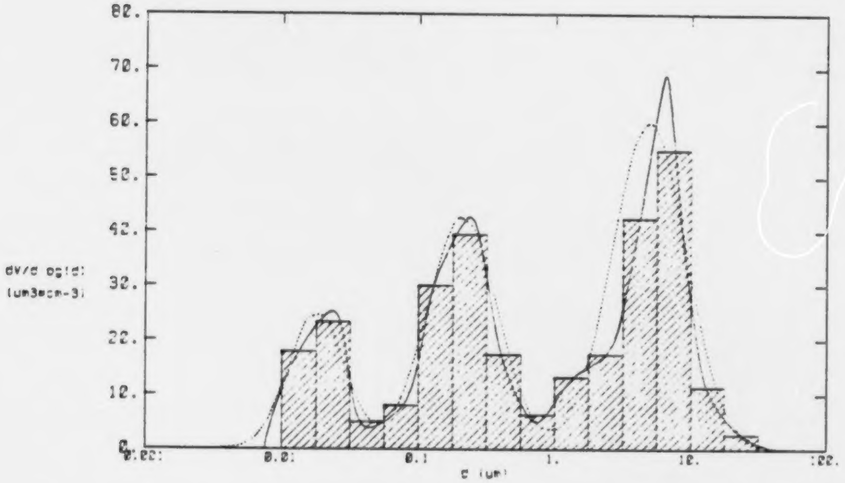

Fig. 6. Representation of an aerosol size distribution with a continuous representation (——), lognormal modal representation (┈┈┈) and sectional representation (▨) --background size distribution. 29 October 1975, General Motors Sulfate Study. Source: (Whitby, 1978).

In the second approach, a discrete approximation is made to the continuous representation of the aerosol size distribution. The accuracy of the solution and the corresponding computational costs depend, therefore, on the resolution of the discrete approximation. As the discrete approximation tends toward the continuous representation, the solution of this approach tends toward the exact solution. This approach is characterized by the ESMAP model for the simulation of coagulation and condensation (Warren and Seinfeld, 1984).

The third approach assumes a known form of the mathematical representation of the aerosol size distribution, and thus the solution of the dynamic equation involves the calculation of the parameters of this mathematical expression. This approach is represented by the AGRO model (Whitby, 1981a; Whitby and McMurry, 1984), which assumes lognormal distributions of the nuclei, accumulation, and coarse aerosol modes.

Of these three methods, the first approach yields the most accurate results. The third approach, because of its parameterization, provides less accurate results. The accuracy of the second approach depends on the resolution of the discrete approximation. Conversely, the computational cost of the numerical solution is highest for the first approach and lowest for the third approach. Both accuracy and computational cost need to be taken into account in modeling aerosol dynamics at the regional scale.

The solution of a continuous representation of the aerosol size distribution is actually obtained by a numerical solution that approximates the size distribution of a finite number of points. Comparisons with analytical solutions suggest that 40 points can accurately represent the size distribution of aerosols whose diameters range from 0.001 to 10 μm. For coagulation, quadrature with spline functions and solution of a set of ordinary differential equations are carried out. For condensation, a finite element method that minimizes numerical dispersion and diffusion is used.

The solution of the discrete, or sectional, representation of the aerosol size distribution is obtained by solving a set of ordinary differential equations. No quadrature is needed for the integration of the coagulation equation since it has already been performed in the calculation of the sectional coagulation coefficients. Solution of the condensation equation may involve some numerical diffusion because of the sectional representation. The number of differential equations to be solved depends on the resolution of the sectional representation.

The solution of the parameterized representation requires the solution of four ordinary differential equations for the total number and volume of the nuclei and accumulation modes, respectively. No quadrature is needed since it is implicitly included in the definition of the parameterized coagulation coefficients of aerosol dynamics.

The AGRO, ESMAP (with 12 and 39 sections), COAGUL and CONFEMM models were applied to the simulation of coagulation and condensation for atmospheric concentrations typical of clear, hazy, and urban conditions. Simulations were conducted for 12 hours for aerosols in the size range 0.001 to 10 μm. Condensation was treated as a diffusion-limited condensation of ammonium sulfate. Condensation amounted to 0.3, 5.4, and 4.4 $\mu m^3 cm^{-3}$ for clear, hazy, and urban conditions, respectively. A summary of the mathematical models is given in Table 3. The results of the model simulations are presented in Table 4. Figure 7 presents the aerosol size distribution calculated after 12 hours of simulation with coagulation and condensation for hazy conditions.

Table 3. Summary of Mathematical Models for Simulation of Aerosol Dynamics in the Size Range 0.001 to 10 μm.

Dynamic Equation	Number of Differential Equations Solved	Model	
		Coagulation	Condensation
Continuous	40	COAGUL	CONFEMM
Sectional	39	ESMAP	ESMAP
	12	ESMAP	ESMAP
Parameterized	4	AGRO	AGRO

Table 4. Preliminary Comparison of Model Simulation Results

Coagulation				Condensation			
Model	Average Percentage Difference			Model	Average Percentage Difference		
	Clear	Hazy	Urban		Clear	Hazy	Urban
COAGUL		(Reference)		CONFEMM		(Reference)	
ESMAP (39 sections)	1%	2%	7%	ESMAP (39 sections)	9%	12%	3%
ESMAP (12 sections)	3%	9%	10%	ESMAP (12 sections)	18%	35%	10%
AGRO	3%	6%	39%	AGRO	19%	37%	13%

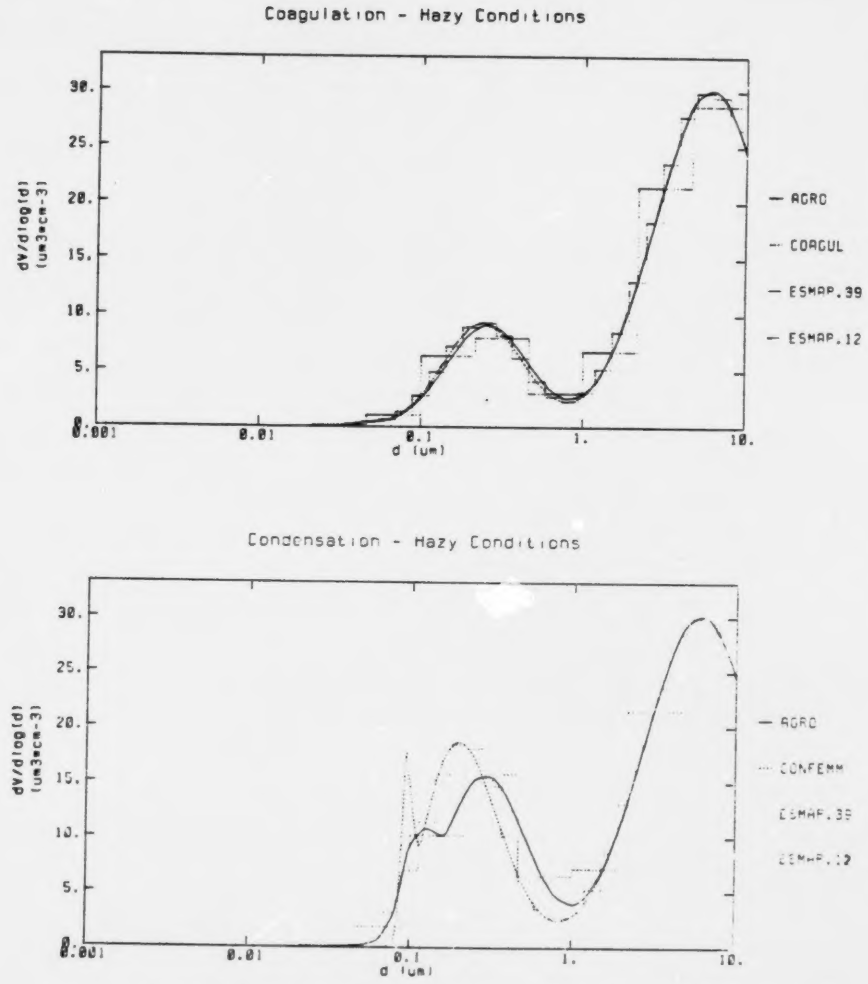

Fig. 7. Simulation of the evolution of an aerosol size distribution undergoing coagulation (top) and condensation (bottom).

In this model comparison, the COAGUL and CONFEMM models were taken as reference since they are based on accurate numerical solutions of the continuous number distribution equation.

The results presented in Table 4 and Figure 7 indicate that the ESMAP model, with either 39 or 12 sections, accurately simulates coagulation. Because the AGRO model assumes a constant standard deviation for the lognormal distributions, it is much less accurate, particularly for urban conditions. The ESMAP and COAGUL models show that the standard deviation actually decreases as coagulation takes place. The AGRO model is being improved to include a time-dependent standard deviation.

The ESMAP model simulates condensation less accurately than it simulates coagulation because of numerical diffusion resulting from the sectional representation. The performance of the AGRO model is reasonable, considering its lower computational requirements. It should be noted that the computational requirements of the AGRO model are about 50 times less than those of the COAGUL and CONFEMM models. The computational requirements of the ESMAP model, which lie between those of the AGRO model and those of the COAGUL and CONFEMM models, depend on the number of sections used to represent the aerosol size distribution. A more detailed comparison of these aerosol dynamics models awaits the development of a final version of the AGRO model and will be reported later.

Aerosol Thermodynamics Models

Models of aerosol thermodynamics considered in this review simulate the thermodynamic equilibrium of sulfate/nitrate/ammonium aerosols. These models include the KEQUIL (Bassett and Seinfeld, 1984), EQUIL (Bassett and Seinfeld, 1983), and MARS (Saxena, 1984) models. These models calculate the amount of sulfate, nitrate, ammonium, and water present in the aerosol as a function of the gas-phase concentrations of sulfuric acid, nitric acid, and ammonia, previous sulfate, nitrate, and ammonium aerosol concentrations, relative humidity, and temperature. These calculations are based upon basic thermodynamic principles.

The KEQUIL model provides an accurate solution of the thermodynamic equations including the Kelvin effect, i.e., the effect of aerosol size on the aerosol chemical composition. The EQUIL model is based on the same thermodynamic equations as is the KEQUIL model but assumes that the aerosol chemical composition is independent of size. The MARS model was developed to provide a computationally less demanding yet fairly accurate solution of the thermodynamic equilibrium problem. It includes several assumptions regarding the aerosol chemical composition that allow reduction of the number of thermodynamic equilibrium relationships considered. Comparison of these models is being carried out and will be reported later.

Formulation of the Aerosol Model

The aerosol model developed for regional applications will require good predictive accuracy as well as reasonable computational costs. For these reasons, we selected a sectional representation of the aerosol size distribution between 0.01 and 10 µm. Seven size sections are included between 0.01 and 2.5 µm (fine aerosol range). Two sections constitute the coarse aerosol range from 2.5 to 10 µm. Aerosols in the fine range undergo coagulation, growth/shrinkage, new aerosol formation at 0.01 µm, thermodynamic equilibrium, aerosol chemical reactions, and dry deposition. Aerosols in the coarse aerosol range undergo dry deposition and sedimentation. All aerosol size ranges are also affected by emissions and atmospheric transport.

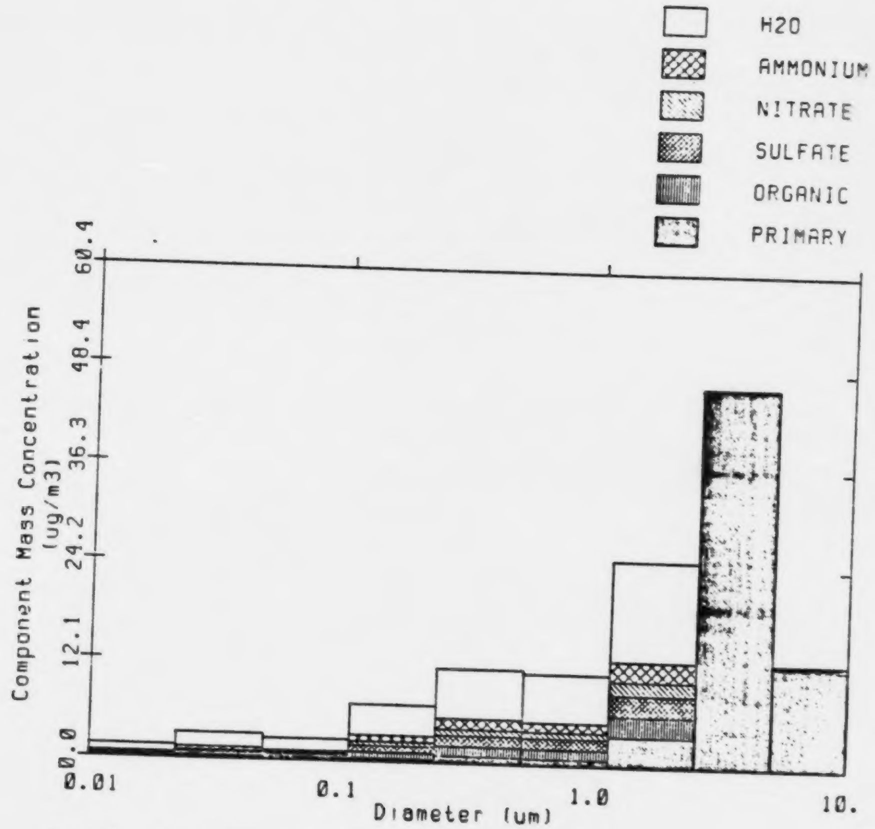

Fig. 8. Example of the concentration and chemical composition of a size-distributed aerosol calculated by the regional aerosol model.

The thermodynamics of the aerosols are treated with the MARS model. A typical aerosol population calculated by the model is presented in Figure 8.

CONCLUSION

We have reviewed the physical and chemical processes that affect the concentration, size distribution, and chemical composition of atmospheric aerosols at the regional scale. Physical processes include coagulation, growth or shrinkage of the aerosols due to condensation or evaporation, nucleation of new aerosols, sedimentation, and dry and wet deposition. Chemical processes include thermodynamic equilibrium between the gas and aerosol phases and within the aerosol phase, gas-phase chemical reactions leading to cendensible vapor, and aerosol-phase chemical reactions.

Our present model for regional aerosols treats aerosols that consist of a nonvolatile solid core, sulfate, nitrate, ammonium, and organic species. The chemical composition is assumed to be independent of the aerosol size. The size distribution is approximated with a sectional representation. This approach was shown to be fairly accurate when compared with more accurate models.

Further work will involve incorporating this model of aerosol dynamics and chemistry in the EPA regional model, some treatment of aerosols in clouds, and the evaluation of this regional aerosol model with field data.

ACKNOWLEDGMENTS

We thank Professors K.T. Whitby, J.H. Seinfeld, and J.R. Brock for providing us with their aerosol models and giving us helpful advice during the course of this work. We thank Mr. E. Whitby and Professor P.H. McMurry for helpful discussions concerning the AGRO model and its computational implementation. We are grateful to Dr. M.C. Dodge for her comments regarding the gas-phase chemistry. We thank Ms. A.B. Hudischewskyj for performing the model simulations and computer graphics, and Ms. J.A. Rodich for editing this manuscript.

REFERENCES

Atkinson, R., and Lloyd, A.C., 1984, Evaluation of kinetic and mechanistic data for modeling of photochemical smog, J. Phys. Chem. Ref. Data, 13:315-444.

Bassett, M.E., and Seinfeld, J.H., 1983, Atmospheric equilibrium model of sulfate and nitrate aerosols, Atmos. Environ., 17:2237-2252

Bassett, M.E., and Seinfeld, J.H., 1984, Atmospheric equilibrium model of sulfate and nitrate aerosols--II. particle size analysis, Atmos. Environ., 18:1163-1170

Calvert, J.G., and Stockwell, W.R., 1983, Acid generation in the troposphere by gas-phase chemistry, Environ. Sci. Technol., 17:428A-443A

Fox, D.L., Gery, M., and Jeffries, H.E., 1984, "Organic Aerosol Formation : OH vs. Ozone Oxidation Pathways," Coordinating Research Council, Inc., Atlanta, Georgia

Franzblau, E., Burton, C.S. and Hidy, G.M., 1984, Aerosol particle formation from ozone-terminal olefin reactions, Aerosol Sci. Technol., 3:167-176

Friedlander, S.K., 1977, "Smoke, Dust and Haze--Fundamentals of Aerosol Behavior," John Wiley, New York

Gautier, O., 1984, "Process Control Optimization Theory Applied to Complex Chemical Systems," M.S. thesis, University of Minnesota, Minneapolis, Minnesota

Gelbard, F., Tambour, Y., and Seinfeld, J.H., 1980, Sectional representation for simulating aerosol dynamics, *J. Colloid Interface Sci.*, 76:541-556

Gillani, N.V., and Wilson, W.E., 1983, Gas-to-particle conversion of sulfur in power plant plumes--II. observations of liquid-phase conversions, *Atmos. Environ.*, 17:1739-1752

Greenfield, S., 1957, Rain scavenging of radioactive particulate matter from the atmosphere, *J. Meteorol.*, 14:115-125

Grosjean, D., 1984, Atmospheric reactions of ortho-cresol : gas phase and aerosol products, *Atmos. Environ.*, 18:1641-1652

Harrison, R.M. and Pio, C.A., 1983, Major ion composition and chemical associations of inorganic atmospheric aerosols, *Environ. Sci. Technol.* 17:167-174

Harrison, R.M., and Sturges, W.T., 1984, Physico-chemical speciation and transformation reactions of particulate atmospheric nitrogen and sulphur compounds, *Atmos. Environ.*, 18:1829-1833.

Heisler, S.L., and Friedlander, S.K., 1977, Gas-to-particle conversion in photochemical smog : aerosol growth laws and mechanisms of organics, *Atmos. Environ.*, 11:157-168

Kerr, J.A., and Calvert, J.G., 1984, "Chemical Transformation Modules for Eulerian Acid Deposition Models--Volume I : The Gas-Phase Chemistry," U.S. Environmental Protection Agency, Research Triangle Park, North Carolina

Killus, J.P., and Whitten, G.Z., 1984, Unpublished manuscript. Systems Applications, Inc., San Rafael, California

Lamb, R.G., 1984a, "A Regional Scale (1000 km) Model of Photochemical Air Pollution, Part 2, Input Processor Network Design," EPA-600/3-84-085, U.S. Environmental Protection Agency, Research Triangle Park, North Carolina

Lamb, R.G., 1984b, Air pollution models as descriptors of cause-effect relationships, *Atmos. Environ.*, 18:591-606.

Lamb, R.G., 1983, "A Regional Scale (1000 km) Model of Photochemical Air Pollution, Part 1, Theoretical Formulation," EPA-600/3-83-03r, U.S. Environmental Protection Agency, Research Triangle Park, North Carolina

Lewis, C.W., and Macias, E.S., 1980, Composition of size-fractionated aerosol in Charleston, West Virginia, *Atmos. Environ.*, 14:185-194

McMurry, P.H., 1983, New particle formation in the presence of an aerosol : rates, time scales, and sub-0.01 μm size distributions, *J. Colloid Interface Sci.*, 95:72-80

McMurry, P.H., 1980, The dynamics of secondary sulfur aerosols, in : "Atmospheric Sulfur Deposition : Environmental Impact and Health Effects," Shriner, Richmond, and Lindberg, eds., Ann Arbor Science Publishers, Inc., Ann Arbor, Michigan.

McMurry, P.H., Takano, H., and Anderson, G.R., 1983, A study of the ammonia (gas)-sulfuric acid (aerosol) reaction rate, Environ. Sci. Technol., 17:347-351

McMurry, P.H., and Wilson, J.C., 1983, Droplet phase (heterogeneous) and gas phase (homogeneous) contributions to secondary ambient aerosol formation as functions of relative humidity, J. Geophys. Res., 88:5101-5108

McMurry, P.H., and Wilson, J.C., 1982, Growth laws for the formation of secondary ambient aerosols : implications for chemical conversion mechanisms, Atmos. Environ., 16:121-134.

Novak, J.H., 1984 "Implementation of the EPA Regional Oxidant Model System", 77th Air Pollution Control Association Annual Meeting, San Francisco, California, 25-29 June 1984.

Radke, L.F., Hobbs, P.V., and Eltgroth, M.W., 1980, Scavenging of aerosol particles by precipitation, J. Appl. Meteorol., 19:715-722

Saxena, P., 1984, Unpublished manuscript. Systems Applications, Inc., San Rafael, California.

Saxena, P., Seigneur, C., and Peterson, T.W., 1983, Modeling of multiphase atmospheric aerosols, Atmos. Environ., 17:1315-1329

Schere, K.L., and Possiel, N.C., 1984, "U.S. EPA Regional Oxidant Model-Background and Overview," 77th Air Pollution Control Association Annual Meeting, San Francisco, California, 25-29 June 1984.

Schwartz, S.E., and White, W.H., 1983, Kinetics of reactive dissolution of nitrogen oxides into aqueous solution, Adv. Environ. Sci. Technol., 12:1-116

Sehmel, G.A., and Hodgson, W.H., 1980, A model for predicting dry deposition of particles and gases to environmental surfaces, AIChE Symposium Series, 76:218-230

Seigneur, C., 1982, A model of sulfate aerosol dynamics in atmospheric plumes, Atmos. Environ., 16:2207-2228

Seigneur, C., and Saxena, P., 1984, A study of atmospheric acid formation in different environments, Atmos. Environ., 18:2109-2124

Seigneur, C., Saxena, P., and Roth, P.M., 1985, Chemistry of sulfate and nitrate formation, in : "Air Pollution Modeling and Its Applications," 4:129-154, C. de Wispelaere, ed., Plenum Press, New York

Seigneur, C., Stephanopoulos, G., and Carr, R.W., 1982, Dynamic sensitivity analysis of chemical reaction systems--a variational method, Chem. Eng. Sci., 37:845-853

Seinfeld, J.H., and Bassett, M., 1980, Effect of the mechanism of gas-to-particle conversion on the evolution of aerosol size distributions, in : "Heterogeneous Atmospheric Chemistry," pp 6-12, D.R. Schryer, ed., American Geophysical Union, Washington, D.C.

Stedman, D., 1985, Private communication.

Stelson, A.W., Friedlander, S.K., and Seinfeld, J.H., 1979, A note on the equilibrium relationship between ammonia and nitric acid and particulate ammonium nitrate, *Atmos. Environ.*, 13:369-371

Stelson, A.W., and Seinfeld, J.H., 1982a, Relative humidity and temperature dependence of the ammonium nitrate dissociation constant, *Atmos. Environ.*, 16:983-992

Stelson, A.W., and Seinfeld, J.H., 1982b, Relative humidity and pH dependence of the vapor pressure of ammonium nitrate-nitric acid solution at 25°C, *Atmos. Environ.*, 16:993-1000

Suck, S.H., and Brock, J.R., 1979, Evolution of atmospheric aerosol particle size distributions via Brownian coagulation : numerical simulation, *J. Aerosol Sci.*, 10:581-590

Tsang, T.H., and Brock, J.R., 1983, Simulation of condensational aerosol growth by condensation and evaporation, *Aerosol Sci. Technol.*, 2:311-320.

Tuazon, E.C., Atkinson, R., Plum, C.N., Winer, A.M., and Pitts, J.N. Jr., 1983, The reaction of gas-phase N_2O_5 with water vapor, *Geophys. Res. Lett.*, 10:953-956

Wang, P.K., Grover, S.N., and Pruppacher, H.R., 1978, On the effect of electric charges on the scavenging of aerosol particles by clouds and small raindrops, *J. Atmos. Sci.*, 35:1735-1743

Warren, D.R., and Seinfeld, J.H., 1984, Simulation of aerosol size distribution evolution in systems with simultaneous nucleation, condensation, and coagulation, *Aerosol Sci. Technol.*, 4:31-43

Whitby, E., and McMurry, P.H., 1984, Private communication.

Whitby, K.T., 1981a, Determination of aerosol growth rates in the atmosphere using lumped aerosol dynamics, *J. Aerosol Sci.*, 12:174-178

Whitby, K.T., 1981b, "Aerosol and Ozone Formations in the Columbus, Ohio Urban Plume on July 29 and 30, 1980 : A Preliminary Report," Particle Technology Laboratory, Depertement of Mechanical Engineering, University of Minnesota, Minneapolis, Minnesota (Publication No. 447)

Wolff, G.T., Kelly, N.A., Ferman, M.A., and Morrison, M.L., 1983, Rural measurements of the chemical composition of airborne particles in the eastern United States, *J. Geophys. Res.*, 88:10769-10775

DISCUSSION

W. WHITE

If you start the model up with no initial aerosol and let it run until it settles down, does it generate an accumulation mode from nuclei-mode and coarse-mode emissions ?

C. SEIGNEUR

Yes, the model will generate an accumulation mode from nuclei-mode emissions since the model treats coagulation and condensational growth. However, if no accumulation mode is initially present, it will take time (either in a experiment or a model simulation) to see nuclei-mode aerosols grow into the accumulation mode by coagulation and condensational growth.

G. SVERDRUP Please compare the performance of algorithms KEQUIL, EQUIL, and MARS for aerosol composition at various relative humidities.

G. SEIGNEUR The KEQUIL, EQUIL and MARS models were compared for a total of 56 case studies that covered a wide range of sulfate, nitrate and ammonium concentrations, relative humidity and aerosol size distributions. The predictions of the MARS model are in the average within 8 percent of the predictions of the KEQUIL model. The MARS model performs best for low relative humidities since the calculations of the aqueous aerosol concentrations at high humidities are more complex then the dry aerosol concentration calculations. The predictions of the EQUIL model are on the average within 4 percent of the predictions of the KEQUIL model. The differences between the EQUIL and KEQUIL models are the largest for cases with aerosol size distributions that have large concentrations of small aerosols. This result occurs because the effect of the aerosol size on the aerosol chemical composition increases as the aerosol size decreases.

K. DEMERJIAN Does the MARS aerosol model have temperature dependence for the various thermodynamic equilibrium processes important in understanding gas phase ⇄ aerosols phase - and absorption - desorption processes on wet aerosol surfaces ?

C. SEIGNEUR The MARS model includes temperature dependence for the gas-phase/aerosol-phase equilibrium constant of ammonia/nitric acid/ammonium nitrate since this equilibrium is strongly temperature sensitive. Other parameters such as the binary data used for the calculation of the activity coefficients of the aqueous aerosol phase are not as strongly temperature dependent and are input for a temperature of 25°C.

Atmospheric Environment Vol. 20, No. 7, pp. 1471–1483, 1986.
Printed in Great Britain.

Pergamon Journals Ltd.

Appendix B

A COMPARATIVE STUDY OF EQUILIBRIUM APPROACHES TO THE CHEMICAL CHARACTERIZATION OF SECONDARY AEROSOLS

PRADEEP SAXENA,* A. BELLE HUDISCHEWSKYJ and CHRISTIAN SEIGNEUR
Systems Applications, Incorporated, 101, Lucas Valley Road, San Rafael, California 94903, U.S.A.

and

JOHN H. SEINFELD
Department of Chemical Engineering, California Institute of Technology, Pasadena, California 91125, U.S.A.

(*First received* 30 *April* 1985 *and in final form* 30 *October* 1985)

Abstract—This paper presents an equilibrium model for prediction of the mass and chemical composition of atmospheric aerosols containing sulfate, nitrate, ammonium, and water. The Model for an Aerosol Reacting System (MARS) is particularly intended for incorporation into larger air quality, visibility, or aerosol dynamics models. Computational efficiency, in addition to satisfactory performance, is an important consideration in such applications. The predictions of MARS agree with those of two comprehensive models currently available. However, the computational efficiency of MARS is shown to be substantially greater than that of the other two models.

Key word index: Aerosol, sulfate, nitrate, thermodynamic equilibrium, size distribution, scattering.

1. INTRODUCTION

The relevance of secondary aerosols to several issues involving air quality is well established. Airborne particulate matter is known to have adverse impacts on human health, materials and visibility. The U.S. Environmental Protection Agency (EPA) enforces air quality standards for total suspended particulate matter (TSP), and a standard for particulate matter with a diameter of less than 10 μm (PM 10) is currently being promulgated. EPA is also studying an ambient standard for particulate matter with a diameter of less than 2.5 μm (PM 2.5). Meanwhile, the State of California has already begun enforcing its own PM 10 standard. The passage of the Clean Air Act Amendments in 1977 identified the protection of visibility in national parks and wilderness areas (Class I areas) as an integral part of air quality management in the United States. In response to this mandate, EPA promulgated visibility regulations for Class I areas. The State of California has a standard for visibility-reducing particles. Atmospheric aerosols play a pivotal role in acid deposition. Acidic species in atmospheric aerosol are deposited on buildings, soil, vegetation, and aquatic systems by dry and wet processes. This deposition may lead to detrimental effects such as increased lake acidity, leaching of toxic material, and damage to flora and monuments.

Among atmospheric aerosols of all sizes, particles in the accumulation mode ($0.1\ \mu\text{m} \leq d_p \leq 2.5\ \mu\text{m}$) are the most critical with respect to health, visibility, and adverse effects caused by acid precipitation. Most of the mass of the secondary aerosols, i.e. the particles formed by gas-to-particle conversion processes, tends to reside in this range. Although numerous chemical species have been identified in secondary aerosols, the most prevalent are sulfate, nitrate, ammonium and water. Therefore, the formation of secondary aerosols from gaseous H_2SO_4, HNO_3, NH_3 and H_2O has been the subject of much theoretical and experimental investigation. These studies have focused on physical and chemical properties such as size distribution, light scattering coefficient, and chemical composition.

Mathematical models have been developed to study aerosol formation in plumes and in urban areas. Such predictive approaches can provide a convenient and reliable means to assess source contributions. If the models perform satisfactorily, they can be employed as effective regulatory tools for emission control strategy design. The nature of information sought from these models varies with the application. For a visibility study it is desirable to know total aerosol mass, as a function of particle size, in the particle size range 0.1–2.5 μm. Knowledge of the chemical composition is essential for acid precipitation modeling, while for PM 10 studies it suffices to know the total mass for particles with $d_p \leq 10\ \mu$m. Therefore, if an aerosol model were to be developed for all these applications, it should be able to predict, with an acceptable degree of accuracy, total aerosol mass and chemical composition as a function of particle size. Furthermore, as such aerosol models will be used in larger regional, urban air quality, or plume models, they must be computationally inexpensive. Saxena *et al.* (1983) and Bassett and Seinfeld (1983, 1984) have developed thermodynamic models of inorganic sulfate and nitrate aerosols. These models determine the equilibrium composition and state of the aerosol by either solving the equilibrium equations or minimizing the Gibbs free energy of the system. Because of their inherent rigorous treatment, these models are computationally expensive when considered for use in large-scale air quality models in which the thermodynamic calculation must be repeated many times. The object of this study is to combine computational efficiency with reasonable accuracy for aerosol thermodynamic models.

---

*To whom correspondence should be addressed.

This paper presents the development and application of an aerosol model for regional and urban applications. The Model for an Aerosol Reacting System (MARS) predicts the quantity and composition of secondary atmospheric aerosols containing sulfate, nitrate, and ammonium compounds. A thermodynamic approach is adopted to predict the chemical composition of multiphase aerosols containing water, $(NH_4)_2SO_4$, NH_4HSO_4, $(NH_4)_3H(SO_4)_2$, H_2SO_4, HNO_3, and NH_4NO_3. This treatment is based on the results of theoretical, laboratory and field studies. Model predictions and computational times are compared with those for two rigorous models available to date (Bassett and Seinfeld, 1983, 1984).

Section 2 summarizes the thermodynamic concepts customarily employed in aerosol studies to date. Also presented in this section are some important conclusions, drawn from these thermodynamic considerations, that were instrumental in the development of MARS. A technical description of MARS is presented in section 3. The salient features of the models of Bassett and Seinfeld (1983, 1984) called EQUIL and KEQUIL are also summarized in this section. EQUIL and KEQUIL are particularly rigorous and comprehensive and thus provide a reasonable basis for the evaluation of MARS' performance. In section 4 we compare the predictions from MARS and EQUIL with those from KEQUIL for aerosol mass, composition, size distribution, and light scattering coefficient. The conclusions of this study are presented in section 5.

2. THERMODYNAMIC CONSIDERATIONS

In this section we examine the principal features of thermodynamic equilibrium involving H_2SO_4, HNO_3, NH_3 and H_2O in the atmosphere. These concepts have been employed in earlier modeling studies and are derived from theoretical as well as experimental evidence.

Inorganic sulfate exhibits a low volatility (Roedel, 1979) and therefore tends to reside in the particle phase. Sulfate produced in the gas phase is transferred to the particle phase by nucleation of $H_2SO_4 \cdot H_2O$ particles, reaction of H_2SO_4 with NH_3, or the condensation of H_2SO_4 on existing particles. Nitrate and ammonia, on the other hand, are significantly more volatile and are therefore distributed between particle (solid and/or aqueous) and gas phases. This distribution is determined by concentrations of sulfate, nitrate and ammonia; relative humidity; and temperature. Due to its high affinity for ammonia, sulfate is completely neutralized in the aerosol phase if enough ammonia is available. In addition to these three species, atmospheric aerosols may contain a significant quantity of water, sufficient to maintain an equilibrium between particle and gas phases. At 90% relative humidity and a temperature of 298 K, a particle composed of pure ammonium sulfate contains over 70% water by weight. Hence, it is necessary to determine the mass of water associated with atmospheric aerosols.

Atmospheric compounds comprising sulfate, nitrate and ammonia are deliquescent and/or hygroscopic. Table 1 presents the relative humidities of deliquescence of some compounds present in the atmosphere. Each of these compounds exists in a dry, solid state at humidities below its relative humidity of deliquescence, while at higher humidities it absorbs water to form an aqueous solution. Sulfuric acid is hygroscopic and does not display a step-function absorption of water. However, several of these compounds may coexist in the atmosphere, yielding aerosols that contain both solid and aqueous compounds. Additionally, compounds such as $(NH_4)_2SO_4$ are known to exhibit hysteresis, wherein an aqueous solution can exist in a supersaturated state below the relative humidity of deliquescence (Charlson *et al.*, 1978; Tang, 1980). However, such behavior is difficult to model.

For submicrometer particles, the equilibrium com-

Table 1. Relative humidities of deliquescence of some atmospheric compounds (temperature = 298 K)

Compound	Relative humidity of deliquescence (%)	Reference
$(NH_4)_2SO_4$	80	Robinson and Stokes (1965)
$(NH_4)_3H(SO_4)_2$	69	Tang (1980)
NH_4HSO_4	40	Tang and Munkelwitz (1977)
NH_4NO_3	62	Robinson and Stokes (1965)

position may vary with particle size because of the Kelvin effect, which tends to increase the equilibrium vapor pressure above a curved surface over that above a flat surface. Moreover, it is desirable to account for nonidealities of aqueous solutions in equilibrium calculations, especially at low humidities. This can be accomplished by estimating and employing solute activity coefficients and solvent activity.

Models are currently available that describe these aspects of aerosol formation with varying degrees of sophistication, thus allowing prediction of aerosol mass and composition from given gas-phase concentrations, and temperature. Equations for interfacial and chemical equilibria are solved in conjunction with those for mass balance and electroneutrality. Current models are designed to treat sulfate, nitrate, ammonia and water; however, the treatment of other ionic species such as Na^+, Cl^-, Mg^{2+} and Fe^{3+} is straightforward and can be incorporated for specific applications. Some models also describe the kinetics of SO_2 oxidation within the aqueous phase. If the size distribution of these aerosols is known, it is possible to predict the light scattering coefficient (b_{scat}) and subsequent reduction in visual range due to their presence in the atmosphere.

3. TECHNICAL APPROACH

This section describes the formulation of MARS. It also notes the main features of two other models, EQUIL and KEQUIL, which have been described in detail by Bassett and Seinfeld (1983, 1984).

3.1. *MARS*

MARS was developed to describe inorganic aerosols comprising sulfate, nitrate, ammonium and water in equilibrium with ambient air. The composition and quantity of aerosols are predicted by this model from total (over all phases) ambient concentrations of the following components: H_2SO_4, HNO_3, NH_3 and H_2O. Several other models that are essentially designed for the same application are currently available (Saxena *et al.*, 1983; Bassett and Seinfeld, 1983, 1984). However, these models are computationally expensive because of their rigorous treatment of chemical and interfacial equilibria. The need for a computationally inexpensive, yet plausibly accurate, aerosol model provided the impetus for MARS development.

MARS is based upon fundamental thermodynamic concepts developed and employed in earlier modeling studies (Saxena and Peterson, 1981; Saxena *et al.*, 1983; Bassett and Seinfeld, 1983, 1984; Stelson and Seinfeld, 1982a, 1982b; Stelson *et al.*, 1979; Hildemann *et al.*, 1984; Russell *et al.*, 1983; Seigneur *et al.*, 1982). The treatment of chemical and interfacial equilibria focuses only on major species for each given set of ambient conditions. Thus, the number of equations to be solved is minimized. Table 2 lists the various species treated in MARS in gas, aqueous and solid phases. Note that the solid phase, when present, is assumed to be an external mixture of compounds such as $(NH_4)_2SO_4$, $(NH_4)_3H(SO_4)_2$, NH_4HSO_4 and NH_4NO_3. Therefore, each of these solid compounds, in reality, constitutes a phase in itself. Not all of these species are present in a particular aerosol/gas system. The presence and amounts of these species in such a system are dictated by the total concentrations of H_2SO_4, HNO_3, NH_3, and the relative humidity. For example, for a particular set of concentrations, there may not be a solid phase at all, and for another, the aqueous phase may be devoid of nitrate. The molar ratio of ammonia to sulfuric acid and relative humidity are the two most important variables in determining the composition of each phase. Another important consideration is the relative humidity of deliquescence (shown in Table 1) for the solids listed in Table 2.

Table 2. Species included in MARS

Phase		
Gas	Aqueous	Solid
H_2SO_4, NH_3, HNO_3, H_2O	SO_4^{2-}, HSO_4^-, NH_4^+, NO_3^-, H^+, $H_2O(l)$	$(NH_4)_2SO_4$ $(NH_4)_3H(SO_4)_2$ NH_4HSO_4 NH_4NO_3

There is evidence of the presence in atmospheric aerosol of mixed sulfate–nitrate salts such as $(NH_4)_2SO_4 \cdot 2NH_4NO_3$ and $(NH_4)_2SO_4 \cdot 3NH_4NO_3$ (Harrison and Sturges, 1984). However, a paucity of thermodynamic data on these compounds prevented us from including them. Bassett and Seinfeld (1983, 1984) included these compounds in their modeling studies by assuming that the thermodynamic properties of $(NH_4)_2SO_4 \cdot 2NH_4NO_3$ and $(NH_4)_2SO_4 \cdot 3NH_4NO_3$ can be approximated by those of $[(NH_4)_2SO_4 + 2NH_4NO_3]$ and $[(NH_4)_2SO_4 + 3NH_4NO_3]$, respectively. For the prediction of masses of $(NH_4)_2SO_4$ and NH_4NO_3, this assumption yields results that do not differ from those obtained when these two compounds are treated in separate phases.

The following discussion of model formulation is divided into two parts: (1) ammonia-rich environment and (2) ammonia-deficient environment. In the following subsections we describe each of these cases and subdivide the entire range of relative humidities into several regimes. MARS is applicable over the entire range of concentrations and relative humidities. For both cases, the binary water activity and solute activity coefficient data are taken from Robinson and Stokes (1965), Wu and Hamer (1969), and Bassett and Seinfeld (1983).

Ammonia-rich environment

This case is defined by $[NH_3] > 2[H_2SO_4]$ where [ ] denotes molar concentration of the component. Sulfate, due to its low volatility, is completely transported to the aerosol phase. In addition, due to its high affinity for ammonia, sulfate exists in the aerosol phase as $(NH_4)_2SO_4$ in solid or aqueous form. The presence of aerosol nitrate is dictated by the concentrations of nitric acid and the remaining ammonia, i.e. ammonia available for nitrate formation (hereafter referred to as free ammonia). If the gas-phase concentrations are high enough to satisfy $NH_3(g)/HNO_3(g)/NH_4NO_3(aq)$ or $NH_3(g)/HNO_3(g)/NH_4NO_3(s)$ equilibrium, aerosol nitrate will also exist. Note that the treatment of sulfate and nitrate is different because sulfate compounds (H_2SO_4, $(NH_4)_2SO_4$) are much less volatile than are nitrate compounds (HNO_3, NH_4NO_3). Table 3 summarizes the species included in the modeling of an ammonia- rich environment. The aqueous-phase species, $(NH_4)_2SO_4$ and NH_4NO_3, are assumed to be completely dissociated; thus $(NH_4)_2SO_4(aq)$, etc. refer only to the stoichiometry.

Case I. Relative humidity $\geqslant 80\%$

Sulfate and nitrate exist in an aqueous phase. The nitrate equilibrium is described by Bassett and Seinfeld (1983) as follows:

$$NH_3(g) + HNO_3(g) \rightleftharpoons NH_4^+(aq) + NO_3^-(aq)$$

$$\frac{[NH_4^+][NO_3^-]\gamma_{NH_4^+}\gamma_{NO_3^-}}{P_{NH_3}P_{HNO_3}} = 3.999 \times 10^{17} \exp\left[64.698\left(\frac{298}{T} - 1\right) + 11.505\left(1 + \ln\frac{298}{T} - \frac{298}{T}\right)\right] \mathrm{mol^2\,kg^{-2}\,atm^{-2}}. \quad (1)$$

where T is the temperature in K.

This equation is solved in conjunction with mass balances for H_2SO_4, HNO_3, and NH_3. Solute activity coefficients are described by Bromley's model, with three parameters, and solvent activity is estimated by the Zdanovskii, Stokes and Robinson (ZSR) method (Saxena and Peterson, 1981).

Case II. $62\% \leqslant$ *relative humidity* $< 80\%$

The treatment here is identical to that in Case I, except that some of the sulfate may exist in the solid phase as $(NH_4)_2SO_4$ because the relative humidity is below the relative humidity of deliquescence for this compound. The aqueous phase is saturated in $(NH_4)_2SO_4$. If the gas-phase concentrations of nitric acid and ammonia are not high enough to make $NH_4NO_3(aq)$ thermodynamically viable, no aqueous phase will exist.

Table 3. Treatment of the aerosol chemical composition for ammonia-rich environment

Relative humidity (%)	Species
100 ↕ 80	$(NH_4)_2SO_4(aq)$ $NH_4NO_3(aq)$ $H_2O(l)$
80 ↕ 62	$(NH_4)_2SO_4(s)$ $(NH_4)_2SO_4(aq)$ $NH_4NO_3(aq)$ $H_2O(l)$
62 ↕ 0	$(NH_4)_2SO_4(s)$ $NH_4NO_3(s)$

Case III. Relative humidity $< 62\%$

Sulfate exists in the aerosol phase as $(NH_4)_2SO_4(s)$. Aerosol nitrate formation is described by Stelson and Seinfeld (1982a) as follows:

$$NH_3(g) + HNO_3(g) \rightleftharpoons NH_4NO_3(s)$$

$$P_{NH_3}P_{HNO_3} = 1.0 \times 10^{-18} \exp\left(84.6 - \frac{24220}{T} - 6.1 \ln\frac{T}{298}\right) \mathrm{atm^2}. \quad (2)$$

This equation is used to distribute nitrate and free ammonia between the aerosol and gas phases. Again, the concentration product of $HNO_3(g)$ and free ammonia, $NH_3(g)$, must exceed the right-hand side of Equation (2) for $NH_4NO_3(s)$ formation to occur. $(NH_4)_2SO_4(s)$ and $NH_4NO_3(s)$ exist as an external mixture, each in its own phase.

Ammonia-deficient environment

If there is insufficient, or barely enough, ammonia available to completely neutralize sulfate, i.e.

$$[NH_3] \leqslant 2[H_2SO_4],$$

then MARS follows the methodology described in this subsection. As was the case in the ammonia-rich environment, all of the sulfate resides in the aerosol phase. Ammonia, as well, is completely transported to the aerosol phase, leading to negligible gas-phase ammonia concentration. As there is insufficient ammonia to neutralize the sulfate, the aqueous phase, if present, is acidic. This may result in concentrations of $[H^+]$ and $[HSO_4^-]$ that are sufficient to accommodate the presence of appreciable quantities of nitrate in the aqueous phase.

Table 4 depicts the species included in MARS for different conditions of relative humidity and the molar ratio of total ammonia to total sulfate. This modeling approach is based upon theoretical considerations and experimental data on the properties of deliquescence of mixed sulfate $[(NH_4)_2SO_4 + H_2SO_4]$ aerosols (Charlson *et al.*, 1978; Tang *et al.*, 1978). Results of model calculations were also taken into account (Bassett and Seinfeld, 1983, 1984; Saxena *et al.*, 1983). Because of their comprehensive and rigorous treatment, these models provided information that allow us to develop a less involved approach.

Compounds such as $(NH_4)_2SO_4(aq)$ and $NH_4HSO_4(aq)$ refer to the overall stoichiometric composition, not the actual ionic state in the aqueous solution. Such stoichiometric terms are essential in

Table 4. Treatment of the aerosol chemical composition for ammonia-deficient environment

Relative humidity %	Species Ratio of total ammonia to total sulfate 0 ⟷ 1	1 ⟷ 1.5	1.5 ⟷ 2
100 ⟷ 80	$NH_4HSO_4(aq)$ $H_2SO_4(aq)$ $NH_4NO_3(aq)$ $HNO_3(aq)$ $H_2O(l)$	$(NH_4)_2SO_4(aq)$ $H_2SO_4(aq)$ $NH_4NO_3(aq)$ $HNO_3(aq)$ $H_2O(l)$	
80 ⟷ 69		$(NH_4)_2SO_4(s)$ $(NH_4)_3H(SO_4)_2(aq)$ $NH_4HSO_4(aq)$ $NH_4NO_3(aq)$ $HNO_3(aq)$ $H_2O(l)$	$(NH_4)_2SO_4(s)$ $(NH_4)_3H(SO_4)_2(aq)$ $NH_4NO_3(aq)$ $HNO_3(aq)$ $H_2O(l)$
69 ⟷ 40		$(NH_4)_3H(SO_4)_2(s)$ $NH_4HSO_4(aq)$ $NH_4NO_3(aq)$ $HNO_3(aq)$ $H_2O(l)$	$(NH_4)_2SO_4(s)$ $(NH_4)_3H(SO_4)_2(s)$
40 ⟷ 0	$NH_4HSO_4(s)$ $H_2SO_4(aq)$ $HNO_3(aq)$ $H_2O(l)$	$(NH_4)_3H(SO_4)_2(s)$ $NH_4HSO_4(s)$	

relating binary water activity data to multicomponent water activity in the ZSR equation. For instance $(NH_4)_3H(SO_4)_2(aq)$ exists as a mixture of NH_4^+, H^+, HSO_4^- and SO_4^{2-}. For a case of relative humidity between 69 and 80% and $[NH_3]/[H_2SO_4]$ between 1 and 1.5, the molar ratio of $(NH_4)_3H(SO_4)_2(aq)$ and $NH_4HSO_4(aq)$ is assumed to be 1. This assumption is based on the results of EQUIL (Bassett and Seinfeld, 1983). For cases in which there is no aqueous phase, the quantities of solid compounds, such as $(NH_4)_2SO_4$ and $(NH_4)_3H(SO_4)_2$, are computed from mass balance on sulfate and ammonia. For the remaining cases, we begin by assuming that there is no nitrate in the aerosol phase, and solve for the amounts of water, aqueous phase sulfate and ammonium, and solid compound from mass balance and the ZSR equation. We then solve the following equations: along with mass balance and electroneutrality, for ionic concentrations $[H^+]$, $[SO_4^{2-}]$, $[HSO_4^-]$ and $[NO_3^-]$. The implicit assumption in this methodology is that the amount of water is not significantly affected by the presence of nitrate in the aqueous phase.

Additional considerations

MARS can also be used to treat the aqueous-phase oxidation of SO_2 to sulfate by H_2O_2, O_3 and O_2 (catalyzed by Mn^{2+} and Fe^{3+}) as described by Seigneur and Saxena (1984). Because such oxidation is strongly pH-dependent, it is necessary to estimate the pH. Once the composition and mass of different phases are computed, the pH is estimated by solving a system of equations including Equation (4) and the following additional equilibrium relationships:

Morgan and Maass (1931) and Hales and Drewes (1979)

$$NH_3(g) \rightleftharpoons NH_3(aq)$$

$$\frac{[NH_3(aq)]}{P_{NH_3}} = 57\exp\left[3.42\times10^3\left(\frac{1}{T}-\frac{1}{298}\right)\right] \text{mol kg}^{-1}\text{atm}^{-1} \qquad (5)$$

Bassett and Seinfeld (1983)

$$HNO_3(g) \rightleftharpoons H^+(aq) + NO_3^-(aq)$$

$$\frac{[H^+][NO_3^-]\gamma_{H^+}\gamma_{NO_3^-}}{P_{HNO_3}} = 3.638\times10^6\exp\left[29.47\left(\frac{298}{T}-1\right)+16.835\left(1+\ln\frac{298}{T}-\frac{298}{T}\right)\right] \text{mol}^2\text{kg}^{-2}\text{atm}^{-1} \qquad (3)$$

$$HSO_4^-(aq) \rightleftharpoons H^+(aq) + SO_4^{2-}(aq)$$

$$\frac{[H^+][SO_4^{2-}]\gamma_{H^+}\gamma_{SO_4^{2-}}}{[HSO_4^-]\gamma_{HSO_4^-}} = 1\times10^{-2}\exp\left[7.59\left(\frac{298}{T}-1\right)+18.825\left(1+\ln\frac{298}{T}-\frac{298}{T}\right)\right] \text{mol kg}^{-1}, \qquad (4)$$

Robinson and Stokes (1965) and Smith and Martell (1976)

$$\mathrm{NH_3(aq)} \rightleftharpoons \mathrm{NH_4^+(aq)} + \mathrm{OH^-(aq)}$$

$$K_{1A} = \frac{[\mathrm{NH_4^+}][\mathrm{OH^-}]\gamma_{\mathrm{NH_4^+}}\gamma_{\mathrm{OH^-}}}{[\mathrm{NH_3(aq)}]} = 1.774 \times 10^{-5} \exp\left[-4.53 \times 10^2\left(\frac{1}{T} - \frac{1}{298}\right)\right] \mathrm{mol\,kg^{-1}} \quad (6)$$

$$\mathrm{H_2O(aq)} \rightleftharpoons \mathrm{H^+(aq)} + \mathrm{OH^-(aq)}$$

$$K_W = \frac{[\mathrm{H^+}][\mathrm{OH^-}]\gamma_{\mathrm{H^+}}\gamma_{\mathrm{OH^-}}}{a_w} = 1.008 \times 10^{-14} \exp\left[-6.72 \times 10^3\left(\frac{1}{T} - \frac{1}{298}\right)\right] \mathrm{mol^2\,kg^{-2}}. \quad (7)$$

Equations (1) to (7) are temperature-dependent. MARS does not account for the effect of temperature variation on relative humidities of deliquescence (Table 1) and binary data for water activity and activity coefficients. All the binary data and relative humidities of deliquescence used in MARS pertain to 298 K. Note that the effect of curvature on chemical composition (i.e. the Kelvin effect) is not considered.

3.2. *EQUIL and KEQUIL*

EQUIL is a rigorous model that explicitly solves for 17 species in eight phases by minimizing the Gibbs free energy of the system (Bassett and Seinfeld, 1983). There are 13 equilibrium reactions among these species. The temperature dependence of all thermodynamic properties is taken into account. EQUIL also treats $(\mathrm{NH_4})_2\mathrm{SO_4} \cdot 2\mathrm{NH_4NO_3}(s)$ and $(\mathrm{NH_4})_2\mathrm{SO_4} \cdot 3\mathrm{NH_4NO_3}(s)$. As previously noted, the thermodynamic properties of these compounds are approximated by those of $[(\mathrm{NH_4})_2\mathrm{SO_4} + 2\mathrm{NH_4NO_3}]$ and $[(\mathrm{NH_4})_2\mathrm{SO_4} + 3\mathrm{NH_4NO_3}]$, respectively, and for the prediction of $(\mathrm{NH_4})_2\mathrm{SO_4}$ and $\mathrm{NH_4NO_3}$ masses, this model produces results that are essentially the same as those obtained by the treatment of $(\mathrm{NH_4})_2\mathrm{SO_4}$ and $\mathrm{NH_4NO_3}$ in separate phases. Like MARS, EQUIL does not consider the Kelvin effect. KEQUIL is derived from EQUIL and does incorporate the Kelvin effect (Bassett and Seinfeld, 1984). In all other respects, KEQUIL is identical to EQUIL. Both EQUIL and KEQUIL employ the Kusik and Meissner (1978) technique to calculate activity coefficients and the water activity. The differences between the ZSR, Bromley and Kusik and Meissner techniques in predicting water activity were found to be generally small (Saxena and Peterson, 1981; Stelson and Seinfeld, 1982c).

4. MODEL APPLICATION AND COMPARISON

The MARS, EQUIL and KEQUIL models were used to simulate a wide range of sulfate, nitrate, ammonia and water vapor concentrations under 56 sets of atmospheric conditions. Table 5 presents these input concentrations. Sulfate, nitrate and ammonia concentrations vary from a low value of 5 μg m^{-3} to significantly high values measured in the Los Angeles area (Russell and Cass, 1984; Doyle *et al.*, 1979). Simulations were performed for relative humidities ranging from 30% to 90%. The first case simulates an ammonia-rich environment, whereas the next three cases are designed to simulate three different regimes of $[\mathrm{NH_3}]/[\mathrm{H_2SO_4}]$ in an ammonia-deficient environment (see Table 4). Cases 5 and 6 are included to test the sensitivity of aerosol-phase nitrate concentrations to total nitrate in ammonia-deficient environments.

Aerosol size distributions are included in our modeling study because we wish to predict and compare b_{scat} values derived from the three models considered here. Additionally, though KEQUIL treats the Kelvin effect, MARS and EQUIL do not. Therefore it is appropriate to test the effect of size distribution on

Table 5. Input to equilibrium aerosol models*

Case†	Total sulfate (μg m^{-3})	Total nitrate (μg m^{-3})	Total ammonia (μg m^{-3})	Relative humidity (%)	Sulfate size distribution‡
1	40	45	70	90	Type I
2	40	45	12	90	Type I
3	40	45	10	90	Type I
4	40	45	5	90	Type I
5	40	5	12	90	Type I
6	40	5	10	90	Type I
7	5	45	5	90	Type II
8	5	5	5	90	Type II

*The molecular weights of sulfate, nitrate and ammonia are 98, 63 and 17, respectively.

†These cases are repeated for the following % relative humidities: 80, 70, 60, 50, 40 and 30; thus cases 9–16 correspond to a relative humidity of 80%, and so on.

‡Hering and Friedlander (1982).

Table 6. Aerosol-phase concentrations and properties predicted by KEQUIL, EQUIL, and MARS at 298 K

	Nitrate* ($\mu g\, m^{-3}$)			Ammonium ($\mu g\, m^{-3}$)			Total mass† ($\mu g\, m^{-3}$)			$b_{scat} \times 10^4$ (m^{-1})		
Case	KEQUIL	EQUIL	MARS	KEQUIL	EQUIL	MARS	KEQUIL	EQUIL	MARS	KEQUIL	EQUIL	MARS
1	44.2	44.2	44.2	27.6	27.6	27.5	386.5	405.6	416.7	20.7	20.2	20.9
2	7.0	7.5	6.8	12.7	12.7	12.7	207.2	221.4	198.8	10.7	11.1	9.8
3	3.8	4.3	4.2	10.6	10.6	10.6	193.3	206.6	201.3	10.0	10.3	10.0
4	0.7	0.8	0.8	5.3	5.3	5.3	195.5	206.4	200.0	10.2	10.6	10.2
5	1.4	1.5	1.5	12.6	12.6	12.7	179.8	189.9	193.5	9.1	9.4	9.6
6	0.6	0.7	0.7	10.5	10.5	10.6	175.5	185.6	197.8	8.9	9.2	9.9
7‡	11.7	11.9	11.2	5.1	5.1	5.1	76.8	84.0	81.5	3.1	2.5	2.5
8‡	3.1	3.3	3.2	2.7	2.8	2.8	35.4	39.7	40.1	1.2	1.2	1.2
49	43.7	43.8	43.2	27.4	27.4	27.2	110.3	110.3	109.6	3.9	3.6	3.6
50	0.0	0.0	0.0	12.7	12.7	12.7	51.9	51.9	51.9	1.7	1.7	1.7
51	0.0	0.0	0.0	10.6	10.6	10.6	49.8	49.8	49.8	1.6	1.6	1.6
52	§	0.0	0.0	§	5.3	5.3	§	55.4	54.6	§	2.0	2.0
53	0.0	0.0	0.0	12.7	12.7	12.7	51.9	51.9	51.9	1.7	1.7	1.7
54	0.0	0.0	0.0	10.6	10.6	10.6	49.8	49.8	49.8	1.6	1.6	1.6
55‡	7.5	7.6	7.1	4.0	4.0	3.9	16.4	16.5	15.9	0.4	0.3	0.3
56‡	0.0	0.0	0.0	1.8	1.8	1.8	6.7	6.7	6.7	0.1	0.1	0.1

*If the predicted nitrate concentration is less than 0.1 $\mu g\, m^{-3}$ (about 0.04 ppb), it is assumed to be 0.

†Total mass includes sulfate, nitrate, ammonium and water. The molecular weights of sulfate, nitrate and ammonium are 96, 62 and 18, respectively.

‡Type II size distribution is used for these cases. For the remaining cases, Type I size distribution is employed.

§The model did not yield a solution for a simulation time of 1000 CPUs on a Prime 750 computer.

model predictions and comparisons. Hering and Friedlander (1982) observed two distinct size distributions (Type I and Type II) of sulfate aerosols in the Los Angeles area. The modal diameters for Type I and Type II distributions were approximately 1 μm and 0.15 μm, respectively (Fig. 4 of Hering and Friedlander, 1982). Type I distribution was associated with high sulfate loading, wheras Type II distribution occurred on days of low sulfate loading. For the first six cases in our study the sulfate mass was apportioned among six sections according to the Type I distribution. In cases 7 and 8, low sulfate concentrations were used in conjunction with the Type II distribution. This procedure enabled us to test the sensitivity of model predictions to the size distribution of sulfate. Cases 1 to 8 were repeated for six other values of relative humidity.

The results of our simulations are presented in Tables 6 and 7. Note that all three models assume sulfate to be non-volatile, which results in complete transfer of sulfate to the aerosol phase. Since there is perfect agreement among these models with respect to predicted sulfate concentration, we do not include aerosol sulfate concentrations in tables or figures dealing with model comparison. For some cases KEQUIL and/or EQUIL do not yield a solution within a simulation time of 1000 CPUs on a Prime 750 computer. The comparison in Tables 6 and 7 is restricted to the 51 cases for which all three models yield a solution. The objective of this comparison is to evaluate the performance of EQUIL and MARS. KEQUIL is the most rigorous and comprehensive model available and is therefore used as a benchmark for model performance.

Table 6 presents nitrate, ammonium and total aerosol mass concentrations predicted by KEQUIL, EQUIL and MARS. Predictions of the aerosol light scattering coefficient are also shown. The values of the scattering coefficient, normalized by aerosol mass, were calculated with a model based upon Mie theory (Dave, 1979; Seigneur *et al.*, 1984). For brevity, the results for only two relative humidities (90% and 30%) are included in this table. Since these relative humidities represent a broad range, the results illustrate the impact of relative humidity on total aerosol mass and on scattering coefficient. Aerosols at high humidities contain relatively large amounts of water to maintain an equilibrium with the gas phase. At lower humidity, aerosols contain less water, and nitrate concentrations are also relatively less. This diminution of aerosol phase nitrate results from the dependence of Equation (1) on relative humidity (Stelson and Seinfeld, 1982a). For a given size distribution, the scattering coefficient is directly proportional to total

Table 7. Comparison of performance and computational efficiency of KEQUIL, EQUIL and MARS

Performance measure*	Parameter	KEQUIL	EQUIL	MARS
Average error† (%)	Nitrate	—	3	7
	Ammonium	—	0	1
	Total	—	2	4
	b_{scat}	—	4	6
Average‡ bias (%)	Nitrate	—	3	0
	Ammonium	—	0	0
	Total	—	2	3
	b_{scat}	—	−1	0
Correlation coefficient	Nitrate	—	1.000	1.000
	Ammonium	—	1.000	1.000
	Total	—	1.000	0.997
	b_{scat}	—	0.999	0.996
Average simulation (CPUs)	Time §	72.4	9.7	0.17

*These performance measures are computed with respect to KEQUIL. For nitrate, if the predicted concentration is less than 0.1 μg m^{-3} (about 0.04 ppb) it is assumed to be zero. For comparison, the measurement threshold for nitrate ranges from 0.04 to about 1 ppb (Anlauf *et al.*, 1985; Kelly *et al.*, 1984). There are 23 cases for which all three models predict nitrate concentrations below 0.1 μg m^{-3}. Perfect agreement among the three models is assumed for these cases.

†Defined as $\frac{1}{N}\sum_{i=1}^{N}\left|\frac{X_i - Y_i}{Y_i}\right| \times 100$, where X_i is the value predicted by EQUIL or MARS, and Y_i is that predicted by KEQUIL. N is the total number of cases.

‡Defined as $\frac{1}{N}\sum_{i=1}^{N}\frac{X_i - Y_i}{Y_i} \times 100$.

§On a Prime 750 computer.

aerosol mass and therefore exhibits lower values at low humidities.

As is evident from Table 7, which summarizes the comparison of model performance and computational efficiency, the difference in performance of EQUIL and MARS is quite small. Both EQUIL and MARS slightly overpredict aerosol mass relative to KEQUIL; however, the disagreement is small and well within 10%. The predictions of b_{scat} by EQUIL and MARS are comparable to those of KEQUIL.

The most noticeable difference among EQUIL, MARS and KEQUIL is observed in their computational efficiency (see Table 7). MARS is about 400 times faster than KEQUIL and about 60 times faster than EQUIL. We now discuss the reasons for remarkable differences in the computational efficiency of the three models despite the good agreement among their predictions.

First, the formulation of EQUIL and KEQUIL is identical except for the treatment of the Kelvin effect, which is included in KEQUIL but not in EQUIL. Therefore, the small disagreement between the two models is entirely due to inclusion of the Kelvin effect in KEQUIL. The magnitude of the impact of the Kelvin effect on equilibrium concentrations increases as the particle diameter decreases. Figures 1 and 2 illustrate this point. In Fig. 1, there is good agreement among the size-segregated compositions predicted by the three models for Type I size distribution (mass median diameter of about 0.5 μm). However, for Type II size distribution (mass median diameter of about 0.2 μm), there is a marked difference between the predictions of KEQUIL and those of EQUIL and MARS. MARS, like EQUIL, does not treat the Kelvin effect; therefore, evaluation of model performance in this study will vary according to input size distribution.

Second, the basic thermodynamic framework of MARS is similar to that of EQUIL and KEQUIL. The major difference is that MARS subdivides the entire domain of sulfate, nitrate, ammonia and water concentrations into several subdomains. This division is consistent with aerosol behavior and with the formulation of EQUIL and KEQUIL. Within each subdomain, there are fewer viable species than there are in the entire domain, which minimizes the number of equations to be solved. Consequently, the computational efficiency of MARS is vastly improved without significant loss of accuracy.

We also performed simulations to investigate the effect of temperature variations on the comparison of model predictions. As noted earlier, KEQUIL and EQUIL treat the temperature dependence of all thermodynamic properties. The treatment of temperature dependence in MARS is not as rigorous, and only the temperature dependence of equilibrium relationships, i.e. Equations (1) to (7), is accounted for. Thus, binary water activities, activity coefficients, and relative humidities of deliquescence, at any given temperature, are approximated by the values of these parameters at 298 K. To check the effect of this approximation on model predictions, we simulated Cases 1 to 8 (see Tables 5 and 6) for a temperature of 288 K. The results are presented in Table 8. All three models predict some variation with temperature in aerosol-phase mass and

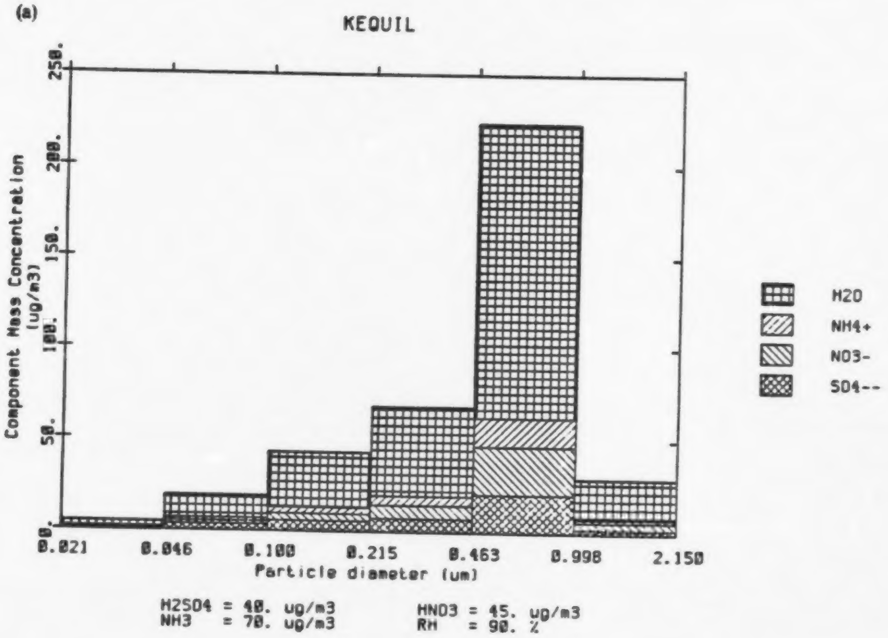

Fig. 1(a).

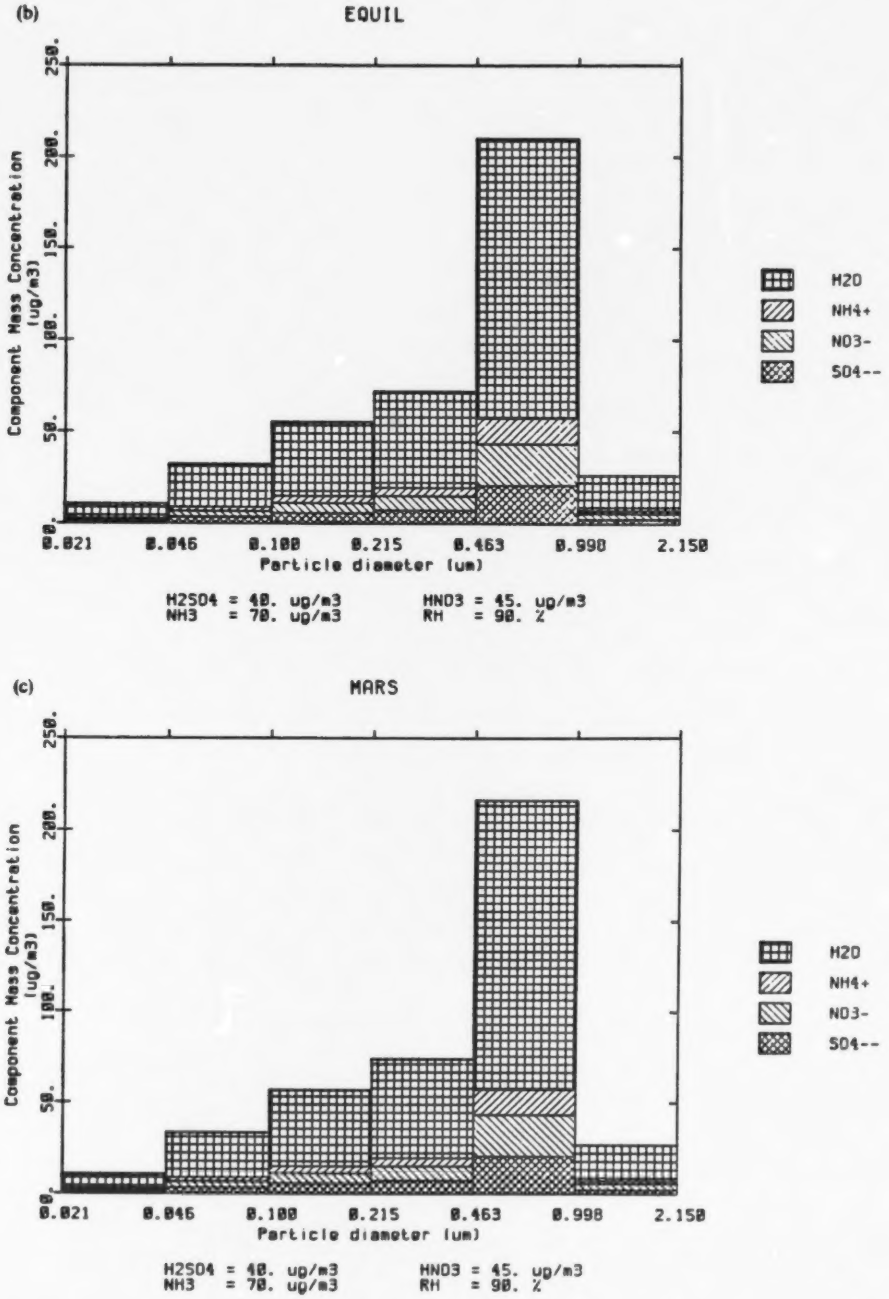

Fig. 1. Size-segregated aerosol composition as predicted by (a) KEQUIL, (b) EQUIL, and (c) MARS for a Type I sulfate size distribution.

composition. The most noticeable changes occur in aerosol-phase nitrate and water; these changes can be explained by the dependence of nitrate volatility on temperature. Furthermore, the change in aerosol-phase water is associated with the change in aerosol-phase nitrate. It should be recognized that the results of such comparisons depend on ambient temperature and relative humidity. Because MARS does not treat the temperature dependence of relative humidities of deliquescence, it is possible that differences between the predictions of MARS and EQUIL or KEQUIL will be slightly more pronounced near points of deliquescence that are sensitive to temperature.

5. SUMMARY AND CONCLUSIONS

This study was prompted by the need for a computationally efficient and yet reasonably accurate aerosol model that can be used as a module in plume, regional and urban air quality models. Current aerosol models tend to be computationally expensive because of their rigorous and comprehensive treatment.

The Model for an Aerosol Reacting System (MARS), applicable over the entire range of atmospheric concentrations, has been developed in this work. The basic thermodynamic framework of this

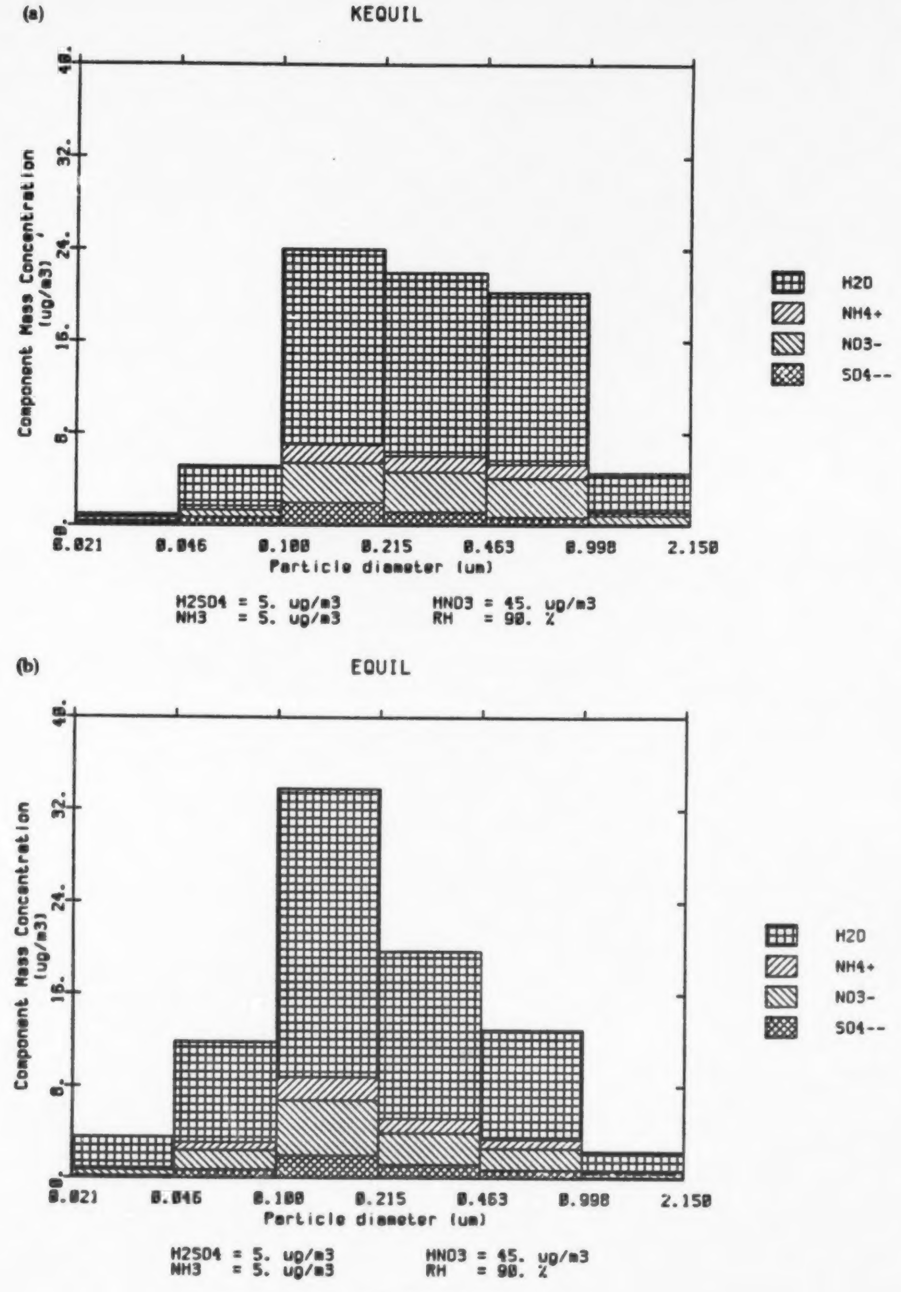

Fig. 2(a) and (b).

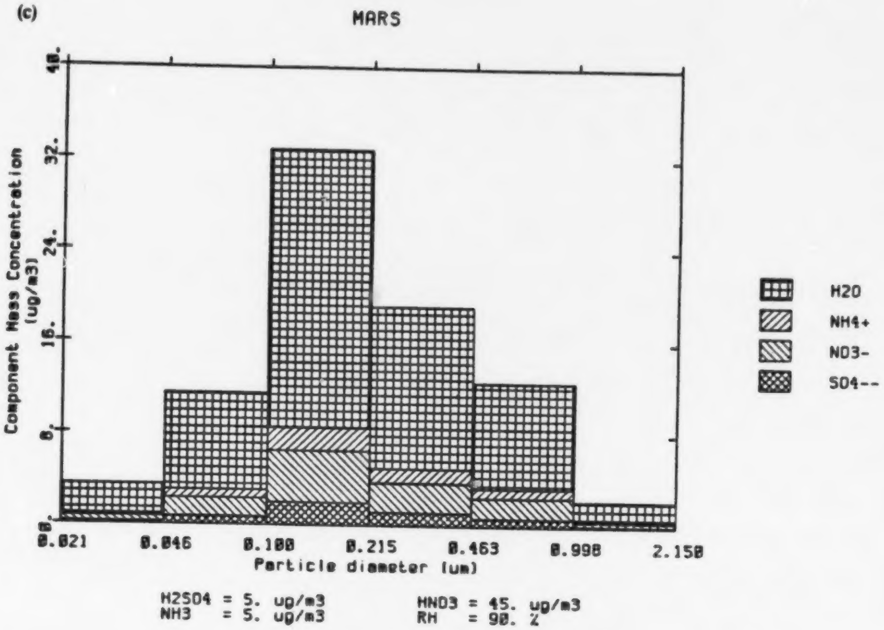

Fig. 2. Size-segregated aerosol composition as predicted by (a) KEQUIL, (b) EQUIL, and (c) MARS for a Type II sulfate size distribution.

Table 8. Aerosol-phase concentrations and total aerosol mass predicted by KEQUIL, EQUIL and MARS at 288 K

	Nitrate ($\mu g\, m^{-3}$)			Ammonium ($\mu g\, m^{-3}$)			Total mass* ($\mu g\, m^{-3}$)		
Case	KEQUIL	EQUIL	MARS	KEQUIL	EQUIL	MARS	KEQUIL	EQUIL	MARS
1	44.3	44.3	44.3	27.6	27.6	27.5	380.6	399.9	417.3
2	10.0	10.6	9.5	12.7	12.7	12.7	218.9	235.5	201.5
3	6.2	6.9	6.5	10.6	10.6	10.6	203.0	218.9	203.6
4	1.5	1.8	1.8	5.3	5.3	5.3	201.0	214.7	201.0
5	2.1	2.3	2.2	12.7	12.7	12.7	180.3	190.8	194.2
6	1.1	1.2	1.3	10.6	10.6	10.6	174.2	184.8	198.3
7	12.9	13.0	11.8	5.3	5.3	5.3	81.4	88.8	84.8
8	4.6	4.7	4.6	3.2	3.2	3.2	41.9	45.8	47.6

*Total mass includes sulfate, nitrate, ammonium and water. The molecular weights of sulfate, nitrate and ammonium are 96, 62 and 18, respectively.

model is consistent with that of the more elaborate models EQUIL and KEQUIL (Bassett and Seinfeld, 1983, 1984), as well as with field and laboratory data. The distinguishing feature of MARS is its division of the entire regime of aerosol species into several subdomains. Since each subdomain contains fewer viable species than does the entire domain of concentrations, the number of equations to be solved is minimized.

The results of MARS and EQUIL were compared with those of KEQUIL, the most comprehensive model currently available. Such comparisons were made for a broad spectrum of atmospheric conditions. Results were compared for concentrations of aerosol-phase ammonium, nitrate and total mass. Since all three models (KEQUIL, EQUIL and MARS) treat sulfate as a nonvolatile species, there was no disagreement among model predictions regarding aerosol-phase sulfate concentration. Model calculations of the light scattering coefficient (b_{scat}) of EQUIL and MARS agreed closely with those of KEQUIL. However, MARS was determined to be on average 400 times faster than KEQUIL and about 60 times faster than EQUIL. This substantial difference in computational efficiency was attained without significant loss of accuracy; the average errors for nitrate, ammonium, total mass and b_{scat} were all well within 10%. It was also discerned that the results of model comparison would be slightly different had we used a different initial size distribution or temperature.

On the basis of the results of this study, we recommend MARS as an efficient and accurate aerosol thermodynamic model for incorporation into larger models for the treatment of aerosol dynamics, or into air quality and visibility models for urban, plume, or regional applications. However, for specific applications, we recommend the use of KEQUIL or EQUIL because these two remain the most comprehensive models currently available.

Acknowledgements—This study was sponsored by the EPA-ASRL Aerosol Research Branch. We would like to thank the Project Officer, Dr H. M. Barnes, for suggesting this study and for his support. We would also like to thank Ms Judy A. Rodich for her editorial effort.

Although the research described in this article was funded wholly by the U.S. Environmental Protection Agency through Contract No. 68-02-4076, it does not necessarily reflect the views of the agency, and no official endorsement should be inferred.

The computer code for MARS is available from the Project Officer at the U.S. Environmental Protection Agency, Atmospheric Sciences Research Laboratory, Research Triangle Park, North Carolina, or from the authors at Systems Applications, Inc.

REFERENCES

Anlauf K. G., Fellin P., Wiebe H. A., Schiff H. I., MacKay G. I., Braman R. S. and Gilbert R. (1985) A comparison of three methods for measurement of atmospheric nitric acid and aerosol nitrate and ammonium. *Atmopsheric Environment* **19**, 325–333.

Bassett M. E. and Seinfeld J. H. (1983) Atmospheric equilibrium model of sulfate and nitrate aerosol. *Atmospheric Environment* **17**, 2237–2252.

Bassett M. E. and Seinfeld J. H. (1984) Atmospheric equilibrium model of sulfate and nitrate aerosols—II. Particle size analysis. *Atmospheric Environment* **18**, 1163–1170.

Charlson R. J., Covert, D. S., Larson T. V. and Waggoner A. P. (1978) Chemical properties of tropospheric sulfur aerosols. *Atmospheric Environment* **12**, 39–53.

Dave J. V. (1979) Computation of an enormous data base. *Solar Energy* **75**, 62–77.

Doyle G. J. Tuazon E. C., Graham R. A., Mischke T. M., Winer A. M. and Pitts J. N., Jr. (1979) Simultaneous concentrations of ammonia and nitric acid in a polluted atmosphere and their equilibrium relationship to particulate ammonium nitrate. *Envir. Sci. Technol.* **13**, 1416–1419.

Hales J. M. and Drewes D. R. (1979) Solubility of ammonia in water at low concentrations. *Atmospheric Environment* **13**, 1133–1147.

Harrison R. M. and Sturges W. T. (1984) Physico-chemical speciation and transformation reactions of particulate atmospheric nitrogen and sulfur compounds. *Atmospheric Environment* **18**, 1829–1833.

Hering S. V. and Friedlander S. K. (1982) Origins of aerosol sulfur size distributions in the Los Angeles basin. *Atmospheric Environment* **16**, 2647–2656.

Hildemann L. M., Russell A. G. and Cass G. R. (1984) Ammonia and nitric acid concentrations in equilibrium with atmospheric aerosols: experiment vs theory. *Atmospheric Environment* **18**, 1737–1750.

Kelly T. J., Tanner, R. L., Newman L., Galvin, P. J. and Kadlecek J. A. (1984) Trace gas and aerosol measurements at a remote site in the northeast U.S. *Atmospheric Environment* **18**, 2565–2576.

Kusik C. L. and Meissner H. P. (1978) Electrolyte activity coefficients in inorganic processing. *A.I.Ch.E. Symp.* **173**, 14–20.

Morgan O. M. and Maass O. (1931) An investigation of the equilibrium existing in gas–water systems forming electrolytes. *Can. J. Res.* **5**, 162–199.

Robinson R. A. and Stokes R. H. (1965) *Electrolyte Solutions*, Butterworths, London.

Roedel W. (1979) Measurements of sulfuric acid saturation vapor pressure: implications for aerosol formation by heteromolecular nucleation. *J. Aerosol Sci.* **10**, 375–386.

Russell A. G. and Cass G. R. (1984) Acquisition of regional air quality model validation data for nitrate, sulfate, ammonium ion and their precursors. *Atmospheric Environment* **18**, 1815–1827.

Russell A. G., McRae G. J. and Cass G. R. (1983) Mathematical modeling of the formation and transport of ammonium nitrate aerosol. *Atmospheric Environment* **17**, 949–964.

Saxena P. and Peterson T. W. (1981) Thermodynamics of multicomponent electrolytic aerosols. *J. Colloid Interface Sci.* **79**, 496–510.

Saxena P., Seigneur C. and Peterson T. W. (1983) Modeling of multiphase atmospheric aerosols. *Atmospheric Environment* **17**, 1315–1329.

Seigneur C. and Saxena P. (1984) A study of atmospheric acid formation in different environments. *Atmospheric Environment* **18**, 2109–2124.

Seigneur C., Bergstrom R. W., Johnson C. D. and Richards L. W. (1984) Measurements and simulations of the visual effects of particulate plumes. *Atmospheric Environment* **18**, 2231–2244.

Seigneur C., Saxena P. and Hudischewskyj A. B. (1982) Formation and evolution of sulfate and nitrate aerosols in plumes. *Sci. total Envir.* **23**, 283–292.

Smith R. M. and Martell A. E. (1976) *Critical Stability Constants*, Vol. 4, Plenum, New York.

Stelson A. W., Friedlander S. K. and Seinfeld J. H. (1979) A note on the equilibrium relationship between ammonia and nitric acid and particulate ammonium nitrate. *Atmospheric Environment* **13**, 369–371.

Stelson A. W. and Seinfeld J. H. (1982a) Relative humidity and temperature dependence of the ammonium nitrate dissociation constant. *Atmospheric Environment* **16**, 983–992.

Stelson A. W. and Seinfeld J. H. (1982b) Relative humidity and pH dependence of the vapor pressure of ammonium nitrate–nitric acid solutions at 25°C. *Atmospheric Environment* **16**, 993—1000.

Stelson A. W. and Seinfeld J. H. (1982c) Thermodynamic prediction of the water activity, NH_4NO_3 dissociation constant, density and refractive index for the NH_4NO_3–$(NH_4)_2SO_4$–H_2O system at 25°C. *Atmospheric Environment* **16**, 2507–2514.

Tang I. N. (1980) Deliquescence properties and particle size change of hygroscopic aerosols. In *Generation of Aerosols and Facilities for Exposure Experiments* (edited by Willeke K.), Ann Arbor Science Publishers, Ann Arbor, Michigan.

Tang I. N. and Munkelwitz H. R. (1977) Aerosol growth studies—III. Ammonium bisulfate aerosols in a moist atmosphere. *J. Aerosol Sci.* **8**, 321–330.

Tang I. N., Munkelwitz H. R. and Davis J. G. (1978) Aerosol growth studies—IV. Phase transformation of mixed salt aerosols in a moist atmosphere. *J. Aerosol Sci.* **9**, 505–511.

Wu Y. C. and Hamer W. J. (1969) Osmotic coefficients and mean activity coefficients of a series of uni-univalent electrolytes in aqueous solutions at 25°C. NASA Contract Report NASA-CR-106045, National Bureau of Standards, Washington, D.C.

Appendix C

Simulation of Aerosol Dynamics: A Comparative Review of Mathematical Models

Christian Seigneur, A. Belle Hudischewskyj
Systems Applications, Inc., 101 Lucas Valley Road, San Rafael, CA 94903

John H. Seinfeld
Department of Chemical Engineering, California Institute of Technology, Pasadena, CA 91109

Kenneth T. Whitby,* Evan R. Whitby
Department of Mechanical Engineering, University of Minnesota, Minneapolis, MN 55455

James R. Brock
Department of Chemical Engineering, University of Texas, Austin, TX 78712

Harold M. Barnes
Atmospheric Sciences Research Laboratory, U.S. Environmental Protection Agency, Research Triangle Park, NC 27711

A comparative review of mathematical models of aerosol dynamics is presented. Three approaches are considered that are based on continuous, discrete (sectional), and parametrized (lognormal) representations of the aerosol size distribution. Simulations of coagulation and diffusion-limited condensation are performed with these modeling approaches for three case studies typical of clear, hazy, and urban atmospheric aerosol concentrations. The relative accuracies and computational costs of models based on these approaches are compared. The models based on a continuous size distribution provide an accurate solution for both coagulation and condensation. Sectional approaches simulate coagulation very well but require a fine size resolution to minimize numerical diffusion in the simulation of condensation. The parametrized model based on log-normal modal size distributions is computationally efficient but tends to overestimate the rate of coagulation and the peak aerosol concentration resulting from condensational growth. The results of this study provide useful information for the selection of an aerosol model, depending on the accuracy requirements and computational constraints associated with a specific application.

INTRODUCTION

The study of aerosol system behavior is relevant to a variety of fields such as air pollution, combustion, and chemical engineering science. To understand the behavior of aerosol systems, it is necessary to be able to simulate by means of mathematical models the dynamic behavior of the aerosol population. Such simulations allow us to reconcile the theoretical description of the physical principles that govern aerosol systems with the experimental observation of these systems. Discrepancies between theory and experiment can then be analyzed and utilized to suggest theoretical advances and further experiments in the study of aerosol dynamics. To that end, several mathematical models have been developed to simulate the physical processes that affect aerosols. Such processes include coagulation, growth due to

---

*Deceased.

Aerosol Science and Technology 5:205–222(1986)
© 1986 Elsevier Science Publishing Co., Inc

condensation of gases, shrinkage due to evaporation, nucleation of new aerosols, sedimentation, and deposition on surfaces.

We focus in this work on the simulation of coagulation and condensation in aerosol systems because most difficulties in solving the equations representing aerosol system dynamics concern the coagulation and condensation terms. The objective of this work is to compare the accuracy and computational requirements of several approaches to simulating aerosol dynamics.

We compare three major approaches that have been developed to simulate aerosol dynamics. These three types of mathematical models are applied to various test cases, and the simulation results and computational requirements are quantitatively compared. The three major approaches differ primarily by their representation of the size distribution of aerosols:

1. Continuous representation
2. Discrete representation
3. Parametrized representation

Each of these approaches is a numerical technique for solving the general dynamic equation for aerosols. They differ only in their degree of approximation of the size distribution. Those techniques that offer any desired degree of approximation are referred to as continuous. Discrete approximations are methods in which the size domain is divided into discrete segments or sections. In principle, discrete approaches can be implemented at an arbitrary degree of approximation; however, there are practical constraints on the number of sections that can be used. Finally, parametrized representations are those methods in which the size distribution is assumed to adhere to a known form depending on a small number of parameters. Both continuous and discrete approaches necessarily assume a certain form of the size distribution but generally at a much finer level of representation than do the approaches that we classify as parametrized.

We present in the next section the basic equations that govern the evolution of a particulate system undergoing coagulation and condensation. The following section describes the modeling techniques that are evaluated in this comparative study. We then describe the simulations for the selected case studies and discuss the resulting accuracy and computational costs for coagulation and condensation, respectively. Concluding remarks and recommendations are provided in the last section.

THE GENERAL DYNAMIC EQUATIONS GOVERNING AEROSOL SYSTEMS

We present in this section the basic equations that govern the dynamics of spatially homogeneous particulate systems undergoing coagulation and condensation. Let $n(v,t)$ be the density function of the aerosol number size distribution, where v is the aerosol volume and t is the time, i.e., $n(v,t)\,dv$ is the number of aerosols per unit volume of air, with volumes between v and $v+dv$.

The evolution of the aerosol size distribution due to coagulation is represented by the following integrodifferential equation:

$$\begin{aligned}\frac{\partial n(v,t)}{\partial t} &= \frac{1}{2}\int_{v^*}^{v}\beta(v-\tilde{v},\tilde{v})\,n(\tilde{v},t)\\ &\quad\times n(v-\tilde{v},t)\,d\tilde{v}\\ &\quad-\int_0^\infty\beta(v,\tilde{v})\,n(v,t)\,n(\tilde{v},t)\,d\tilde{v},\\ n(v,0) &= n_0(v), \qquad\qquad (1)\\ n(v,t) &= 0, \qquad v<v^*,\end{aligned}$$

where β is the coagulation coefficient and v^* is the minimum aerosol volume. Difficulties in solving this equation arise in the evaluation of the integrals on the right-hand side.

The coagulation coefficient β is a function of the size of the two coagulating aerosols. Its form depends on the coagulation process, i.e., Brownian, turbulent, or gravitational motion. For the purpose of this study, we consider coagulation by Brownian motion since it is the most relevant to coagulation of atmospheric fine aerosols (e.g., Seigneur and Barnes, 1985). The aerosol coagulation coefficient used in this study is the Fuchs coefficient (Fuchs, 1964; Sitarski and Seinfeld, 1977):

$$\beta(v_i, v_j) = 4\pi(D_i + D_j)(r_i + r_j) \times \left[\frac{r_i + r_j}{r_i + r_j + g_{ij}} + \frac{4(D_i + D_j)}{(\bar{C}_i^2 + \bar{C}_j^2)^{1/2}(r_i + r_j)} \right]^{-1} \tag{2}$$

where r_i is the radius of aerosols of volume v_i, d_i is the diffusion coefficient of aerosols of volume v_i, g_{ij} is a function of the aerosol radius and mean free path of the air, and $\bar{C}_i$ is the mean thermal velocity of aerosols of volume v_i.

The evolution of the aerosol size distribution due to condensation/evaporation is represented by the following equation:

$$\begin{aligned} \frac{\partial n(v,t)}{\partial t} &= -\frac{\partial}{\partial v}[n(v,t)I(v,t)], \\ n(v,0) &= n_0(v), \\ n(v,t) &= 0, \qquad v < v^*. \end{aligned} \tag{3}$$

where $I(v, t) = dv/dt$, the rate of growth/shrinkage of a particle of volume v.

Equation (3) is a hyperbolic partial differential equation. The numerical solution of such an equation is hindered by the difficulty in accurately representing the fronts that move with velocity dv/dt. The errors in the solution give rise to numerical diffusion and dispersion (Tsang and Brock, 1983). Numerical diffusion leads to a decrease of the peak values of the number distribution and to concurrent increases in the values of the number distribution around these peak values. Numerical dispersion leads to wakes in the ranges below and above the area of large values of the number distribution. If one is interested only in condensation/evaporation processes, then Eq. (3) can be solved exactly by the method of characteristics. However, in the presence of coagulation, the condensation/evaporation term of the general dynamic equation must be treated numerically in accordance with the coagulation terms.

In this study the condensation growth law, dv/dt, which depends on the condensing vapor and aerosol size, is represented by the Fuchs–Sutugin formula (Fuchs and Sutugin, 1971):

$$\frac{dv}{dt} = \frac{4\pi r D}{1 + \left(\frac{1.333\mathrm{Kn} + 0.71}{1 + \mathrm{Kn}}\right)\mathrm{Kn}} \times v_m \left[P - P_s \exp\left(\frac{2\sigma v_m}{rkT}\right) \right], \tag{4}$$

where r is the aerosol radius, D is the diffusion coefficient of the condensing vapor, Kn is the Knudsen number equal to λ/r, λ is the mean free path of the condensing vapor, v_m is the molecular volume of the condensing vapor, and P and P_s are the ambient and equilibrium vapor pressure of the condensing vapor, respectively. The exponential term represents the Kelvin effect, where σ is the surface tension of the condensed species, k is Boltzmann's constant, and T is the absolute temperature.

Species such as condensible organics generally have a nonnegligible equilibrium vapor pressure; thus the Kelvin effect becomes important and can lead to evaporation from small aerosols while condensation occurs on larger aerosols (Tsang and Brock, 1983, 1984). In this study, we focus on the treatment of condensation only and therefore assume that the equilibrium vapor pressure of the condensing vapor is zero. This is a reasonable assumption for a condensing species with very low volatility such as sulfuric acid.

DESCRIPTION OF THE MATHEMATICAL MODELS OF AEROSOL DYNAMICS

This section describes the mathematical models that were selected for our comparative study of the continuous, discrete, and parametrized approaches to simulating aerosol dynamics. We consider the models of Brock and co-workers based on the continuous aerosol size distribution, the model of Seinfeld and co-workers based on a discrete representation of the aerosol size distribution, and the parametrized aerosol model of Whitby and co-workers.

Models Based on the Continuous Representation of the Aerosol Size Distribution

Suck and Brock (1979), Tsang and Brock (1982, 1983), and Yom and Brock (1984) have developed mathematical models to simulate the evolution of the aerosol number distribution, $n(v,t)$, when it is affected by either coagulation or condensation/evaporation. We briefly describe in this section the formulation of the models COAGUL and CONFEMM, which simulate coagulation and condensation, respectively.

The model COAGUL is based on the solution of the coagulation equation, Eq. (1). Suck and Brock (1979) then performed the following change of variable, the so-called J-space transformation:

$$v(J) = v(J_0)\exp[\alpha(J - J_0)], \tag{5}$$

where J and J_0 are integers such that $J \geq J_0$, $J_0 > 0$, and α is an adjustable parameter.

The aerosol distribution function in J space is then represented by the following function:

$$\psi(J,t) = \alpha v(J) n(v(J),t). \tag{6}$$

The coagulation equation may then be rewritten for the J-space distribution function as follows:

$$\begin{aligned}\frac{\partial\psi(J,t)}{\partial t} &= \int_{J_0}^{J_h} \beta_J(\tilde{J},J')\frac{v(J)}{v(\tilde{J})}\psi(\tilde{J},t)\psi(J',t)\,dJ' \\ &\quad - \int_{J_0}^{\infty} \beta_J(J,J')\psi(J,t)\psi(J',t)\,dJ',\end{aligned} \tag{7}$$

where

$$\tilde{J} = J + \frac{1}{\alpha}\ln\{1 - \exp[\alpha(J - J')]\};$$

$$J_h = J - \frac{\ln 2}{\alpha};$$

and

$$\beta_J(\tilde{J},J') = \beta(v - v', v').$$

The integrals in Eq. (7) are then represented by means of cubic spline functions, and a subroutine based on the method of Gear (1971) is used to integrate the resulting ordinary differential equations with respect to time. The solution $\psi(J,t)$ is then converted back to the number distribution function $n(v,t)$ according to Eq. (6).

The model CONFEMM is based on the solution of the condensation equation for the continuous number distribution, as described by Eq. (3). Tsang and Brock (1983) developed numerical schemes for solving this equation that minimize numerical diffusion and dispersion to any desired level of accuracy. They used two different finite-element methods for the condensation ($dv/dt > 0$) and evaporation ($dv/dt < 0$) equations. The method of Varoglu and Finn (1980) was modified and applied to the solution of the condensation equation. The method of Neuman (1981), together with cubic spline interpolation on finite elements, was applied to the solution of the evaporation equation. These two approaches yield solutions with any specified degree of accuracy. In addition, the two techniques have been coupled to solve the equation representing the case in which both condensation and evaporation simultaneously affect the aerosol size distribution (Tsang and Brock, 1984). In the present study, we consider the condensation equation only.

Model Based on the Discrete Representation of the Aerosol Size Distribution

In the discrete approach to modeling aerosol dynamics, the aerosol size range is divided into a discrete number of sections.

The aerosol volumes of section l range from v_{l-1} to v_l, where $l = 1, \ldots, L$. Approximating the number, surface area, or volume distribution function as a constant within each section results in a set of differential equations for the properties of each section. For example, the number distribution is approximated as follows:

$$N_l(t) = \int_{v_{l-1}}^{v_l} n(v,t)\,dv, \qquad l = 1, \ldots, L, \tag{8}$$

where $N_l(t)$ is the aerosol number concentration in section l, L is the total number of aerosol size sections, and v_0 and v_L are the aerosol volume of the lower and upper ranges of the aerosol size distribution, respectively.

The number distribution $n(v,t)$ is then approximated by the step functions $N_l(t)(v_l - v_{l-1})^{-1}$. The volume size distribution is approximated in a similar manner, as follows:

$$Q_l(t) = \int_{v_{l-1}}^{v_l} n(v,t)\,v\,dv, \qquad l = 1, \ldots, L. \tag{9}$$

The aerosol dynamic equations can be solved for any representation of the size distribution, i.e., number, volume, etc. Generally, the sectional equations are solved for the mass or volume distribution. This solution is convenient because it allows direct conservation of mass or volume. In addition, it is computationally more accurate because the volume distribution covers a lesser range of concentration values than does the number distribution.

The coagulation equation for the sectional volume distribution can be deduced from Eq. (1) to give the following ordinary differential equations (Gelbard, Tambour, and Seinfeld, 1980):

$$\frac{dQ_l(t)}{dt} = \int_{i=1}^{l-1} {}^a\bar{\beta}_{i,l-1} Q_i(t) Q_{l-1}(t) - \sum_{i=1}^{L} {}^b\bar{\beta}_{i,l} Q_i(t) Q_l(t), \qquad l = 1, \ldots, L, \tag{10}$$

where the first term is not evaluated for $l = 1$.

The first term represents the formation of new aerosols in section l by coagulation of aerosols from lower sections, and the second term represents the coagulation of aerosols from section l with other aerosols to form aerosols in higher sections.

The sectional coagulation coefficients ${}^a\bar{\beta}_{i,l-1}$ and ${}^b\beta_{i,l}$ are calculated by integrating the coagulation coefficient $\beta(v_1, v_2)$ given by Eq. (2) over the sections of interest (see Gelbard, Tambour, and Seinfeld, 1980, for the derivation of the sectional coagulation coefficients). These coefficients are generally calculated with the constraint that $v_l > 2v_{l-1}$. The advantage of this method is that for a fixed sectionalization of the aerosol size distribution, the sectional coagulation coefficients are integrated only once, and the coagulation equation is then reduced from an integrodifferential equation to a set of ordinary differential equations.

Similarly, the condensation equation governing the sectional volume distribution can be deduced from Eq. (3) to give the following equation (Gelbard and Seinfeld, 1980):

$$\frac{dQ_l(t)}{dt} = {}^a\bar{\phi}_l Q_l(t) + {}^b\bar{\phi}_{l-1} Q_{l-1}(t) - {}^b\bar{\phi}_l Q_l(t), \qquad l = 1, \ldots, L, \tag{11}$$

where the second term is not evaluated for $l = 1$. The first term represents the growth of the aerosol volume in section l due to condensation; the second term represents the growth of the aerosol volume from section $(l-1)$ into section l; and the third term represents the growth of the aerosol volume from section l into section $(l+1)$. The sectional condensation coefficients are calculated by integrating the growth law given by Eq. (4) over the sections (Gelbard and Seinfeld, 1980; Seigneur, 1982). If the sectionalization of the aerosol size distribution is fixed, these sectional condensation coefficients are calculated only once, and the condensation equation is then reduced from a partial differential equation to a set of ordinary differential equations. In addition to including the treatment of condensation and evaporation processes in Eq. (11), Warren and Seinfeld (1985) improved the sectional treatment of gas/aerosol conversion by calculating coefficients that allow conservation of the aerosol number concentration. Their formulation was used in this study.

The model ESMAP (Warren and Seinfeld, 1985)—an extension of the model MAEROS (Gelbard and Seinfeld, 1980; Gelbard, 1984)—combines the treatment of both coagulation and condensation to describe the evolution of a sectional aerosol size distribution affected by these two processes. The sectional coagulation and condensation coefficients are calculated by Gaussian quadrature. The set of ordinary differential equations is solved by the numerical intergration scheme EPISODE, a revised version of the numerical integration scheme of Gear (Byrne and Hindmarsh, 1975).

Model Based on the Parametrized Representation of the Aerosol Size Distribution

Whitby (1981a) developed the model AGRO, which simulates the evolution of a bimodal aerosol size distribution. The model is based on the parametrization of the coagulation and condensation processes and describes the evolution of the number and volume concentrations of the two models. The fixed number of parameters involved in the model formulation does not allow for variation of the resolution of the aerosol size distribution as was possible in the models described above, and the parametrized approach is constrained by this definition of the two modes. These two modes represent fine aerosols (i.e., up to 3 μm in diameter) and consist of a nuclei mode and an accumulation mode. The coarse mode is assumed to be affected by emissions, sedimentation, and deposition processes but not by coagulation and condensation processes. It is therefore treated separately from the two fine aerosol modes. The bimodal number distribution for fine aerosols, $n(d,t)$, represents the aerosol number concentration as a function of $\log(d)$, where d is the aerosol diameter. This distribution is represented by two lognormal distributions as follows:

$$
\begin{aligned}
n(d,t) = {} & \frac{N_n(t)}{(2\pi)^{1/2}\log[\sigma_n(t)]} \\
& \times \exp\left[-\frac{1}{2}\left(\frac{\log[d/d_{Nn}(t)]}{\log\sigma_n(t)}\right)^2\right] \\
& + \frac{N_a(t)}{(2\pi)^{1/2}\log[\sigma_a(t)]} \\
& \times \exp\left[-\frac{1}{2}\left(\frac{\log[d/d_{Na}(t)]}{\log\sigma_a(t)}\right)^2\right].
\end{aligned}
\tag{12}
$$

where the subscripts n and a refer to the nuclei and accumulation modes, respectively. N_n and N_a represent the total aerosol number concentrations in each mode, d_{Nn} and d_{Na} are the geometric mean aerosol diameters, and σ_n and σ_a are the standard deviations. Similarly, the bimodal volume distribution, $V(d,t)$, represents the aerosol volume concentration as a function of $\log(d)$. It is represented by the sum of two log-normal distributions as follows:

$$
\begin{aligned}
V(d,t) = {} & \frac{V_n(t)}{(2\pi)^{1/2}\log[\sigma_n(t)]} \\
& \times \exp\left[-\frac{1}{2}\left(\frac{\log[d/d_{Vn}(t)]}{\log[\sigma_n(t)]}\right)^2\right] \\
& + \frac{V_a(t)}{(2\pi)^{1/2}\log[\sigma_a(t)]} \\
& \times \exp\left[-\frac{1}{2}\left(\frac{\log[d/d_{Va}(t)]}{\log[\sigma_a(t)]}\right)^2\right].
\end{aligned}
\tag{13}
$$

where V_n and V_a represent the total aerosol volumes in each mode, and d_{Vn} and d_{Va}

represent the geometric mean aerosol diameters. A third log-normal distribution with constant parameters was added in this study to represent the coarse mode.

In the original formulation (Whitby, 1981a), the coagulation equations consist of a set of four ordinary differential equations representing the temporal evolution of these four parameters, and four algebraic equations calculating the mean diameters; the standard deviations were kept constant:

$$\begin{aligned}
\frac{dN_n(t)}{dt} &= -K_{nn}N_n^2(t) - K_{na}N_n(t)N_a(t),\\
\frac{dN_a(t)}{dt} &= K_{na}N_n(t)N_a(t) - K_{aa}N_a^2(t),\\
\frac{dV_n(t)}{dt} &= -K_{na}N_a(t)N_n(t)\frac{\pi}{6}(d_{Nn})^3\\
&\quad \times \exp\left(4.5\, l\mathrm{n}^2 \sigma_n\right),\\
\frac{dV_a(t)}{dt} &= K_{na}N_a(t)N_n(t)\frac{\pi}{6}(d_{Nn})^3\\
&\quad \times \exp\left(4.5\, l\mathrm{n}^2 \sigma_n\right).
\end{aligned} \tag{14}$$

The parameters K_{nn}, K_{aa}, and K_{na} are the nuclei intramodal, accumulation intramodal, and nuclei/accumulation intermodal coagulation coefficients, respectively. They are derived from the Fuchs coagulation coefficient given in Eq. (2) integrated over log-normal distibutions. These parameters depend therefore on the standard deviations and mean diameters of the modal distribution (Whitby, 1985). The first equation represents the decrease in aerosol number in the nuclei mode due to intramodal coagulation of nuclei mode aerosols and intermodal coagulation of nuclei mode aerosols with accumulation mode aerosols. The second equation represents the change in aerosol number in the accumulation mode due to intermodal coagulation of nuclei mode aerosols with accumulation mode aerosols and intramodal coagulation of accumulation mode aerosols. The change in volume concentrations results from intermodal coagulation only. This value is calculated from the intermodal coagulation term of the number concentrations and converted into volume concentrations.

In a new version of the model AGRO, both the mean diameters for the number and volume distributions and the standard deviations are allowed to change with time. Two additional equations are therefore introduced to calculate the temporal evolution of the standard deviations. The algorithms for calculating the evolution of these parameters are given by Whitby (1985).

The effect of condensation on the aerosol size distribution is treated similarly by a set of ordinary differential equations:

$$\begin{aligned}
\frac{dV_n(t)}{dt} &= Q_{Vn},\\
\frac{dV_a(t)}{dt} &= Q_{Va},
\end{aligned} \tag{15}$$

where Q_{Vn} and Q_{Va} are the rates of condensation of the nuclei and accumulation modes, respectively. These condensation rates depend on the rate of condensible species formation in the gas phase given by Eq. (4) and the distribution of condensation between the two modes. This distribution is determined according to the Fuchs–Sutugin condensation formula given in Eq. (4).

These differential equations representing coagulation and condensation are combined into the model AGRO. The numerical solution is obtained by a finite-difference technique with variable time steps.

SIMULATION OF AEROSOL COAGULATION AND CONDENSATION

The models AGRO, ESMAP, COAGUL, and CONFEMM were applied to the simulation of (1) coagulation, and (2) condensation for atmospheric aerosol concentrations typical of clear, hazy, and urban conditions. The aerosol size distributions were modeled for the 0.001–10-μm-diam size range. Two resolutions were used for ESMAP: 12 and 39 sections for this size range.

The simulations were conducted for 12 hr. The condensation rates were calculated with a gas-phase chemical kinetic mechanism for sulfuric acid formation. The sulfuric acid

TABLE 1. Initial Log-Normal Size Distributions Used in the Aerosol Dynamics Model Simulations

Parameter[a]	Conditions		
	Clear	Hazy	Urban
Mean diameter (μm)			
d_n	0.03	0.044	0.038
d_a	0.2	0.24	0.32
d_c	6.0	6.0	5.7
Standard deviation			
σ_n	1.8	1.2	1.8
σ_a	1.6	1.8	2.16
σ_c	2.2	2.2	2.21
Total volume ($\mu m^3 cm^{-3}$)			
V_n	0.03	0.09	0.63
V_a	1.0	5.8	38.4
V_c	5.0	25.9	30.8
Reference	Seigneur (1982)	Whitby (1981b)	Whitby (1978)

[a] Subscripts *n*, *a*, and *c* refer to nuclei, accumulation, and coarse modes, respectively.

formation rates amounted to 0.3, 5.5, and 4.6 μm^3 cm^{-3} of aerosol for 12 hr for typical clear, hazy, and urban conditions, respectively. The condensation rates were assumed to be constant throughout the simulation.

The initial size distributions were chosen to be log–normal to allow all three models to be initialized with identical size distributions. These initial size distributions are presented in Table 1. The models AGRO, COAGUL, and CONFEMM used the parameters of the log-normal size distributions as direct inputs. The log-normal size distributions were integrated exactly over 12 and 39 size sections to provide the inputs to ESMAP.

The aerosol size distributions were quantitatively compared after 12 hr of simulation as follows. The COAGUL and CONFEMM simulation results were taken as reference since they are capable of the most highly resolved solutions of the coagulation and condensation equations, respectively. Test simulations of COAGUL were made using 79, 39, and 13 grid points. The maximum local error between the simulations using 39 grid points and those using 79 grid points was 3% over the diameters of interest. The maximum error for the simulations using 13 grid points was 5%. The CONFEMM simulations used 80, 40, and 12 grid points. The maximum error between the 40- and 80-point simulations was 1.5%. The maximum error using 12 points was 16%. Computational costs increased significantly as the number of grid points increased. The increase in cost is nearly proportional to the number of grid points for CONFEMM and more than proportional for COAGUL. Since reasonable accuracy was obtained in the simulations using 39 and 40 points for COAGUL and CONFEMM, respectively, these model results were used as reference in this study.

Once satisfactory grid point numbers were selected, it was then necessary to allow a common representation of the size distributions. To that end, the COAGUL and CONFEMM results were cast into a sectional form with 12 and 39 size ranges. This sectionalization was carried out by interpolating between the points of the COAGUL and CONFEMM distributions by means of a cubic spline function and integrating the resulting size distributions over the desired size ranges. The results of the model ESMAP with 12 and 39 sections were compared with the results of COAGUL and CONFEMM sectionalized with 12 and 39 size ranges, respectively. The size distributions calculated by AGRO were cast into a sectional size distribution by means of an exact analytical transformation. The AGRO results could then be compared with the COAGUL and CONFEMM results using the 39-section size resolution. The accuracy of this technique for comparing the size distributions calculated by the various models was assessed by applying it to the initial size distributions, which are necessarily identical for all models. This evaluation showed that the technique was accurate over the entire size range within 1% and locally within 2%.

A quantitative comparison of model accuracy was conducted for aerosols with diameters in the size range 0.07–2.5 μm. Below 0.07 μm, aerosol concentrations were very low after 12 hr of simulated coagulation or condensation, and comparison of predicted aerosol concentrations would therefore be of little value. Above 2.5 μm, aerosols are little affected by coagulation and condensation, and all calculated size distributions after 12 hr are nearly identical to the initial size distribution; thus, model comparison in the upper size range is irrelevant. It may be noted that the size range 0.07–2.5 μm comprises the aerosols that are optically the most active and generally includes the largest volume of secondary aerosols.

The model comparison was performed with the following measure:

$$D = \frac{1}{15} \sum_{i=19}^{33} \frac{|Q_i - Q_i^*|}{Q_i^*}, \tag{16}$$

where i is the section number of the 39-section representation and corresponds to the size range 0.07–2.5 μm, Q_i^* is the aerosol volume in section i calculated by either COAGUL (coagulation simulations) or CONFEMM (condensation simulations), and Q_i is the aerosol volume in section i calculated by ESMAP (39 sections), ESMAP (12 sections), or AGRO. A model that provides the same result as the reference model will ideally have a performance measure of 0% (actually, the limitations of the interpolation method may lead to a value of D of 1%), whereas a model that differs widely from the reference model will have a large value of D.

Simulation of Coagulation

The results of the simulations of coagulation are presented for the volume size distribution in Figures 1–3 for clear, hazy, and urban conditions. The results of the model performance evaluation [Equation (16)] are presented in Table 2. In theory, total aerosol mass is conserved during coagulation. Total aerosol mass conservation was checked for COAGUL, ESMAP (both 12 and 39 sections), and AGRO. After 12 hr of simulation time, all models were found to conserve mass to within 0.5% for all three cases.

It appears that for clear conditions, where aerosol concentrations are very low, coagulation has little effect on the aerosol size distribution. Thus, after 12 hr of simulation, all models provide results that are very close to the initial size distribution, and the ESMAP and AGRO simulation results are within 1% and 2% of the COAGUL simulation results, respectively.

For hazy conditions, a similar result is obtained; aerosol concentrations are not high enough to allow coagulation to significantly affect the initial size distribution. It may be noted, however, that AGRO tends to predict a slightly larger peak in the accumulation mode than do COAGUL and ESMAP. The performance of ESMAP and AGRO is still excellent for this case.

The simulation of urban aerosol concentrations is a more stringent test for coagulation models since there is a significant change in the aerosol size distribution during the 12-hr simulation. The COAGUL simulation shows that aerosols below 0.15 μm coagulate with aerosols of larger sizes to lead to an increase in the peak concentration of the accumulation mode. The mean diameter of the coagulation mode is not noticeably

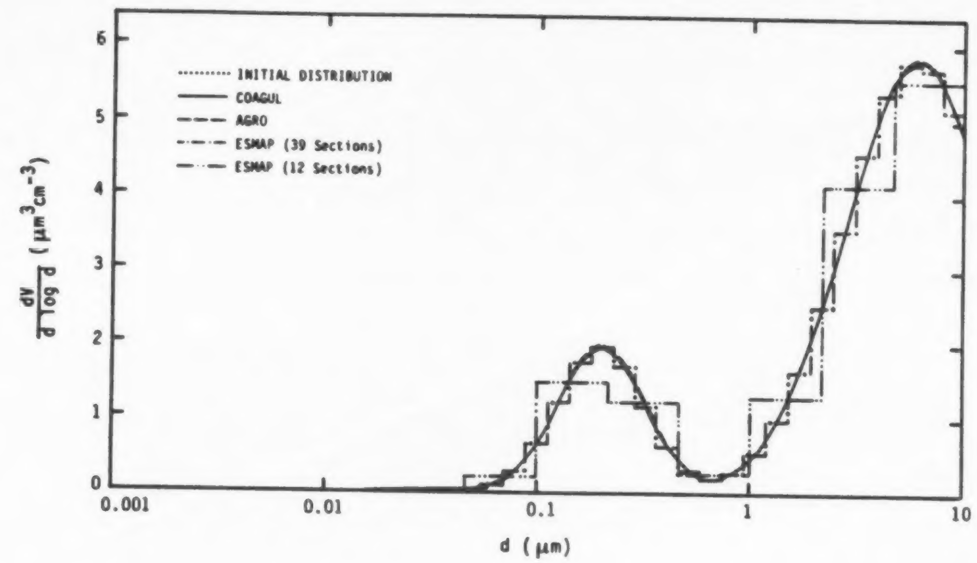

FIGURE 1. Simulation of coagulation for clear conditions; aerosol volume distributions, initially and after 12 hr.

affected by the coagulation process. The change in the aerosol size distribution is negligible above 0.7 μm. The ESMAP simulation results closely approximate those of COAGUL, producing size distributions that are within a few percent. The AGRO simulation tends to overestimate the rate of coagu-

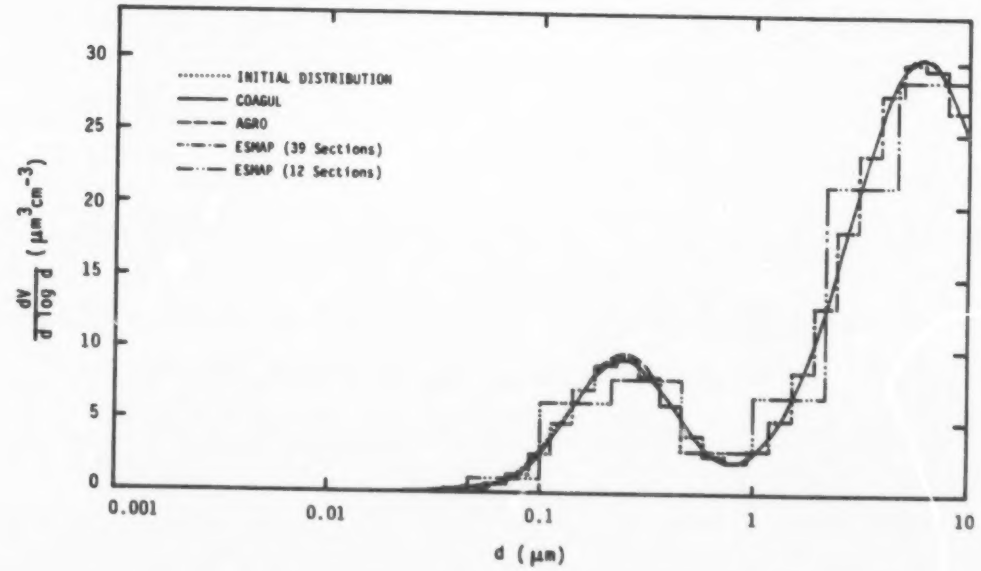

FIGURE 2. Simulation of coagulation for hazy conditions; aerosol volume distributions, initially and after 12 hr.

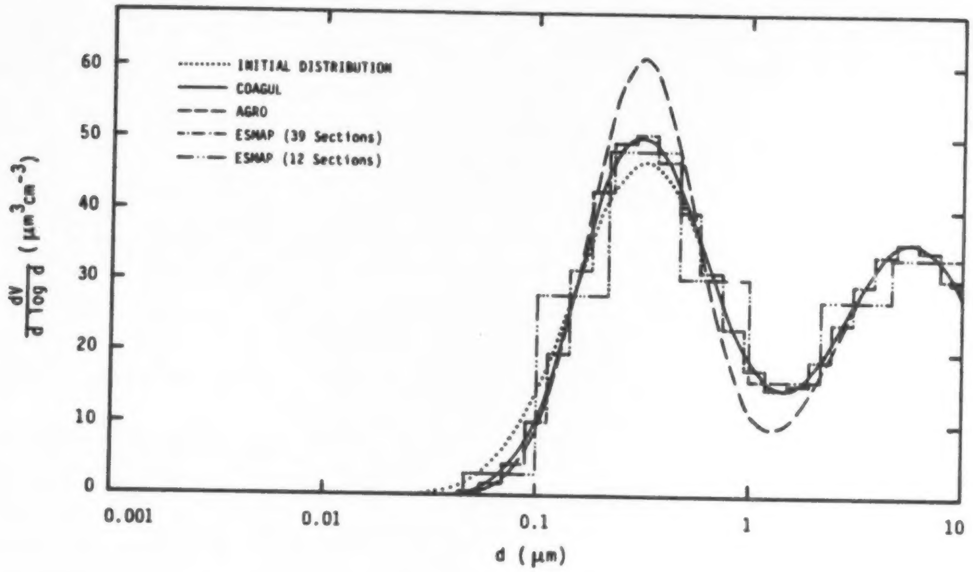

FIGURE 3. Simulation of coagulation for urban conditions; aerosol volume distributions, initially and after 12 hr.

lation and leads to results that are, on average, within 20% of the COAGUL simulation results. The mean diameter of the accumulation mode is well predicted by AGRO; however, the standard deviation is too small, resulting in overprediction of the aerosol concentration at the mean diameter size and underprediction at the tails of the accumulation mode distribution. This overprediction of the overall coagulation rate by AGRO is due to the inherent assumption of a log-normal distribution.

This discrepancy between the results of AGRO and COAGUL can be better exemplified by analyzing the evolution of the number distributions since the coagulation equation is based on the number concentrations. As shown in Figure 4, COAGUL does not predict a log-normal distribution for the aerosol number distribution, and there is a sharp cutoff in the number concentrations at the lower size end. In contrast, AGRO requires the assumption of a log-normal distribution and, therefore, the number distribution extends further toward the lower size range. The coagulation rate increases as the difference between the aerosol sizes increases. Therefore, the AGRO number size

TABLE 2. Comparison of Model Simulation Results for Coagulation

	Average absolute normalized difference (percent)		
Model	Clear conditions	Hazy conditions	Urban conditions
COAGUL		(Reference)	
ESMAP (39 sections)	1	1	2
ESMAP (12 sections)	1	1	3
AGRO	2	2	18

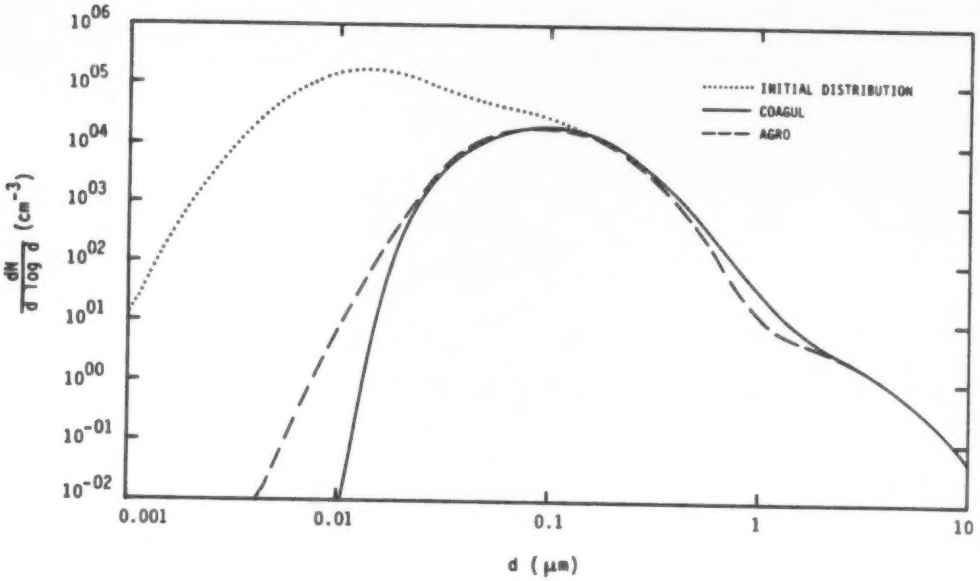

FIGURE 4. Simulation of coagulation for urban conditions; aerosol number distributions, initially and after 12 hr.

distribution allows coagulation to proceed at a faster rate than does the COAGUL number size distribution.

For the model simulations performed here, Gear's method of solving stiff ordinary differential equations was employed by COAGUL (Gear, 1971), and a modified version of Gear's method (Byrne and Hindmarsh, 1975) was used by ESMAP. In AGRO, the nonstiff ordinary differential equations were solved by a finite-difference method.

The computational times on a PRIME 750 computer were as follows. AGRO required less than 1 CPU s for the 12-hr simulation. COAGUL required from 100 to 1000 CPU s, depending on the case study. ESMAP required from 180 to 2500 CPU s with 39 sections and from 40 to 350 CPU s with 12 sections. For the initial ESMAP simulation, approximately 500 extra CPU s were required to calculate the sectional coefficients for the simulations with 39 sections and 70 extra CPU s for those with 12 sections. The coefficients were stored and used for subsequent simulations. These computational times are given to indicate the magnitude of the computational requirements; they may vary if different numerical techniques are used to integrate the model's differential equations. It should also be noted that, when the aerosol dynamics equations are solved along with other differential equations such as those for chemical kinetics (e.g., Seigneur, 1982), the incremental cost of the aerosol dynamics computation may be significantly less than the computational costs reported here.

Simulation of Condensation

The results of the simulations of condensation are presented for the volume size distribution in Figures 5–7 for clear, hazy, and urban conditions. The results of the model performance evaluation are listed in Table 3.

In theory, total aerosol number is conserved during condensation. The total aerosol number conservation was checked for

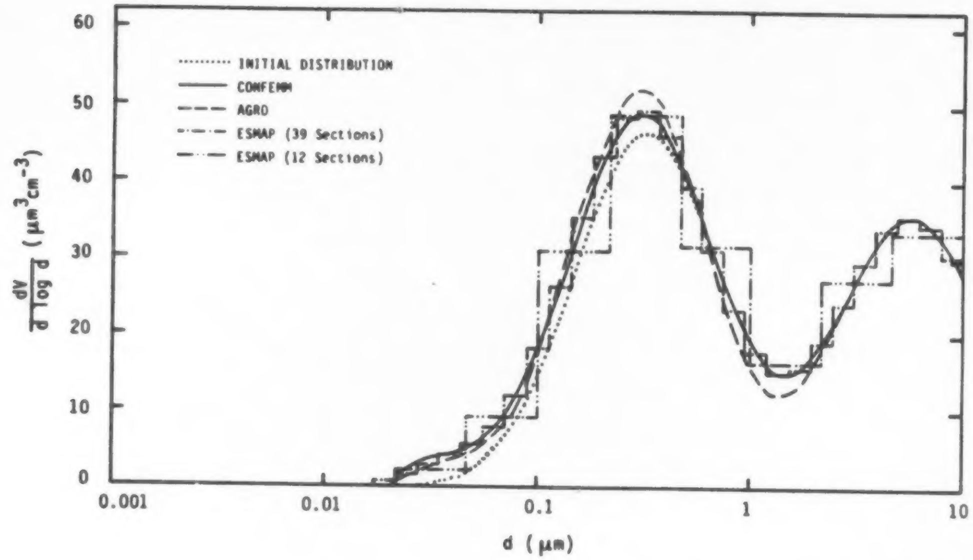

FIGURE 7. Simulation of condensation for urban conditions; aerosol volume distributions, initially and after 12 hr.

the lower range of the size distribution, where the very low mass concentrations and very high number concentrations induce errors in the calculation of the total number concentration by interpolation between grid points. This localized error in the total number concentration has very little effect on the accuracy over the entire size range, as demonstrated by the good agreement obtained between simulations performed with 40 and 80 grid points.

The CONFEMM simulation of condensation for clear conditions shows that secondary aerosols condense on two modes, with peak concentrations at about 0.03 and 0.2 μm. The mode centered at 0.03 μm results from the larger rate of condensation on smaller aerosols that is expressed by Eq. (4). The mode centered at 0.2 μm results from condensation that takes place at a slower rate but on a larger number of existing aerosols. It should be noted that if coagulation were simulated simultaneously, the lower mode would vanish owing to coagulation of these small aerosols with aerosols from the accumulation mode (Seigneur and Barnes, 1985).

ESMAP with 39 sections reproduces the existence of these two modes. However, because of numerical diffusion associated with

TABLE 3. Comparison of Model Simulation Results for Condensation

	Average absolute normalized difference (percent)		
Model	Clear conditions	Hazy conditions	Urban conditions
CONFEMM		(Reference)	
ESMAP (39 sections)	4	12	1
ESMAP (12 sections)	13	35	4
AGRO	6	18	7

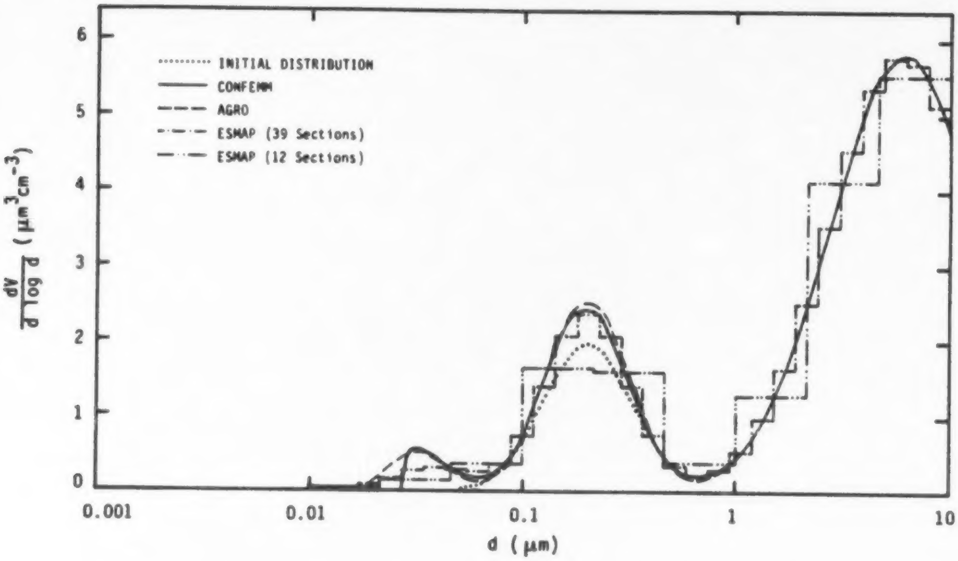

CONFEMM, ESMAP (both 12 and 39 sections), and AGRO. AGRO and ESMAP were found to conserve aerosol number to within at least 0.5% after 12 hr of simulation. CONFEMM was within 8.2%, 0.02%, and 3.7% for the clear, hazy, and urban cases. The larger error for CONFEMM occurs at

FIGURE 5. Simulation of condensation for clear conditions; aerosol volume distributions, initially and after 12 hr.

FIGURE 6. Simulation of condensation for hazy conditions; aerosol volume distributions, initially and after 12 hr.

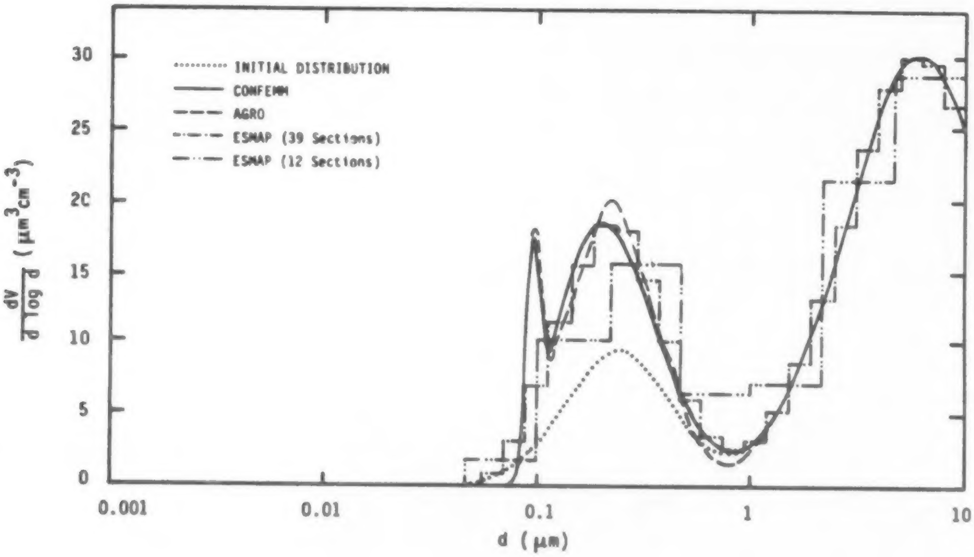

the solution of the sectional condensation equation, the lower mode is more spread out in the ESMAP simulation. For aerosols with diameters above 0.07 μm, the ESMAP simulation results with 39 sections agree well with the CONFEMM simulation results. ESMAP with 12 sections underpredicts the formation of a mode below 0.1 μm. Too much numerical diffusion is associated with the size resolution used in ESMAP with 12 sections. Nevertheless, the ESMAP (12 sections) simulation results are within 13% of the CONFEMM simulation results, on average.

AGRO reproduces the two submicron modes. The lower mode is more spread out than in the CONFEMM simulation because of the log-normal distribution constraint of AGRO. Good agreement is obtained between the AGRO and CONFEMM simulation results above 0.03 μm.

The simulation of condensation for hazy conditions is a more difficult test of the condensation models because the volume of condensed aerosol amounts to about 50% of the initial fine aerosol volume. In the CONFEMM simulation, the lower mode is centered at about 0.1 μm and is more accentuated than it was in the clear-condition simulation. ESMAP fails to reproduce this lower mode because of numerical diffusion. AGRO reproduces the peak at 0.1 μm predicted by CONFEMM but predicts a slightly larger diameter for the accumulation mode peak. Because of numerical diffusion, ESMAP with 12 sections also predicts a larger median diameter for the accumulation mode. ESMAP with 39 sections performs better than ESMAP with 12 sections and AGRO and is able to reproduce the diameter of the peak of the accumulation mode predicted by CONFEMM. None of these models agrees within less than 10% with CONFEMM.

The simulation of condensation for urban conditions is not as difficult a test because the condensing volume relative to the initial fine aerosol volume is less, and the predominance of the accumulation mode over the nuclei mode precludes the formation of a distinct lower mode as shown in the CONFEMM simulation results. Therefore, this case is easier to simulate than were the previous cases. ESMAP performs very well with 39 sections and still offers very satisfactory performance with 12 sections. AGRO tends to overpredict the peak concentration of the accumulation mode because of the assumption of a log-normal size distribution. All models predict the same median diameter of the accumulation mode, which is nearly identical to that of the initial size distribution.

As was done in the ESMAP simulations of coagulation, the ESMAP simulations of condensation also employed the modified version of Gear's method to solve stiff ordinary differential equations (Byrne and Hindmarsh, 1975). AGRO used the same finite-difference technique used for coagulation. In CONFEMM, a finite-element method was used (Tsang and Brock, 1983).

The computational times on a PRIME 750 computer were as follows. AGRO required less than 1 CPU s for the 12-hr simulation. CONFEMM required about 150 CPU s. ESMAP with 12 sections required about 90 CPU s, and ESMAP with 39 sections required about 300 CPU s. Unlike the coagulation cases simulated with ESMAP, the extra CPU s required when the sectional coefficients were calculated for the first time were minimal, on the order of 10 s.

These CPU times are only approximate since, as mentioned in the previous section, they depend on the numerical technique of integration and could eventually be reduced by further optimizing the integration techniques.

CONCLUSION

A comparative review of mathematical models of aerosol coagulation and condensation has been presented. This review should provide useful guidance in selecting models according to computational requirements and the level of accuracy desired for a particular application. Three approaches were presented that differ by their representation of the size distribution of aerosols and include continuous, sectional, and parametrized (log-normal) representations. The models COAGUL and CONFEMM were selected as representative of the continuous approach for simulating coagulation and condensation, respectively. These models appear to provide the most accurate solution to the aerosol dynamics equations and are thus used as references in this model comparison. The model ESMAP represents the sectional approach and was applied here with 39 sections (the finest size resolution allowed in its standard formulation) and 12 sections over the 0.001 to 10 μm aerosol diameter range. The model AGRO represents the parametrized approach; it is based on a trimodal log-normal representation of the aerosol size distribution.

COAGUL and CONFEMM require the solution of 40 differential equations; ESMAP, 39 and 12, depending on sectional resolution, and AGRO, 6. The computational times on a PRIME 750 computer for 12 hr of simulation of coagulation or condensation are less than 1 CPU s for the AGRO model and range from 90 to 3000 CPU s for the other models.

Simulations of coagulation and condensation were conducted for 12 hr with initial aerosol size distributions typical of clear, hazy, and urban atmospheric conditions. The results of these simulations may be summarized as follows.

For coagulation ESMAP with either 39 or 12 sections performs very well relative to COAGUL, i.e., the aerosol size distributions calculated by these models are within a few percent. AGRO performs well for clear and hazy conditions where coagulation has little effect on the initial size distribution but is less accurate (within 18% of COAGUL on average) for urban conditions. This poorer performance of AGRO is due to its inherent assumption of the log-normal distribution, which leads to overprediction of the coagulation rate.

For condensation, ESMAP requires a relatively large number of sections to minimize numerical diffusion. The performance of ESMAP with 39 sections is satisfactory for all cases, whereas with 12 sections it produces reasonable results when condensation occurs primarily on the accumulation mode but poorer results when condensation also occurs on smaller aerosols to form a mode below 0.1 μm in addition to the accumulation mode. AGRO tends to overestimate the peak concentration of the accumulation mode, but it predicts the median diameter of the mode fairly well.

These results suggest that, for the conditions considered, ESMAP accurately simulates aerosol dynamics, although the presence of numerical diffusion may require the use of a larger number of sections to simulate condensation accurately. AGRO performs satisfactorily but tends to overestimate coagulation rates and the peak concentration of the accumulation mode resulting from condensation. Its substantially lower computational time compared to that of the other models makes AGRO attractive for applications that have large calculational requirements; however, the model-accuracy limitations must be kept in mind.

Both AGRO and ESMAP can treat coagulation and condensation simultaneously. Because coagulation has a strong effect on the size distribution of an aerosol undergoing condensational growth (Seigneur and Barnes, 1985), it would be useful to compare these two models with one based on the models of the continuous representation of the aerosol size distribution that simulates simultaneous coagulation and condensation. Tsang and Brock (1985) recently developed such a model to solve the general dynamic equation for simultaneous coagulation, condensation, and evaporation processes with changing saturation ratio.

For application purposes, each one of these three methods has its merits, and the selection of a specific approach will depend on the requirements of the application. For example, if aerosol dynamics is incorporated within a larger model describing fluid dynamics and ambient chemistry, a low computational cost may be required for the aerosol dynamics calculation to keep the overall computational cost within a reasonable range. This constraint may preclude use of a computationally expensive approach and favor the less expensive but less accurate approaches. On the other hand, the simulation of a laboratory experiment conducted to elucidate the details of a physical process of aerosol dynamics will require an accurate solution, and the accurate but computationally more expensive approaches may then be needed.

The results of this comparative study apply to atmospheric aerosols and depend on the test cases chosen. However, the conclusions of this work can be qualitatively extended to the simulation of particulate systems in general and should prove helpful for the selection of a mathematical model for studies of particulate dynamics.

We thank Dr. Peter H. McMurry, University of Minnesota, Dr. Tate Tsang, University of Kentucky, Dr. K. Yom, University of Texas, and Mr. Dale Warren, California Institute of Technology, for helpful discussions during the course of this study. We would also like to thank Ms. Judy A. Rodich for her editorial effort. The models described in this study are available with user's manuals from their authors, from the project officer, Dr. H. M. Barnes, at the U.S. Environmental Protection Agency, or from Dr. A. Belle Hudischewskyj at Systems Applications, Inc. Although the research described in this article was funded wholly by the U.S. Environmental Protection Agency through Contract No. 68-02-4076, it does not necessarily reflect the views of the agency, and no official endorsement should be inferred.

REFERENCES

Byrne, G. D., and Hindmarsh, A. C. (1975). A polyalgorithm for the numerical solution of ordinary differential equations. *ACM Trans. Math. Software* 1:71–96.

Fuchs, N. A. (1964). *Mechanics of Aerosols*. Pergamon, New York.

Fuchs, N. A., and Sutugin, A. G. (1971). High dispersed aerosols. In *Topics in Current Aerosol Research* (G. M. Hidy and J. R. Brock, eds.), Pergamon Press, Oxford, Vol. 2, pp. 1–60.

Gear, C. W. (1971). The automatic integration of ordinary differential equations. *Commun. ACM* 14:176–179.

Gelbard, F. (1984). MAEROS. *Aerosol Sci. Technol.* 3:117–118.

Gelbard, F., and Seinfeld, J. H. (1980). Simulation of multicomponent aerosol dynamics. *J. Colloid Interface Sci.* 78:485–501.

Gelbard, F., Tambour, Y., and Seinfeld, J. H. (1980). Sectional representation for simulating aerosol dynamics. *J. Colloid Interface Sci.* 76:541–556.

Neuman, S. P. (1981). A Eulerian–Lagrangian numerical scheme for the dispersion–convection equation using conjugate space-time grids. *J. Comp. Phys.* 41:270–294.

Seigneur, C. (1982). A model of sulfate aerosol dynamics in atmospheric plumes. *Atmos. Environ.* 16:2207–2228.

Seigneur, C., and Barnes, H. M. (1985). Technical considerations in regional aerosol modeling. In *Air Pollution Modeling and Its Application*. (C. de Wispleaere, ed.), Plenum Press, New York (in press), Vol. 5.

Sitarski, M., and Seinfeld, J. H. (1977). Brownian coagulation in the transition regime. *J. Colloid Interface Sci.* 61:261–271.

Suck, S. H., and Brock, J. R. (1979). Evolution of atmospheric aerosol particle size distributions via Brownian coagulation: Numerical simulation. *J. Aerosol Sci.* 10:581–590.

Tsang, T. H., and Brock, J. R. (1982). Aerosol coagulation in the plume from a cross-wind line source. *Atmos. Environ.* 16:2229–2235.

Tsang, T. H., and Brock, J. R. (1983). Simulation of condensation aerosol growth by condensation and evaporation. *Aerosol Sci. Technol.* 2:311–320.

Tsang, T. H., and Brock, J. R. (1984). On Ostwald ripening. *Aerosol Sci. Technol.* 3:283–292.

Tsang, T. H., and Brock, J. R. (1985). Dynamics of Ostwald ripening with coalescence. *Aerosol Sci. Technol.* in press.

Varoglu, E., and Finn, W. D. L. (1980). Finite elements incorporating characteristics for one-dimensional diffusion–convection equations. *J. Comp. Phys.* 34:371–389.

Warren, D. R., and Seinfeld, J. H. (1985). Simulation of aerosol size distribution evolution in systems with simultaneous nucleation, condensation, and coagulation. *Aerosol Sci. Technol.* 4:31–43.

Whitby, K. T. (1978). The physical characteristics of sulfur aerosols. *Atmos. Environ.* 12:135–159.

Whitby, K. T. (1981a). Determination of aerosol growth rates in the atmosphere using lumped aerosol dynamics. *J. Aerosol Sci.* 12:174–178.

Whitby, K. T. (1981b). Aerosol and ozone formations in the Columbus, Ohio urban plume on July 29 and 30, 1980: A preliminary report (Publication No. 447). Particle Technology Laboratory, Department of Mechanical Engineering, University of Minnesota, Minneapolis, Minnesota.

Whitby, E. R. (1985). The modal aerosol dynamics model. Part I. Solution of the internal terms of the general dynamic equation of aerosols. Report to the U.S. Environmental Protection Agency, Department of Mechanical Engineering, University of Minnesota, Minneapolis, Minnesota.

Yom, K., and Brock, J. R. (1984). Private communication, Department of Chemical Engineering, University of Texas, Austin, Texas.

Received 19 July 1985; accepted 28 January 1986

Appendix D

DEVELOPMENT OF A PARAMETERIZED CHEMICAL KINETIC MECHANISM FOR SECONDARY ORGANIC AEROSOL FORMATION

Appendix D

MODELING SECONDARY ORGANIC AEROSOL FORMATION

INTRODUCTION

Secondary organic aerosol constitutes an important fraction of atmospheric aerosol concentrations. It is therefore important to incorporate some treatment of secondary organic aerosol formation into a mathematical model of atmospheric aerosol dynamics and chemistry. However, no general chemical kinetic mechanism has been developed to treat the formation of secondary organic aerosols. Some chemical kinetic mechanisms can treat specific hydrocarbons, but these mechanisms are still tentative; thus there is clearly a need for more detailed kinetic and mechanistic studies of the chemistry of secondary organic aerosol formation. We present here an overview of the current state of knowledge of the chemistry and dynamics of secondary organic aerosols and infer from this review the formulation of a lumped model of secondary organic aerosol formation for the EPA regional particulate model.

REVIEW OF ORGANIC AEROSOL CHEMISTRY

Several studies of organic aerosol formation have been conducted in smog chambers and chemical reactors. The report titled "Ozone and Other Photochemical Oxidants" by the National Academy of Sciences (NAS, 1977) presents a comprehensive review of organic aerosol formation based on experimental work carried out before 1976. This review is summarized as follows: (1) carbonyls, acetylene, and most paraffins do not lead to organic aerosol formation; (2) some branched paraffins may lead to aerosol formation; (3) olefins can lead to aerosol formation: cyclic olefins and diolefins lead to more aerosol formation than do terminal single olefins; the amount of organic aerosol formed among the terminal olefins increases with the length of the olefin. The NAS report discusses the chemical composition of organic aerosols and recommends further investigation of aromatics. Oxygenated compounds such as carbonyls, acids, and nitrate esters are considered to constitute the main fraction of organic aerosol products. However, identification of the organic aerosol products for given precursor hydrocarbons is not usually precise.

We review next the results of six major studies that were reported after the NAS review: the smog chamber experiments of Heisler and Friedlander (1977); the reactor experiments of Franzblau, Burton, and Hidy (1984); the smog chamber experiments of Grosjean and McMurry (Grosjean and McMurry, 1982; Grosjean, 1984a, 1984b, 1985); the smog chamber experiments of Fox, Gery, and Jeffries (1984); the smog chamber and reactor experiments of Hatakeyama et al. (1985); and the smog chamber experiments of Kamens et al. (1982).

Heisler and Friedlander (1977) investigated the formation of organic aerosols in outdoor smog chamber experiments. They conducted 11 experiments with mixtures of one hydrocarbon and nitrogen oxides. Seven hydrocarbons were considered: cyclohexene, 2-methyl-2-butene, 1-heptene, 2,3-dimethyl-2-butene, 1,7-octadiene, cyclopentene, and toluene. The total aerosol number concentration and light scattering coefficient were monitored during the experiment to characterize aerosol formation. The scattering coefficient increased notably for the experiments involving cyclohexene, octadiene, and cyclopentene. Less significant changes in the scattering coefficient were observed for the monoolefins and toluene. The products of some experiments were analyzed by gas chromatography-mass spectrometry. Cyclohexene and 1,7-octadiene led primarily to hexanedioic acid and 6-nitratohexanoic acid. Cyclopentene oxidation resulted mainly in 1,5-pentanedial and pentanedioic acid.

Franzblau, Burton, and Hidy (1984) studied the formation of organic aerosols resulting from the reactions of ozone with terminal olefins. The two olefins considered were 1-hexene and 1-octene. The experiments were conducted in a glass tube reactor at atmospheric pressure and room temperature. Chemical characterization of the aerosol produced in the experiments was not reported. The amount of organic aerosol formed was less than 2 percent of the initial organic species. The rates of aerosol formation were measured to be 6.2×10^{-2} and 1.2×10^{-1} $\mu g \cdot m^{-3}$ ppm^{-2} s^{-1} for 1-hexene and 1-octene, respectively. Water vapor inhibited aerosol formation.

Grosjean and McMurry (1982) studied organic aerosol formation in an outdoor smog chamber in the presence of hydrocarbons and nitrogen oxides. The hydrocarbons studied included n-heptane, cyclohexane, 1-hexene, 1-heptene, o-cresol, and methylsulfide. Organic aerosol formation from n-heptane and cyclohexane was negligible. Aerosol formation occurred in more significant amounts for the other hydrocarbons. 1-hexene led to aerosol formation that accounted for less than 0.4 percent of the initial hydrocarbon. 1-heptene led to more aerosol formation--1 to 10 percent of the initial hydrocarbon; hexanoic acid was a major aerosol product, but more than 90 percent of the aerosol mass was not identified. o-cresol led to organic aerosol, accounting for 5 to 20 percent of the initial o-cresol concentration. Hydroxynitrocresols were the main aerosol products; other aerosol products included nitrocresols and traces of pyruvic acid and, possibly, dinitrocresol. Methylsulfides led to inorganic sulfate and organic aerosol formation; 4 to 7 percent of the initial hydrocarbon was converted to organic aerosol. Formation of organic aerosol from 1-hexene was inhibited by water vapor.

Fox, Gery, and Jeffries (1984) investigated the formation of organic aerosols in an outdoor smog chamber. The precursor hydrocarbons studied included 1-hexene, 1,7-octadiene, cyclopentene, cyclohexene, toluene, m-xylene, and 1,3,5-trimethylbenzene. Three types of conditions for organic aerosol formation were investigated: (1) O_3 oxidation, (2) OH oxidation, and (3) simultaneous O_3 and OH oxidations. Organic aerosols were formed in the reactions of olefins with OH and O_3 and in the reaction of aromatics with OH. The amounts of organic aerosol formed relative to the initial hydrocarbon concentration for the O_3 oxidation pathways were 1.6 to 4 percent for cyclohexene, 2.3 percent for 1,7-octadiene, 1.2 percent for cyclopentene, and only 0.1 percent for 1-hexene. The amounts of organic aerosol formed relative to the initial hydrocarbon concentration for the OH oxidation pathways were 1.6 percent for m-xylene, 1.5 percent for trimethylbenzene, 1.3 percent for toluene, 1.7 percent for 1-hexene, 0.2 to 1.4 percent for cyclopentene, and 0.1 to 0.4 percent for cyclohexene. A combination of OH and O_3 oxidation led to organic aerosol formation that was sometimes less than that observed for the individual oxidation pathways. The amounts of organic aerosol formed relative to the initial hydrocarbon concentration were 0.1 to 8 percent for cyclohexene, 5.3 percent for 1,7-octadiene, 4.4 percent for cyclopentene, 0.3 to 0.7 percent for 1-hexene, 0.2 to 5.2 percent for toluene, and 1 percent for m-xylene and trimethylbenzene. Chemical characterization of the aerosol products was not performed. Chemical kinetic mechanisms were developed to simulate 1-hexene and cyclohexene oxidation. In the 1-hexene mechanism, peroxypentylnitrate was considered to be the major source of organic aerosol. Organic diacids and organic acids with nitrate groups were considered to be the condensible species in the cyclohexene mechanism.

Hatakeyama et al. (1985) investigated the aerosol products of the reaction of ozone with cyclohexene using three types of reactors: (1) a smog chamber, (2) a cylindrical quartz vessel, and (3) pyrex bulbs. The following aerosol products were identified: adipaldehyde, 6-oxohexanoic acid, adipic acid, glutaraldehyde, 5-oxopentanoic acid, and glutaric acid. About 13 percent of cyclohexene was converted to organic aerosol carbon. This percentage of conversion is higher than that observed by Fox, Gery, and Jeffries (1984).

Kamens et al. (1982) studied the reactions of isoprene and α-pinene with ozone in an outdoor smog chamber. Secondary organic aerosols were formed as a result of the reactions of these natural hydrocarbons with O_3. The dark isoprene/O_3 system led to the nucleation of small aerosols; however, only 1 percent of the isoprene yields condensible products. Thus, most of the aerosols produced in this system did not grow by subsequent condensation and remained at sizes well below 0.3 μm. The α-pinene/O_3 system led to more secondary aerosol formation and these aerosols grew by condensation to sizes of the order of 0.5 μm. No chemical characterization of the aerosol products was performed.

REVIEW OF ORGANIC AEROSOL DYNAMICS

The dynamics of aerosol formation is important because it determines the evolution of the aerosol size distribution as organic aerosols grow by condensation of organic species of low volatility or shrink by evaporation of volatile organic aerosols.

Aerosol formation may occur via gas-to-aerosol formation of condensible products formed in the gas phase or via heterogeneous formation of aerosol products in the aerosol phase. Gas-to-aerosol conversion occurs via nucleation of new aerosols or condensation on existing aerosols when the vapor pressure of a gaseous species exceeds its saturation vapor pressure. The Kelvin effect slightly modifies this theory by allowing the saturation vapor pressure at the surface of a small particle to be higher than the reference saturation vapor pressure (i.e., over a flat surface). Thus, condensation of an organic species may occur over large aerosols while evaporation from small aerosols takes place concurrently. The phenomenon of simultaneous evaporation/condensation is due to the Kelvin effect and modifies the aerosol size distribution by allowing large particles to grow and smaller particles to shrink.

The saturation vapor pressure of organic species is generally not well known. The following qualitative trends are given in the report of the National Academy of Science (NAS, 1977). The saturation vapor pressure decreases as the length of the hydrocarbon chain increases. For a given number of carbon atoms, the condensibility of organic species increases roughly as follows: alkane, aldehyde, alcohol, nitrate ester, carboxylic acid, dialdehyde, diol, dinitrate, acid aldehyde, and dicarboxylic acid.

More recent studies of the dynamics of organic aerosol formation include the works of Heisler and Friedlander (1977) and McMurry and Grosjean (1985). Heisler and Friedlander (1977) followed the change in the aerosol size distribution as organic aerosols were formed in an outdoor smog chamber. Comparison of the theoretical condensational growth laws of aerosol formation with the experimental data of the evolution of aerosol sizes suggested that gas-phase formation of condensible organic products followed by diffusion-limited condensation on existing aerosols was the major mechanism. They also noted that aerosol growth did not occur below critical diameter sizes because of the Kelvin effect and aerosol chemical composition effect on the equilibrium vapor pressure of the condensible organic species. These critical diameter sizes were estimated to have the following values: between 0.1 and 0.3 μm for cyclohexene, between 0.25 and 0.3 μm for 1,7-octadiene. For cyclopentene, two critical sizes were suggested by the data, implying two different condensation products. The lower critical size was between 0.2 and 0.5 μm, and the larger was between 0.7 and 1.0 μm.

McMurry and Grosjean (1985) investigated the growth laws of organic aerosols resulting from the reactions of o-cresol, nitrocresol, 1-heptene, and methylsulfide in the presence of nitrogen oxides and ammonia in an outdoor smog chamber. Their experimental measurements extended to aerosol sizes as small as 0.01 μm in diameter, whereas the measurements of Heisler and Friedlander were limited to a smaller aerosol size of about 0.3 μm. The growth law analyses indicated that condensation of organic species occurred on existing aerosols above a critical diameter size, whereas evaporation occurred below that critical size. The critical aerosol diameters were between 0.02 and 0.06 μm for 1-heptene experiments and about 0.06 μm for an o-cresol experiment. These results can be explained by the Kelvin effect and suggest that the condensing organic species have a nonnegligible saturation vapor pressure.

Least square analysis of the aerosol growth laws led to estimates of the average saturation vapor pressure of the condensible organic species that range from 0.06 to 2.0 ppb. The average saturation vapor pressures of the organic condensible products were 0.14 ppb for products of 1-heptene reacting in the presence of NO_x, 1.3 ppb for products of 1-heptene reacting in the presence of NO_x and NH_3, 1.6 ppb for products of o-cresol reacting in the presence of NO_x with sunlight, 0.06 ppb for o-cresol reacting in the presence of NO_x and O_3 in the dark, 2.0 ppb for nitrocresol products, and 1.4 ppb and 0.2 ppb for products of methylsulfide under dry and humid conditions, respectively. It appears that there is a large variation--about an order of magnitude--in the estimated saturation vapor pressure of products of a given hydrocarbon under different conditions. The saturation ratios (i.e., the ratio of the actual organic species vapor pressure to its saturation vapor pressure) ranged from 1.03 to 2.23. In the 1-hexene experiments, the growth law at large aerosol sizes suggested the presence of a second condensible organic species with a critical aerosol diameter between 0.15 μm and 0.5 μm for the reported experiment. This result is consistent with the observation of two critical sizes reported for the cyclohexene experiments by Heisler and Friedlander (1977).

The results of the growth law analyses of McMurry and Grosjean (1985) indicate that, for the chemical systems considered, secondary organic aerosol formation occurs via gas-phase formation of condensible organic products and subsequent diffusion-limited condensation on existing aerosols.

FORMULATION OF THE LUMPED ORGANIC AEROSOL MODEL

The organic aerosol model must be consistent with both the gas-phase chemical kinetic mechanism and the aerosol dynamics model. In this section we present the development of a lumped model of organic aerosols that is consistent with the carbon-bond formulation of the gas-phase chemistry and the aerosol sectional model.

Our knowledge of the chemistry of organic aerosol formation is still insufficient to develop a detailed chemical kinetic mechanism. Consequently, we opted for the development of a lumped mechanism in which the stoichiometric coefficients are derived from smog chamber experiments. This mechanism is formulated as follows:

$$\mathrm{RHC}_i + \mathrm{OXIDANT} \rightarrow \alpha_i\ \mathrm{ORG}_i$$

where

RHC_i = a reactive hydrocarbon from the Carbon-Bond Mechanism,

OXIDANT = either the OH radical or O_3,

ORG_i = a surrogate organic aerosol product, and

α_i = an empirical stoichiometric coefficient.

The coefficient α_i may be decomposed as follows:

$$\alpha = a\ b\ c\ d$$

where

a = yield of organic aerosol product (on a C basis)

b = conversion factor of ppm of precursor to ppmC

c = conversion factor of ppmC of precursor to ppmC of organic aerosol product

d = conversion factor of ppmC of organic aerosol product to $\mu g/m^3$ of normalized organic aerosol

For example, the formation of organic aerosol from toluene oxidation was determined to be a yield of 3 percent on a ppmC basis by Grosjean and McMurry (1982); thus, the value of the parameter a would be 0.03. In the Carbon-Bond Mechanism formulation (CBM IV and CBM X), toluene is represented by TOL and contains 7 carbon atoms; thus, the parameter b is equal to 7. The major organic aerosol product was hydroxynitrocresol, which also contains 7 carbon atoms; thus, the value of the parameter c is 1. However, the molecular weight of hydroxynitrocresol is higher than the weight of an alkane with 7 carbon atoms. To normalize the organic aerosol products with respect to mass per carbon, we use the molecular weight of methane as a norm for 1 ppmC, and normalize the aerosol product ppmC with respect to methane ppmC. In this case, the molecular weight of hydroxynitrocresol is 169 g; 1 ppmC of hydroxynitrocresol equals 981 $\mu g/m^3$.

According to the review of the chemistry of organic aerosol formation, aromatics, long-chain olefins, cyclic olefins, and diolefins are the major precursors of organic aerosols. Aromatics are distributed in two classes in the CBM-IV and CBM-X formulations: Toluene (TOL) and xylenes (XYL). These products are oxidized by reaction with OH radicals, and phenolic compounds such as cresol are formed. These phenolic compounds are represented by PHEN in the CBM formulation.

Cresols have been identified as an important source of organic aerosols with hydroxynitrocresol as the major aerosol product. Thus there are two possibilities for treating aerosol formation from aromatics: (1) relate the formation of organic aerosols to the primary precursors TOL and XYL, (2) relate the formation of organic aerosols to the intermediate species such as cresol (PHEN).

The first alternative leads to the following lumped reactions for organic aerosol formation:

$$\mathrm{TOL} + \mathrm{OH} \rightarrow \alpha_1\ \mathrm{ORG1}$$

$$\mathrm{XYL} + \mathrm{OH} \rightarrow \alpha_2\ \mathrm{ORG2}$$

where ORG1 and ORG2 represent the surrogate aerosol organic products for the toluene and xylene oxidations, respectively, and α_1 and α_2 represent stoichiometric coefficients deduced from smog chamber experiments. The second alternative leads to the following lumped reaction:

$$\mathrm{PHEN} + \mathrm{OH} \rightarrow \alpha_1'\ \mathrm{ORG1}$$

where ORG1 and α_1' are the surrogate organic aerosol product and the empirical stoichiometric coefficient, respectively.

Toluene oxidation leads to cresol, which contributes about 15 percent of the toluene oxidation products. Comparison of the toluene and cresol yields of organic aerosol products suggests that, in the toluene chemistry, cresol is a major precursor of organic aerosols. However, some other toluene oxidation pathways may also lead to organic aerosol formation. Consequently, it appears more appropriate to apply our lumped mechanism to the primary hydrocarbon ARO to encompass all organic aerosol products.

The surrogate organic species ORG1 is assumed to be hydroxynitrocresol in agreement with the findings from Grosjean (1984b) that this compound is the major organic aerosol product of o-cresol chemistry. By analogy, we assumed that ORG2 represents hydroxynitrodimethylphenol.

The experimental yield of organic aerosol products from toluene was 3 percent in the work of Grosjean and McMurry (1982) and between 0.2 to 5.2 percent in the work of Fox et al. (1984). The yield of organic aerosol products from o-cresol was between 5 and 19 percent (Grosjean and McMurry, 1982); if we assume that o-cresol accounts for 15 percent of toluene oxidation products, the yield of organic aerosol from toluene via the cresol pathway would be between 1 and 3 percent. From these results, we assumed that the yield of organic aerosols from toluene was 3 percent. The value of the parameter a is therefore 0.03. The values of the other parameters b, c, and d are calculated according to the assumption that the surrogate organic species is hydroxynitrocresol. The values of these parameters are given in Table 1.

The experimental yield of organic aerosol from m-xylene was reported to be between 0.4 and 1.6 percent (Fox et al., 1984). For trimethylbenzene, this yield was reported to be between 1 and 1.5 percent. We assumed that the yield of organic aerosol from xylenes was 1 percent. The value of the other parameters b, c, and d were deduced by assuming that the surrogate organic species was hydroxynitrodimethylphenol. The values of the parameters are given in Table 1.

The olefins are represented in the Carbon-Bond Mechanism by the double-bonded group OLE and single-bonded carbons PAR. We present the formation of organic aerosols from olefins by the following two reactions:

$$\mathrm{OLE} + \mathrm{OH} \rightarrow \alpha_3' \,\mathrm{ORG3}$$

$$\mathrm{OLE} + \mathrm{O_3} \rightarrow \alpha_4' \,\mathrm{ORG4}$$

The parameters α_3' and α_4' are defined as follows:

$$\alpha' = \kappa\, \alpha$$

TABLE 1. Parameters of the lumped organic aerosol reactions.

Chemical Reaction	Surrogate Organic Aerosol Product	a	b	c	d	α
TOL + OH	Hydroxynitrocresol	0.3	7	1	981	206
XYL + OH	Hydroxynitrodimethylphenol	0.01	8	1	845	67.6
OLE + OH	1-hydroxy-hexane-2,5-dione	0.008	2	3	877.5	42.3
OLE + O_3	Hexanoic acid	0.012	2	3	780	55.9
ISOP + O_3	Unknown	0.01	5	1	845	45.5

where κ represents the fraction of olefins that can lead to condensible organic products (i.e., long-chain olefins, cyclic olefins, and diolefins). A review of ambient concentrations of olefins measured in urban areas shows a wide range of values for the ratio of long-chain olefins (i.e., with more than 5 carbon atoms) to total olefins (Calvert, 1976; Kopczynski et al., 1972). The upper limit of this ratio--0.5--was selected here as the value of κ to provide an upper limit for organic aerosol formation.

Heisler and Friedlander (1977) and McMurry and Grosjean (1985) inferred from the measurements of the size distributions of organic aerosols resulting from terminal olefins that there were two major organic aerosol species (see previous section). However, Grosjean (1984a) identified only one major organic product--hexanoic acid--from the reaction of 1-heptene with O_3. To calculate the parameters b, c, and d of this lumped model, we assumed that the surrogate organic products ORG4 are hexanoic acid. Although the products of the reaction of 1-hexene with OH were not identified, the tentative chemical kinetic mechanism developed by Grosjean and McMurry (1982) suggests that 1,hydroxy-hexane-2,5-dione is a major product. Thus, we assumed that ORG3 was represented by this compound. However, the model is flexible, and when more data on the organic product speciation become available, the surrogate species ORG3 and ORG4 can be represented by the appropriate compounds.

The measured yields of organic aerosols from 1-hexene were less than 0.4 percent (Grosjean and McMurry, 1982), less than 2 percent (Franzblau et al., 1984) and between 0.1 and 1.7 percent (Fox et al., 1984). The measured yield of aerosols from 1-heptene was between 1 and 10 percent (Grosjean and McMurry, 1982; Grosjean, 1984a). The measured yield of aerosols from 1-octene was less than 2 percent (Franzblau et al., 1984). The measured yields of aerosols from cyclohexene and cyclopentene were between 0.1 and 13 percent and between 1.2 and 4.4 percent, respectively (Fox et al., 1984; Hatakeyama et al., 1985). The measured yield of aerosol from 1,7-octadiene was between 0.4 and 5.3 percent (Fox et al., 1984). There is clearly a large variation in the yields of aerosol products from olefins--from 0.1 to 10 percent. A yield of 2 percent was assumed in this model. This yield appears to be representative of an upper limit for terminal olefins (1-hexene, 1-heptene, and 1-octene) and of a lower limit for cyclic olefins and diolefins. A value of the yield tailored to the speciation of the olefin emissions could be developed later when more data became available.

A theoretical investigation of the oxidation of 1-hexene suggested that 40 percent of organic aerosol was produced through the OH-1-hexene pathway, and 60 percent through the O_3-1-hexene pathway (Fox et al., 1984). Thus, the values of a_3 and a_4 are 0.008 and 0.012, respectively, providing the total assumed yield is 0.02. The values of the parameters c and d were calculated assuming that hexanoic acid was the major aerosol product for the 1-hexene-O_3 pathway and that 1,hydroxy-hexane-2,5-dione was the major aerosol product for the 1-hexene-OH pathway (Grosjean and McMurry, 1982). The value of κ is assumed to be 0.5. The stoichiometric coefficients are summarized in Table 1.

Presently, biogenic hydrocarbons are represented in the Carbon-Bond Mechanism solely by isoprene (ISOP). Terpenes, such as α-pinene, are not treated. It appears from the work of Kamens et al. (1982) that it would be worthwhile to include some treatment of terpenes in the gas-phase chemical kinetic mechanism since these compounds may lead to significant amounts of aerosol formation. For the moment, we limit our treatment of organic aerosol formation from natural hydrocarbons to isoprene oxidation by ozone.

$$\mathrm{ISOP} + O_3 \rightarrow \alpha_5\ \mathrm{ORG5}$$

Kamens et al. (1982) reported a yield of about 1 percent for the reaction of isoprene with O_3. There was no chemical characterization of the aerosol products. We used this value for the parameter a. Therefore, other parameters were selected by assuming that the condensible product had five carbon atoms. The value of the parameter d was selected as an average value of this parameter for other organic aerosols.

The mechanism for secondary organic aerosol formation may then be cast in the following form:

$$\begin{aligned}
\mathrm{TOL} + \mathrm{OH} &\rightarrow 206\ \mathrm{AERO}\\
\mathrm{XYL} + \mathrm{OH} &\rightarrow 68\ \mathrm{AERO}\\
\mathrm{OLE} + \mathrm{OH} &\rightarrow 42\ \mathrm{AERO}\\
\mathrm{OLE} + O_3 &\rightarrow 56\ \mathrm{AERO}\\
\mathrm{ISOP} + O_3 &\rightarrow 46\ \mathrm{AERO}
\end{aligned}$$

where AERO stands for the lumped organic aerosol product. Because of the large uncertainties in the saturation vapor pressure of condensible organic species, no attempt was made to treat the evaporation of organics from the aerosols, and organic aerosol condensation was assumed to be irreversible.

REFERENCES

Fox, D. L., M. Gery, and H. E. Jeffries. 1984. "Organic Aerosol Formation: OH vs. Ozone Oxidation Pathways." Final Report to Coordinating Research Council, Inc., Atlanta, Georgia.

Franzblau, E., C. S. Burton, and G. M. Hidy. 1984. Aerosol particle formation from ozone-terminal olefin reactions. *Aerosol Sci. Technol.*, 3:167-176.

Grosjean, D. 1984. Atmospheric reactions of ortho. cresol: gas phase and aerosol products. *Atmos. Environ.*, 18:1641-1652.

Grosjean, D., and P. H. McMurry. 1982. "Secondary Organic Aerosol Formation: Homogeneous and Heterogeneous Chemical Pathways." Final Report to Coordinating Research Council, Inc., Atlanta, Georgia.

Heisler, S. L., and S. K. Friedlander. 1977. Gas-to-particle conversion in photochemical smog: aerosol growth laws and mechanisms for organics. *Atmos. Environ.*, 11:157-168.

McMurry, P. H., and D. Grosjean. 1985. Photochemical formation of organic aerosols: growth laws and mechanisms. *Atmos. Environ.*, 19:in press.

NAS. 1977. "Aerosols." In *Ozone and Other Photochemical Oxidants*. National Academy of Sciences, Washington, D.C., pp. 45-125.

Atmospheric Environment Vol. 21, No. 4, pp. 807–812, 1987.
Printed in Great Britain.

© 1987 Pergamon Journals Ltd.

NTIS is authorized to reproduce and sell this report. Permission for further reproduction must be obtained from the copyright owner.

Appendix E

ON THE OXIDATION OF SO_2 TO SULFATE IN ATMOSPHERIC AEROSOLS

PRADEEP SAXENA* and CHRISTIAN SEIGNEUR†
Systems Applications, Inc., 101 Lucas Valley Road, San Rafael, California 94903, U.S.A.

(*First received* 1 *July* 1986 *and in final form* 12 *August* 1986)

Abstract—This paper presents the results of a study to investigate the atmospheric oxidation of sulfur dioxide (SO_2). A detailed model of gas-phase chemistry, aerosol thermodynamics and aerosol chemistry is employed to simulate atmospheric sulfate formation. The calculations indicate that, in addition to the gas-phase oxidation by hydroxyl (OH) radicals, SO_2 oxidation in aqueous aerosols may also contribute significantly to sulfate formation. Reactions of SO_2 with hydrogen peroxide (H_2O_2) and O_2 (catalyzed by Fe^{3+} and Mn^{2+}) are identified as principal aqueous-phase oxidation mechanisms. The results of this study confirm the conclusions drawn from the analysis of ambient aerosol data qualitatively. However, some discrepancies also exist between the results of our modeling study and field data. Such discrepancies emphasize the need for the collection of ambient data for a more rigorous and quantitative evaluation of atmospheric aerosol models.

Key word index: Aerosols, sulfur dioxide, oxidation, kinetics, sulfate.

1. INTRODUCTION

The atmospheric oxidation of sulfur dioxide (SO_2) to sulfate may take place in the gas phase, the aqueous phase, or heterogeneously on the surface of soot aerosols. The gas-phase oxidation of SO_2 leads to the formation of sulfuric acid which, due to its low vapor pressure, is subsequently transported to the aerosol phase. The aqueous-phase oxidation of SO_2 may take place in either clouds/fog or in aerosols. Recent studies indicate that catalytic oxidation by soot is not a significant pathway for sulfate formation (Hoffmann and Calvert, 1985). In the absence of clouds and fog, sulfate is formed in the gas phase and in aerosols containing an aqueous phase.

The oxidation of SO_2 in the gas phase occurs primarily via its reaction with hydroxyl (OH) radicals (Atkinson and Lloyd, 1984). Major aqueous sulfate formation mechanisms include the reactions of dissolved SO_2 with H_2O_2, O_3, and O_2 (catalyzed by Mn^{2+} and Fe^{3+}) (Jacob and Hoffmann, 1983; Seigneur and Saxena, 1984). The diffusion-limited condensation of gaseous H_2SO_4 leads to the formation of sulfate aerosols that are typically of smaller sizes than sulfate aerosols resulting from aqueous-phase oxidation of SO_2 (Seinfeld and Bassett, 1982; Seigneur and Barnes, 1986). This difference between size distributions of aerosols formed by H_2SO_4 condensation and aqueous-phase oxidation has been used to analyze the relative importance of these mechanisms in the atmosphere (McMurry *et al*., 1981; McMurry and Wilson, 1982, 1983; Hering and Friedlander, 1982). The results of these studies indicate that both gas- and aerosol-phase oxidation pathways are important in the atmosphere and their relative contributions to total sulfate formation are functions of atmospheric conditions. However, these studies did not identify the chemical mechanisms for aqueous-phase sulfate formation. For example, McMurry and Wilson (1983) analyzed ambient aerosol data to study the mechanisms for sulfate formation. They concluded that at higher relative humidities, aqueous-phase oxidation mechanisms contributed significantly to total sulfate but they did not elucidate the aqueous-phase oxidation mechanisms. Middleton *et al*. (1980) theoretically investigated the relative contributions of different pathways to overall sulfate formation. Their calculations suggest that under daytime conditions, the gas-phase formation of H_2SO_4 and its subsequent condensation on aerosols, and aqueous-phase oxidation of SO_2 by H_2O_2 are the principal mechanisms for atmospheric sulfate formation. Middleton *et al*. (1980) also found that sulfate formation at night was dominated by aqueous-phase mechanisms and was generally lower than daytime sulfate formation.

It is evident that the importance of various SO_2 oxidation pathways to aerosol sulfate formation needs to be evaluated because the rates of SO_2 oxidation by these pathways will determine the atmospheric concentrations of sulfate—a species critical to air quality issues such as acid deposition, suspended particulate matter concentrations and acid sulfate concentrations. Furthermore, the relative contributions of these pathways are relevant to visibility impairment because (1) the aerosol size distribution is affected by SO_2 oxidation mechanisms, and (2) light scattering is a strong function of the aerosol size distribution.

---

*Present address: Pacific Gas & Electric Company, Department of Engineering Research, 3400 Crow Canyon Road, San Ramon, CA 94583, U.S.A.

†Present address: Bechtel National, Inc., Environmental Services Department, P.O. Box 3965, San Francisco, CA 94119, U.S.A.

We investigate here the importance of various SO_2 oxidation pathways in clear atmospheres, *i.e.* atmospheres characterized by the absence of clouds and fog. A detailed model is employed to simulate atmospheric sulfate formation. This model provides a more comprehensive treatment of atmospheric gas-phase chemistry, aerosol thermodynamics and aerosol chemistry than the model used by Middleton *et al.* (1980). The conditions selected are typical of regional continental pollution. Section 2 presents an overview of the mathematical model and assumptions used to perform the calculations. Section 3 describes the results of our investigation. Concluding remarks are presented in section 4.

2. TECHNICAL APPROACH

Simulations of the atmospheric oxidation of SO_2 to sulfate were performed with a mathematical model that describes the gas- and aqueous-phase chemistry of SO_2, NO, NO_2, oxidants and reactive hydrocarbons (RHC). This model is described in detail elsewhere (Hudischewskyj and Seigneur, 1986) and only a brief overview is presented here.

The gas-phase chemistry of RHC, NO, NO_2, and oxidants is simulated by means of the Carbon-Bond Mechanism (Killus and Whitten, 1983). The gas-phase oxidation of SO_2 is represented by its reaction with OH radicals. The rate constant for this reaction was taken from Atkinson and Lloyd (1984), with a value of 1500 $\text{ppm}^{-1}\,\text{min}^{-1}$ at 25°C.

The aerosol chemical composition, including the pH of the aqueous phase if present, is calculated by the Model for an Aerosol Reacting System (MARS) (Saxena *et al.*, 1986a). The aqueous-phase oxidation of SO_2 is described by the following reactions:

$$S(IV) + 1/2O_2 \xrightarrow{Mn^{2+},\,Fe^{3+}} S(VI) \text{ (Martin, 1984)}$$

$$S(IV) + H_2O_2 \dashrightarrow S(VI) + H_2O \text{ (McArdle and Hoffmann, 1983)}$$

$$S(IV) + O_3 \dashrightarrow S(VI) + O_2 \text{ (Maahs, 1983).}$$

Although other chemical pathways exist for the aqueous-phase oxidation of SO_2, these three pathways have been shown to be the most important for polluted environments (Jacob and Hoffmann, 1983; Seigneur and Saxena, 1984).

Multicomponent atmospheric aerosols can be highly concentrated, especially at low relative humidities (Saxena and Peterson, 1981). Although MARS is applicable to the entire range of relative humidities and hence ionic strengths, the aqueous-phase chemical kinetic mechanisms have not been tested at high ionic strengths. For instance, Martin (1986, private communication) indicated that the mechanism used for metal-catalyzed oxidation of SO_2 (Martin, 1984) may overpredict sulfate formation at high ionic strengths. The liquid water content of atmospheric aerosols is another source of uncertainty. Because of limited available data (Ho *et al.*, 1980), predictions of MARS and other models cannot be evaluated for liquid water content.

The initial concentrations were selected to be typical of the northeastern United States and are presented in Table 1. Each simulation was for a 3-h period. The base case simulation started at 1030 LST. The relative humidity and the temperature for the base case simulation were 90% and 25°C, respectively. In addition to the base case simulation, sensitivity simulations were performed to investigate the effect of various atmospheric parameters on SO_2 oxidation. The parameters selected for these sensitivity simulations are presented in Table 2.

3. DISCUSSION OF THE RESULTS

The evolution of the sulfate concentration in the base case simulation is presented in Fig. 1. Results

Table 1. Initial concentrations typical of those found in the northeastern United States

Species	Concentration
SO_2	11 ppb
NO_x	5.3 ppb
O_3	48 ppb
HNO_3	1.8 ppb
NH_3	5 ppb
H_2O_2	1 ppb
Sulfate	14 $\mu g\,m^{-3}$
RHC	17 ppb
Fe^{3+}	0.06 $\mu g\,m^{-3}$
Mn^{2+}	0.02 $\mu g\,m^{-3}$

Table 2. Sensitivity simulations

Simulation No.	Parameter changed	Value
1 (Base case)	None	...
2	Time	Night-time
3	Relative humidity	80%
4	Temperature	5°C
5	Trace metal concentrations	$[Mn^{2+}] = 0.10\,\mu g\,m^{-3}$ $[Fe^{3+}] = 1.0\,\mu g\,m^{-3}$

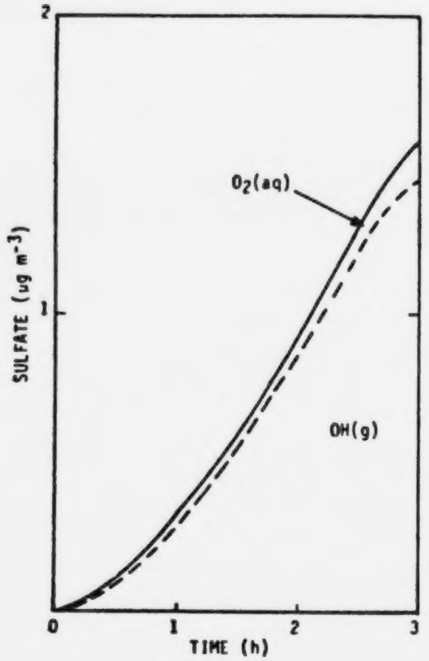

Fig. 1. Sulfate formation in the base-case simulation. (- -) Sulfate formed via OH (g); (——) sulfate formed via OH (g) and via O_2 (aq).

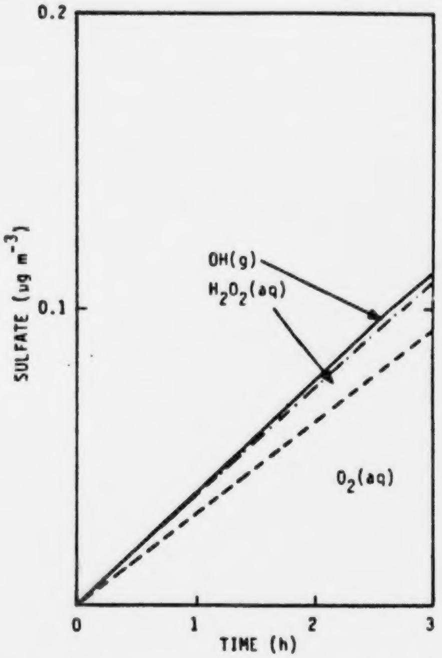

Fig. 2. Sulfate formation in the night-time simulation. (- -) Sulfate formed via O_2 (aq); (— · —) sulfate formed via O_2 (aq) and via H_2O_2 (aq); (——) sulfate formed via O_2 (aq), H_2O_2 (aq) and OH(g).

show that the gas-phase SO_2 oxidation pathway clearly dominates the sulfate formation and accounts for over 90% of the sulfate formed in 3 h. Oxidation of SO_2 by O_2, catalyzed by trace metals, is the only aerosol-phase reaction that contributes appreciably to total sulfate formation.

The results for the night-time simulation are presented in Fig. 2. At night, the OH concentrations are low and the aqueous-phase oxidation of SO_2 by O_2 (catalyzed by Mn^{2+} and Fe^{3+}) and by H_2O_2 account for 82 and 15%, respectively, of the total sulfate formed. Note that the amount of sulfate formed during the night-time simulation is about 10 times smaller than that formed during the daytime simulation. The difference between sulfate formation rates during day and night will depend upon atmospheric conditions such as pollutant concentrations and solar radiation. For example, during the winter, daytime SO_2 oxidation by OH radicals will be significantly slower than during the summer. Therefore, the contribution of aqueous-phase mechanisms to overall sulfate formation will likely be more significant during the winter than during the summer.

Figure 3 presents the results of the daytime simulation with a relative humidity of 80%. As expected, the contribution of the aerosol-phase reactions to sulfate formation decreases as the relative humidity decreases because the amount of liquid water available for aqueous-phase reaction diminishes. This result is consistent with the conclusion of McMurry and

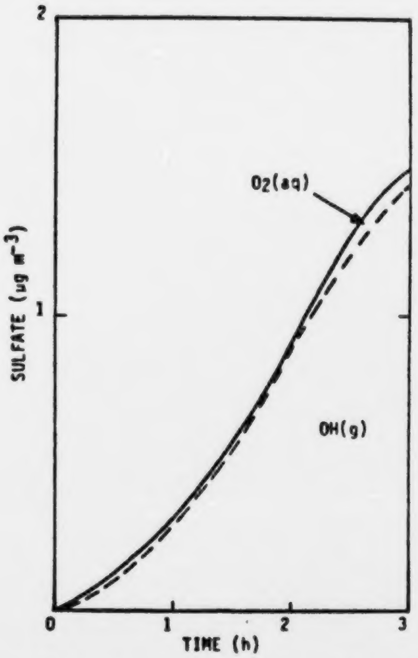

Fig. 3. Sulfate formation in the relative humidity sensitivity simulation. (- -) Sulfate formed via OH(g); (——) sulfate formed via OH(g) and via O_2 (aq).

Wilson (1983), based upon field experiments, that aerosol-phase sulfate formation diminished with decreasing relative humidity. It is interesting to note that the amount of sulfate formed by the $(SO_2 + O_2)$ reaction does not display a diminution which is proportional to the liquid water volume. This can be explained as follows. As the liquid water volume decreases, the pH also decreases and consequently the concentration of dissolved SO_2 decreases. However, the reductions in liquid water volume and dissolved SO_2 concentration are compensated, to some degree, by an increase in the concentrations of trace metals because these concentrations are inversely proportional to the liquid water volume.

The effect of temperature on sulfate formation is evident from the comparison between Fig. 1 (for 25°C) and Fig. 4 (for 5°C). The contribution of the gas-phase reaction decreases with decreasing temperature. This phenomenon results from two different effects: (1) the rate constant for the $(SO_2 + OH)$ reaction increases as the temperature decreases and (2) the OH concentration level decreases as the temperature decreases. The second effect predominates. The reduction in the $(SO_2 + O_2)$ aqueous-phase reaction, when the temperature changes from 25°C to 5°C, is small. This slight change results from a slower kinetic at lower temperature which is partially compensated by an increase in SO_2 solubility. Figure 4 also shows that the $(SO_2 + H_2O_2)$ reaction is very sensitive to temperature and it contributes appreciably to the total sulfate formed at 5°C but not at 25°C. The increase in the solubilities of both SO_2 and H_2O_2, as the temperature decreases, overwhelms the slight decrease in the value of the rate constant.

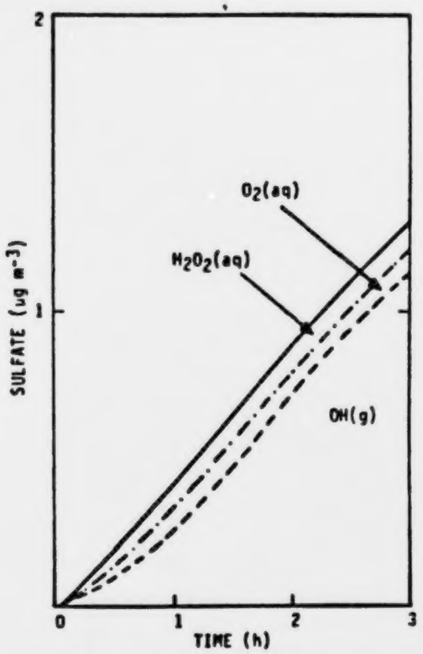

Fig. 4. Sulfate formation in the temperature sensitivity simulation. (-·-) Sulfate formed via OH(g); (— · —) sulfate formed via OH(g) and via O_2(aq); (——) sulfate formed via OH(g), O_2(aq) and H_2O_2(aq).

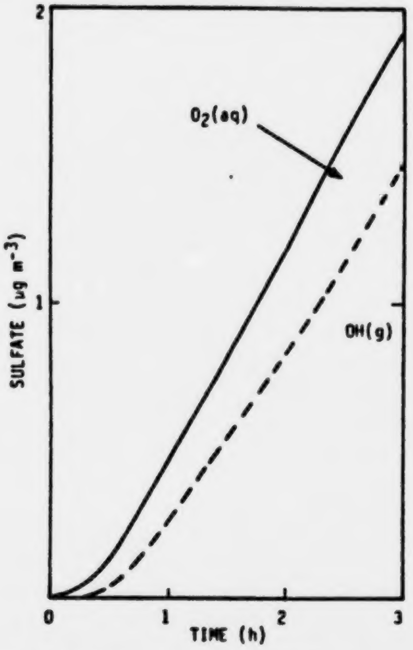

Fig. 5. Sulfate formation in the trace-metal concentrations sensitivity simulation. (- -) Sulfate formed via OH(g); (——) sulfate formed via OH(g) and via O_2(aq).

The effect of changes in trace metal concentrations is presented in Fig. 5. As the manganese and iron concentrations are increased by factors of 5 and 17, respectively, the amount of sulfate formed via the $(SO_2 + O_2)$ aqueous-phase reaction increases from 0.14 to 0.45 $\mu g\ m^{-3}$. It is, therefore, of primary importance to obtain accurate data on ambient concentrations of trace metals, if one wants to assess with reasonable certainty the rate of aqueous oxidation of SO_2 to sulfate in aerosols. This result reinforces the need for data on emissions and ambient concentrations of trace metals (Saxena *et al.*, 1986b).

4. CONCLUSION

The results of our simulations of the atmospheric oxidation of SO_2 to sulfate indicate that, in addition to the gas-phase oxidation by OH, the aqueous-phase oxidation by O_2 and H_2O_2 may contribute significantly to sulfate formation. The conditions selected for simulations were typical of polluted background environments, free of clouds and fog. Furthermore, our simulations indicate that the gas-phase oxidation pathway dominates sulfate formation for summer daytime conditions, whereas at night, atmospheric sulfate production is dominated by aqueous-phase pathways. The contribution of the aqueous-phase reaction of SO_2 with O_2 depends strongly on Fe and Mn concentrations and on the liquid water content of aerosols which, in turn, is dependent on the relative humidity and the background concentrations of sulfate, nitrate and ammonia (Saxena *et al.*, 1986a). The aqueous reaction of SO_2 with H_2O_2 becomes important only at low temperatures when the solubility of these gases is relatively high. The aqueous-phase oxidation of SO_2 by O_3 and other oxidants such as PAN, HNO_2, CH_3COO_2H and CH_3O_2H are not important for aerosols because atmospheric aerosols are generally too acidic for these reactions which become significant only at relatively high pH. Therefore, the study of SO_2 oxidation in polluted background atmospheres needs to include only the gas-phase reaction of SO_2 with OH radicals and the aerosol-phase reactions of SO_2 with O_2 and H_2O_2. Other chemical pathways appear to be insignificant.

The results of our study confirm, qualitatively, the observations made by McMurry and Wilson (1983) in their analysis of ambient aerosol data and suggest that these data can be explained by a few major mechanisms for the oxidation of SO_2 to sulfate. However, some discrepancies also exist between our model predictions and the conclusions reached by McMurry and Wilson (1983). For instance, they showed that liquid-phase reactions tend to dominate aerosol sulfate formation for relative humidities greater than 75% for daytime conditions. In contrast, our model predicts the gas-phase oxidation of SO_2 to be the dominant sulfate production mechanism for all the daytime scenarios we simulated. This discrepancy may be due to the uncertainty in the kinetics of SO_2 oxidation by O_2 and/or an underestimation of the liquid water available for SO_2 oxidation. Our model considers only sulfate, nitrate and ammonium salts; the presence of other hygroscopic salts in the atmosphere would lead to higher liquid water content than predicted by the model. McMurry and Wilson (1983) observed aerosol sulfate formation, by both liquid- and gas- phase mechanisms, only in air parcels exposed to daylight. Although we do predict aerosol sulfate formation at night, it is approximately ten times smaller than during the day and, therefore, the inconsistency between the data and model predictions is not very significant.

No data were acquired in the McMurry and Wilson (1983) study on the ambient concentrations of such species as nitrate, ammonia, H_2O_2 and trace metals which constitute important input parameters for our model. Therefore, it is not possible to perform a quantitative comparison of model predictions and ambient data to determine whether aforementioned discrepancies emanate from uncertainty in model input or from limitations of the model itself. However, such discrepancies emphasize the need for the collection of ambient data for more rigorous and quantitative evaluation of aerosol models and for the enhancement of our understanding of atmospheric aerosol formation.

Acknowledgments—This study was sponsored by the EPA-ASRL Aerosol Research Branch. We would like to thank the Project Officer, Dr H. M. Barnes, for suggesting this study and for his support. We also thank Mr B. M. Lal for his editorial suggestions.

Although the research described in this article was funded wholly by the U.S. Environmental Protection Agency through Contract No. 68-02-4076, it does not necessarily reflect the views of the agency, and no official endorsement should be inferred.

The computer code for the aerosol model used in this study is available from the Project Officer at the U.S. Environmental Protection Agency, Atmospheric Sciences Research Laboratory, Research Triangle Park, North Carolina.

REFERENCES

Atkinson R. and Lloyd A. C. (1984) Evaluation of kinetic and mechanistic data for modeling of photochemical smog. *J. Phys. Chem. Ref. Data* **13**, 315–444.

Hering S. V. and Friedlander S. K. (1982) Origins of aerosol sulfur size distributions in the Los Angeles basin. *Atmospheric Environment* **16**, 2647–2656.

Ho W. W., Hidy G. M. and Govan R. M. (1980) Microwave measurements of the liquid water content of atmospheric aerosols. In *The Character and Origins of Smog Aerosol* (edited by Hidy G. M., Mueller P. K., Grosjean D., Appel B. R. and Wesolowski J. J.). Wiley-Interscience, New York.

Hoffmann M. R. and Calvert J. G. (1985) Chemical transformation modules for Eulerian acid deposition models: Vol. II. The aqueous-phase chemistry. National Center for Atmospheric Research, Boulder, Colorado.

Hudischewskyj A. B. and Seigneur C. (1986) Simulation of the formation of acidic aerosol species in power plant and smelter plumes. In *Proceedings of the 79th Annual Meeting of the Air Pollution Control Association*, 22–27 June, Minneapolis, Minnesota.

Jacob D. J. and Hoffmann M. R. (1983) A dynamic model for the production of H^+, NO_3^-, and SO_4^{2-} in urban fog. *J. geophys. Res.* **88**, 6611–6621.

Killus J. P. and Whitten G. Z. (1983) A new carbon-bond mechanism for air quality simulation modeling. Report No. SYSAPP-81/245, Systems Applications, Inc., San Rafael, California.

Maahs H. G. (1983) Kinetics and mechanism of the oxidation of S(IV) by ozone in aqueous solution with particular reference to SO_2 conversion in nonurban tropospheric clouds. *J. geophys. Res.* **88C**, 10721–10732.

Martin L. R. (1984) Kinetic studies of sulfite oxidation in aqueous solution. In *SO_2, NO, and NO_2 Oxidation Mechanisms: Atmospheric Considerations* (edited by Calvert J. G.). Butterworth, Boston, Massachusetts.

McArdle J. V. and Hoffmann M. R. (1983) Kinetics and mechanism of the oxidation of aquated sulfur dioxide by hydrogen peroxide at low pH. *J. phys. Chem.* **87**, 5425–5429.

McMurry P. H., Rader D. J. and Stith J. L. (1981) Studies of aerosol formation in power plant plumes—I. Growth laws for secondary aerosols in power plant plumes: implications for chemical conversion mechanisms. *Atmospheric Environment* **15**, 2315–2327.

McMurry P. H. and Wilson J. C. (1982) Growth laws for the formation of secondary ambient aerosols: implications for chemical conversion mechanisms. *Atmospheric Environment* **16**, 121–134.

McMurry P. H. and Wilson J. C. (1983) Droplet phase (heterogeneous) and gas phase (homogeneous) contributions to secondary ambient aerosol formation as functions of relative humidity. *J. geophys. Res.* **88C**, 5101–5108.

Middleton P., Kiang C. S. and Mohnen V. A. (1980) Theoretical estimates of the relative importance of various urban sulfate aerosol production mechanisms. *Atmospheric Environment* **14**, 463–472.

Saxena P., Hudischewskyj A. B., Seigneur C. and Seinfeld J. H. (1986a) A comparative study of equilibrium approaches to the chemical characterization of secondary aerosols. *Atmospheric Environment* **20**, 1471–1484.

Saxena P. and Peterson T. W. (1981) Thermodynamics of multicomponent electrolytic aerosols. *J. Colloid Interface Sci.* **79**, 496–510.

Saxena P., Seigneur C. and Pollack A. K. (1986b) A critical assessment of existing data bases for acid deposition modeling studies. *J. Air Pollut. Control Ass.* **36**, 48–54.

Seigneur C. and Barnes H. M. (1986) Technical considerations in regional aerosol modeling. In *Air Pollution Modeling and Its Application*, Vol. 5 (edited by C. de Wispelaere). Plenum Press, New York.

Seigneur C. and Saxena P. (1984) A study of atmospheric acid formation in different environments. *Atmospheric Environment* **18**, 2109–2124.

Seinfeld J. H. and Bassett M. (1982) Effect of the mechanism of gas-to-particle conversion on the evolution of aerosol size distributions. In *Heterogeneous Atmospheric Chemistry* (edited by Schryer D. R.). American Geophysical Union, Washington, D.C.

APPENDIX F

REDUCTION OF THE CARBON-BOND MECHANISM X (CBM-X) USING VARIATIONAL SENSITIVITY ANALYSIS

INTRODUCTION

The CBM-X was developed by Whitten and co-workers (Whitten, Killus, and Johnson, 1985) as an expanded representation of atmospheric chemistry based on the carbon-bond formulation. The carbon-bond treatment of the atmospheric chemistry of reactive hydrocarbons offers several advantages when mixtures of hydrocarbon species are simulated (Whitten et al., 1980). The previous carbon-bond mechanisms typically involved fewer than 100 reactions, whereas the CBM-X includes about 170 reactions and therefore provides a more detailed treatment of hydrocarbon chemistry. The carbon groups of hydrocarbon species that are considered in the CBM-X include carbonyl groups of formaldehyde, higher aldehydes, and ketones, single-bonded (paraffinic) carbons, double-bonded carbon (olefinic) groups, ethylene, toluene, xylenes, and isoprene. Several other organic compounds that result from the oxidation of these carbon groups are also included.

Because the carbon-bond mechanisms are primarily intended to be incorporated into large-scale air quality models such as plume, urban airshed, or regional models, it is imperative to minimize the number of chemical species and reactions involved in the mechanism while maintaining reasonable predictive accuracy. To that end, we developed a reduced version of the CBM-X by eliminating reactions that do not significantly affect the concentration of major pollutants. The relative importance of the reactions was determined by means of a sensitivity analysis of the chemical kinetic mechanism. The results of this analysis were used as the basis for the development of a reduced version of the CBM-X, i.e., the CBM-IV (Whitten and Gery, 1985).

We first present the chemical species and reactions that constitute the CBM-X. We then describe the method of variational sensitivity analysis used to determine the relative importance of reactions in the CBM-X. Next we discuss the results of the application of this method to the reduction of the CBM-X, and last, we describe the CBM-IV that resulted from the CBM-X reduction and from further reduction procedures.

THE CARBON-BOND MECHANISM X

The expanded version of the Carbon-Bond Mechanism (CBM-X) was developed specifically for use in atmospheric models such as EKMA, whereas previous versions of the CBM were designed to be used in complex photochemical dispersion models such as the Systems Applications' urban airshed model (UAM) (Reynolds et al., 1979) or the PARIS model (Seigneur et al., 1983). The size of these earlier versions was limited (i.e., number of reactions and species) to provide computational efficiency, whereas little effort was made to limit the size of the CBM-X since OZIPM-3 computer requirements are typically not extensive.

The expanded Carbon-Bond Mechanism (CBM-X) is actually a hybrid of explicit chemistry, surrogate approximations, and lumped/generalized chemistry designed to simulate the broad features of urban smog chemistry. Explicit chemistry is used to treat the inorganic and carbonyl species plus the chemistries of ethylene, toluene, and xylene. Surrogate approximations are utilized by treating mono-substituted aromatics--such as propylbenzene--as toluene. The carbon-bond lumping method is used primarily for paraffins and olefins.

Each part of the CBM-X chemistry, such as the inorganic subset or the ethylene chemistry, conforms to current literature review studies and has been extensively validated in separate organics/NO_x systems. In addition, the entire CBM-X was used to simulate a new series of auto exhaust and synthetic auto exhaust experiments involving a variety of conditions. Most of the smog chamber experiments used for CBM-X validation were performed in the outdoor dual-chamber facility of the University of North Carolina, which is a well-characterized chamber with extensive analytical capabilities. The CBM-X also successfully simulated multiple-day experiments using a synthetic urban mixture of hydrocarbons performed in the outdoor dual smog chamber at the University of California at Riverside.

The CBM-X mechanism consists of 67 chemical species and 148 chemical reactions (see Table 8). The CBM-X contains 8 primary organic species and their corresponding number of carbon atoms (see Table 9).

TABLE 9. Carbon numbers of carbon-bond groups for primary species.

Carbon-Bond Group	Carbon Number (carbon atoms per molecule)
PAR	1
ETH	2
OLE	2
TOL	7
XYL	8
FORM	1
ALD2	2 (acetaldehyde)
NR	1

The species NR represents the nonreactive part of molecular species such as benzene, ethane, and acetylene.

OVERVIEW OF VARIATIONAL SENSITIVITY ANALYSIS

Sensitivity analysis of a chemical kinetic mechanism provides a rigorous approach to establishing the relative importance of chemical reactions and species involved in the mechanism. Several mathematical approaches can be used to determine the sensitivity of chemical kinetic mechanisms to reaction parameters; however, sensitivity analysis techniques based on variational calculus are considered to be more appropriate to the study of mechanisms that involve a large number of chemical reactions (Seigneur, Stephanopoulos, and Carr, 1982; Carr and Seigneur, 1985). We present in this subsection a brief overview of the variational method of sensitivity analysis.

The mathematical representation of a chemical kinetic mechanism consists of a set of N ordinary differential equations involving M kinetic parameters, where N corresponds to the number of chemical species, and M corresponds to the number of chemical reactions:

$$\frac{dC_i(t)}{dt} = f_i[C(t), k(t)]$$

$$C_i(t = 0) = C_i \qquad i = 1, \ldots, N \qquad (1)$$

where C(t) is the N vector of concentrations and k(t) is the M vector of parameters. Let $C^*(t)$ be the solution of this system. When perturbations are introduced in the rate parameters, the perturbed vector of parameters is defined as follows:

$$^{P}k(t) = [u_1 k_1(t), \ldots, u_m k_m(t)] \tag{2}$$

Equation (1) may be rewritten for the perturbed kinetic system as follows:

$$\frac{dC_i(t)}{dt} = f_i[c(t), {}^{P}k(t)]$$

$$C_i(t = 0) = C_i^0 \qquad i = 1, \ldots, N \tag{3}$$

Let C(t) be the solution to this system.

We define the following objective function as a measure of the perturbation of the chemical kinetic mechanism:

$$J = \frac{1}{t_\delta - t_0} \int_{t_0}^{t_f} \left[\left([NO] - [NO]^* \right)^2 + \left([NO_2] - [NO_2]^* \right)^2 + \left([O_3] - [O_3]^* \right)^2 \right]^{1/2} dt \tag{4}$$

where t_0 and t_f are the initial and final times of the chemical kinetic simulation, respectively. Clearly, the objective function J is 0 when the perturbation parameters are equal to 1, and increases as the perturbation parameters are varied away from 1, i.e., when the kinetic parameters are perturbed away from their original values. We then define the sensitivity coefficient as follows:

$$S_j = \frac{\Delta J}{\Delta u_j} \qquad j = 1, \ldots, M \tag{5}$$

where Δu_j is the normalized perturbation in k_j

$$\Delta u_j = \frac{\Delta k_j}{k_j} = u_j - 1 \qquad j = 1, \ldots, M \tag{6}$$

The sensitivity coefficient S_j is a measure of the sensitivity of the system, represented by the objective function, J, to variations in the reaction rate parameter k_j, represented by the normalized perturbation Δu_j. A reaction with a large value of S_j will have a large effect on the concentrations of NO, NO_2, or O_3 when its rate varies. Conversely, a reaction with a small value of S_j will have little influence on these concentrations.

In the variational method of sensitivity analysis, the sensitivity coefficients S_j are calculated by introducing N adjoint variables $\lambda(t)$, which are governed by a set of N adjoint equations:

$$\frac{d\lambda_i(t)}{dt} = -\frac{\partial H}{\partial C_i}$$

$$\lambda_i(t_f) = 0 \qquad i = 1, \dots, N \tag{7}$$

where H is the Hamiltonian of the system.

$$H = \frac{1}{t_f - t_0}\left[([NO] - [NO]^*)^2 + ([NO_2] - [NO_2]^*)^2 + ([O_3] - [O_3]^*)^2\right]^{1/2} \tag{8}$$

It can be shown that the desired sensitivity coefficients are given by the following equations:

$$S_j = \int_{t_0}^{t_f} \frac{\partial H}{\partial u_j}\, dt \tag{9}$$

A more detailed mathematical description of the variational method is provided by Seigneur, Stephanopoulos, and Carr (1982). The computational implementation of the method is given by Gautier, Carr, and Seigneur (1985).

The results of a sensitivity analysis can be used to evaluate the relative importance of chemical reactions in a chemical kinetic mechanism (Seigneur, 1978). A large value of S_j generally indicates that a reaction is very important in the calculation of chemical concentration, whereas a small value of S_j indicates that this reaction can be omitted from the mechanism without significantly affecting the calculated species concentrations. There are, however, a few exceptions, which are discussed next when we apply the variational method of sensitivity analysis to the reduction of the CBM-X.

REDUCTION OF THE CBM-X BASED ON VARIATIONAL SENSITIVITY ANALYSIS

Oliver Gautier (1984) determined the relative importance of the 170 reactions used by the CBM-X model by analyzing a CBM-X simulation for 11 August 1983 (case UNCR 081183). The results of his analysis were displayed in a computer output that listed the reactions, ranked according to an absolute sensitivity index, ranging from least important to most important.

In our effort to reduce the number of reactions of the CBM-X, we examined the results of Gautier at 600 minutes and 60 minutes of simulation time. The first 30 reactions with nonzero indices at 600 minutes were listed. Each of the 30 reactions listed for the 600-minute case was sequentially checked against the 30 reactions for the 60-minute case. If a reaction appeared in both lists, it was added to a new list (again sequentially) as a possible candidate for omission. When the matching was completed, the new list comprised 15 reactions. Reactions, in blocks of 10, were then sequentially taken from Gautier's output list and added to the 600-minute and 60-minute case lists. As each block of data was added, the reactions previously listed for the 600-minute case were sequentially checked to see if any of them appeared in the new block of data added for the 60-minute case. Next, the 10 reactions added for the 600-minute case were sequentially checked for a match with reactions listed for the 60-minute case list. Each time a match was made, the reaction was added to the list of reactions that were possible candidates for omission. This process was repeated using blocks of 10 reactions until 120 reactions were listed for both the 600-minute and 60-minute cases. This cross-matching of reactions produced a list of 99 reactions that were candidates for omission. Of these, 30 could not be omitted from the mechanism because their low sensitivity index resulted from the fact that their rate was governed by one or more precursor reactions. For example, the reaction of NO with ANO_2 is insensitive to the value of its rate parameter because its rate is determined by the rate of the reaction of AONE with OH:

$$AONE + OH \rightarrow ANO_2 \qquad \text{(Reaction 70)}$$

$$ANO_2 + NO \rightarrow NO_2 + FORM + C_2O_3 \qquad \text{(Reaction 71)}$$

The list of candidates for omission was reduced to 69 reactions.

We performed a base case simulation of the CBM-X chemistry, using all 170 reactions. The time at which the maximum O_3 concentration occurred was noted. The NO_2, NO, and O_3 concentrations at this time (540 minutes) were also noted. We then performed a CBM-X simulation in which the first of the 69 candidate reactions was omitted. The NO_2, NO, and O_3 concentrations at 540 minutes were compared to the base case concentrations. Because the concentrations were within 3 percent of the base case values, the reaction was not reinstated. The second of the 69 reactions was then also omitted, bringing the total number of reactions to 168. Another CBM-X simulation was performed with the remaining 168 reactions. The resultant NO_2, NO, and O_3 concentrations were still within 3 percent of the base case values; thus this reaction continued to be omitted. This process was repeated with all 69 reactions. In 13 cases, the omission of a single reaction caused at least one of the three key concentrations to exceed 3 percent of the base case value. Each time this occurred, the reaction in question was reinstated in the mechanism. Table 8 lists all 170 reactions. Table 10 lists, in order of omission, the 67 omitted reactions. Note that 56 reactions were omitted according to the results of the sensitivity analysis. The other 11 reactions were omitted because the precursor reaction was omitted. It should be noted that this reduction procedure is specific to the simulation for which the sensitivity analysis was carried out. The isoprene chemistry was not considered in the condensation process since isoprene was not input in this simulation.

THE CARBON-BOND MECHANISM IV

The results of the reduction of the CBM-X were used along with other standard procedures to reduce the number of species and reactions involved in a chemical kinetic mechanism. CBM-IV, the reduced version of the CBM-X, includes 27 inorganic and organic chemical species and a total of 70 reactions (see Table 11). The development of the CBM-IV is described by Whitten and Gery (1985).

REFERENCES

Gautier, O. 1984. MS Thesis. University of Minnesota, Minneapolis, Minnesota.

Gautier, O., and R. W. Carr, Jr. 1985. Variational sensitivity analysis of a photochemical smog mechanism. Int. J. Chem. Kinet., 17:1347-1364.

Reynolds, S. D., T. W. Tesche, and L. E. Reid. 1979. "An Introduction to the SAI Airshed Model and Its Usage." Systems Applications, Inc., San Rafael, California (EF78-53R4-EF79-31).

Seigneur, C. 1978. Ph.D. Thesis, University of Minnesota, Minneapolis, Minnesota.

Seigneur, C., G. Stephanopoulous, and R. W. Carr, Jr. 1982. Dynamic sensitivity analysis of chemical reaction systems--a variational method. Chem. Eng. Sci., 37:845-853.

Seigneur, C., T. W. Tesche, P. M. Roth, and M. K. Liu. 1983. On the treatment of point source emissions in urban air quality modeling. Atmos. Environ., 17:1655-1676.

Whitten, G. Z., and M. W. Gery. 1985. "Development of CBM-X Mechanisms for Urban and Regional AQSMs." Systems Applications, Inc., San Rafael, California.

Whitten, G. Z., J. P. Killus, and H. Hogo. 1980. The carbon-bond mechanism--a condensed kinetic mechanism for photochemical smog. Environ. Sci. Technol., 14(6).

Whitten, G. Z., J. P. Killus, and R. G. Johnson. 1985. "Development of a Chemical Kinetic Mechanism for the U.S. EPA Regional Oxidant Model." Systems Applications, Inc., San Rafael, California.

Appendix G

FORMATION OF AEROSOLS IN CLOUDS

INTRODUCTION

As an air parcel is advected into a cloud, the aerosol and gaseous pollutants present in the air partially dissolve in droplets, and aqueous chemical reactions take place. Formation of sulfate in clouds has been shown to occur at significant rates when SO_2 reacts with the oxidants H_2O_2, O_3, and O_2 in the presence of trace metal catalysts. When the air parcel is transported out of the cloud, droplet evaporation leads to the formation of sulfate aerosols consisting of both the sulfate present initially and the sulfate formed in the cloud.

The size distribution of sulfate aerosols formed during oxidation of SO_2 in cloud droplets differs from the size distribution of sulfate aerosols formed through gas-phase oxidation of SO_2. Thus, it is necessary to calculate the formation of sulfate in clouds as well as the aerosol size distribution that remains after the liquid water has evaporated. To that end, we developed a mathematical model that calculates the oxidation of SO_2 to sulfate in a cloud and the aerosol size distribution resulting from cloud droplet evaporation.

We first describe the model formulations for the treatment of cloud chemistry and aerosol dynamics. We then examine the evolution of an aerosol size distribution as the air parcel is transported through a cloud.

CHEMICAL KINETIC MECHANISM

The formation of sulfate in clouds occurs primarily through oxidation of SO_2 by O_3, O_2 (catalyzed by Mn^{2+} and Fe^{3+}), and H_2O_2 (Seigneur and Saxena, 1984; Saxena, Hudischewskyj, and Seigneur, 1986). The relative importance of these oxidation mechanisms varies according to the environmental conditions, i.e., cloud type, pollutant concentrations, season, and time of day. The (SO_2 + O_3) oxidation pathway is important only at pH values above about 4; this condition seems to occur in raining clouds in which pollutant concentrations have been rained out, in remote unpolluted areas, and during the winter, when sulfate and H_2O_2 concentrations are low. The importance of the (SO_2 + O_2) oxidation pathway depends on the availability of the trace metals Fe^{3+} and Mn^{2+}. The (SO_2 + H_2O_2) reaction is considered to be the major oxidation mechanism during the summer, when H_2O_2 conditions are of the order of 1 ppb.

Because the simulation of secondary aerosol formation with the Regional Particulate Model will initially focus on summertime conditions, we selected the (SO_2 + H_2O_2) reaction as the sole pathway for sulfate formation in clouds. A more detailed mechanism of cloud chemistry is being developed by the U.S. EPA and will be included in future studies to provide a more comprehensive treatment of sulfate formation in clouds. In our model, the kinetics of aqueous SO_2 oxidation is as follows:

$$S(IV) + H_2O_2 \rightarrow S(VI) + H_2O$$

$$\frac{d[S(VI)]}{dt} = \frac{7.2 \times 10^7}{1 + 16\,[H^+]}\,[H_2O_2(aq)][SO_2(aq)]\,\exp\left[4430\left(\frac{1}{298} - \frac{1}{T}\right)\right] \quad M\ min^{-1}\ .$$

Because this reaction is very rapid, we can assume that it will be completed during the residence of the air parcel in the cloud. Consequently, we simulate the formation of sulfate in clouds as follows.
If $[SO_2]_0 \geq [H_2O_2]_0$,

$$\Delta[\text{sulfate}] = [H_2O_2]_0 \ , \ \Delta[SO_2] = - [H_2O_2]_0, \ \Delta[H_2O_2] = - [H_2O_2]_0$$

where Δ represents the change in concentration between the times the air parcel leaves the cloud and enters the cloud, and subscript 0 denotes concentrations before the air parcel enters the cloud. If $[SO_2]_0 < [H_2O_2]_0$,

$$\Delta[\text{sulfate}] = [SO_2]_0, \ \Delta[SO_2] = - [SO_2]_0, \ \Delta[H_2O_2] = - [SO_2]_0 \ .$$

This approach reflects the fact that the $(SO_2 + H_2O_2)$ reaction is limited by the minimum concentration of the reactants. If the reaction is oxidant-limited (i.e., $[H_2O_2]_0 < [SO_2]_0$), there is nonlinearity in the SO_2/sulfate relationship (Seigneur, Saxena, and Roth, 1984).

AEROSOL SIZE DISTRIBUTION

The aerosol size distribution that results from the evaporation of cloudwater is calculated as follows.

The size distribution of primary aerosols is identical to the size distribution existing before the air parcel entered the cloud. Sulfate aerosols consist of the sulfate aerosols that were present before the air parcel entered the cloud, and the sulfate that was formed by aqueous oxidation of SO_2 in the cloud. We assume that the initial sulfate aerosols are dissolved in the cloud droplets either through nucleation scavenging or coagulation with cloud droplets. Thus, all sulfate is present in the cloud droplets when the cloud begins to evaporate.

The size distribution selected for the droplets is typical of that of a cumulus cloud (Telford, Keck, and Chai, 1984) and ranges from 8 to 28 μm for a total liquid water content of 0.08 g m^{-3}. The cloud sulfate size distribution is identical since we assume that sulfate concentrations are independent of cloud droplet size. Note that this size distribution is a model input parameter and that another one could be used if desired.

As the water evaporates, all droplets shrink until they reach thermodynamic equilibrium with the ambient relative humidity. The new aerosol size distribution is then calculated for aerosols composed of sulfate, nitrate, ammonium, and water in equilibrium with the ambient gas phase. Calculation of the new aerosol size distribution is performed with the Model of an Aerosol Reacting System--MARS (Saxena et al., 1986), using the cloud droplet size distribution as the initial size distribution.

SIMULATION OF AN AIR PARCEL TRAJECTORY WITH DRY/WET/DRY TRANSITIONS

To demonstrate the major features of this model of intermittent cloud chemistry and gas/aerosol chemistry, we simulated an air parcel trajectory that is initiated in a dry environment, transported through a cloud and back to a dry environment. The simulation is initiated at 0800 LST and continues until 0825 LST. The air parcel enters the cloud at 0805 LST and is transported out of the cloud at 0820 LST. The values of temperature, relative humidity, and liquid water content along the trajectory are listed in Table 6. The initial concentrations are listed in Table 7.

TABLE 6. Temperature, relative humidity, and liquid water content used in the model simulation.

Time (LST)	Temperature (°C)	Relative Humidity (percent)	Liquid Water Content (g·l)
0800	15	90	1.0×10^{-6}
0805	15	90	1.0×10^{-6}
0810	15	90	1.0×10^{-3}
0815	15	90	1.0×10^{-3}
0820	15	90	1.0×10^{-6}
0825	15	90	1.0×10^{-6}

TABLE 7. Initial concentrations.

Species	Concentration
NO_x	7.9×10^{-3} ppm
SO_2	9.3×10^{-3} ppm
O_3	3.5×10^{-2} ppm
H_2O_2	5.0×10^{-4} ppm
PAR	1.11×10^{-2} ppm
OLE	1.9×10^{-4} ppm
ETH	6.5×10^{-4} ppm
ARO	3.2×10^{-4} ppm
CARB	1.5×10^{-3} ppm
NH_3	1.0×10^{-2} ppm
CO	1.0×10^{-1} ppm
CO_2	3.2×10^{2} ppm
HNO_3	0
PAN	2.0×10^{-4} ppm
Sulfate	0.75 $\mu g\ m^{-3}$
Fe^{3+}	0
Mn^{2+}	0
Mg^{2+}	0.155 $\mu g/m^3$
Na^+	0.102 $\mu g/m^3$
Cl^-	0.610 $\mu g/m^3$
QS1	2.03×10^{-3} $\mu g\ m^{-3}$
QS2	1.12×10^{-2} $\mu g\ m^{-3}$
QS3	6.89×10^{-2} $\mu g\ m^{-3}$
QS4	3.95×10^{-1} $\mu g\ m^{-3}$
QS5	1.64×10^{-1} $\mu g\ m^{-3}$
QS6	2.85×10^{-2} $\mu g\ m^{-3}$

Continued

TABLE 7. Concluded.

Species	Concentration
QS7	8.33×10^{-2} μg m^{-3}
QP1	3.00×10^{-3} μg m^{-3}
QP2	1.65×10^{-2} μg m^{-3}
QP3	1.021×10^{-1} μg m^{-3}
QP4	5.86×10^{-1} μg m^{-3}
QP5	5.00×10^{-3} μg m^{-3}
QP6	4.22×10^{-2} μg m^{-3}
QP7	1.237×10^{-1} μg m^{-3}
Q8	1.50 μg m^{-3}
Q9	3.00 μg m^{-3}

Figure 2 presents the simulation results for the chemical composition and size distribution of the aerosol. The initial aerosol size distribution consists only of primary and sulfate aerosols. The initial sulfate concentration is 0.75 $\mu g\ m^{-3}$. After 5 minutes of simulation, the sulfate concentration increases to 0.82 $\mu g\ m^{-3}$ due to gas-phase SO_2 oxidation and subsequent condensation of H_2SO_4. The thermodynamic equilibrium calculations show the formation of an aqueous aerosol with the composition of ammonium sulfate. As the air parcel enters the cloud, gases and aerosols are dissolved, and reaction of SO_2 with H_2O_2 takes place in the cloud droplets. Sulfate is formed, and after 20 minutes of simulation, the sulfate concentration is 18.6 $\mu g\ m^{-3}$. As the cloud evaporates, the sulfate aerosols that are found range in size from 1 to 2 μm. Some nitrate is also present due to dissolution of HNO_3. No major change occurs during the next 5 minutes of simulation, since gas-phase oxidation of SO_2 yields a small amount of sulfuric acid formation.

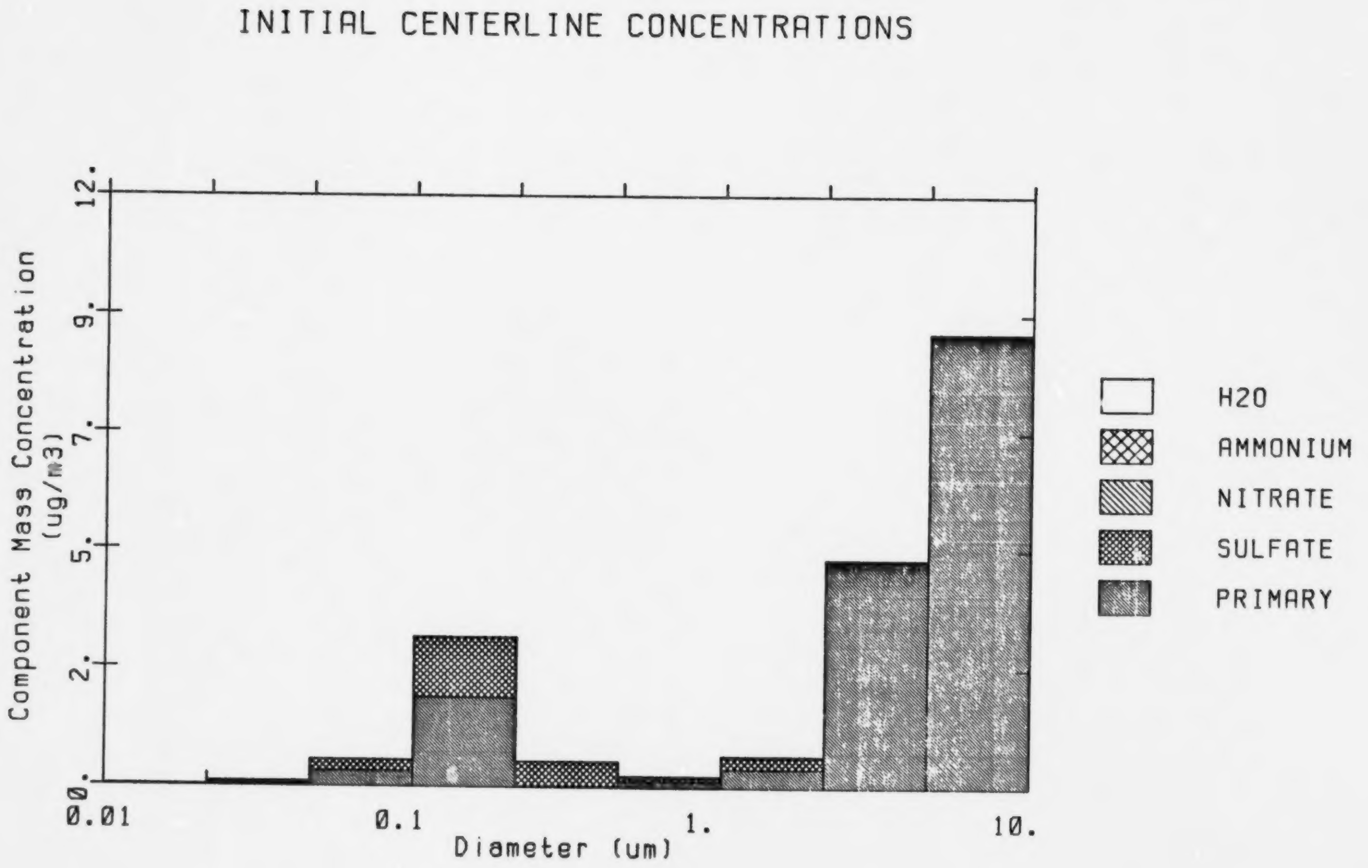

FIGURE 2.Evolution of the chemical composition and size distribution of aerosols transported through a cloud.

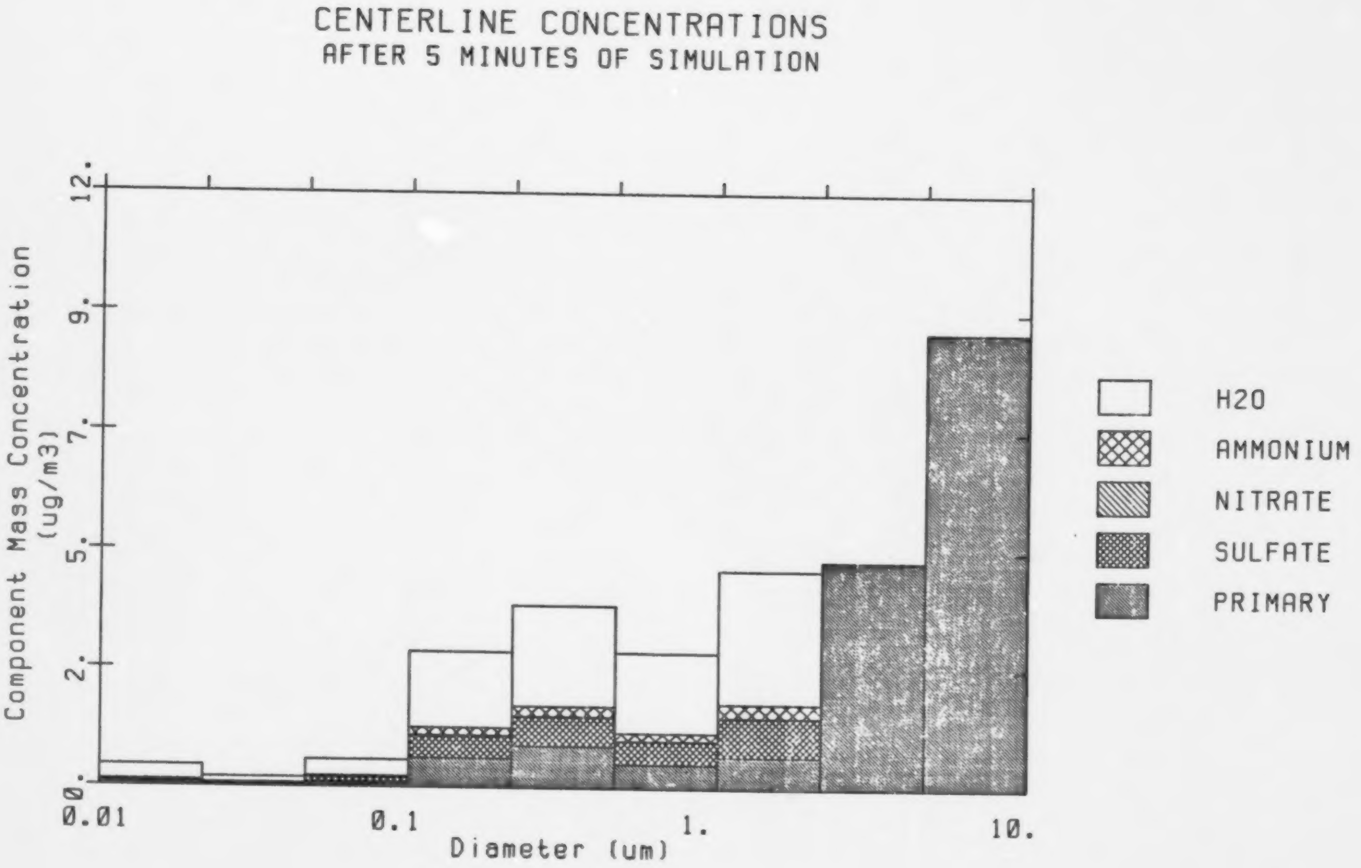

CENTERLINE CONCENTRATIONS
AFTER 5 MINUTES OF SIMULATION

FIGURE 2 Continued.

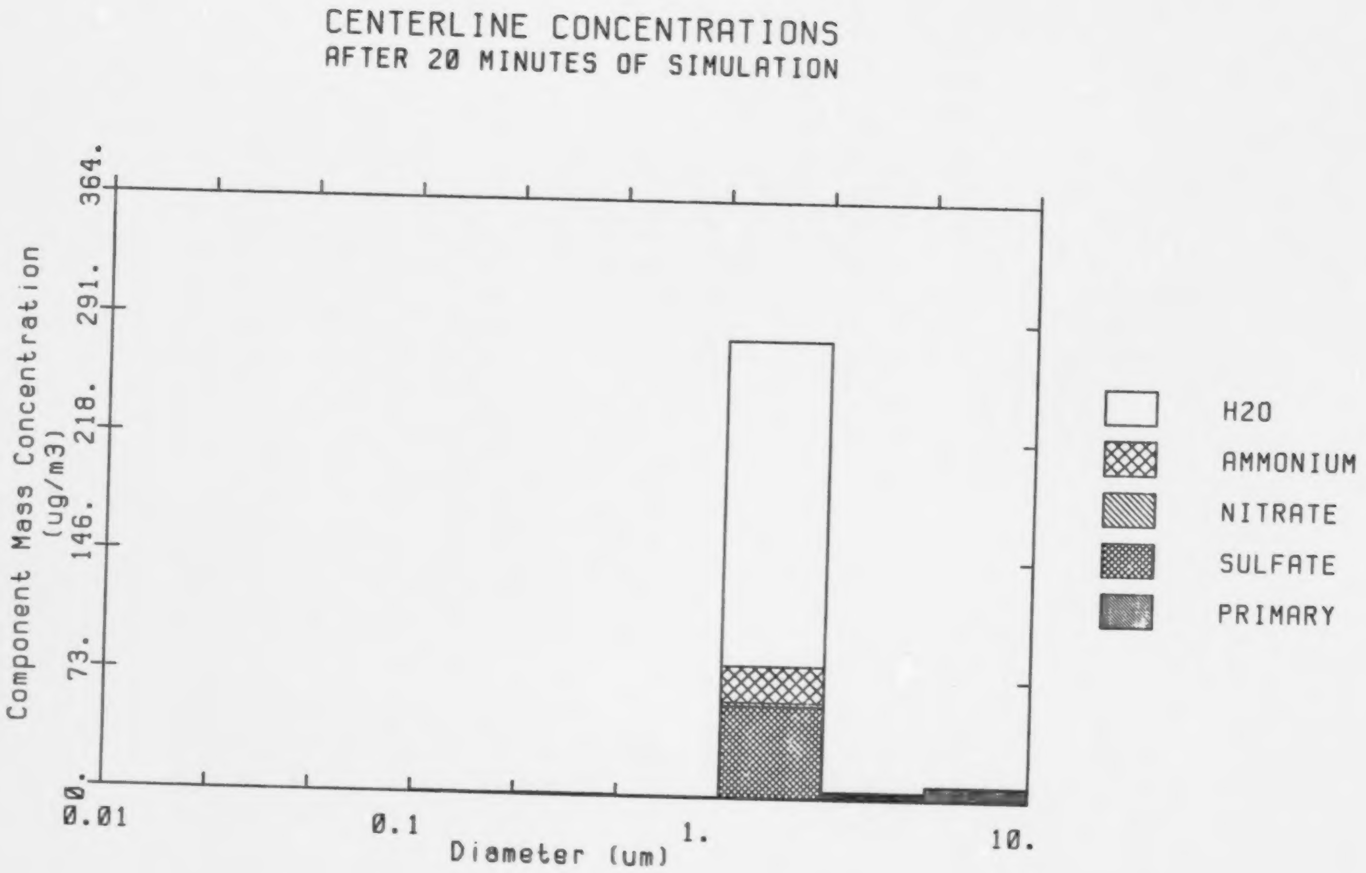

FIGURE 2 Continued.

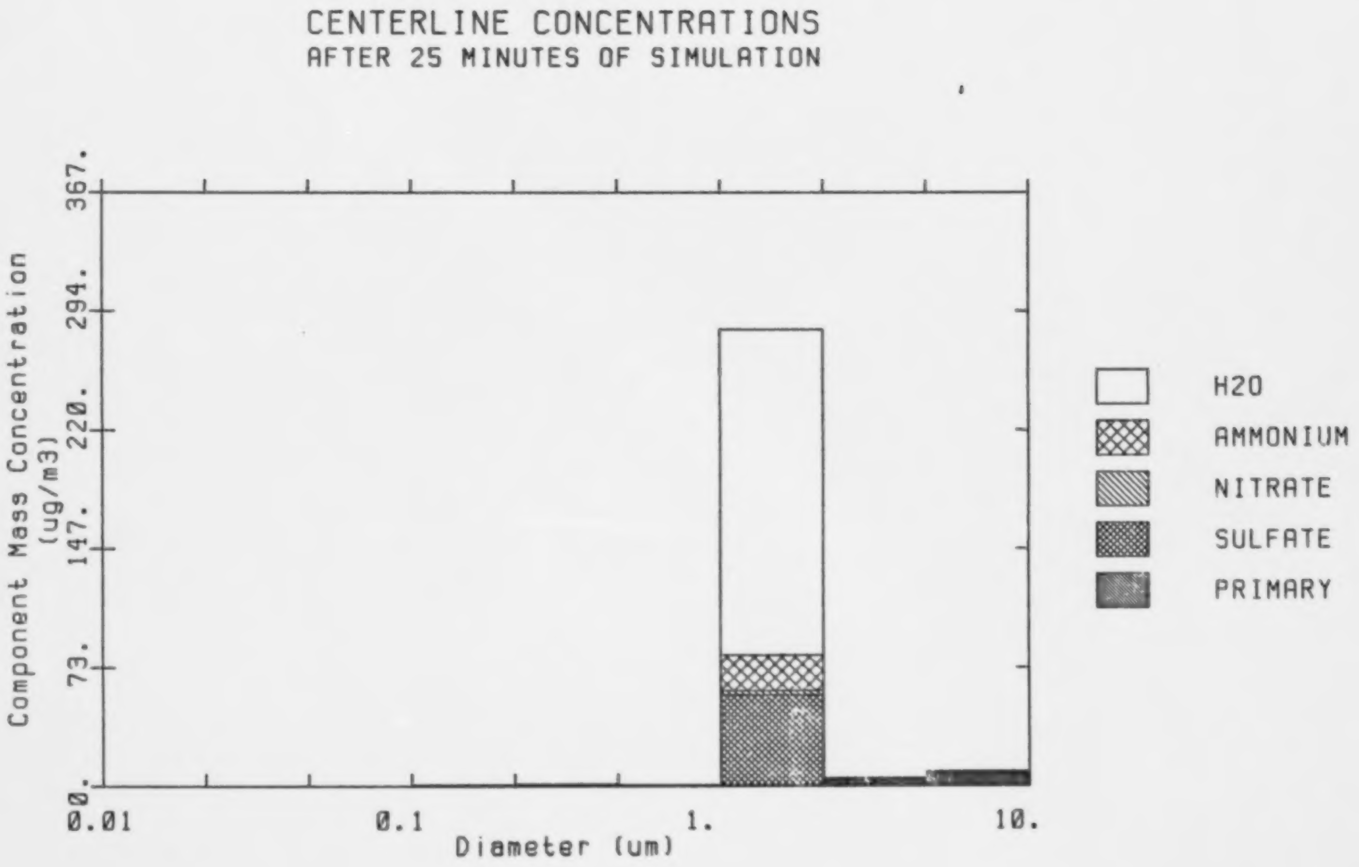

FIGURE 2 Concluded.

REFERENCES

Businger, J. A., and S.P.S. Arya. 1974. Height of the mixed layer in the stably stratified planetary boundary layer. Adv. Geophys., 18A:73-92.

Calvert, J. G. 1976. Hydrocarbon involvement in photochemical smog formation in Los Angeles atmosphere. Environ. Sci. Technol., 10:256-262.

EPRI. 1982. "The Sulfate Regional Experiment: Data Base Inventory and Summary of Major Source File Programs." Electric Power Research Institute, Palo Alto, California (EPRI EA-1904).

Ferman, M. A., N. A. Kelly, and G. T. Wolff. 1985. "Nonurban Hydrocarbons and Their Effect on Ozone and Haze." Environmental Science Department, General Motors, Warren, Michigan (GMR-5040, ENV-211).

Fox, D. L., M. Gery, and H. E. Jeffries. 1984. "Organic Aerosol Formation: OH vs. Ozone Oxidation Pathways." Final Report to Coordinating Research Council, Inc., Atlanta, Georgia.

Franzblau, E., C. S. Burton, and G. M. Hidy. 1984. Aerosol particle formation from ozone-terminal olefin reactions. Aerosol Sci. Technol., 3:167-176.

Gillani, N. V., R. B. Husar, J. D. Husar, D. E. Patterson, and W. E. Wilson. 1978. Project MISTT: Kinetics of particulate sulfur formation in a power plant plume out to 300 km. Atmos. Environ., 12:589-598.

Grosjean, D. 1984a. Photooxidation of 1-heptene. Sci. Total Environ., 37:195-211.

Grosjean, D. 1984b. Atmospheric reactions of ortho-cresol: gas phase and aerosol products. Atmos. Environ., 18:1641-1652.

Grosjean, D. 1985. Reactions of o-cresol and nitrocresol with NO_x in sunlight and with ozone-nitrogen dioxide mixtures in the dark. Environ. Sci. Technol., 19:968-974.

Grosjean, D., and P. H. McMurry. 1982. "Secondary Organic Aerosol Formation: Homogeneous and Heterogeneous Chemical Pathways." Final Report to Coordinating Research Council, Inc., Atlanta, Georgia.

Hatakeyama, S., T. Tanonaka, J. H. Weng, H. Bandow, H. Takagi, and H. Akimoto. 1985. Ozone-cyclohexene reaction in air: quantitative analysis of particulate products and the reaction mechanism. Environ. Sci. Technol., 19:935-942.

Heikes, B. G., A. L. Lazrus, and G. L. Kok. 1985. "Measurements of H_2O_2 in the Lower Troposphere." 17th International Symposium on Free Radicals, Granby, Colorado (18-23 August).

Heisler, S. L., and S. K. Friedlander. 1977. Gas-to-particle conversion in photochemical smog: aerosol growth laws and mechanisms for organics. Atmos. Environ., 11:157-168.

Holzworth, G. C. 1972. "Mixing Heights, Wind Speeds, and Potential for Urban Air Pollution Throughout the Contiguous United States." U.S. Environmental Protection Agency, Research Triangle Park, North Carolina (AP-101).

Hudischewskyj, A. B., and C. Seigneur. 1986. "Simulation of the Formation of Acidic Aerosol Species in Power Plant and Smelter Plumes." 79th Annual Meeting of the Air Pollution Control Association, Minneapolis, Minnesota (22-27 June).

Kamens, R. M., M. W. Gery, H. E. Jeffries, M. Jackson, and E. I. Cole. 1982. Ozone-isoprene reactions: product formation and aerosol potential. Int. J. Chem. Kinet., 14:955-975.

Killus, J. P., and G. Z. Whitten. 1982. "A New Carbon-Bond Mechanism for Air Quality Simulation Modeling." U.S. Environmental Protection Agency, Research Triangle Park, North Carolina (EPA-600/3-82-041).

Kopczynski, S. L., W. A. Lonneman, F. D. Sutterfield, and P. E. Darley. 1972. Photochemistry of atmospheric samples in Los Angeles. Environ. Sci. Technol., 6:342-347.

Lamb, R. G., and D. R. Duran. 1977. Eddy diffusivities derived from a numerical model of the convective boundary layer. Nuov. Cimento, 1C:1-17.

Lindberg, S. E. 1982. Factors influencing trace metal, sulfate, and hydrogen ion concentrations in rain. Atmos. Environ., 16:1701-1709.

McMurry, P. H., and D. Grosjean. 1985. Photochemical formation of organic aerosols: growth laws and mechanisms. Atmos. Environ., 19:1445-1451.

NAS. 1977. Aerosols. In Ozone and Other Photochemical Oxidants. National Academy of Sciences, Washington, D.C., pp. 45-125.

Saxena, P., A. B. Hudischewskyj, and C. Seigneur. 1986. The effect of meteorology on the SO_2/sulfate relationship. In The Meteorology of Acidic Deposition.

Saxena, P., A. B. Hudischewskyj, C. Seigneur, and J. H. Seinfeld. 1986. A comparative study of equilibrium approaches to the chemical characterization of secondary aerosols. Atmos. Environ., 20(7):1478-1483.

Seigneur, C., A. B. Hudischewskyj, J. H. Seinfeld, K. T. Whitby, E. R. Whitby, J. R. Brock, and H. M. Barnes. 1986. Simulation of aerosol dynamics: a comparative review of mathematical models. Aerosol Sci. Technol., 5:205-222.

Seigneur, C., and P. Saxena. 1984. A study of atmospheric acid formation in different environments. Atmos. Environ., 18:2109-2124.

Seigneur, C., P. Saxena, and P. M. Roth. 1984. Computer simulations of the atmospheric chemistry of sulfate and nitrate formation. Science, 225:1028-1030.

Tanner, R. L. 1982. "Temporal and Spatial Variability of Ammonia Concentrations in the Nonurban Troposphere." Second Symposium on the Composition of the Nonurban Troposphere, Williamsburg, Virginia (25-28 May).

Telford, J. W., T. S. Keck, and S. K. Chai. 1984. Entrainment at cloud tops and the droplet spectra. J. Atmos. Sci., 41:3170-3179.

Whitby, K. T. 1978. The physical characteristics of sulfur aerosols. Atmos. Environ., 12:135-159.

Whitby, K. T. 1981. "Aerosol and Ozone Formation in the Columbus, Ohio, Urban Plume on July 29 and 30, 1980: A Preliminary Report." Particle Technology Laboratory, Department of Mechanical Engineering, University of Minnesota, Minneapolis, Minnesota (No. 447).

Whitby, E. R., and K. T. Whitby. 1985a. "The Modal Aerosol Dynamics Model--Part I--Solution of the Internal Terms for the General Dynamics Equation of Aerosols." Department of Mechanical Engineering, University of Minnesota, Minneapolis, Minnesota (Particle Technology Laboratory Publication No. 580).

Whitby, E. R., and K. T. Whitby. 1985b. "AGR01: A Fortran Implementation of the Modal Aerosol Dynamics Model for the IBM PC/XT/AT." Department of Mechanical Engineering, University of Minnesota, Minneapolis, Minnesota (Particle Technology Laboratory Publication No. 581).

Wilson, W. E. 1978. Sulfates in the atmosphere: A progress report on project MISTT. Atmos. Environ., 12:537-547.

Wolff, G. T., N. A. Kelly, M. A. Ferman, and M. L. Morrissey. 1983. Rural measurements of the chemical composition of airborne particles in the eastern United States. J. Geophys. Res., 88C:10769-10775.

Atmospheric Environment Vol 21, No. 4, pp. 943–955, 1987.
Printed in Great Britain.

© 1987 Pergamon Journals Ltd.
NTIS is authorized to reproduce and sell this
report. Permission for further reproduction
must be obtained from the copyright owner.

Appendix H

MATHEMATICAL MODELING OF THE DYNAMICS OF MULTICOMPONENT ATMOSPHERIC AEROSOLS

CHRISTODOULOS PILINIS and JOHN H. SEINFELD*
Department of Chemical Engineering, California Institute of Technology, Pasadena, CA 91125, U.S.A.

and

CHRISTIAN SEIGNEUR†
Systems Applications, Inc., 101 Lucas Valley Road, San Rafael, CA 94903, U.S.A.

(*First received* 12 *May* 1986 *and in final form* 1 *August* 1986)

Abstract—A model is developed to simulate the dynamics of multicomponent atmospheric aerosols, including new particle formation by homogeneous heteromolecular nucleation, gas-to-particle conversion, coagulation and dry deposition. Both equilibrium and non-equilibrium aspects involving sulfate, nitrate and ammonium compounds are considered. The model is used to predict the dynamics of the composition of the aerosol observed on an air trajectory in the Los Angeles basin on 31 August 1982.

Key word index: Aerosols, mathematical model.

INTRODUCTION

Atmospheric aerosols are, in general, multicomponent particles with sizes ranging roughly from 0.01 to 10 μm in diameter. These particles evolve as a result of gas-to-particle conversion and coagulation, are augmented through the formation of fresh particles by nucleation and through the continuous introduction of primary particles, and are removed by wet and dry deposition.

To predict how atmospheric aerosol levels depend on gaseous and particulate source emissions, and specifically how such levels might be expected to vary given changes in primary emissions, requires the development of aerosol air quality models. Whereas the development, evaluation and use of gas-phase air quality models has received considerable attention, there has not been available an air quality model capable of simulating the dynamics of multicomponent atmospheric aerosols that includes new particle formation by nucleation, growth or evaporation due to gas-to-particle or particle-to-gas conversion, and coagulation. The object of the present work is to present the first urban multicomponent aerosol model and to illustrate its application to the Los Angeles basin.

A considerable body of work has preceded the model we will present and it is useful to review that work briefly to provide the context within which the current model lies.

A spatially-uniform, dynamic multicomponent aerosol can be characterized by its size-composition distribution function $n(m,t)$, where $m = (m_1, m_2, \ldots, m_k)^T$, such that $n(m,t)dm$ is the number of particles per volume of gas with mass composition in the range $[m_1, m_1 + dm_1]$, $[m_2, m_2 + dm_2]$, etc. (Specification of the complete chemical composition of a particle in principle specifies the particle's size.) For an aerosol that can be completely characterized by its size, e.g. one comprised of a single chemical component, its size distribution function is just $n(D_p,t)$, where $n(D_p,t)dD_p$ is the number of particles per volume of gas with diameters in the range $[D_p, D_p + dD_p]$. The dynamic behavior of n is governed by the so called general dynamic equation (Gelbard and Seinfeld, 1979; Seinfeld, 1986). The numerical solution of the general dynamic equation serves as the central core of a model simulating the evolution of aerosols. Significant work has been carried out on techniques for the numerical solution of the general dynamic equation, largely devoted to its form for $n(D_p,t)$ (Gelbard and Seinfeld, 1978; Middleton and Brock, 1976; Tsang and Brock, 1983). Recently several of these approaches have been reviewed and compared (Seigneur *et al.*, 1986). Some previous work does exist on the numerical simulation of single-component atmospheric aerosols through solution for $n(D_p,t)$ (Bassett *et al.*, 1981; Eltgroth and Hobbs, 1979; Middleton and Kiang, 1978; Seigneur, 1982; Suck and Brock, 1979; Tsang and Brock, 1982).

An approximate composition of the Los Angeles aerosol is 20% sulfates, 25% nitrates, 10% elemental carbon, 20% organic carbon (primary and secondary), 25% soil, metals and water. The following picture is considered to represent the evolution of such a 'typical' particle. Say that a primary carbonaceous particle is emitted and advected from its source by the wind. In the gas-phase, photochemical reactions are occurring converting NO_x to nitric acid (HNO_3), SO_2 to sulfuric acid (H_2SO_4), and reactive organic gases to low vapor pressure condensable species. Water vapor is ubiquitous, and ammonia (NH_3) may also be present in the gas phase. Gas-to-particle conversion of sulfate, nitrate, ammonium and organics occurs as these gas-phase reactions proceed, with the composition of the aerosol continuously adjusting to maintain equilibrium at the local relative humidity and temperature. At high relative humidity the aerosol consists of an aqueous solution of sulfate, nitrate and ammonium ions, while at low relative humidity the resulting aerosol may be completely dry. In the latter case the solid phase is an external mixture of four simple salts, NH_4HSO_4, $(NH_4)_3H(SO_4)_2$, $(NH_4)_2SO_4$ and NH_4NO_3, as well as two mixed salts, $(NH_4)_2SO_4 \bullet 2NH_4NO_3$ and $(NH_4)_2SO_4 \bullet 3NH_4NO_3$ (Stelson and Seinfeld, 1982c; Harrison and Sturges, 1984). It is this overall process that we seek to simulate.

---

* To whom correspondence should be addressed.

† Present address: Bechtel National, Inc., Environmental Sciences Department, 50 Beale Street, P.O. Box 3965, San Francisco, CA 94119, U.S.A.

We begin with a brief summary of the calculation of aerosol thermodynamic equilibria, followed by a discussion of the simulation of multicomponent aerosol dynamics. The remainder of the paper is devoted to a detailed application of the model developed to simulate the evolution of aerosol along a particular air trajectory in the Los Angeles basin on 31 August 1982.

AEROSOL THERMODYNAMIC EQUILIBRIUM

When the multicomponent nature of the aerosol is considered, one must account for the individual rates of transfer of the various species between the gas and particulate phases. If the sticking coefficient is equal to one then the characteristic time for gas-particle transport for certain species is short enough that chemical equilibrium is established on a time scale much shorter than that over which other changes are taking place. This situation is in fact estimated to be the case for species such as water and ammonium nitrate (Hildelmann et al., 1984; Tanner, 1982; Russell et al., 1983; Russell and Cass, 1984). Consequently, chemical equilibrium can be assumed to be instantaneously established for such species. Considerable effort has been devoted to developing the capability to predict the equilibrium chemical composition and physical state of atmospheric sulfate, nitrate and ammonium aerosols (Bassett and Seinfeld, 1983, 1984; Saxena et al., 1986; Stelson et al., 1979; Stelson and Seinfeld, 1982a, b, c). As noted above, to simulate the evolution of an atmospheric aerosol containing water, sulfates, nitrates and ammonium it will be necessary to merge the thermodynamic equilibrium calculation into the dynamic solution of the multicomponent general dynamic equation.

From the point of view of numerical simulation we can divide the aerosol evolution into a short time step of non-equilibrium gas-to-particle conversion and coagulation, followed by an instantaneous relaxation to equilibrium. Then more gas-to-particle conversion and coagulation occur over the next time step, followed again by adjustment of the particle composition (and size) to equilibrium. Thus the structure of the numerical solution will consist of successive steps of non-equilibrium transport and coagulation followed by the re-establishment of gas and particulate phase chemical equilibrium.

Sulfate is produced in the gas phase by oxidation of SO_2 (Middleton et al., 1980), and it is transferred to the particulate phase by either condensation on already existing particles or nucleation. Because of the relatively low vapor pressure of sulfuric acid, the gas-to-particle conversion process can be assumed to be irreversible. In addition, sulfate may be formed through oxidation of SO_2 on the surface of soot aerosol or in aqueous aerosols.

Volatile compounds, such as NH_3, HNO_3 and water, on the other hand, are distributed between the gas and aerosol phases as determined by thermodynamic equilibrium. The distribution by particle size of non-volatile species, such as sulfate, serves as a 'core' upon which the distribution of volatile species can be determined.

In considering the equilibrium in the sulfate, nitrate, ammonium system the following components are possible (Bassett and Seinfeld, 1983, 1984; Harrison and Sturges, 1984; Saxena et al., 1986):

gas phase NH_3, H_2O, HNO_3

liquid phase NH_4^+, H^+, HSO_4^-, SO_4^{2-}, NO_3^-, H_2O

solid phase NH_4HSO_4, $(NH_4)_3H(SO_4)_2$, $(NH_4)_2SO_4$, NH_4NO_3
$(NH_4)_2SO_4 \bullet 2NH_4NO_3$, $(NH_4)_2SO_4 \bullet 3NH_4NO_3$.

Three methods have been developed to determine the thermodynamic equilibrium in this system and the computer codes that have resulted are summarized in Table 1. The basic idea of each method is, given the sulfate, HNO_3 and NH_3 concentrations, as well as relative humidity and temperature, to determine the equilibrium phases and their composition by minimizing the total Gibbs free energy of the system, i.e.

$$\min_{n_i} G_{\text{total}}$$

subject to

(a) conservation of mass
(b) $n_i \geq 0$ for all i.

Table 1. Computer codes for aerosol sulfate/nitrate/ammonium/water equilibria

	KEQUIL*	EQUIL†	MARS‡
Method used	Minimization of the Gibbs free energy, using conjugate gradient and Newton's methods. Use of homotopy method, to include the Kelvin effect.	Minimization of the Gibbs free energy, using conjugate gradient and Newton's methods.	The domain of feasible solutions is divided into several subdomains. Then the Gibbs free energy is minimized into the specific subdomain that corresponds to the given atmospheric conditions.
Kelvin effect	Included	Not included	Not included
Mixed salts	Included	Included	Not included
Aqueous phase reactions	Not included	Not included	Included
Typical simulation time for an equilibrium calculation‡ (CPU s)	72	10	0.2

* Bassett and Seinfeld (1984). † Bassett and Seinfeld (1983). ‡ Saxena *et al.* (1986).

AEROSOL DYNAMICS

A spatially homogeneous aerosol undergoing nucleation, condensation and coagulation is simulated by numerical solution of the general dynamic equation. A particularly powerful technique for solving the multicomponent general dynamic equation is the so- called sectional method (Gelbard and Seinfeld, 1980; Gelbard *et al.*, 1980; Gelbard, 1984; Warren and Seinfeld, 1985).

The sectional representation of an aerosol distribution approximates the continuous size distribution function with a series of step functions. The particle size may be represented by x, the natural logarithm of the mass of a particle. If one defines $q(x)$ as the continuous aerosol mass distribution function, i.e. $q(x)\mathrm{d}x$ is the mass corresponding to particles with logarithm of mass in the range $[x, x+\mathrm{d}x]$, then the total mass within each section is given by

$$Q^l = \int_{x_l}^{x_{l+1}} q(x)\mathrm{d}x \quad l = 1,2,\ldots \tag{1}$$

where x_l, x_{l+1} are the lower and upper bounds of section l, respectively. One assumes that the mass is uniformly distributed within each section. Thus,

$$\bar{q}_l(x) = \frac{Q^l}{x_{l+1} - x_l} \quad l = 1,2,\ldots \tag{2}$$

The number of particles in each section is linearly related to the total aerosol mass within the section, specifically

$$N^l = Q^l \frac{e^{-x_l} - e^{-x_{l+1}}}{x_{l+1} - x_l}. \tag{3}$$

Thus the sectional general dynamic equation that describes the evolution of the concentration of species i in the l^{th} section, Q_i^l, takes the following form

$$\frac{\partial Q_i^l}{\partial t} = \left[\frac{\partial Q_i^l}{\partial t}\right]_{\text{cond./evap.}} + \left[\frac{\partial Q_i^l}{\partial t}\right]_{\text{coag.}} + \left[\frac{\partial Q_i^l}{\partial t}\right]_{\text{sources/sinks}} \tag{4}$$

where the first term on the right hand side represents growth due to condensation or shrinkage due to evaporation, the second term represents coagulation and the third term represents sources of new particles through nucleation and primary emissions and removal through wet and dry deposition.

Multicomponent condensation/evaporation

The flux of vapor molecules of species i onto an aerosol particle of diameter d_p, F_i in the case that gas-phase diffusion is the rate determining step, can be described by the Fuchs–Sutugin formula (Fuchs and Sutugin, 1971)

$$F_i = 2\pi d_p D_i \frac{(p_i - p_{d_i}) f_0(Kn)}{kT} \tag{5}$$

with

$$f_0(Kn) = \frac{1 + Kn}{1 + 1.71\,Kn + 1.33\,Kn^2} \tag{6}$$

where Kn is the Knudsen number, D_i is the diffusion coefficient of species i in the gas phase and $(p_i - p_{di})$ is the difference between the partial pressure of species i in the bulk phase and that at the particle surface. The rate of change of the mass of species i in particles of diameter d_p due to the flux F_i is

$$\frac{\mathrm{d}M_i}{\mathrm{d}t} = H_i M_{\mathrm{tot}} \tag{7}$$

where

$$H_i = \frac{12 D_i (p_i - p_{di}) f_0(Kn) m_{1i}}{\rho_i d_p^2 kT} \tag{8}$$

and where M_{tot} is the total aerosol mass at time t, ρ_i is the species density as a liquid or a solid, and m_{1i} is the molecular mass of species i. An assumption associated with Equation (7) is that ρ_i remains constant as a function of time.

When the aerosol mass distribution has been represented by sections, the growth rate of the mass of component i in section l,

$$\bar{H}_i^l = \frac{\int_{x_l}^{x_{l+1}} q(x) H_i \,\mathrm{d}x}{\int_{x_l}^{x_{l+1}} q(x)\,\mathrm{d}x} \tag{9}$$

from Equation (2) becomes

$$\bar{H}_i^l = \frac{\int_{x_l}^{x_{l+1}} H_i \,\mathrm{d}x}{x_{l+1} - x_l}. \tag{10}$$

Therefore, $\bar{H}_i^l Q^l$ is the rate of change of the mass of species i on particles in section l. This growth causes some of the largest particles of the section to migrate into the $(l+1)^{\text{th}}$ section while, at the same time, some of the largest particles in the $(l-1)^{\text{th}}$ section grow into section l. Exactly the reverse behavior takes place in the case of evaporation. To account for this phenomenon the intersectional condensation rate, $\bar{T}_i^{l+1}$, is defined, such that $\bar{T}_i^{l+1}\,\mathrm{d}t$ is the mass of species i that goes from section l to section $l+1$ in the time interval $[t, t+\mathrm{d}t]$. As a result the net rate of change of the mass of species i, in section l is given by

$$\left[\frac{\mathrm{d}Q_i^l}{\mathrm{d}t}\right]_{\text{condensation}} = \bar{H}_i^l Q^l - \bar{T}_i^{l+1} + \bar{T}_i^l. \tag{11}$$

Particle number conservation for an aerosol undergoing condensational growth can be used to set the rates of the intersectional condensation (Warren and Seinfeld, 1985). The overall intersectional mass flux from the l^{th} section, defined as $\bar{T}^{l+1} = \Sigma_i \bar{T}_i^{l+1}$, is given by

$$\bar{T}^{l+1} = \frac{\sum_i \bar{H}_i^l Q^l}{1 - e^{-(x_{l+1} - x_l)/2}} \tag{12}$$

in the case of condensation, and

$$\bar{T}^{l+1} = \frac{\sum_i \bar{H}_i^{l+1} Q^{l+1}}{1 - e^{(x_{l+1} - x_l)/2}} \tag{13}$$

in the case of evaporation.

The intersectional condensation rate of species i is proportional to the overall intersectional mass flux and it is also proportional to the mass fraction of species i in the l^{th} and $(l+1)^{\text{th}}$ sections for condensation and evaporation, respectively, i.e.

$$\bar{T}_i^{l+1} = \frac{Q_i^l}{Q^l} \bar{T}^{l+1} \tag{14}$$

for condensation, and

$$\bar{T}_i^{l+1} = \frac{Q_i^{l+1}}{Q^{l+1}} \bar{T}^{l+1} \tag{15}$$

for evaporation. Substitution of (12) and (13) into (14) and (15), respectively, gives

$$\bar{T}_i^{l+1} = \frac{Q_i^l \sum_i \bar{H}_i^l}{1 - e^{-(x_{l+1} - x_l)/2}} \tag{16}$$

for the case of condensation, and

$$\bar{T}_i^{l+1} = \frac{Q_i^{l+1} \sum_i \bar{H}_i^{l+1}}{1 - e^{(x_{l+1} - x_l)/2}} \tag{17}$$

for the case of evaporation.

Note that the largest section must be specified large enough so that no particles can grow out of it. Also, the lower bound of the first section must be larger than the size of the critical nucleus for homogeneous necleation, so that freshly nucleated particles grow into the first section. It is assumed here that the rate of growth of aerosols into the lowest size section is equal to the rate of nucleation of fresh aerosols.

One difficulty that arises when applying the sectional method to atmospheric aerosols is dealing with those species the mass of which in the aerosol phase is thermodynamically controlled. We need to estimate the intersectional coefficients of the nonvolatiles due to condensation or evaporation of the equilibrium species, the volatiles. Let $Q(t)$ be the overall aerosol mass at time t, i.e. $Q(t) = \Sigma_l Q^l(t)$. Then, one can define a time average rate of aerosol change due to condensation or evaporation of the volatiles, $\bar{H}_v$, so that Equation (7) is satisfied, i.e.

$$\frac{\mathrm{d}Q}{\mathrm{d}t} = \bar{H}_v Q \tag{18}$$

subject to $Q(t_0) = Q_0$. Equation (18) gives

$$\bar{H}_v = \frac{1}{\Delta t} \ln\left[\frac{Q(t_0 + \Delta t)}{Q_0}\right] \tag{19}$$

where $Q(t_0 + \Delta t)$ is the sum of the nonvolatile species mass, obtained from the non-equilibrium computation, and the volatile species mass, found from the equilibrium portion of the computation, at time $(t_0 + \Delta t)$.

The distribution of the volatiles between sections depends, in general, on the particle size in each section, because the tendency for molecules to escape a small drop into the vapor phase will depend on the size of the drop. If, though, one neglects the effect of surface curvature on vapor pressure, the Kelvin effect, an assumption reasonable for particles for which $d_p \geqslant 0.01\ \mu m$, the mass of volatiles that condenses in one section is proportional to the mass fraction of the total nonvolatiles in that section. As a result, the intrasectional time average rate of aerosol mass change in the l^{th} section, due to condensation or evaporation of volatile species, is given by

$$\bar{H}^l_v = \frac{1}{\Delta t}\frac{Q^l_{nv}}{Q_{nv}}\ln\left[\frac{Q(t_0+\Delta t)}{Q_0}\right] \quad (20)$$

where Q^l_{nv} is the mass of the nonvolatiles in the l^{th} section, and Q_{nv} is the total nonvolatile mass in the aerosol phase.

Given $\bar{H}^l_v$ Equations (16) and (17) can be used to determine the intersectional rates.

Coagulation

Assuming that only binary collisions occur, the coagulation part of Equation (4) has the form

$$\frac{dQ^l}{dt} = \sum_{n=1}^{l-1} \beta^a_{n,l-1} Q^l Q^n - \sum_{n=1}^{L} \beta^b_{n,l} Q^l Q^n \quad (21)$$

where $\beta^a_{n,l-1}$ and $\beta^b_{n,l}$ are the sectional coagulation coefficients depending on the total masses of the coagulating particles and L is the total number of sections (Gelbard and Seinfeld, 1980; Gelbard *et al.*, 1980; Gelbard, 1984). These coagulation calculations are simplified if a geometric constraint for the sectional boundaries is imposed, namely $x_{l+1} - x_l \geqslant \ln 2$.

Homogeneous heteromolecular nucleation

New particles may form by homogeneous nucleation. In the system we are considering nucleation may be either homomolecular or heteromolecular. The candidates for nucleation are H_2SO_4, HNO_3 and secondary organics formed from the atmospheric conversion of hydrocarbons.

Under atmospheric conditions, H_2SO_4 and HNO_3 heteromolecular nucleation with H_2O occurs at a rate many orders of magnitude above that of homogeneous homomolecular nucleation, because heteromolecular nucleation can take place when a mixture of vapors is undersaturated with respect to the pure vapors, as long as it is supersaturated with respect to the critical solution (Middleton and Kiang, 1978; Mirabel and Katz, 1974; Yue and Hamill, 1979).

Since H_2SO_4–H_2O nucleates at 6–8 orders of magnitude lower concentration than does nitric acid at the same relative humidity, we account only for homogeneous heteromolecular nucleation of sulfuric acid with water here. For the present study we neglect any nucleation that might be occurring involving secondary organics.

The classical rate of binary nucleation of H_2SO_4–H_2O when the vapor number concentration of water is much larger than that of sulfuric acid is given by (Middleton and Kiang, 1978; Mirabel and Katz, 1974; Yue and Hamill, 1979)

$$J = 4\pi r^{*2}\frac{p_{H_2SO_4}}{(2\pi m_{H_2SO_4} kT)^{1/2}}\exp\left[-\frac{\Delta G^*}{kT}\right] \quad (22)$$

where r^* and ΔG^* are the critical cluster radius and free energy, respectively, and where $p_{H_2SO_4}$ and $m_{H_2SO_4}$ are the partial pressure and molecule mass of sulfuric acid, respectively.

To calculate J from Equation (22) one needs to know the quantities ΔG^* and r^*. The free energy of formation of a cluster containing n_1 and n_2 molecules of H_2SO_4 and H_2O, respectively, is given by

$$\Delta G = n_1(\mu_{1l} - \mu_{1g}) + n_2(\mu_{2l} - \mu_{2g}) + 4\pi r^2 \gamma \quad (23)$$

where μ_{1l}, μ_{2l}, μ_{1g}, μ_{2g} are the chemical potentials of the two components in the liquid and gas phase, respectively, for a macroscopic amount of liquid, and γ is the surface tension.

To find the Gibbs free energy, the radius and the composition of the critical cluster one has to solve Equation (23) together with the saddle point conditions (Middleton and Kiang, 1978; Mirabel and Katz, 1974; Yue and Hamill, 1979).

$$\left.\frac{\partial \Delta G}{\partial n_1}\right)_{n_2} = \mu_{1l} - \mu_{1g} + \frac{2\gamma V_1}{r^*} - \left.\frac{3X^*V}{r^*}\frac{d\gamma}{dX}\right)_{X=X^*} = 0 \quad (24)$$

$$\left.\frac{\partial \Delta G}{\partial n_2}\right)_{n_1} = \mu_{2l} - \mu_{2g} + \frac{2\gamma V_2}{r^*} + \left.\frac{3(1-X^*)V}{r^*}\frac{d\gamma}{dX}\right)_{X=X^*} = 0 \quad (25)$$

$$X = \frac{n_2}{n_1+n_2} \quad (26)$$

$$\tfrac{4}{3}\pi r^{*3} = (n_1^* + n_2^*)V, \quad (27)$$

where V_1 and V_2 are the partial molar volumes, and V is the molar volume of the binary solution, at critical composition.

The location of the saddle point is obtained by solving the system of Equations (23)–(27) numerically, using Newton's method. Since in the atmosphere the gas densities of sulfuric acid and water are very low, the ideal gas law can be used to obtain the terms $\mu_{ig}-\mu_{il}$ appearing in Equations (24) and (25). Molar volumes have been calculated from the data on density and composition given in Perry (Perry and Chilton, 1973). Calculated values were then fitted by a fifth degree polynomial. Partial molar volumes were determined by calculating the intercepts of the tangent to the polynomial with the axes. Vapor pressure data for aqueous sulfuric acid have been taken from the work of Gmitro and Vermeulen (1964) and were fitted with a logarithmic function. Surface tensions for the mixture of sulfuric acid and water were obtained from the data of Sabinina and Terpugow (1935) and have been fitted by a fifth degree polynomial.

TRAJECTORY AEROSOL MODEL

A form commonly used for air quality models is the Lagrangian trajectory model used to simulate the changes occurring in a hypothetical air parcel advected by the mean wind field (Liu and Seinfeld, 1975; Tilden and Seinfeld, 1982). The model is particularly useful in providing a means to examine the sensitivity of air quality to changes in key variables without incurring the computational requirements of a three-dimensional grid model. As applied to the aerosol model, the governing equations for Q_i^l are

$$\frac{\partial Q_i^l}{\partial t} = \frac{\partial}{\partial z}\left(K_{zz}\frac{\partial Q_i^l}{\partial z}\right) + \left[\frac{\partial Q_i^l}{\partial t}\right]_{\text{growth/shrinkage}} + \left[\frac{\partial Q_i^l}{\partial t}\right]_{\text{coagulation}} - \left[\frac{\partial Q_i^l}{\partial t}\right]_{\text{deposition}} + S_i^l(x, y, z, t) \tag{28}$$

with initial conditions

$$Q_i^l(x, y, z, 0) = Q_{i0}^l(x, y, z) \tag{29}$$

and boundary conditions

$$K_{zz}\frac{\partial Q_i^l}{\partial z} = 0 \quad \text{for } z = H \tag{30}$$

$$E_i^l + K_{zz}\frac{\partial Q_i^l}{\partial z} - v_{gi}Q_i^l = 0 \quad \text{for } z = 0 \tag{31}$$

where $K_{zz}(z)$ is the eddy vertical diffusion coefficient, H is the height of the vertical column, E_i^l is the emission flux per unit area of species i in the l^{th} section, v_{gi} is the deposition velocity, and $S_i^l(x, y, z, t)$ is the rate of increase of species i in the l^{th} section due to nucleation or direct injection of aerosol into the atmosphere.

Given the emission inventory, meteorological conditions and concentrations of all the gaseous pollutants at time t, the trajectory model calculates the concentrations of the various gases at time $t + \Delta t$, as well as the evolution of Q_i^l in the aerosol phase due to eddy diffusion and deposition. Then the non-equilibrium portion of the aerosol model is used to update the sulfate distribution in the aerosol phase through the condensation, coagulation and nucleation portions of the general dynamic equation. Subsequently the equilibrium solution is used to calculate the total aerosol mass and chemical composition, as well as to update the size distribution of the aerosol, by calculating the intersectional movement of particles, due to re-establishment of the equilibrium of the volatile species. The resulting aerosol size and chemical composition distribution at time $t + \Delta t$ is used as input for the subsequent step.

The initial size and chemical composition distribution of the aerosol is required. Since the rates of generation of various condensable organics are not yet well established, we neglect here the organic contribution to gas-to-particle conversion, although the model has the ability to include organics as data become available. For convenience the initial sulfate distribution is assumed to be log-normal. At the prevailing gas-phase conditions at the beginning of the trajectory the volatiles are assumed to be distributed between the gaseous and the aerosol phase so that equilibrium is achieved.

A compromise between reasonable accuracy and computational cost is obtained by assuming that the aerosol size distribution is described by nine sections in the range between 0.01 and 20 μm, while the air parcel is divided into ten equally spaced vertical grids.

The vertical diffusion coefficient depends on atmospheric stability and height. The gas-phase chemical kinetics are simulated using the reaction mechanism presented by Russell *et al.* (1983). Dry deposition of aerosols is calculated on the basis of a single, size-independent deposition velocity v_g (Russell *et al.*, 1983). Nitrate aerosol results from the formation of nitric acid vapor by a variety of paths, including reaction of NO_2 with OH radical. Formation of sulfuric acid takes place through the gas-phase oxidation of SO_2:

$$SO_2 + OH \xrightarrow{H_2O, O_2} H_2SO_4 + HO_2.$$

Oxidation of SO_2 in the aerosol phase by catalytic reactions with O_2 and H_2O_2 is not considered here, but could easily be included in the model formulation.

MODEL APPLICATION

We will compute the formation of aerosol along an air trajectory in the Los Angeles basin on 31 August 1982 that started at about 1300 (PST) at Anaheim and arrived at Rubidoux between 1700 and 1800 (Fig. 1). For the simulation of the thermodynamic equilibrium between the particulate and gas phases the Kelvin

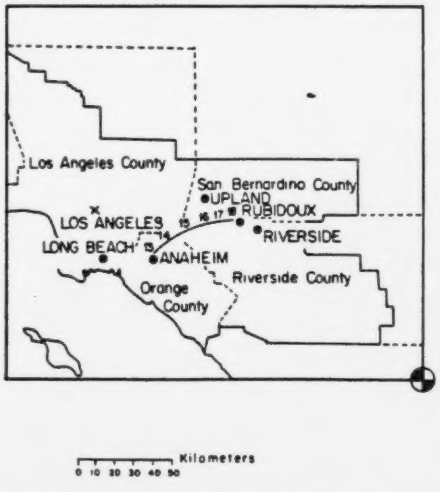

Fig. 1. Trajectory of the air mass that started on 31 August 1982 at 1300 (PST) at Anaheim, CA and arrived at Rubidoux, CA at about 1800.

effect has been neglected. The EQUIL model will be used for the base case calculation. A simulation will also be performed with the MARS model to compare the relative prediction accuracy and computational cost of these two thermodynamic submodels.

Gas and aerosol phase monitoring data are available at these locations against which to compare the predictions of our model. Emission rates, relative humidity, temperature, mixing depth and wind speed data are available for 31 August 1982 (Hildelmann *et al.*, 1984). Temperature was in the range 25–31°C, while relative humidity varied from 30 to 40%. Figure 2 shows the initial size composition distribution determined on the basis of chemical equilibrium at Anaheim at 1300.

The measured and predicted concentrations at Rubidoux are given in Table 2. The predicted NO_2 concentrations have been corrected to include the other nitrogen containing species that interfere with the NO_2 measurement (Winer *et al.*, 1974). The resulting NO_2 prediction is slightly lower than the measured concentrations at Rubidoux. The predicted concentration for O_3 matches the observed value, while NH_3 matches the measured values at Rubidoux within the measurement uncertainties. Comparison of the predicted and observed sulfate, nitrate and ammonium concentrations at Rubidoux indicates that we have adequately represented the formation of those aerosol species along the trajectory.

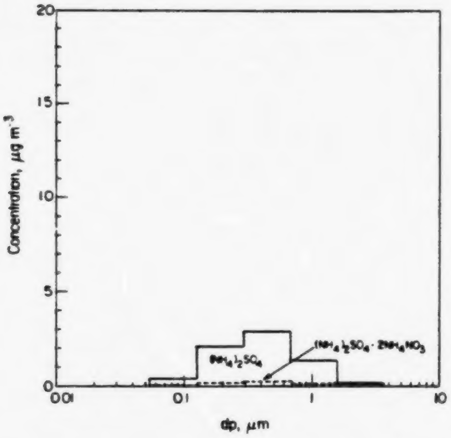

Fig. 2. Predicted aerosol size–composition distribution at Anaheim, CA at 1300 h on 31 August 1982. The aerosol mass is an external mixture of $(NH_4)_2SO_4 \bullet 2NH_4NO_3$ and $(NH_4)_2SO_4$. The mass below the solid line indicates the total amount of aerosol, and the incremental components of that total are indicated.

Table 2. Measured and predicted gaseous and particulate concentrations at Rubidoux, CA at 1700–1800 h on 31 August 1982

Species	Concentration	
	Measured	Predicted
NO_3^- (μg m^{-3})	14.2–29.8	24.9
NH_4^+ (μg m^{-3})	11.2–14.7	9.6
SO_4^{2-} (μg m^{-3})	4.3–16.9	6.5
O_3 (ppb)	130.0	125.0
NO_2 (ppb)	50.0	31.0
SO_2 (ppb)	10	7.1
HNO_3 (ppb)	1.8–5.3	1.0
NH_3 (ppb)	59.8–89.0	58.0

The evolution of the total sulfate–nitrate–ammonium concentrations along the trajectory is presented in Fig. 3. The first few hours, due to the substantial quantity of OH radical in the atmosphere, SO_2 is predicted to react relatively rapidly to produce sulfuric acid in the gas phase, which then transfers to the aerosol phase. Thus, the sulfate aerosol mass keeps increasing until it reaches a maximum of about 7 μg m^{-3} at about 1600, between Anaheim and Rubidoux. Late in the afternoon, the reduction in the photochemical activity causes a decrease in the OH radical concentration, resulting in a reduction of the production rate of sulfuric acid in the gas-phase. Hence turbulent diffusion and deposition predominate and the sulfate aerosol concentration declines smoothly to about 6.5 μg m^{-3} at Rubidoux.

As shown in Table 5, condensation of sulfuric acid is the predominant source of sulfate mass increase in the aerosol phase, while dry deposition and eddy diffusion to the upper layers are the major removal mechanisms for aerosol sulfates. Since the ambient relative humidity on 31 August, 1982 was very low, about 40%, the rate of particle formation, due to binary nucleation is negligible and no new particles are predicted to be produced.

The predicted aerosol nitrate has its minimum at about 1330, near Anaheim. At that time the ambient temperature reaches its maximum of about 31°C. Such high temperature does not favor the formation of aerosol ammonium nitrate, and most of the nitrate exists in the gas-phase as HNO_3.

Later in the afternoon, near Rubidoux, the substantial increase in the ammonia concentration, due to production near Riverside, combined with a decrease of the ambient temperature to about 25°C, cause NH_3 and HNO_3 to condense as ammonium nitrate. Thus, both the ammonium and nitrate concentrations increase sharply and reach their maxima at about 1800, near Rubidoux.

Effect of thermodynamic submodel

In Table 1 we indicated that two size-independent thermodynamic submodels are available, EQUIL and MARS. Figure 3 shows the aerosol sulfate, nitrate and ammonium concentrations calculated by using both these submodels. Since the sulfate concentration is controlled by gas-phase reaction and gas-to-particle diffusion, the sulfate prediction is unaffected by the choice of thermodynamic model.

The nitrate predictions differ between the two thermodynamic submodels. The curve corresponding to MARS shows lower nitrate concentrations

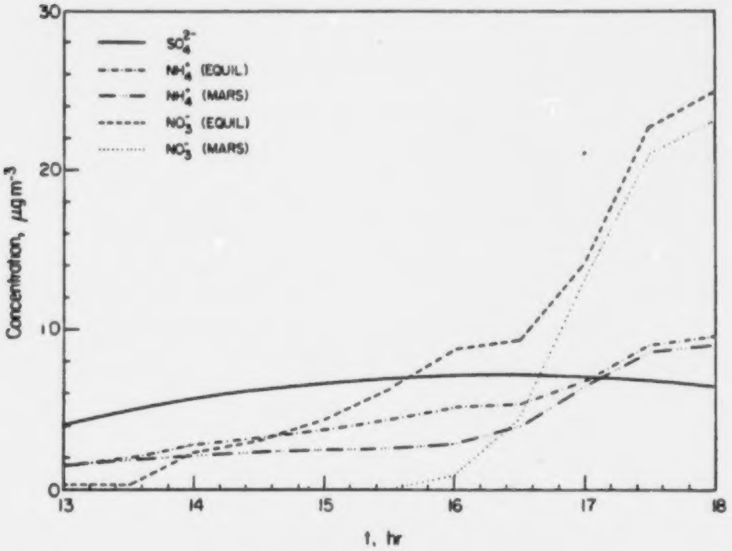

Fig. 3. Predicted evolution of total aerosol nitrate, ammonium and sulfate along the trajectory from Anaheim to Rubidoux, CA from 1300 to 1800 h on 31 August 1982. Predictions are shown for the two thermodynamic models, EQUIL and MARS (Table 1).

along the course of the trajectory until close to Rubidoux. The reason for this difference is that EQUIL takes into account the existence of two mixed salts, $(NH_4)_2SO_4 \bullet 2NH_4NO_3$ and $(NH_4)_2SO_4 \bullet 3NH_4NO_3$, whereas MARS does not. As a result, at low relative humidities, whenever NH_3 is in high enough concentration to form $(NH_4)_2SO_4$, but not so abundant to form pure solid NH_4NO_3, MARS predicts that no nitrates should be present in the aerosol phase. On the other hand, under the same conditions EQUIL predicts that nitrates exist in the solid phase in the form of mixed salts.

Near Rubidoux, due to the large production of NH_3 in the E portion of the Los Angeles basin, the ammonium nitrate solid phase becomes thermodynamically favored. As a result, MARS predicts fairly well the existence of nitrates in the aerosol phase. EQUIL also predicts accurately the nitrate concentration over Rubidoux, showing, as presented in Fig. 4, that most of the nitrate is in the form of $(NH_4)_2SO_4 \bullet 3NH_4NO_3$.

Computationally the program that uses MARS is considerably faster than the one using EQUIL. For the specific trajectory examined here, the first one consumed 3 h of CPU time, while the second one 4.5 h of CPU time, on a VAX 11/780. Therefore MARS, even though less accurate than EQUIL, might be preferred in an Eulerian regional air quality model, where computational efficiency is of paramount importance.

ANALYSIS OF MODEL SENSITIVITY

We now focus on an analysis of parameters that affect the aerosol chemical composition and size distribution. This sensitivity analysis was conducted using the EQUIL submodel. The parameters studied are NH_3 initial conditions and emissions, ambient temperature and relative humidity, together with initial aerosol and SO_2 concentrations. Table 3 summarizes the sensitivity tests we will present with the changes of the various parameters from their base case values, while Table 4 presents the results of the sensitivity runs for major species and aerosol concentrations, at Rubidoux.

The first sensitivity test examines the effect of the ammonia concentration on the formation of aerosols.

Table 3. Parameters varied in sensitivity study

Sensitivity study	Parameter	Variation
1	NH_3 initial conc. and emissions	50% decrease
2	Temperature	3°C increase
3	Relative humidity	increase to 95%
	SO_2 initial concentration	factor of 10 increase
	Initial sulfate concentration	factor of 10^3 decrease

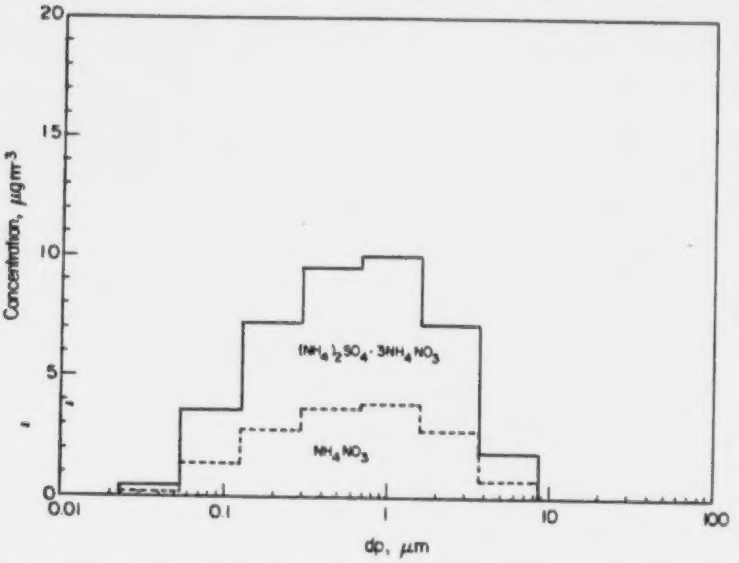

Fig. 4. Predicted size–composition distribution at Rubidoux, CA at 1800 h on 31 August 1982. The aerosol mass is an external mixture of $(NH_4)_2SO_4 \bullet 3NH_4NO_3$ and NH_4NO_3. The mass below the solid line indicates the total amount of aerosol, and the incremental components of that total are indicated.

Table 4. Predicted gaseous and particulate concentrations at Rubidoux, CA for the sensitivity studies

	Base case	Test 1	Test 2	Test 3
SO_4^{2-} ($\mu g\ m^{-3}$)	6.5	6.5	6.6	20.7
NO_3^- ($\mu g\ m^{-3}$)	24.9	17.6	20.0	30.8
NH_4^+ ($\mu g\ m^{-3}$)	9.6	7.4	8.2	16.5
H_2O ($\mu g\ m^{-3}$)	0.0	0.0	0.0	400.0
Total mass ($\mu g\ m^{-3}$)	41.0	31.5	34.8	468.0
SO_2 (ppb)	7.1	7.0	7.0	42.0
HNO_3 (ppb)	1.0	2.1	1.8	0.04
NH_3 (ppb)	58.0	25.0	60.0	43.8

In this test both the initial ammonia concentration and the ammonia emissions along the course of the trajectory were reduced by 50%. The resulting size–composition distribution at Rubidoux is shown in Fig. 5. As expected, the sulfate concentration remains unaffected. An interesting point is that the pure ammonium nitrate phase decreases more than 50%, causing an overall 30% reduction of the nitrate mass and a 23% reduction in the ammonium mass, while the ammonium nitrate, that is contained in the mixed salt, remains, practically, unaffected.

The second sensitivity test was designed to examine the influence of temperature on the aerosol formation and chemical composition. The ambient temperature was increased by 3°C. The resulting size–composition distribution at Rubidoux is shown in Fig. 6. The sulfate mass in the aerosol phase is not seriously affected (only 1.5% increase from the base case). The pure ammonium nitrate phase decreases more than 50% as the result of the increase in temperature, due to the strong temperature dependence of the ammonium nitrate dissociation constant.

In these two sensitivity tests condensational growth is the only route of gas-to-particle conversion (Table 5). The last sensitivity test was designed to investigate conditions under which nucleation is a pathway for gas-to-particle conversion, thus we selected a high humidity situation with the initial concentration of pre-existing aerosol very low. The initial sulfate concentration was reduced to 0.004 $\mu g\ m^{-3}$, while the

Table 5. Contribution of nucleation, condensation, and loss by deposition to final sulfate concentration ($\mu g\ m^{-3}$)

		Sensitivity study		
	Base case	1	2	3
Initial	4.0	4.0	4.0	0.004
Nucleation	0.0	0.0	0.0	0.023
Condensation	4.85	4.85	4.96	29.06
Loss by deposition	−2.35	−2.35	−2.36	−8.38
Final	6.50	6.50	6.60	20.71

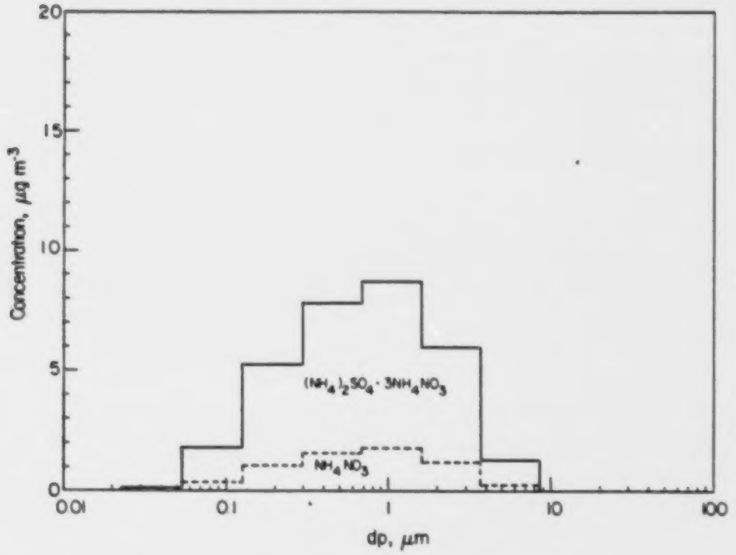

Fig. 5. Predicted size-composition distribution at Rubidoux, CA at 1800 h on 31 August 1982. Conditions changed according to Test 1 in Table 3, namely 50% decrease in initial concentration and emission level of NH_3 from those of the base case, Fig. 4. The aerosol mass is an external mixture of $(NH_4)_2SO_4 \bullet 3NH_4NO_3$ and NH_4NO_3. The mass below the solid line indicates the total amount of aerosol, and the incremental components of that total are indicated.

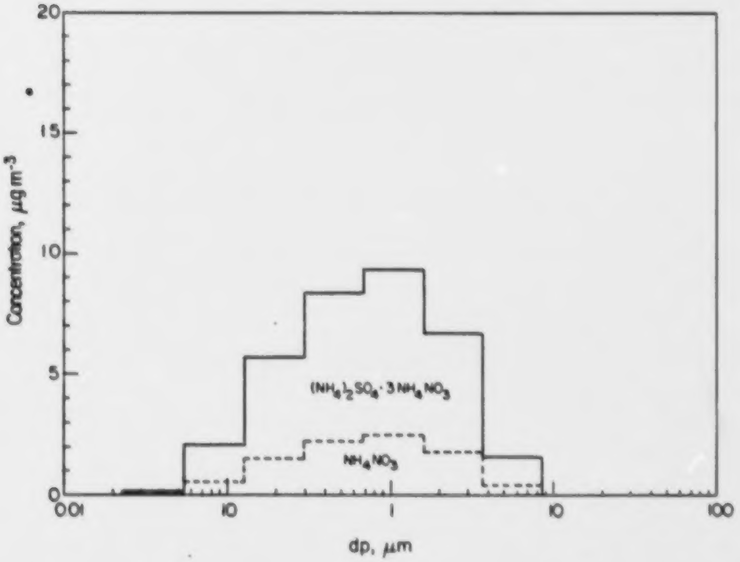

Fig. 6. Predicted size-composition distribution at Rubidoux, CA at 1800 h on 31 August 1982. Conditions changed according to Test 2 in Table 3, namely 3°C increase in temperature from that of the base case, Fig. 4. The aerosol mass is an external mixture of $(NH_4)_2SO_4 \bullet 3NH_4NO_3$ and NH_4NO_3. The mass below the solid line indicates the total amount of aerosol, and the incremental components of that total are indicated.

SO_2 concentration was increased by a factor of ten and the relative humidity maintained at 95%.

The resulting size–composition distribution at Rubidoux is presented in Fig. 7. It is clear that the physical state of the resulting aerosol is completely different from the previous cases. Since the relative humidity is higher than the deliquescence humidity of all the possible salts, the aerosol consists of an aqueous solution of sulfate, nitrate and ammonium ions. The increased SO_2 concentration causes a substantial increase in the sulfate mass, and, as presented in Table 4, the overall sulfate concentration has been tripled, as compared to the previous cases. The total aerosol mass has been increased by an order of magnitude, as compared to the base case, basically due to the 400 $\mu g\,m^{-3}$ of condensed water.

As it is shown in Table 5, in contrast to the previous cases, here, nucleation does take place. High relative humidity provides a more favorable condition for nucleation. The critical cluster contains many more water molecules per molecule of sulfuric acid than it does in low relative humidities. Therefore, lower sulfuric acid partial pressure is necessary for binary nucleation to occur, at the same rate, in humid environments than in dry ones.

What is crucial, though, for the formation of new particles by nucleation is the concentration of pre-existing aerosol particles. The cleaner environment provides less total surface area of aerosols, hence there is less consumption of sulfuric acid vapors by condensation and, therefore, more H_2SO_4 available for nucleation (Middleton and Kiang, 1978). In this sensitivity test all the new particle production by nucleation took place in the first 30 min of the simulation, when the concentration of pre-existing aerosol was relatively low. After that time, the increasing aerosol mass accelerated the condensation process, resulting in no further particle production by nucleation. Under urban conditions, though, since background aerosol is always present, homogeneous nucleation of H_2SO_4–H_2O appears to be negligible.

New particles formed by nucleation are very small and do not contribute substantially to the total aerosol mass. They do, though, affect the number concentration density function in the range below 0.01 μm. In this sensitivity test, for example, the 0.023 $\mu g\,m^{-3}$ of sulfate produced by nucleation corresponds to about 10^{11} particles m^{-3}, one order of magnitude more than that initially existing in the system. Since the coagulation process is strongly dependent on the particle number density, these small particles move rapidly into the higher sections by coagulating among themselves and with pre-existing small particles. This is the reason no particles smaller than 0.05 μm are predicted to exist when the trajectory reaches Rubidoux, as presented in Fig. 7.

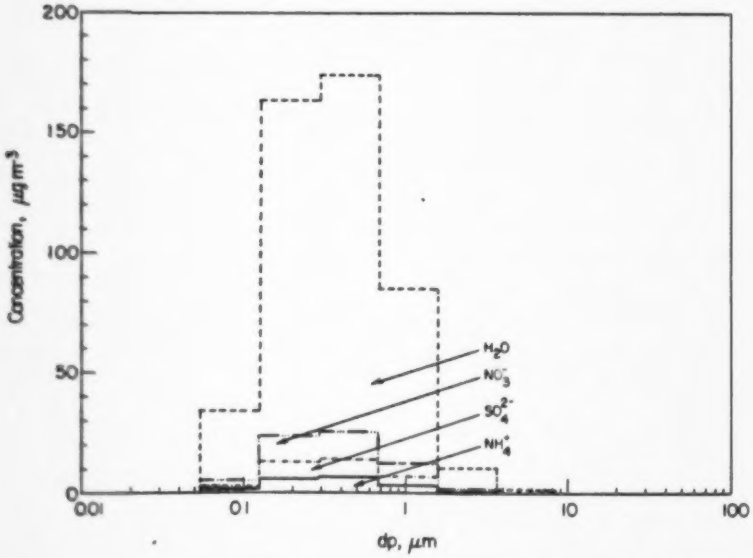

Fig. 7. Predicted size–composition distribution at Rubidoux, CA at 1800 h on 31 August 1982. Conditions changed according to Test 3 in Table 3, namely increase of the relative humidity to 95%, increase of the initial SO_2 concentration by a factor of 10, and decrease of the initial sulfate level by a factor of 1000 from those of the base case, Fig. 4. The aerosol consists of an aqueous solution of sulfate, nitrate and ammonium ions. The mass below the upper line indicates the total amount of aerosol, and the incremental components of that total are indicated.

CONCLUSIONS

A mathematical model that describes the evolution of the size and chemical composition distribution of atmospheric aerosols has been developed. The model, based on a sectional representation of the size distribution, treats dynamics and thermodynamics of multicomponent atmospheric aerosols, including new particle formation by homogeneous heteromolecular nucleation, gas-to-particle conversion, coagulation and dry deposition.

The aerosol model was used to simulate the aerosol size and chemical composition on a trajectory from Anaheim to Rubidoux in the Los Angeles basin, for which measured particulate concentrations were available. Comparison between the predicted and observed aerosol concentrations showed that the model adequately predicted the concentrations of the major particulate compounds along that trajectory.

The particular day of the trajectory in question was characterized by low relative humidity, and as a result the aerosol consisted solely of dry ammonium sulfate and ammonium nitrate. The results of the simulation showed that mixed salts rather than pure phases were thermodynamically favored along the course of the trajectory.

Three tests were conducted to investigate the sensitivity of the model to various atmospheric parameters. As expected, reduction of the ammonia and increase in the ambient temperature cause a decrease in the aerosol ammonium nitrate concentration. Although a condition of high relative humidity, combined with very low initial aerosol concentration, leads to the formation of new particles, by nucleation, condensation is predicted to be the predominant mechanism for gas-to-particle conversion.

Future studies to be carried out with the model include extension to organic aerosols and evaluation of the effect of proposed control strategies on atmospheric aerosol levels.

Acknowledgement—This work was supported by State of California Air Resources Board Agreement A4-146-32 to the California Institute of Technology and by U.S. Environmental Protection Agency contract 68-02-4076 to Systems Applications, Inc. Although the research described in this article has been funded in part by the U.S. Environmental Protection Agency, it does not necessarily reflect the views of the agency and no official endorsement should be inferred.

REFERENCES

Bassett M. E., Gelbard F. and Seinfeld J. H. (1981) Mathematical model for multicomponent aerosol formation and growth in plumes. *Atmospheric Environment* **15**, 2395–2406.

Bassett M. E. and Seinfeld J. H. (1983) Atmospheric equilibrium model of sulfate and nitrate aerosol. *Atmospheric Environment* **17**, 2237–2252.

Bassett M. E. and Seinfeld J. H. (1984) Atmospheric equilibrium model of sulfate and nitrate aerosol—II. Particle size analysis. *Atmospheric Environment* **18**, 1163–1170.

Eltgroth M. W. and Hobbs P. V. (1979) Evolution of particles in the plumes of coalfired power plants—II. A numerical model and comparison with field measurements. *Atmospheric Environment* **13**, 953–975.

Fuchs N. A. and Sutugin A. G. (1971) *Topics in Current Aerosol Research* (edited by Hidy G. M. and Brock J. R.), Vol. II, pp. 1–60. Pergamon Press, Oxford.

Gelbard F. MAEROS (1984) *Aerosol Sci. Technol.* **3**, 117–118.

Gelbard F. and Seinfeld J. H. (1978) Numerical solution of the dynamic equation for particulate systems. *J. Computat. Phys.* **28**, 357–375.

Gelbard F. and Seinfeld J. H. (1979) The general dynamic equation for aerosols—theory and application to aerosol formation and growth. *J. Colloid Interface Sci.* **69**, 363–382.

Gelbard F. and Seinfeld J. H. (1980) Simulation of multicomponent aerosol dynamics. *J. Colloid Interface Sci.* **78**, 485–501.

Gelbard F., Tambour Y. and Seinfeld J. H. (1980) Sectional representation for simulating aerosol dynamics. *J. Colloid Interface Sci.* **76**, 541–556.

Gmitro J. I. and Vermeulen T. (1964) Vapor-liquid equilibrium for aqueous sulfuric acid. *AIChE J.* **10**, 740–746.

Harrison R. M. and Sturges W. T. (1984) Physico-chemical speciation and transformation reactions of particulate atmospheric nitrogen and sulfur compounds. *Atmospheric Environment* **18**, 1829–1833.

Hildelmann L. M., Russell A. G. and Cass G. R. (1984) Ammonia and nitric acid concentrations in equilibrium with atmospheric aerosols: experiment vs theory. *Atmospheric Environment* **18**, 1737–1750.

Liu M. K. and Seinfeld J. H. (1975) On the validity of grid and trajectory models of urban air pollution. *Atmospheric Environment* **9**, 555–574.

Middleton P. and Brock J. (1976) Simulation of aerosol kinetics. *J. Colloid Interface Sci.* **54**, 249–264.

Middleton P. and Kiang C. S. (1978) A kinetic aerosol model for the formation and growth of secondary sulfuric acid particles. *J. Aerosol Sci.* **9**, 359–385.

Middleton P., Kiang C. S. and Mohnen V. A. (1980) Theoretical estimates of the relative importance of various urban sulfate aerosol production mechanisms. *Atmospheric Environment* **14**, 463–472.

Mirabel P. and Katz J. L. (1974) Binary homogeneous nucleation as a mechanism for the formation of aerosols. *J. Chem. Phys.* **60**, 1138–1144.

Perry R. H. and Chilton C. H. (1973) *Chemical Engineers' Handbook*, 5th edn, pp. 3–80, 3–81. McGraw-Hill, New York.

Russell A. G. and Cass G. R. (1984) Aquisition of regional air quality model validation data for nitrate, sulfate, ammonium ions, and their precursors. *Atmospheric Environment* **18**, 1815–1827.

Russell A. G., McRae G. J. and Cass G. R. (1983) Mathematical modeling of the formation and transport of ammonium nitrate aerosol. *Atmospheric Environment* **17**, 949–964.

Sabinina L. and Terpugow L. (1935) Die oberflächenspannung des systems schwefelsäure-wasser. *Z. Phys. Chem.* **A173**, 237.

Saxena P., Hudischewskyj A. B., Seigneur C. and Seinfeld J. H. (1986) A comparative study of equilibrium approaches to the chemical characterization of secondary aerosols. *Atmospheric Environment* **20**, 1471–1483.

Seigneur C. (1982) A model of sulfate aerosol dynamics in atmospheric plumes. *Atmospheric Environment* **16**, 2207–2228.

Seigneur C., Hudischewskyj A. B., Seinfeld J. H., Whitby K. T., Whitby E. R., Brock J. R. and Barnes H. M. (1986) Simulation of aerosol dynamics: comparative review of mathematical models. *Aerosol Sci. Technol.* **5**, 205–221.

Seinfeld J. H. (1986) *Atmospheric Chemistry and Physics of Air*

Pollution. John Wiley, New York.

Stelson A. W., Friedlander S. K. and Seinfeld J. H. (1979) A note on the equilibrium relationship between ammonia and nitric acid and particulate ammonium nitrate. *Atmospheric Environment* **13**, 369–371.

Stelson A. W. and Seinfeld J. H. (1982a) Relative humidity and temperature dependence of the ammonium nitrate dissociation constant. *Atmospheric Environment* **16**, 983–992.

Stelson A. W. and Seinfeld J. H. (1982b) Relative humidity and pH dependence of the vapor pressure of ammonium nitrate-nitric acid solutions at 25°C. *Atmospheric Environment* **16**, 993–1000.

Stelson A. W. and Seinfeld J. H. (1982c) Thermodynamic prediction of the water activity, NH_4NO_3 dissociation constant, density and refractive index for the NH_4NO_3–$(NH_4)_2SO_4$–H_2O system at 25°C. *Atmospheric Environment* **16**, 2507–2514.

Suck S. H. and Brock J. R. (1979) Evolution of atmospheric aerosol particle size distributions via Brownian coagulation: numerical simulation. *J. Aerosol Sci.* **10**, 581–590.

Tanner R. L. (1982) An ambient experimental study of phase equilibrium in the atmospheric system: aerosol-H^+, NH_4^+, SO_4^{2-}, NO_3^-–$NH_{3(g)}$, $HNO_{3(g)}$. *Atmospheric Environment* **16**, 2935–2942.

Tilden J. W. and Seinfeld J. H. (1982) Sensitivity analysis of a mathematical model of photochemical air pollution. *Atmospheric Environment* **16**, 1357–1364.

Tsang T. H. and Brock J. R. (1982) Aerosol coagulation from a crosswind line source. *Atmospheric Environment* **16**, 2229–2235.

Tsang T. H. and Brock J. R. (1983) Simulation of aerosol growth by condensation and evaporation. *Aerosol Sci. Technol.* **2**, 311–320.

Warren D. R. and Seinfeld J. H. (1985) Simulation of aerosol size distribution evolution in systems with simultaneous nucleation, condensation and coagulation. *Aerosol Sci. Technol.* **4**, 31–43.

Winer A. M., Peters J. W., Smith J. P. and Pitts J. N. (1974) Response of commercial chemiluminescent NO–NO_2 analyzers to other nitrogen containing compounds. *Envir. Sci. Technol.* **8**, 1118–1121.

Yue G. K. and Hamill P. (1979) The homogeneous nucleation of H_2SO_4–H_2O aerosol particles in air. *J. Aerosol Sci.* **10**, 609–614.

Appendix I

MATHEMATICAL MODELING OF LIGHT SCATTERING BY ATMOSPHERIC AEROSOLS

A. Belle Hudischewskyj

Pradeep Saxena*, Christian Seigneur#,
Systems Applications, Inc.
101 Lucas Valley Road
San Rafael, California 94903

Scattering of light by aerosols is generally the major component of atmospheric light extinction. Because light scattering by atmospheric aerosols is a strong function of the aerosol size, it is imperative to predict the aerosol size distribution with accuracy in order to calculate the aerosol scattering coefficient (b_{scat}). Mathematical models have been developed to describe the evolution of the size distribution, chemical composition, and concentration of aerosols as chemical reactions and aerosol dynamics processes (coagulation, growth, deposition) take place in the atmosphere. These models can be applied to calculate b_{scat} due to aerosols by means of Mie theory. Three models available for determining the chemical composition and concentration of secondary aerosols are reviewed --one of these models considers the Kelvin effect, i.e., the effect of aerosol size on aerosol/gas phase equilibrium, and the other two do not. Their predictions of b_{scat} are compared over a wide range of initial conditions for sulfate, nitrate, ammonium, and relative humidity. The treatment of the Kelvin effect has been shown to have a negligible effect on the calculation of b_{scat}. A model is used to simulate the formation of aerosols in power plant and smelter plumes. A comparison of calculated and measured b_{scat} values shows that the model tends to underpredict b_{scat}, although the correlations between calculated and measured b_{scat} values are quite satisfactory.

---

* Present Address: Pacific Gas and Electric Company, Department of Engineering Research, 3400 Crow Canyon Road, San Ramon, CA 94583.
# Present Address: Bechtel National, Inc. Environmental Services Department, P.O. Box 3965, San Francisco, CA 94119.

MATHEMATICAL MODELING OF LIGHT SCATTERING BY ATMOSPHERIC AEROSOLS

Introduction

Scattering of light by aerosols is generally the major component of light extinction. Scattering of light by molecules (Rayleigh scattering) and absorption by aerosols (e.g. soot particles) and gases (e.g., NO_2) are the other components contributing to light extinction. Light scattering by atmospheric aerosols is a strong function of the aerosol size; it is therefore imperative to predict the aerosol size distribution with accuracy if one wants to calculate the aerosol scattering coefficient (b_{scat}). Mathematical models have been developed to describe the evolution of the size distribution, chemical composition, and concentration of aerosols as chemical reactions and aerosol dynamics processes (coagulation, growth, deposition) take place in the atmosphere. These models can be applied to calculate light scattering due to aerosols by means of Mie theory.[1]

In this paper we present a mathematical model that predicts the aerosol scattering coefficient, b_{scat}, based on a rigorous treatment of aerosol dynamics, chemistry, and thermodynamics. First we present an overview of the various components of this model and their incorporation into a reactive plume model. Then we briefly review several models available for determining the equilibrium chemical composition of secondary aerosols. We compare their predictions of b_{scat} over a wide range of initial conditions for sulfate, nitrate, and ammonium concentrations, and relative humidity to determine the importance of the Kelvin effect (the effect of aerosol size on aerosol/gas phase equilibrium), on the calculation of b_{scat}.

We simulated the formation of aerosols in the plumes from three power plants (Navajo in Arizona, Mohave in Nevada, and Labadie in Missouri), and a copper smelter (San Manuel in Arizona) and compared the calculated and measured b_{scat} values. The simulations of the plumes of these four emission sources span a wide range of atmospheric chemical and physical conditions.

Description of the Mathematical Model

The mathematical modeling of light scattering by aerosols comprises several components that are depicted in Figure 1. The simulation of aerosol chemistry takes into account the gas-phase concentrations of chemical species, relative humidity, temperature, and the initial chemical composition and size distribution of the aerosols. Aerosol dynamics treats the changes in the aerosol size distribution that result from chemical processes (growth or shrinkage due to condensation or evaporation, respectively) and physical processes (coagulation, sedimentation, and deposition). The aerosol scattering coefficient is deduced from the size distribution using the Mie theory of light scattering.[1]

Chemical processes that affect atmospheric aerosols have been reviewed by Seigneur and Barnes.[2] A key question in the simulation of the aerosol chemistry is the dependence of the aerosol chemical composition on the aerosol size. The effect of aerosol size (and therefore curvature) on the saturation vapor pressure of condensible species (i.e., the Kelvin effect) may affect the chemical concentrations of species in aerosols of different sizes. This phenomenon is investigated in the next section with models that predict the mass and equilibrium chemical composition of atmospheric aerosols.

The oxidation of SO_2 to sulfate in aqueous aerosols occurs primarily in the presence of trace metals (iron and manganese) and H_2O_2 and must be included into the aerosol model.[3] Treatment of condensation and evaporation requires the coupling of the aerosol model with a gas-phase chemical kinetic mechanism. The modeling of aerosol dynamics can be approached in different manners depending on the method used to represent the aerosol size distribution (e.g. continuous, parameterized, or discrete). The sectional (discrete) representation, in which the aerosol size distribution is represented by a series of step functions, was shown to be computationally efficient and reasonably accurate.[4]

From the aerosol size distribution, aerosol light scattering can be calculated by means of Mie theory.[1] If the sectional approach is used, the scattering coefficient can be calculated for each section and then summed over all sections.

The treatment of light scattering by aerosols in this model may be described as follows. Let the aerosol volume size distribution be $V(x)$, where $x = \log(d_p)$ and d_p is the aerosol aerodynamic diameter. The total aerosol scattering coefficient, $b_{scat}(\lambda)$, is given by the integral equation

$$b_{scat}(\lambda) = \int_0^{\infty} G(m,x,\lambda)\, V(x)\, dx$$

where $G(m,x,\lambda)$ is the volume extinction efficiency, m is the aerosol refractive index, and λ is the wavelength of the light. Note that for our model we chose a sectional representation of the aerosol size distribution. If $\bar{b}(\lambda,x)$ is the scattering coefficient per aerosol unit volume, the sectional scattering coefficient, $\bar{b}_\ell(\lambda)$, is given by the following relationship:

$$\bar{b}_\ell(\lambda) = \frac{1}{x_\ell - x_{\ell-1}} \int_{x_{\ell-1}}^{x_\ell} b(\lambda,x)\, dx$$

where X_ℓ and $X_{\ell-1}$ are the upper and lower bounds of section ℓ respectively. Then, the total aerosol scattering coefficient is given by the following algebraic equation:

$$b_{scat}(\lambda) = \sum_{i=1}^{N} \bar{b}_\ell(\lambda) \frac{Q_\ell}{\rho}$$

where Q_ℓ is the aerosol mass in section ℓ, N is the total number of sections, and ρ is the aerosol density. The aerosol sectional scattering coefficients were calculated for a wavelength of 550 nm and a refractive index equal to 1.5 - 0 i using a standard solution to the Mie equations.[5]

The components of aerosol chemistry, thermodynamic equilibrium, dynamics, and light scattering have been integrated to form a comprehensive and theoretically rigorous mathematical model of light scattering by atmospheric aerosols.[6] The formulation of the coupling between the sectional equations for aerosol dynamics and the thermodynamic equilibrium equation has been described by Pilinis and co-workers.[7]

For our model we selected the Model for an Aerosol Reacting System (MARS) to simulate aerosol thermodynamics.[8] This model is discussed in the next section. We selected a sectional aerosol size distribution that covers the range of 0.01 to 10 μm with 9 size sections. Aerosol chemistry includes oxidation of SO_2 to sulfate in the liquid aerosol phase.[3] This aerosol model was coupled with a gas-phase chemical kinetic mechanism, the Carbon-Bond Mechanism (CBM) III,[9] and incorporated into a Lagrangian gridded plume model (PLMSTAR)[10] that simulates transport, dispersion, and dry deposition.[11]

Importance of the Size Dependence of the Aerosol Chemical Composition (Kelvin Effect)

Several models that calculate the aerosol chemical composition based on the thermodynamic equilibrium between the aerosol and the gas phase have been developed in recent years. Such models are an important component of an aerosol model that calculates scattering since they provide the amount of sulfate, nitrate, ammonium, and water present in the aerosol phase. These species have been shown to contribute significantly to light scattering.

Three thermodynamic models were compared to determine the most computationally efficient, while still accurate, model to incorporate into a Lagrangian reactive plume model; EQUIL and KEQUIL developed by Bassett and Seinfeld,[12,13] and MARS developed by Saxena and co-workers.[8] All three models assume sulfate to be present entirely in the aerosol phase. The aerosol concentrations of nitrate, ammonium, and water, on the other hand, are determined by the sulfate, gas-phase ammonia, and nitric acid concentrations, relative humidity, and temperature.

EQUIL is a rigorous model that explicitly solves the thermodynamic equilibrium problem for 17 species in eight phases by minimizing the Gibbs free energy of the system. Thirteen equilibrium reactions are taken into account among these 17 species. The temperature dependence of all thermodynamic properties is also incorporated. The formulation of KEQUIL is identical to that of EQUIL except that the treatment of the Kelvin effect is included in KEQUIL and not in EQUIL.

The basic thermodynamic framework of MARS is similiar to that of EQUIL and KEQUIL but was developed with computational efficiency (while still maintaining reasonable accuracy) in mind.[8] Unlike EQUIL and KEQUIL, MARS focuses only on major species for each given set of ambient conditions in its treatment of chemical and interfacial equilibria. It does so by subdividing the entire domain of sulfate, nitrate, ammonium, and water concentrations into several subdomains. This minimizes the number of equations to be solved, since within each subdomain, there are fewer species than there are in the entire domain. The thermodynamic equilibrium parameters are temperature dependent. However, MARS does not account for the effect of temperature variation on relative humidities of deliquescence, binary data for water activity and activity coefficients, nor the Kelvin effect.

Simulations were performed for 51 sets of atmospheric conditions using the EQUIL, KEQUIL, and MARS models.[8] For these simulations, sulfate, nitrate, and ammonia concentrations ranged from 5 $\mu g/m^3$ for all three species, to 40 $\mu g/m^3$ for sulfate, 45 $\mu g/m^3$ for nitrate, and 70 $\mu g/m^3$ for ammonia. Relative humidity ranged from 30% to 90%. The ambient temperature was 298 K for all cases. To test the effect of aerosol size distributions on model predictions of b_{scat}, two size distributions were included, one with a modal diameter of 1 µm and the other with a modal diameter of 0.15 µm.

Simulation results are presented in detail elsewhere.[8] Since KEQUIL is the most rigorous and comprehensive model, it was used as a benchmark for model performance. The predictions of b_{scat} by EQUIL and MARS are comparable to those of KEQUIL, since the correlation coefficients are 0.999 and 0.996, and the absolute errors are 4 and 6 percent, respectively. The efficiency of MARS is much greater than those of EQUIL and KEQUIL; MARS is approximately 400 times faster than KEQUIL and 60 times faster than EQUIL. Because of its computational efficiency as well as reasonable accuracy, MARS was selected for the thermodynamic portion of our model.

Simulation of Light Scattering by Atmospheric Aerosols in Plumes

The aerosol/plume model described earlier was used to simulate the formation of aerosols in power plant and smelter plumes.[11] The data base consisted of plume data collected at three power plants--Navajo (Arizona),[14,15] Labadie (Missouri),[15,16] and Mohave (Nevada)[17,18]--and one copper smelter, San Manuel(Arizona).[15,19] By performing simulations of the plumes of these four emission sources, we were able to study a wide range of chemical and physical conditions. The Navajo power plant is well controlled for particulate matter and sited in a clean environment; the Mohave power plant is located in the desert downwind of the Los Angeles basin; the Labadie power plant is located in an urban environment near St. Louis. Smelters, like power plants, emit particulate matter and SO_2, but not significant amounts of nitrogen oxides (NO_x). The results of the b_{scat} calculations for the wavelength of 550 nm are shown in Table I.

Correlation coefficients were calculated for the seven Mohave cases alone and again for all cases combined. Insufficient data precluded the calculation of correlation coefficients for Navajo, Labadie, and San Manuel, individually. Scatter diagrams of measured versus calculated b_{scat} values for Mohave alone and all cases combined are presented in Figures 2 and 3, respectively. For the most part, agreement between measured and calculated b_{scat} values is good. The correlation coefficient for the Mohave data alone is 0.64; for all data combined, 0.88. In only one case (Mohave, 28 August 1979, 5.5 km) did the model overpredict the b_{scat} value. In 9 of the remaining 11 cases it underpredicted the b_{scat} value. In one case (Labadie) the calculated value of b_{scat} is within the range of the measurements. The model underestimation of b_{scat} is consistent with the underestimation of sulfate formation found previously.[11] In 7 cases out of 12 the model predictions are within a factor of two of the measured values. The average absolute error between predicted and measured values is 44 percent. Although the model tends to underpredict, it is able to reproduce the large variations in aerosol scattering that occur under various conditions.

Since many atmospheric visibility models use a b_{scat}/aerosol mass relationship without any consideration of aerosol size distribution, we compared the performance of such an approach with our more rigorous approach. Table I presents the b_{scat} values obtained using the empirical b_{scat}/aerosol mass relationship.[20] This relationship takes into account sulfate aerosols, other fine aerosols, and coarse aerosols:

$$b_{scat} = 4 * f(RH) * [SO_4^{2-}] + 3 * [FA] + 0.4\ [CA]$$

where f(RH) is a function whose value is 1 for relative humidities up to 40 percent and an increasing function of relative humidity above 40%; FA represents fine aerosols (below 2.5 μm in diameter); and CA represents coarse aerosols (above 2.5 μm in diameter).

The results presented in Table I show that the empirical formula is not as consistent in predicting b_{scat} as is the mathematical model. The formula underpredicted b_{scat} in 6 of the 12 cases and overpredicted b_{scat} in 5. In one case, the calculated and measured b_{scat} values were equal. The correlation between measured b_{scat} and empirical b_{scat} is 0.72 for all data points, and 0.43 for the Mohave data alone. The average absolute error is 74%. These results indicate that an empirical formula based solely on the sulfate aerosol mass would produce some large discrepancies with the measurements since it is not able to reproduce the large variation in the aerosol size distribution and hence the value of the scattering coefficient. It is therefore important to include the modeling of the aerosol size distribution in the calculation of the aerosol scattering coefficient.

Conclusion

A mathematical model has been presented that allows simulation of the evolution of the multicomponent aerosol size distribution in the atmosphere. The Kelvin effect was shown to have little influence of the aerosol size distribution and was therefore neglected in the model formulation. The model was incorporated into a Lagrangian reactive plume model and then applied to the simulation of the aerosol evolution in plumes of three power plants and one smelter. Although the model tended to underpredict bscat, agreement between calculated and measured bscat was good. The correlation between the calculated and measured b_{scat} values is 0.88 and the average absolute error is 44 percent. Results indicate that the model performance appears promising. Because light scattering by aerosols is a strong function of their size distribution, this model of atmospheric aerosols should be used in studies of plume visibility and regional haze instead of models which use the b_{scat}/aerosol mass relationship and consequently neglect the evolution of the aerosol size distribution.

Acknowledgements

The portion of this study dealing with the aerosol model development and the comparison of the thermodynamic models was sponsored by the EPA-ASRL Aerosol Research Branch. We would like to thank the project officer, Dr. H. M. Barnes for suggesting this study and for his support. The remainder of this study was sponsored by Southern California Edison (SCE). We acknowledge the continuous support and interest of Mr. Stan Marsh and Mr. Vince Mirabella, the SCE project officers, throughout the course of this work. Sincere thanks are also due to Dr. L. W. Richards and Dr. D. L. Hegg, for providing valuable information regarding the experimental data and to Mr. Howard Beckman for his technical editing.

REFERENCES

1. G. Mie, Ann. Physik, 25:377 (1908).

2. C. Seigneur C. and H. M. Barnes, "Technical considerations in aerosol modeling." In Air Pollution Modeling and Its Application, Volume 5, pp. 343-369 (edited by C. de Wispelaere, F. Schiermeier, and N. Gillani) Plenum Press, New York, New York (1986).

3. P. Saxena and C. Seigneur, "On the oxidation of SO_2 to sulfate in atmospheric aerosols." Atmos. Environ., in press (1987).

4. C. Seigneur, A. B. Hudischewskyj, J. H. Seinfeld, K. T. Whitby, E. R. Whitby, J. R. Brock, and H. M. Barnes, "Simulation of aerosol dyanamics: A comparative review of mathematical models," Aerosol Sci. Technol., 5:205-222 (1986).

5. C. Seigneur, R. W. Bergstrom, C. D. Johnson, and L. W. Richards, "Measurements and simulations of the visual effects of particulate plumes," Atmos. Environ., 18:2231-2244 (1984).

6. C. Seigneur, A. B. Hudischewskyj, and P. Saxena, "Mathematical modeling of the concentration, chemical composition, and size distribution of aerosols in plumes," Systems Applications, Inc., San Rafael, California, SYSAPP-85/026 (1985).

7. C. Pilinis, J. H. Seinfeld, and C. Seigneur, "Mathematical modeling of the dynamics of multicomponent atmospheric aerosols," Atmos. Environ., in press (1987).

8. P. Saxena, A. B. Hudischewskyj, C. Seigneur, and J. H. Seinfeld, "A comparative study of equilibrium approaches to the chemical characterization of secondary aerosols," Atmos. Environ., 20, 1471-1484 (1986).

9. J. P. Killus, and G. E. Whitten, "Technical discussions relating to the use of the Carbon-Bond Mechanism in OZIPM/EKMA," U.S. Environmental Protection Agency, Research Triangle Park, North Carolina, EPA-450/4-84-009 (1984).

10. D. Godden and F. Lurman, "Development of the PLMSTAR model and its application to ozone episode conditions in the South Coast Air Basin," Environmental Research and Technology, Inc., Westlake Village, California, P-A702-200 (1983).

11. A. B. Hudischewskyj and C. Seigneur, "Simulation of the formation of acidic aerosol species in power plant and smelter plumes," In Proceedings of the 79th Annual Meeting of the Air Pollution Control Association (1986).

12. M. E. Bassett and J. H. Seinfeld, "Atmospheric equilibrium model of

sulfate and nitrate aerosol," Atmos. Environ., 17:2237-2252 (1983).

13. M. E. Bassett and J. H. Seinfeld, "Atmospheric equilibrium model of sulfate and nitrate aerosols--II. Particle size analysis," Atmos. Environ., 18:1163-1170 (1984).

14. L. W. Richards et al., "The chemistry, aerosol physics, and optical properties of a western coal-fired power plant plume," Atmos. Environ., 15:2111-2134 (1981).

15. L. W. Richards, Sonoma Technology, Inc., personal communication, 1985.

16. L. W. Richards et al., "Chemical, aerosol, and optical measurements in the plumes of three midwestern coal-fired power plants," Atmos. Environ., 19(10):1685-1704 (1985).

17. D. A. Hegg, P. V. Hobbs, and J. H. Lyons, "Field studies of a power plant plume in the arid southwestern United States," Atmos. Environ., 19(7):1147-1167 (1984).

18. D. A. Hegg, University of Washington, personal communication, 1985.

19. L. W. Richards et al., "Nitrogen and sulfur chemistry and aerosol formation in plumes," Proceedings of the 75th Annual Meeting of the Air Pollution Control Association (1982).

20. Systems Applications, Inc., "Modeling Regional Haze in the Southwest: A Preliminary Assessment of Source Contributions," San Rafael, CA (SYSAPP/85-039).

Table I. COMPARISON OF MEASURED AND CALCULATED SCATTERING COEFFICIENTS (b_{scat}) IN VARIOUS PLUMES

		b_{scat} (10^{-4} m^{-1})		
Plant and Date	Downwind Distance (km)	Measured	Calculated (Mathematical (Model)	Calculated (Empirical Relationship)
Navajo				
13 July 1979	58.0	0.26	0.10	0.14
Mohave				
27 August 1979	5.5	1.6	1.1	2.2
	27.8	0.51	0.48	0.72
28 August 1979	5.5	0.63	0.90	2.4
	55.5	0.33	0.27	0.48
31 August 1979	5.5	0.62	0.32	0.58
	25.9	0.40	0.19	0.40
11 August 1980	5.5	1.6	0.56	0.81
Labadie				
23 August 1981	5.5	0.10-0.19	0.16	0.52
San Manuel				
6 September 1981	10.0	4.7	2.5	2.9
	13.0	2.7	0.63	1.6
	14.0	2.7	1.0	1.3

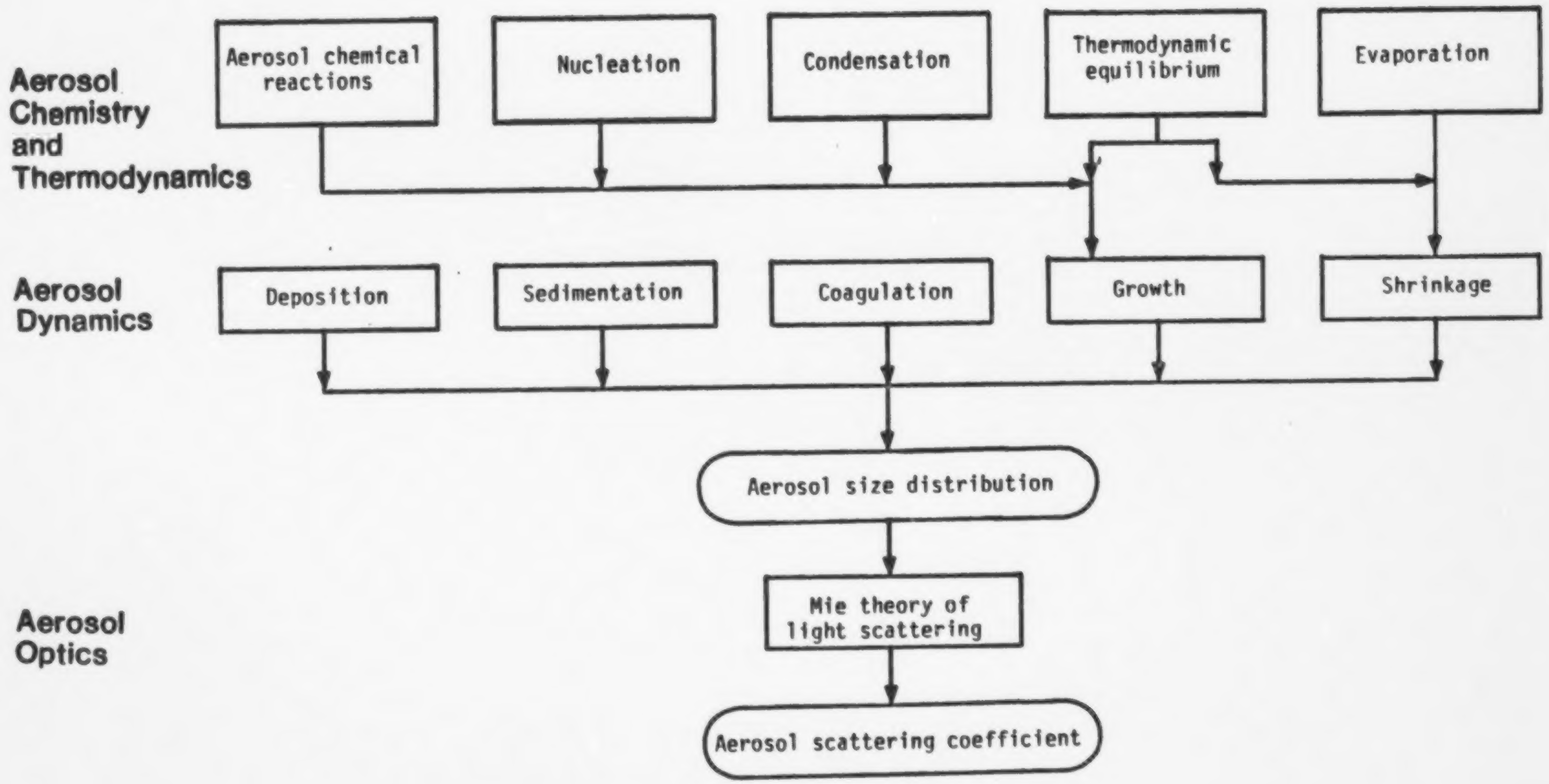
Aerosol Chemistry and Thermodynamics
Aerosol chemical reactions
Nucleation
Condensation
Thermodynamic equilibrium
Evaporation
Aerosol Dynamics
Deposition
Sedimentation
Coagulation
Growth
Shrinkage
Aerosol size distribution
Aerosol Optics
Mie theory of light scattering
Aerosol scattering coefficient

FIGURE 1. Schematic description of the mathematical modeling of light scattering by atmospheric aerosols.

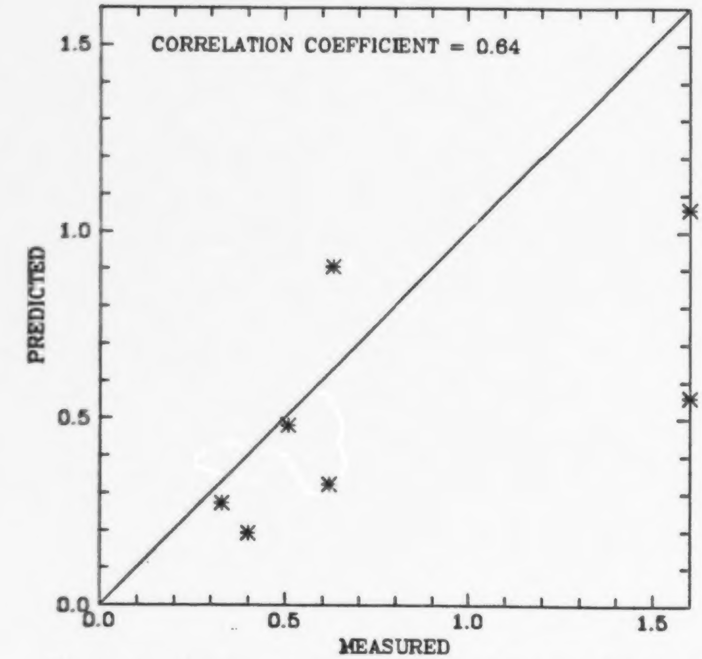

Figure 2. Measured vs predicted scattering coefficients for the Mohave power plant plume, August 1979 and 1980. Units are 10^{-4} m^{-1}.

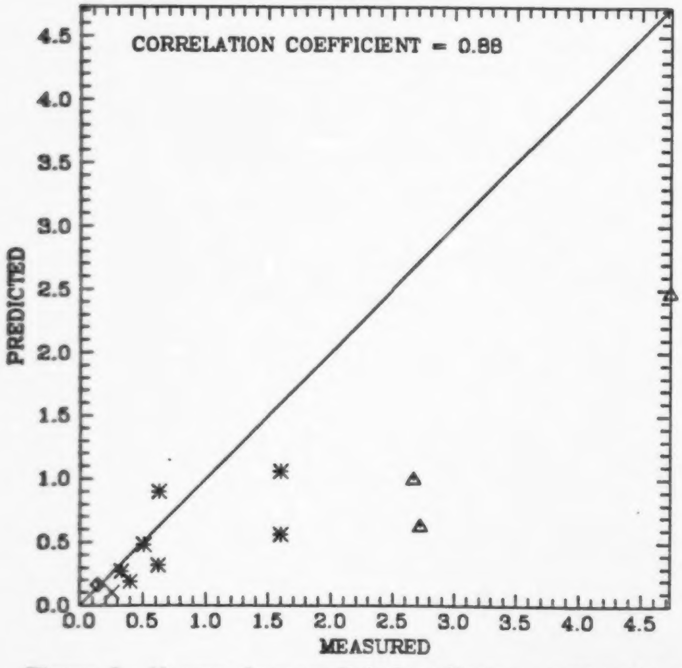

Figure 3. Measured vs predicted scattering coefficients for the Navajo (✕), Mohave (✱), and Labadie (◇) power plant plumes and for the San Manuel (△) smelter plume. Units are 10^{-4} m^{-1}.

Key Words:

Aerosol
Plume
Scattering coefficient
Visibility

Appendix J

USER'S GUIDE TO THE AEROSOL MODEL

The aerosol model developed during the course of this project has been installed in a number of transport models including the SAI Airshed Model (Hogo et al., 1986), the Reactive Plume Model (RPM) (Seigneur and Hudischewskyj, 1986), PLMSTAR (Seigneur et al., 1986a), and for this project, the EPA Regional Oxidant Model (ROM). The following discussion of the model pertains to its use in ROM. Figure 1 is a flow diagram of the aerosol model as it is used in ROM. The original ROM subroutines are enclosed in boxes with dotted lines; the new aerosol subroutines are enclosed in solid boxes.

The species incorporated into ROM have been divided into two groups: differential species that are treated with the transport algorithm (i.e., species governed by differential equations) and the algebraic species that are treated at a given time and location regardless of their value at other times and locations (i.e., species governed by algebraic equations).

The ROM aerosol model contains 24 differential species:

SO_2	Sulfur dioxide (gas phase and aerosol)
NH_3	Total of ammonia (gas phase) and ammonium (aerosol)
QP_1 to QP_7	Total of primary and organic aerosol mass in 7 size ranges from 0.01 to 2.5 μm: 0.01-0.022 μm, 0.022-0.048 μm, 0.048-0.107 μm, 0.107-0.235 μm, 0.235-0.516 μm, 0.516-1.136 μm, 1.136-2.5 μm.
QP_8 and QP_9	Primary aerosol mass in two size ranges: 2.5 to 5 μm and 5 to 10 μm
QS_1 to QS_7	Sulfate aerosol mass in seven size ranges from 0.01 to 2.5 μm: 0.01-0.022 μm, 0.022-0.048 μm, 0.048-0.107 μm, 0.107-0.235 μm, 0.235-0.516 μm, 0.516-1.136 μm, 1.136-2.5 μm.

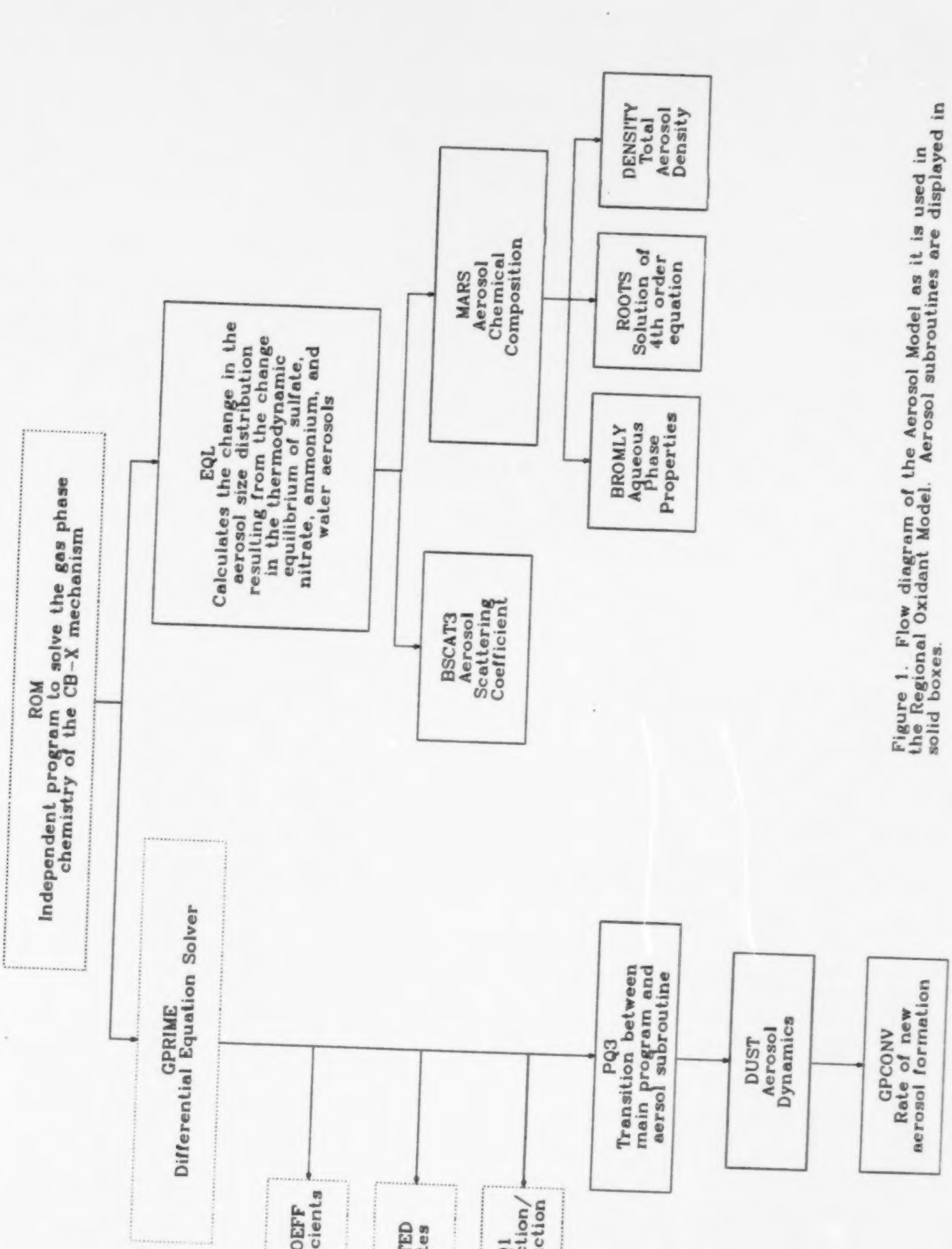
ROM
Independent program to solve the gas phase chemistry of the CB-X mechanism
GPRIME
Differential Equation Solver
EQL
Calculates the change in the aerosol size distribution resulting from the change in the thermodynamic equilibrium of sulfate, nitrate, ammonium, and water aerosols
PQCOEFF
Coefficients
RATED
Rates
PQ1
Production/
Destruction
PQ3
Transition between main program and aerosol subroutine
DUST
Aerosol
Dynamics
GPCONV
Rate of new aerosol formation
BSCAT3
Aerosol
Scattering
Coefficient
MARS
Aerosol
Chemical
Composition
BROMLY
Aqueous
Phase
Properties
ROOTS
Solution of 4th order equation
DENSITY
Total
Aerosol
Density

Figure 1. Flow diagram of the Aerosol Model as it is used in the Regional Oxidant Model. Aerosol subroutines are displayed in solid boxes.

AERO	Total mass of organic aerosol
λ	Parameter equal to the ratio of the total of sulfate, nitrate, ammonium, and water aerosol to sulfate aerosol (i.e., $\lambda = (AERS + AERN + AERA + AERW)/AERS$)
FE^{3+}	Iron
Mn^{2+}	Manganese
NaCl	Sodium chloride
$NaNO_3$	Sodium nitrate

The ROM aerosol model contains 15 algebraic species:

Q_1 to Q_7	Total aerosol mass in seven size ranges from 0.01 to 2.5 µm ($Q_i = QP_i + \lambda\ QS_i$). Note that $Q_8 = QP_8$ and $Q_9 = QP_9$, which are already included in the differential species list.
AERS	Total sulfate aerosol ($AERS = QS_1 + QS_2 + \ldots + QS_7$)
AERN	Total nitrate aerosol present as ammonium nitrate (calculated by subroutine MARS)
AERA	Total ammonium aerosol (calculated by MARS)
AERW	Total water aerosol (calculated by MARS)
PM10	Total aerosol mass below 10 µm ($PM10 = Q_1 + Q_2 + \ldots + Q_9$)
RHO	Aerosol density
BSCAT	Aerosol scattering coefficient
PH	Aerosol pH

The following input data are needed to perform the calculation for the aerosol model:

CB-IV mechanism

Relative humidity

Temperature

Note that ROM keeps track of total ammonia (i.e., NH_3(g) + AERA) and total "free" nitrate (i.e., HNO_3(g) + AERN). The partitioning between the gas phase and the aerosol phase is calculated by MARS at each location and time. It is necessary to keep track of the parameter, λ, as a function of time because the change in λ affects the aerosol size distribution (i.e., the distribution of the aerosol mass among the QP_i and QS_i, $i = 1, \ldots, 7$). The subroutines that were added to treat aerosol processes include EQL, MARS (Saxena et al., 1986), BROMLY, ROOT, DENSITY, BSCAT, PQ3, DUST, and GPCONV.

SUBROUTINE EQL is called by the main program. It calculates the distribution of ammonia/ammonium, nitric acid/nitrate, and water between the gas and aerosol phases as the total sulfate, ammonia, and nitrate concentrations, relative humidity, and temperature change. Changes in aerosol size distribution and chemical composition are also calculated. EQL is currently called by the main program only once every print-out interval to minimize the computational cost. It can be called for the same interval as the gas-phase chemistry time step, but the computational cost may go up significantly. Subroutines MARS and BSCAT are called from EQL.

SUBROUTINE MARS (SO4, NO3, NH3, RH, TEMP, NSO2, H2O2, XMN, FE, SO2, NUNIT, NDROP, GSO4, GNO3, GNH3, ASO4, A96SO4, ANO3, ANH4, AQSSO4, AQSNO3, AQSNH4, HPLUS, S1, S2, S3, S4, WH2O, RHO, RKHP, RKO2, PH) is called from EQL. It calculates the distribution of NH_3, HNO_3, and H_2O between the gas phase and the aerosol phase. This subroutine also calculates the rate parameters for the heterogeneous formation of sulfate in the aerosol phase. Subroutines BROMLY, ROOT, and DENSITY are called from MARS. The arguments that are required for the call to MARS are

SO4 = total sulfate in $\mu g/m^3$ as sulfuric acid

NO3 = total nitrate in $\mu g/m^3$ as nitric acid

NH3 = total ammonia in $\mu g/m^3$ as ammonia

RH = fractional relative humidity

TEMP = temperature in degrees Kelvin

NSO2 = a flag to indicate whether SO_2 oxidation by H_2O_2 and metals is to be included: Yes = 1, NO = 2

XMN = Mn^{2+} concentration in $\mu g/m^3$ (required only if NSO2 = 1)

FE = Fe^{3+} concentration in $\mu g/m^3$ (required only if NSO2 = 1)

NUNIT = unit for writing error messages

NDROP = number of aerosol particles per m^3 (required only if NSO2 = 1). If a value of zero is specified, MARS will compute NDROP from the aerosol phase volume (cc/m^3) and an average particle size diameter of 0.3 μm

The arguments returned by MARS to EQL are

GSO4 = gas phase sulfuric acid in $\mu g/m^3$

GNO3 = gas phase nitric acid in $\mu g/m^3$

GNH3 = gas phase ammonia in $\mu g/m^3$

ASO4 = aerosol phase sulfate (solid + liquid) with associated H^+ in $\mu g/m^3$

A96SO4 = aerosol phase sulfate (solid + liquid) as SO_4^{-2} in $\mu g/m^3$

ANO3 = aerosol phase nitrate (solid + liquid) in $\mu g/m^3$

ANH4 = aerosol phase ammonium (solid + liquid) in $\mu g/m^3$

AQSSO4 = aqueous phase sulfate in $\mu g/m^3$ with a molecular weight of 96.

AQSNO3 = aqueous phase nitrate in $\mu g/m^3$

AQSNH4 = aqueous phase ammonium in $\mu g/m^3$

HPLUS = hydrogen ion concentration (moles/kg)

S1 = solid phase $(NH_4)_2 SO_4$ in $\mu g/m^3$

S2 = solid phase $(NH_4)_3 (SO_4)_2$ in $\mu g/m^3$

S3 = solid phase NH_4HSO_4 in μg/m^3

S4 = solid phase NH_4NO_3 in μg/m^3

WH2O = aerosol phase NH_4NO_3 in μg/m^3

RHO = average density in g/cc

RKMP, RKO2 = pseudo-first-order oxidation rates of SO_2 by H_2O_2 and trace metals, respectively, in $(ppm\ min)^{-1}$ or $(min)^{-1}$

The arguments used both in the call to MARS and returned to EQL are

H2O2 = H_2O_2 concentration in ppm (required only if NSO2 = 1)

O3 = O_3 concentration in ppm (required only if NSO2 = 1)

SO2 = SO_2 concentration in ppm (required only if NSO2 = 1)

The arrays used internally in MARS are AWAS, AWAB, AWSA, AWLC, and AWAN. These five arrays are inverse-water-activity functions in the form of arrays dimensioned to 99. For a given water activity (corresponding to relative humidities of 1 to 99 %), these arrays contain the molality of the binary solutions of ammonium sulfate (AWAS) ammonium bisulfate (AWAB), sulfuric acid (AWSA), letrovicite $(NH_4)_3\ H(SO_4)_2$ (AWLC), and ammonium nitrate (AWAN).

SUBROUTINE BROMLY (CAT1, CAT2, AN1, AN2, AN3, NUNIT, YY1, YY2, YY3, YY4, YY5) is called from MARS. It computes the activity coefficients of ($2NH_4^+$, SO_4^{-2}), (NH_4^+, NO_3^-), ($2H^+$, SO_4^{2-}), (H^+, NO_3^-), and (H^+, HSO_4^-) in aqueous multicomponent solution using Bromly's model with four parameters.

The arguments required for the call to BROMLY are

CAT1 = concentration of H^+ (moles/kg)

CAT2 = concentration of NH_4^+ (moles/kg)

AN1 = concentration of SO_4^{2-} (moles/kg)

AN2 = concentration of NO_3^- (moles/kg)

AN3 = concentration of HSO_4^- (moles/kg)

NUNIT = unit for writing error messages.

Arguments returned by BROMLY to EQL are

YY1 = mean molal ionic activity coefficient for ($2NH_4^+$, SO_4^{2-})

YY2 = mean molal ionic activity coefficient for (NH_4^+, NO_3^-)

YY3 = mean molal ionic activity coefficient for ($2H^+$, SO_4^{2-})

YY4 = mean molal ionic activity coefficient for (H^+, NO_3^-)

YY5 = mean molal ionic activity coefficient for (H^+, HSO_4^-)

SUBROUTINE ROOT (METHOD, ERRMAX, A, B, XO, NUNIT, F, DF, R, MSG)
This subroutine is called by MARS. It finds a root of the function F(x) or the function DF(x) in a user-specified interval to within a user-specified accuracy. The interval (A, B) must be such that F(A)* F(B) < 0. Function G(x) and DG(x) may be substituted for F(x) and DF(x) in the call.

Arguments required for the call to ROOT are

NUNIT = unit to write error messages

METHOD = method to be employed

1 = Bisection
2 = Newton-Raphson
3 = Both 1 and 2

ERRMAX = maximum acceptable error

A = lower limit for bisection (for METHOD=1 or 3 only)

B = upper limit for bisection (for METHOD=1 or 3 only) (note that the subroutine will still work if B is the lower limit and A is the upper limit)

F = externally defined function for which a root is being sought

DF = externally defined function for which a root is being sought

Arguments returned by ROOT are

XO = initial guess for the Newton Raphson method (for METHOD=2 only)

MSG = a message to indicate that no more than one root is in this interval

Note that the functions F(x), DF(x), and G(x), DG(x) must be externally specified as

$$F(x) = x^4 + C_3 x^3 + C_2 x^2 + C_1 x + C_0$$

$$DF(x) = 4 x^3 + 3C_3 x^2 + 2C_2 + x + C_1$$

$$G(x) = x^3 + C_2 x^2 + C_1 x + C_0$$

$$DG(x) = 3x^2 + 2C_2 x + C_1$$

where C_0, C_1, C_2, and C_3 are coefficients of the quartic equation.

SUBROUTINE DENSITY (X, RHO) is called by MARS. It computes the density of an aerosol comprising several components. The argument required for the call to DENSITY is the array X, which contains the components of the aerosol in $\mu g/m^3$:

X(1) = water

X(2) = ammonium sulfate

X(3) = letrovicite $(NH_4)_3 H(SO_4)_2$

X(4) = ammonium bisulfate

X(5) = sulfuric acid

X(6) = ammonium nitrate

X(7) = nitric acid

The argument returned by DENSITY to MARS is RHO, which is the density of the aerosol in g/cc.

SUBROUTINE BSCAT3 (CC, BSCAT, PM10, XLAM) is called from EQL. It calculates the aerosol scattering coefficient of the aerosol sectional distribution using the MIE scattering efficiencies. The arguments required for the call to BSCAT are

CC = array of aerosol concentrations

XLAM = parameter equal to the ratio of the total of sulfate, nitrate, ammonium, and water aerosol to the sulfate aerosol (i.e., XLAM = (AERS+AERN+AERA+AERW)/AERS)

The arguments returned by BSCAT3 to EQL are

PM10 = total aerosol mass below 10 μm

BSCAT = the aerosol scattering coefficient

SUBROUTINE PQ3 (P1, Q1, RSA, RCAN, RKENRT, RORG) is called from the ROM subroutine GPRIME. It allows for the transition between the main program and the other aerosol subroutines. The arguments required for the call to PQ3 are

RSA = rate of sulfuric acid formation in the gas phase

RCAN = rate of coarse aerosol formation

RKENRT = rate of sulfate formation in the aerosol phase

RDRG = rate of condensible organics formation in the gas phase

The arguments returned by PQ3 are

P1 = array containing the normalized rates of destruction

Q1 = array containing the normalized rates of production

Subroutine PQ3 calls subroutine DUST.

SUBROUTINE DUST (CC, PROD, DEST, RSA, RCAN, RKENRT, RORG) is called from PQ3. It calculates the aerosol dynamics, i.e., the change in the aerosol size distribution due to coagulation, sulfate condensation, sulfate heterogeneous formation, and new aerosol formation. This is done through computations using the kinetic rate equations for a sulfate/nitrate /ammonium/primary aerosol with a sectional aerosol size distribution (Seigneur et al., 1986b). The arguments required for the call to DUST are

CC = array containing the concentrations of gas-phase, liquid-phase, and aerosol species

RSA = rate of sulfuric acid formation in the gas phase

RCAN = rate of coarse aerosol formation

RKENRT = rate of sulfate formation in the aerosol phase

RORG = rate of condensible organics formation in the gas phase

The arguments returned by DUST are

PROD = array containing the rates of production

DEST = array containing the rates of destruction

Subroutine DUST calls subroutine GPCONV.

SUBROUTINE GPCONV (R, AREA, RATIO, RO, WM) is called by DUST. It computes the ratio of new particle formation to total gas-to-particle conversion for sulfate and organic species according to the steady-state-monomer balance theory (McMurry, 1982). The arguments required for the call to GPCONV are

R = rate of condensible species formation in the gas phase

AERA = total aerosol area

RO = density of the condensed species

WM = molecular weight of the condensed species

The argument returned by GPCONV is RATIO, which is the ratio of new particle formation to total gas-to-particle conversion for sulfate and organic species.

REFERENCES

Hogo, H., M. A. Yocke, and C. S. Liu. 1986. "Extension of the Urban Airshed Model to Estimate PM10 and Visibility in Los Angeles." Presented at the Air Pollution Control Association International Specialty Conference on Visibility Protection, Grand Teton National Park, Wyoming, 7-10 September 1986.

McMurry, P. H. 1983. New particle formation in the presence of an aerosol: Rates, time scales, and sub-0.01 μm size distribution. J. Colloid Interface Sci., 95:72-80.

Saxena, P., A. B. Hudischewskyj, C. Seigneur, and J. H. Seinfeld. 1986. A comparative study of equilibrium approaches to the chemical characterization of secondary aerosols. Atmos. Environ., 20:1471-1483.

Seigneur, C., and A. B. Hudischewskyj. 1986. "Description of the Reactive Plume Model with Aerosol Chemical Composition and Size Distribution." Systems Applications, Inc., San Rafael, California (SYSAPP-86/055).

Seigneur, C., A. B. Hudischewskyj, and P. Saxena. 1986a. "Further Development and Application of a Mathematical Model of Sulfate and Nitrate Formation in Plumes." Systems Applications, Inc., San Rafael, California (SYSAPP-86/163).

Seigneur, C., A. B. Hudischewskyj, J. H. Seinfeld, K. T. Whitby, E. R. Whitby, J. R. Brock, and H. M. Barnes. 1986b. Simulation of aerosol dynamics: A comparative review of mathematical models. Aerosol Sci. Technol., 5:205-222.